

Chapter One

Introduction

“...when you can measure what you are speaking about and express it in numbers, you know something about it; but when you cannot express it in numbers, your knowledge is of a meagre and unsatisfactory kind; it may be the beginning of knowledge, but you have scarcely in your thoughts advanced to the state of science, whatever the matter may be.”

Lord Kelvin

1.1 INTRODUCTION

All engineering design incorporates uncertainty in one form or another. In fact, the overall, or total, uncertainty associated with any particular design may incorporate one or more of the following:

- uncertainties due to variabilities of material properties;
- inconsistencies associated with the magnitude and distribution of design loads;
- uncertainties associated with the measurement and conversion of design parameters;
- inaccuracies that arise from the models which are used to predict the performance of the design;
- anomalies that occur as the result of construction variabilities;
- gross errors and omissions.

While the traditional forms of geotechnical engineering design, which are based on deterministic constitutive relationships, are unable to account for these uncertainties in any quantifiable manner, the *probabilistic* design approach, which has gained greater acceptance

over the last 20 years or so, is able to incorporate these uncertainties. The value of probabilistic, or stochastic, analyses is that, in accounting for uncertainties and errors, they enable the designer to make estimates regarding the reliability and risk of failure associated with a particular engineering design.

An important uncertainty that sets geotechnical engineering apart from other disciplines of civil engineering, and which is one aspect of the probabilistic design approach, is the variability associated with the properties of soils and rock or, more precisely, the *probabilistic characterisation of soil profiles*. This problem, which is central to geotechnical engineering, as well as other geosciences, arises from the fact that the engineering properties of geotechnical materials, such as soils, rock and fill, exhibit variability from one location to another, even within seemingly homogeneous profiles. This is in contrast to other civil engineering materials, such as steel, concrete and timber, which are essentially homogeneous in comparison. The reason for this is due largely to the complex and varied physical processes associated with the formation of geotechnical materials. The divergence of properties from one location to another, within a soil or rock mass, is termed *spatial variability*.

Since the performance of a geotechnical structure depends on local extremes of the properties within a subsurface profile, it is important to probabilistically characterise a soil profile (Vanmarcke, 1978). This is best illustrated by referring to the following two examples. Firstly, the failure, or settlement, of a foundation will occur if the shear strength, or stiffness, within a sufficiently large enough volume of soil lying beneath it, falls below some critical value. Secondly, sliding failure of an embankment will occur if the shear strength along a given surface drops below some minimum strength. The same can be said for other geotechnical failure conditions, such as differential settlement, liquefaction, piping and erosion, and retaining wall failures. Each of these examples illustrates the fact that failures occur within some region whose *spatially averaged* property falls below some critical value. Vanmarcke (1978) describes the probabilistic characterisation of soil profiles as having essentially two main purposes:

- (i) it provides a format for quantifying geotechnical engineering information regarding the subsurface conditions at a particular site;
- (ii) it provides the basis for predicting the performance of a geotechnical engineering structure and for quantifying the probability of failure.

Kulatilake and Varatharajah (1986) suggested an additional benefit of quantifying the spatial variability of soil deposits, that is, it enables a geotechnical engineer to critically assess and

compare various site investigation and testing programmes, and also to evaluate their effectiveness.

A probabilistic design approach has a number of significant benefits when compared to traditional deterministic design. These are best illustrated by looking at the design of embankments. The traditional deterministic design approach expresses the stability of an embankment by means of the factor of safety, *FoS*, which is the ratio of the forces *resisting* failure to those *causing* failure. It has been shown by several researchers (e.g. Matsuo and Asaoka, 1977; Li and Lumb, 1987; Li and White, 1987b; Mostyn and Li, 1993) that the *FoS* is a wholly unsatisfactory description of the stability of a slope. This is because it is uncertain whether some parameters which affect the stability of the slope, such as the weight of the soil at the toe of the slope, should contribute to the *FoS* by adding to the *forces resisting sliding* or by subtracting from the *forces causing sliding*. However, more importantly, depending on the level of uncertainty associated with the various parameters, a slope based on data with large scatter and, therefore, reduced confidence in the mean value, may produce a higher factor of safety than a slope based on data with a reduced spread, that is, one with more reliable information. The probabilistic approach, on the other hand, would apportion the former case with a higher probability of failure than the latter, as one would normally expect. In addition, by quantifying the failure probability, the designer is able to quantify the expenditure needed to reduce the risk of failure, or alternatively, the consequences associated with reducing the overall cost of a project. As a result, the probabilistic design approach provides much more useful design information than that provided by traditional deterministic techniques.

Whilst some research has been undertaken in the study of the probabilistic characterisation of soil profiles, this thesis seeks to add to the existing body of knowledge in this field. In particular, there is a distinct lack of accurate, closely-spaced data with which to examine the spatial variability of soils (Orchant et al., 1988).

1.2 AIMS AND SCOPE OF THE STUDY

This research has aimed to investigate and quantify the spatial variation of soils and seeks to examine its influence on geotechnical engineering design. This study has focused on two stiff, overconsolidated clays, known as the *Keswick and Hindmarsh Clays*, and has been confined to a section of the central business district of Adelaide known as the *Adelaide city area*. The research has concentrated on the undrained shear strength, s_u , of these clays, however some attention has also been given to the internal angle of friction, ϕ , and the undrained Young's modulus, E_u , as well as those properties defining the state of the clays,

that is, the moisture content, w , void ratio, e , specific gravity of solids, G_s , and the coefficient of earth pressure at rest, K_0 .

This study has aimed to provide:

- an understanding of the nature of the spatial variation of the Keswick and Hindmarsh Clays, and soils like them;
- a model to allow the preliminary estimation of geotechnical properties;
- an understanding of the influence of spatial variability on geotechnical engineering design.

The Keswick and Hindmarsh Clays were chosen as the basis of this study for a number of reasons. These include:

- The Keswick and Hindmarsh Clays are relatively homogeneous and underlie much of the metropolitan and central business district of Adelaide;
- Keswick Clay is internationally significant since its geotechnical properties are similar to the well-documented London Clay and, as a result, conclusions made in this study may be directly applicable to similar soils in other countries;
- Keswick Clay is locally significant since many of Adelaide's high rise buildings are founded on it and, as a consequence, a relatively large quantity of in situ and laboratory test information is available;
- From a pragmatic point of view, the Keswick Clay can be intercepted at reasonably shallow depths resulting in relatively cost-effective sampling and testing programmes.

In order to investigate and quantify the spatial variability of a soil or rock mass, a large volume of closely-spaced, accurate data is needed. This is because the mathematical techniques used to quantify spatial variation, namely *random field theory* and *geostatistics*, require large amounts of data, otherwise large uncertainties will be associated with the results of these analyses. Vast resources of capital, equipment and labour are needed to sample and test the large number of specimens required for these mathematical analyses. Lumb (1975) suggested that for a full, three-dimensional analysis of spatial variability, a minimum of 10^4 test samples are needed. As a consequence, to date, little data has been published in the field of spatial variability of geotechnical materials.

In order to obtain large quantities of reliable data efficiently and economically, it was necessary and desirable to make use of existing test information. As a consequence, a data base of test results was compiled from records stored in private and government geotechnical engineering offices. Such a data base is able to provide the information necessary to develop a *large-scale* spatial variability model of the Keswick and Hindmarsh Clays, but would provide little data for quantifying the *small-scale* variability of the clay. This is because very few geotechnical site investigations sample and test closely-spaced soil specimens. Therefore, in order to quantify the small-scale spatial variability of these clays, it was necessary to conduct a specific, carefully-controlled experimental programme. It was decided to base this experimental programme on data obtained using the electrical *cone penetration test* (CPT). Factors which influenced this decision are given below.

- *In situ testing has a number of advantages over laboratory testing* - Wroth (1984) suggested that, as the understanding of the behaviour of real soils increases, the appreciation of the suitability of conventional laboratory testing diminishes. In situ testing, unlike its laboratory counterpart, does not suffer from the consequences of sample disturbance, and the soil in question is tested at the appropriate level of effective stress; provided that changes due to insertion of the instrument are kept to a minimum.
- *Large amounts of data can be collected efficiently and economically* - By virtue of its continuous and simultaneous recording of test parameters, the CPT is able to provide, for a particular linear sounding, a large volume of closely-spaced data, as is required for spatial variability analyses. In addition, the CPT is able to measure these data efficiently, economically, and with a high level of reliability.
- *Accuracy* - The CPT, along with the Marchetti Flat Plate Dilatometer, has been shown to exhibit the lowest measurement error (*coefficient of variation*¹ of between 5% and 15%) of any of the common in situ test methods in current practice (Wu and El-Jandali, 1985; Orchant et al., 1988).
- *Availability* - The Department of Civil and Environmental Engineering, at the University of Adelaide, currently owns and maintains a cone penetrometer and associated equipment, and employs technicians who are proficient in its operation.

This small-scale study has been confined to the investigation of the spatial variability of the undrained shear strength of the Keswick and Hindmarsh Clays within the Adelaide city area, using the cone penetration test. The analytical techniques of random field theory and geostatistics have been employed to examine the spatial variability of the Keswick Clay.

¹ ratio of the standard deviation, σ , to the mean, m .

Finally, the assessment of the significance of spatial variability on geotechnical engineering design has been restricted to the analysis of embankments, and the design of piled foundations.

1.3 LAYOUT OF THE THESIS

The thesis details the present research undertaken to quantify and model the spatial variability of the Keswick and Hindmarsh Clays. In Chapter 2 the study area is described, and a review of the existing literature regarding the development in the understanding of the Keswick and Hindmarsh Clays is given, including their geological history, stratigraphy and geotechnical properties. In addition, matters relating to the CPT, which are relevant to this study, are presented, and techniques currently used to characterise the spatial variability of soils, as well as published experimental and theoretical research relevant to the spatial variability of geotechnical materials, are examined.

Chapter 3 describes a micro-computer based data acquisition system for the CPT which was developed in order to enable the recording, storage and post-processing of accurate, reliable and closely-spaced CPT measurements. The data acquisition system consists of both hardware and software components. Chapter 3 describes these, as well as the design criteria on which they are based. Each of the elements of the data acquisition system is then tested and calibrated, and treatment of the results is given, as well as discussion relating to the limitations of the overall system.

Chapter 4 describes the experimental programme undertaken to examine the small-scale spatial variability of the Keswick and Hindmarsh Clays. This programme consisted of:

- 222 vertical CPTs, at various lateral spacings, to a typical depth of 5 metres. These CPTs were performed at the *South Parklands site* which is situated within the Adelaide city area;
- a single horizontal CPT, performed to a lateral extent of 7.62 metres at the *Keswick site*;
- continuous and discrete sampling;
- a series of 12 unconsolidated undrained triaxial tests.

In addition, Chapter 4 discusses the relevant sites, the equipment used to obtain the measurements, the conditions under which they were recorded, and the results of these tests.

In Chapter 5 analyses are presented which are based on the data detailed in Chapter 4. These analyses have been performed using random field theory and geostatistics, and spatial variability models are generated for the undrained shear strength, s_u , of the Keswick Clay. The techniques of random field theory and geostatistics are then employed to generate predictions and simulations of the s_u data.

The compilation of the data base of geotechnical properties of the Keswick and Hindmarsh Clays, known as *KESWICK*, is detailed in Chapter 6. This data base, which provides information relating to the large-scale spatial variation of the Keswick and Hindmarsh Clays, was compiled from various site investigations and laboratory results. In this chapter, these data are discussed, and trends and relationships between them, are examined.

In Chapter 7 the data and relationships presented in Chapter 6 are used to develop a model which describes the lateral spatial variation of the undrained shear strength of the Keswick Clay. This model is then used to develop a stochastic framework which provides preliminary estimates of the undrained shear strength of the Keswick Clay within the Adelaide city area.

The results obtained in Chapters 5 and 7 are then employed in Chapter 8 to examine the influence of spatial variability on the design of geotechnical engineering systems, in particular, earth embankments and piled foundations.

A summary and conclusions of this study, as well as areas for future research, are then presented in Chapter 9.

Chapter Two

Literature Review

2.1 INTRODUCTION

This chapter provides a background for later chapters of this thesis and briefly reviews the historical developments in: the understanding of the nature and properties of the Keswick and Hindmarsh Clays; the cone penetration test; and the spatial variability of soils. Where possible, the review has followed a chronological sequence.

2.2 THE STUDY AREA

Adelaide, the capital and largest city of South Australia, is located approximately ten kilometres east of the Gulf St. Vincent, as shown in Figure 2.1, and is bounded to the east by the Adelaide foothills which form part of the Mount Lofty Ranges.

This research focuses on a region of the Adelaide city bounded by Park, Fitzroy and Robe Terraces to the north; Port Road and the Railway to the west; Greenhill Road to the south; and Fullarton Road, Dequetteville Terrace and Hackney Road to the east, as shown in Figure 2.2. This region was originally studied by Cox (1970) and was referred to as the *Adelaide city area* in his paper. Stapledon (1970) and Selby and Lindsay (1982) also referred to this region as the Adelaide city area.

This portion of the Adelaide city varies in mean height above sea level from approximately 20 metres to the west, to approximately 60 metres to the east, and includes the central business district and a region of parklands locally referred to as the *green belt*. The River Torrens bisects the city area into North Adelaide, chiefly residential, and Adelaide, to the south, which is predominantly commercial.



Figure 2.1 Locality plan.

2.3 THE KESWICK AND HINDMARSH CLAYS

A brief treatment of the geological history and geotechnical characteristics of the Keswick and Hindmarsh Clays are presented below, in order to provide a broad overview of properties of these soils.

2.3.1 Geological History

The city of Adelaide is situated on the western portion of an upthrust block bounded to the west by the Para Fault and to the east by the Eden-Burnside Fault. It is predominantly these two faults which have influenced the present day topography of the city. The major stratigraphic units that underlie the Adelaide city area are summarised in Table 2.1.

The St. Vincent Basin, shown in Figure 2.3, was formed by a downfaulted block bounded by the Ardrossan Fault to the west and a series of major faults to the east. The Adelaide city area is located in one of the eastern embayments of the St. Vincent Basin, referred to by Selby and Lindsay (1982) as the *Highbury - Golden Grove Embayment* and later by Sheard and Bowman (1987a) as the *Adelaide - Golden Grove Embayment*. The sediments

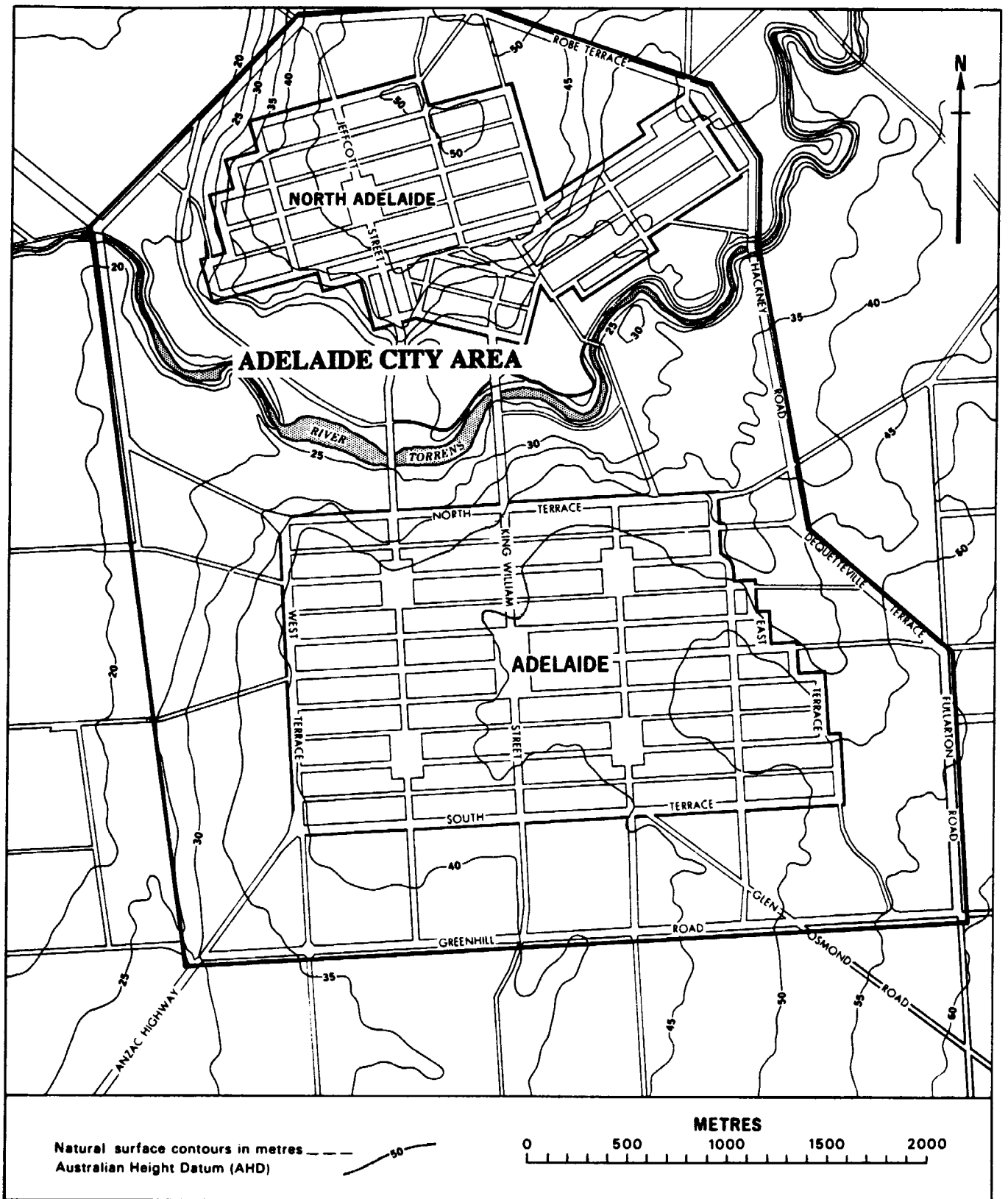


Figure 2.2 The Adelaide city area.
(After Cox, 1970 and Selby and Lindsay, 1982).

Table 2.1 Summary of stratigraphic units underlying the Adelaide city area.
(After Selby and Lindsay, 1982).

Era, Period, Epoch	Age in Millions of years	Geological Classification Name	Maximum Thickness (m)	Material Description
Cainozoic Quaternary <i>Holocene</i>	10,000 years	Alluvium of the River Torrens	21	Red brown Silty CLAY; grades downwards to SAND and GRAVEL (SP-GP).
		Callabonna Clay		Red brown CLAY (CH).
		Pooraka Formation		Light brown Silty CLAY (CL-ML), calcareous with layers of calcrete GRAVEL (GM).
Cainozoic Quaternary <i>Pleistocene</i>	1.5	Keswick Clay	7	Grey-green CLAY (CH) with red and brown mottling, stiff to hard, fissured.
		Hindmarsh Clay	16	Grey-green CLAY (CH) with yellow and red mottling with overlying SAND (SC).
		Carisbrooke Sand	13	Yellow, orange brown and grey, fine to medium Clayey and Silty SAND (SC/SM)
		Burnham Limestone	1 - 2	White Clayey, Sandy and rubbly LIMESTONE.
Cainozoic Tertiary <i>Pliocene</i>	3	Hallett Cove Sandstone	12	Pale grey to brown calcareous SANDSTONE with layers of SAND (SP).
Cainozoic Tertiary <i>Eocene</i>	30-38	Port Willunga Formation	39	Sandy SILT and CLAY with strong CHERT nodules (GC-GP, ML, SM).
		Chinaman Gully Formation	12	Dark grey to black SILT and CLAY (ML-CL) with layer of Gravelly, Clayey SAND (SC-GW).
		Blanche Point Formation	25	Alternating bands of cherty siltstone and grey SILT (SM) overlying green to dark grey Clayey SAND (SC) and LIMESTONE.
	40	South Maslin Sand	12	Grey to brown or yellow, Silty SAND (SM) with pyrite lumps.
		Clinton Formation	27	Dark grey CLAY (CL) with lignite; irregular Clayey SAND zones (SC).
Proterozoic	≈ 800+	Adelaidean System		Brown, pink, grey to white, weathered SILTSTONE with quartz veinlets.

that filled these embayments were deposited first in swamps and from streams, followed by several cycles of marine deposition. During the Tertiary period, movement along the faults continued, as is evidenced by the variation of strata thickness adjacent to, and on either side, of the faults.

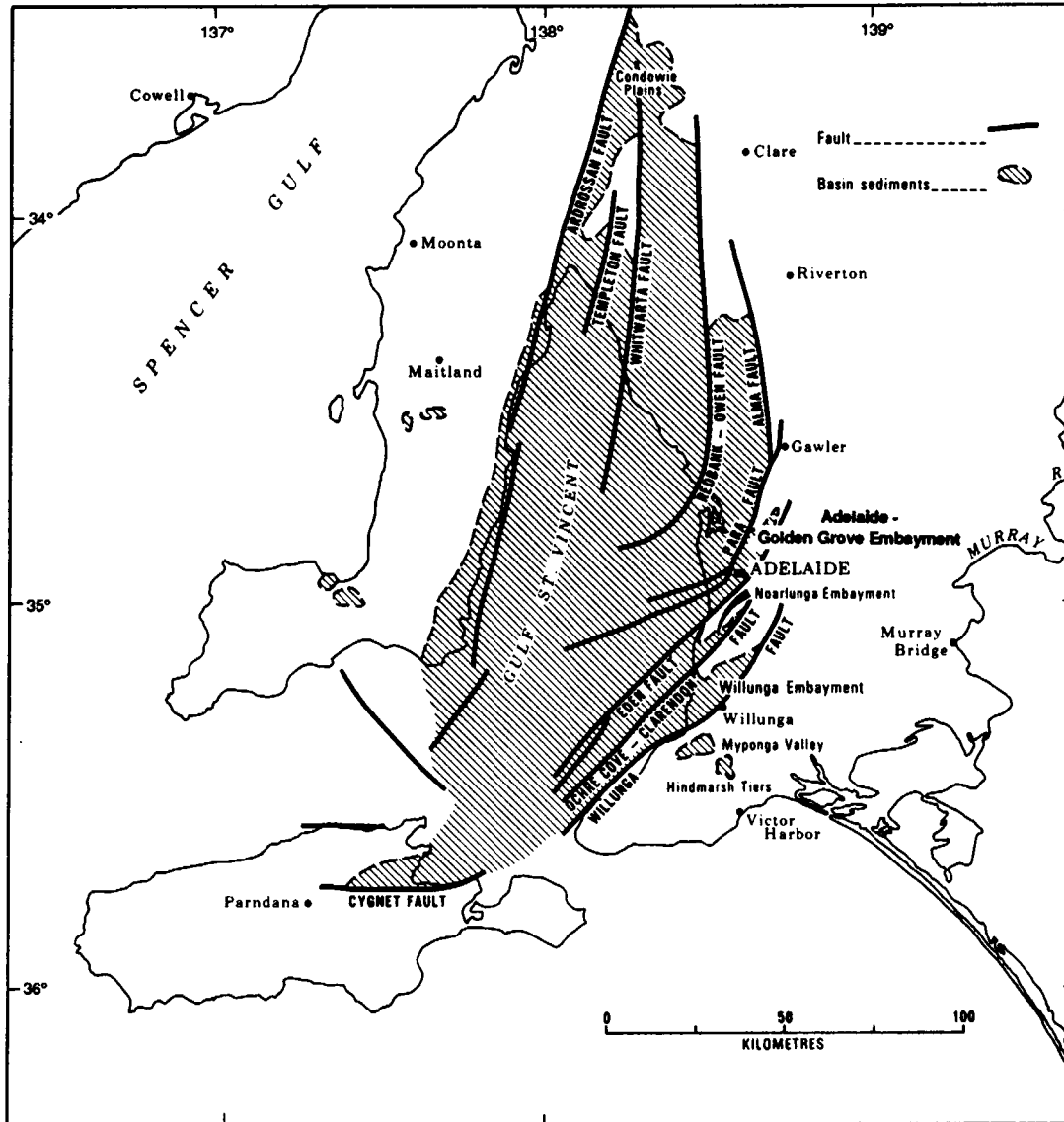


Figure 2.3 The St. Vincent basin.
(After Selby and Lindsay, 1982).

Selby and Lindsay (1982) suggested that approximately 1.5 million years ago the clayey sands and gravels of the *Carisbrooke Sand* were deposited. Following a depositional break and a period of subsequent weathering, the *Hindmarsh Clay* was alluvially deposited on a flat riverine plain (Selby and Lindsay, 1982; Sheard and Bowman, 1987b).

The *Keswick Clay* disconformably overlies the *Hindmarsh Clay*, the basal contact of which is an erosion surface, and is often sharp. The *Keswick Clay* is thought to have been deposited in the Middle Pleistocene (Sheard and Bowman, 1987a).

Following the deposition of the Keswick Clay, a major cold, dry and windy period began in the Middle Pleistocene about 700,000 years ago. This led to the accumulation of a wind-blown calcareous dust, or *loess*, known as the *calcareous mantle*. This is an extremely variable soil profile which varies from nodular lime gravel to soft calcareous silt and clay. Usually the calcareous material appears in white, yellow or pink patches within grey or green sand, silt, or clay. In the Adelaide city area the calcareous mantle grades downwards into the Keswick, or Hindmarsh, Clay, a transition which is marked by: the gradual disappearance of carbonate nodules and patches; a change to stiff clay of high plasticity; and development of mottling and structuring in the clay.

Approximately 20,000 years ago, following a period of faulting and erosion, alluvial silts and clays of the *Pooraka Formation* were deposited. Another cold, dry period caused further accumulation of windblown calcareous sediments which modified the Pooraka Formation. Finally, a red-brown, non-calcareous, alluvial clay, known as the *Callabonna Clay*, or *Soil-B Horizon*, was deposited over much of the Adelaide city area, where it is usually less than one metre in thickness. In some parts of the Adelaide city area, the Callabonna Clay is absent due to erosion, weathering, gilgai and shallow earthmoving activities.

Subsequent to the deposition of the Keswick and Hindmarsh Clays, sediments were deposited in the River Torrens valley. Though, at present, the River Torrens occupies a relatively narrow channel within the Adelaide city area, below it lies a much wider ancient valley. The sediments that have been deposited within this buried valley are known as the *Alluvium of the River Torrens*, and deposition is thought to have occurred during the recent Quaternary, since the Keswick and Hindmarsh Clays have been completely removed from this valley (Selby and Lindsay, 1982). The composition of these sediments consists generally of sandy gravel overlain by silt and clay, but vary greatly, both laterally and with depth.

2.3.2 Geotechnical Characteristics

This section details the geotechnical characteristics of the Keswick and Hindmarsh Clays relevant to this research. These characteristics include: stratigraphy; mineralogy; plasticity; moisture regime; specific gravity; degree of saturation; instability index; and coefficient of earth pressure at rest.

2.3.2.1 Stratigraphy

Since the late 1800's, many geoscientists have described the clay-rich deposits overlying the Tertiary marine sediments of the Adelaide plains. These clays have been referred to as *Plio-Pleistocene 'pipe clay'*, *Mammaliferous Drift*, *'alluvial mottled clays'*, *Adelaide Clay*, *'mottled clay'* and the *Pleistocene Clay*. Recently, Selby and Lindsay (1982) referred to these clays as the *Hindmarsh Clay* and they described it as consisting of three layers: the *upper clay layer*; the *middle sand member*; and the *lower clay layer*. Based on a joint Department of Mines and Energy, S.A. and CSIRO project that incorporated the drilling of 62 boreholes in the Adelaide metropolitan area, Sheard and Bowman (1987a & b) suggested that a disconformable erosion surface exists between the upper clay layer and the lower sediments. They subsequently redefined the upper clay layer as the *Keswick Clay* and the middle sand member and lower clay layer as the *Hindmarsh Clay*. However, it is somewhat ambiguous to refer to this soil deposit, which consists of a layer of clay and a layer of sand, as the "Hindmarsh Clay." As a consequence, for the remainder of this thesis, the term *Hindmarsh Clay Formation* will refer to both, the *Hindmarsh Clay sand member* (the middle sand member of Selby and Lindsay, 1982), and the *Hindmarsh Clay layer* (the lower clay layer of Selby and Lindsay, 1982), and the term *Keswick Clay* will be consistent with that defined by Sheard and Bowman (1987a).

(i) Keswick Clay

The Keswick Clay underlies much of the Adelaide city area and pockets of the Adelaide metropolitan area, as shown in Figure 2.4, and has been eroded by the River Torrens. It stratigraphically overlies the Hindmarsh Clay Formation; the basal contact surface being a disconformable erosion surface.

Keswick Clay is a relatively uniform, very stiff to hard, silty clay of high plasticity. It has a Unified Soil Classification System (USCS) symbol of **CH** and is heavily fissured, with fissure spacings of approximately 10 to 25 mm. Its colour varies from grey-green to yellow-grey (gley colours) with red (haematite) and yellow (limonite) mottling of varying proportions. Sheard and Bowman (1994) suggest that the gley colours may have resulted from post-depositional chemical reduction in oxygen-poor groundwaters. Within the Adelaide city area, its thickness varies to a maximum of approximately 7 metres. Tree roots have been found at all depths and are probably the remains of old eucalypts removed during urbanisation (Cox, 1970).

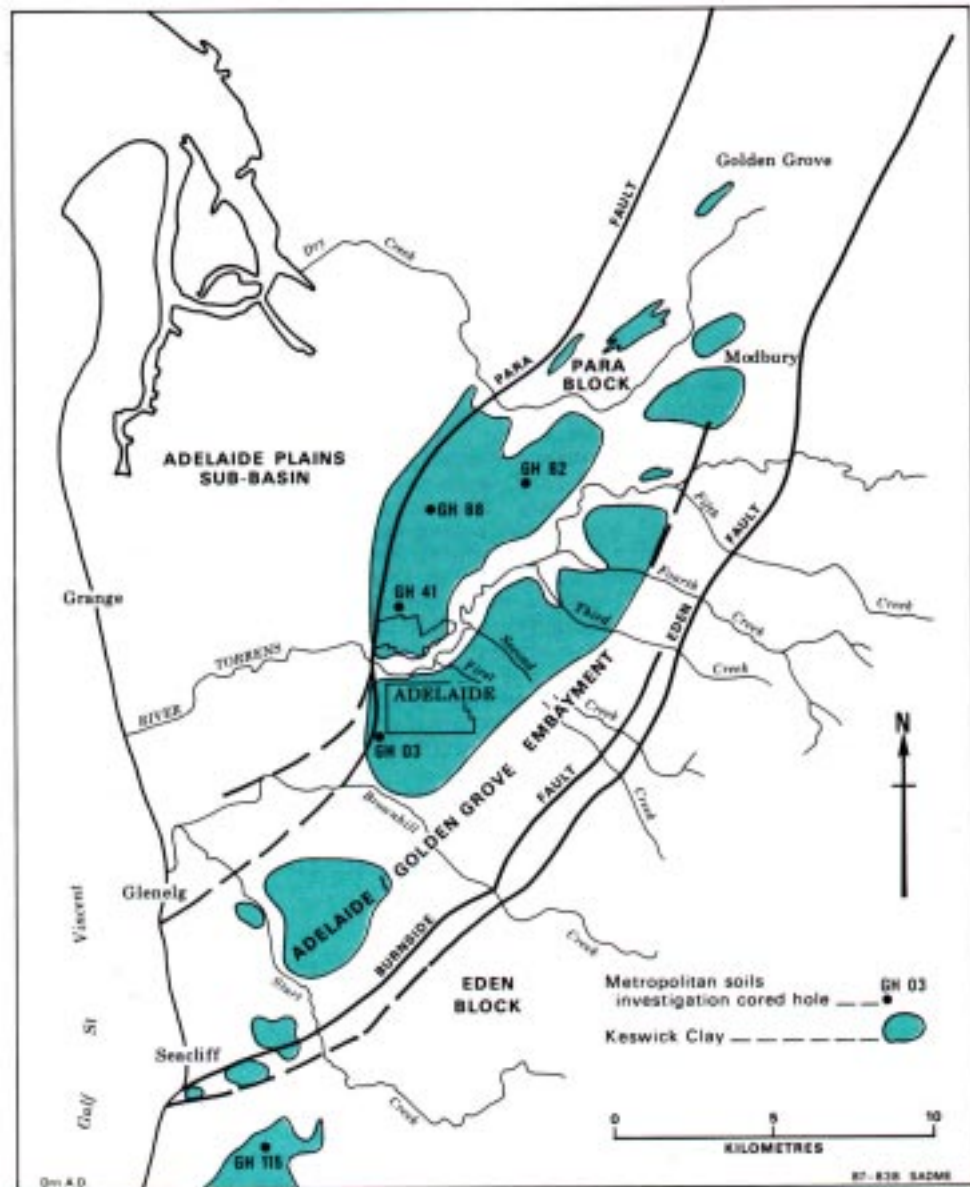


Figure 2.4 Distribution of the Keswick Clay.
(After Sheard and Bowman, 1987a).

Stapledon (1970) and Selby and Lindsay (1982) suggested that the Keswick Clay has been overconsolidated due mainly to desiccation, with preconsolidation pressures in excess of 400 kPa.

(ii) Hindmarsh Clay Sand Member

The Hindmarsh Clay sand member consists of a grey and brown, dense, coarse clayey sand (USCS symbol SC). It directly overlies either the clay member of the Hindmarsh Clay Formation, the Hallett Cove Sandstone, or the Blanche Point Formation (Cox, 1970). The

sand has many red lateritic and sand/rock pebbles, some horizontal interbedded clay layers and traces of calcareous material.

Selby and Lindsay (1982) suggested that the sand member is distributed in an elongated zone extending south-southwest across the central city area and that the member probably represents a river channel deposit.

(iii) **Hindmarsh Clay Layer**

The Hindmarsh Clay Layer underlies the Adelaide city area and much of the Adelaide metropolitan area, as shown in Figure 2.5. In the Adelaide - Golden Grove Embayment the River Torrens has dissected the unit.

The Hindmarsh Clay layer is similar in appearance and properties to that of the Keswick Clay. It is a very stiff to hard, highly plastic silty clay (USCS symbol **CH**). Selby and Lindsay (1982) attribute stiffening of the upper 1 to 2 metres of the clay, which they term '*pseudo-consolidation*', to post-depositional desiccation. Its colour is the same as the Keswick Clay, that is, grey-green with red and yellow mottling at depth. The Hindmarsh Clay Layer directly overlies the Carisbrooke Sand or, where it has been removed by erosion, it overlies the Hallett Cove Sandstone. (The Burnham Limestone is often seen only as a transitional zone within the Hallett Cove Sandstone). The Hindmarsh Clay Layer is relatively uniform, both in properties and in surface level.

Where no sand separator bed exists, and where the Hindmarsh and Keswick Clays are similar in character, the boundary between the two units is difficult to establish (Sheard and Bowman, 1987b). Like the Keswick Clay, the Hindmarsh Clay layer is heavily fissured with large and numerous slickensides which occur at 30° to 45° to the horizontal. Structural features associated with these clays are treated in greater detail in §2.3.3.

2.3.2.2 Mineralogy

In general, very few tests have been carried out in order to determine the mineralogy of the Keswick and Hindmarsh Clays. This holds true not only for these clays, but for all Adelaide soils in general. Cox (1970) cited X-ray diffraction tests carried out on the Keswick Clay which indicated that the soil consists predominantly of three clay minerals: illite; kaolinite; and montmorillonoid minerals. Illite appears in quantities generally greater than 50%, whereas kaolinite was found in quantities in excess of 20%. Minerals of the montmorillonoid group were observed in amounts of less than 20%.

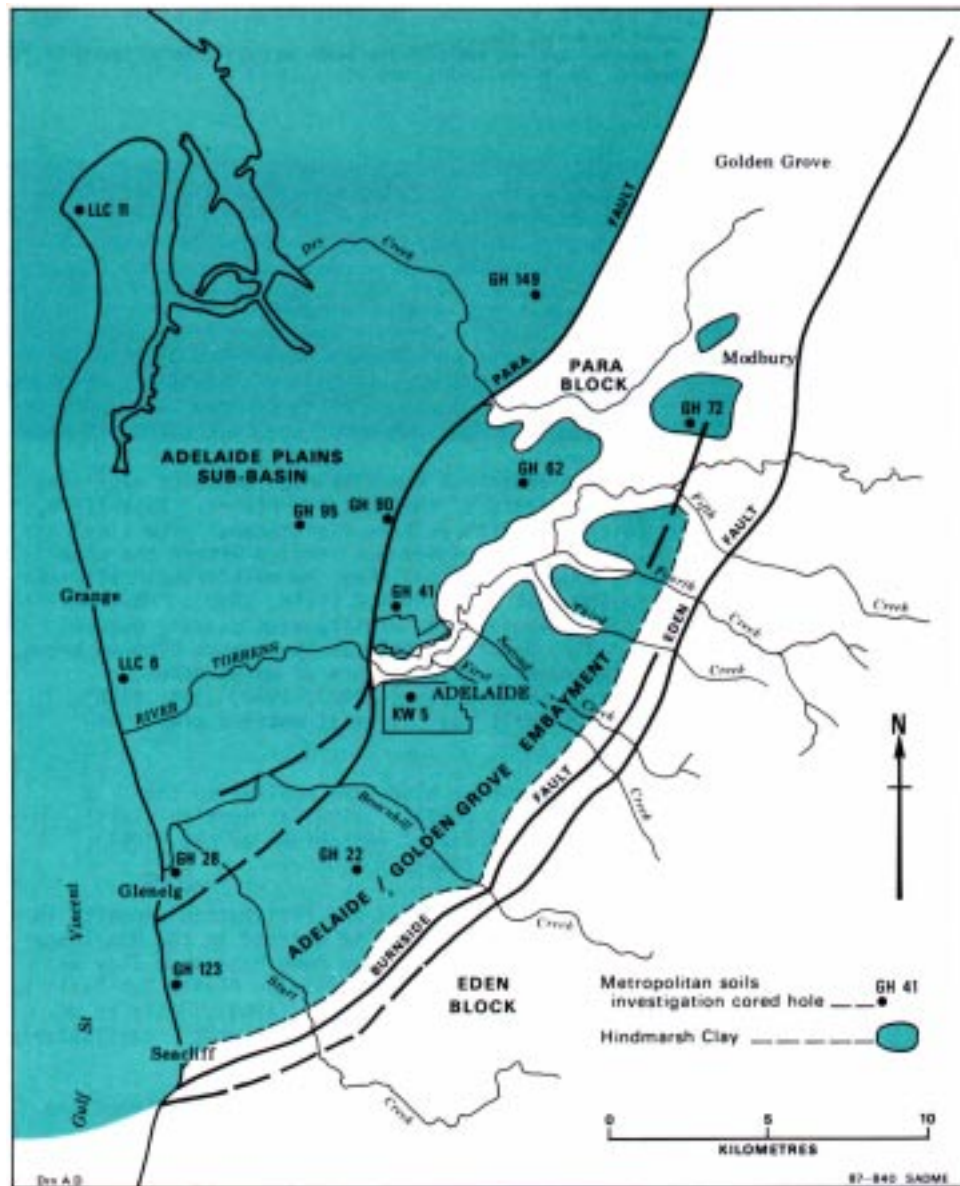


Figure 2.5 Distribution of the Hindmarsh Clay.
(After Sheard and Bowman, 1987b).

Stapledon (1970) suggested that the Hindmarsh Clay consists of illite and kaolinite in proportions of greater than 50%, and lesser amounts of montmorillonite. It is not evident whether Stapledon was referring to the Keswick Clay or the Hindmarsh Clay layer, however, Stapledon (1995) confirmed that he was referring to both.

2.3.2.3 Plasticity

Cox (1970) presented the results of many Atterberg limit tests performed on samples of Keswick Clay and the Hindmarsh Clay layer in the Adelaide city area. The ranges of results from these tests are summarised in Table 2.2.

Table 2.2 Summary of Atterberg limit tests. (*Reported by Cox, 1970*).

Member	No. of tests	w_P (%)	w_L (%)	I_P (%)	Clay Content (%)	Activity
Keswick Clay	75	18-29	60-117	42-88	52-67	0.8-1.2
Hindmarsh Clay layer	11	16-30	55-100	40-70	50-70	0.7-1.0

Cox suggested that the plastic limit, liquid limit, plasticity index and activity increase to the north. Sheard and Bowman (1994) also reported Atterberg limit results based on their extensive study of soils in the metropolitan area of Adelaide. Those results that pertain to soils within the Adelaide city area are summarised in Table 2.3, with average values shown in parentheses. *Undifferentiated Keswick-Hindmarsh Clay* refers to soil that the authors were unable to classify as Keswick Clay or the Hindmarsh Clay layer.

Table 2.3 Summary of Atterberg limit tests. (*Reported by Sheard and Bowman, 1994*).

Member	No. of tests	w_P (%)	w_L (%)	I_P (%)
Keswick Clay	17	21-35 (27)	46-98 (74.6)	25-63 (47.6)
Hindmarsh Clay layer	14	17-42 (26.9)	46-100 (72.4)	27-66 (45.5)
Undifferentiated Keswick-Hindmarsh Clay	9	12-32 (23.8)	77-96 (83.7)	53-84 (59.9)

Note: Average values are shown in parentheses.

2.3.2.4 Moisture Regime

Cox (1970) suggested that the in situ moisture content of the Keswick Clay generally decreases from 34% at the surface of the layer to 30% at depth, with moisture contents of

up to 40% beneath old basement floors. He also reported that the in situ moisture content of the Hindmarsh Clay is much lower than that of the Keswick Clay, varying from 20% at the surface of the clay layer to 30% at depth.

Jaksa and Kaggwa (1992) presented a moisture distribution of far greater variation than that suggested by Cox. Based on the results of 451 separate tests performed on samples of Keswick Clay obtained throughout the Adelaide city area, Jaksa and Kaggwa suggested that the in situ moisture content varied anywhere between 15% and 40% at depths between one and 20 metres below ground surface. These data are examined in greater detail in Chapter 6.

2.3.2.5 Specific Gravity

Based on the results of three laboratory tests performed on samples of Keswick Clay, Cox (1970) reported that the average specific gravity of solids, G_s , was 2.70. The values of the individual tests, however, were not published. Jaksa and Kaggwa (1992) suggested that a mean value of 2.75 ± 0.02 would be a more appropriate value for the G_s of the Keswick Clay. Their estimate was not based on laboratory test measurements of G_s , but on a statistical analysis of 451 moisture content and dry density test results, as well as an estimation based on the mineralogy of the clay particles. Islam (1994) reported the result of a single laboratory test which was carried out on a sample of Keswick Clay obtained from the Myer-Remm development, which lies within the Adelaide city area. He reported the G_s of the clay to be 2.73. To date, no values of the G_s of the Hindmarsh Clay have been published.

2.3.2.6 Degree of Saturation

In general, the in situ degree of saturation, S_r , is obtained from the measured in situ moisture content, w , and dry density, ρ_d ; tabulated values of the density of water, ρ_w (usually assumed constant at 1000 kg/m^3); and the value of the specific gravity of solids, G_s , via the relationship shown in Equation (2.1), below.

$$S_r = \frac{w G_s \rho_d}{(G_s \rho_w) - \rho_d} \quad (2.1)$$

Using this relationship, and a G_s of 2.70, Cox (1970) found that the majority of his samples of Keswick Clay, taken from 20 separate sites within the Adelaide city area, had degrees of saturation between 95% and 100%. He inferred that the Keswick Clay was fully saturated

by suggesting the 0% to 5% air which was measured could be attributed to air entering the fissure system during sampling and testing. Cox claimed, based on theoretical calculations, “that fissures with a spacing of one inch [25 mm] need open only 0.0001 in. [0.0025 mm] to give a degree of saturation of 95%.” Similar calculations performed by the author suggest that the fissures need to open 0.02 mm to yield an S_r of 95%. In addition, Stapledon (1970) stated that the Hindmarsh Clay (the Keswick Clay and Hindmarsh Clay Formation) is either unsaturated or *quasi-saturated*, that is, apparently saturated, but showing appreciable negative porewater pressures.

Using 451 test results, Jaksa and Kaggwa (1992) also concluded that the majority of the Keswick Clay is “saturated or very close to being saturated.” They also described the clay as being *quasi-saturated* due to the fact that, though it is saturated, no free moisture is observed. These data will be examined in greater detail in Chapter 6.

2.3.2.7 Instability Index, I_{pt}

The instability index, I_{pt} , is defined as the ratio between the vertical strain, ϵ_v , and the change in total suction, Δu , as shown in Equation (2.2).

$$I_{pt} = \frac{\epsilon_v}{\Delta u} \quad (2.2)$$

The I_{pt} is a measure of the *reactivity* or *expansiveness* of a soil, or in other words, the amount of shrinkage or swelling that the soil will undergo upon drying or wetting, respectively. It is widely accepted that the Keswick and Hindmarsh Clays are extremely expansive with recorded measurements of I_{pt} up to 6% not uncommon (Sheard and Bowman, 1994). One would suspect that the reactivity of these clays is related to the amount of montmorillonoid minerals present in the soil mass, however, no published mineralogical tests have yet been carried out to investigate this assumption.

2.3.2.8 Coefficient of Earth Pressure at Rest, K_0

The coefficient of earth pressure at rest, K_0 , is defined as the ratio between the horizontal effective stress, σ'_h , and the vertical effective stress, σ'_v , at some depth below the ground surface, as shown in Equation (2.3).

$$K_0 = \frac{\sigma'_h}{\sigma'_v} \quad (2.3)$$

Richards and Kurzeme (1973) installed earth pressure cells and psychrometer probes behind a 7.5 metre deep basement wall, much of which was retaining undifferentiated Keswick-Hindmarsh Clay. They found that after a period of approximately two years, the earth pressures stabilised to a value of 1.3 to 4 times the overburden pressure. Similar results have been obtained from self-boring pressuremeter tests performed in the Keswick and Hindmarsh Clays (Kaggwa, 1992).

While Richards and Kurzeme's measurements were based on total stresses, many geotechnical engineering practitioners used these results to imply that the Keswick and Hindmarsh Clays have values of K_0 up to 4. This high value of K_0 has been used by some engineers to hypothesise that the lateral earth pressure is close to the passive resistance of the soil (Kaggwa, 1992).

Kaggwa (1992) examined self-boring pressuremeter, triaxial and psychrometer test results obtained from an extensive site investigation for a proposed tunnel within the Adelaide city area (Coffey and Partners Pty. Ltd., 1979). He found, by assuming that measurements of soil suction could be equated to negative porewater pressures, that the derived values of K_0 reduced to more realistic figures in agreement with laboratory K_0 triaxial tests. Kaggwa suggested that values close to 1 are appropriate for the K_0 of the Keswick and Hindmarsh Clays.

2.3.3 Structural Features

Stapledon (1970) detailed many structural features and defects within the Keswick Clay and the Hindmarsh Clay Formation. These included:

- **Steeply dipping joints:** These dip between 60° and vertical, are generally less than 4 m² in areal extent and, upon drying, cause the clays to break into prismatic or polyhedral blocks 20 to 200 mm in width. The faces are slickensided, which suggests that they may have been initially formed by tension due to drying out, and then modified by shearing due to movement of adjacent blocks.
- **Gently dipping joints:** Slickensided joints with dips ranging from 20° to 60° and extending for several metres. These joints generally occur in two sets striking approximately parallel to one another, but dipping in opposite directions.

- **Fissures:** These are joints of small areal extent, generally less than 0.2 metres, which may have originated during deposition of the clay in large open-structure floccs.

- **Dykes:** These are found only in the Keswick Clay and are numerous where the clay has come in contact with sandy topsoil. They are generally 1 to 5 mm wide and are thought to have formed by the percolation of the sandy topsoil into the vertical joints.

- **Other minor defects:** These include *roots*, ranging up to 10 mm in diameter; tubes; tube-casts; and tunnels and sinkholes.

In addition, Stapledon (1970) stated that some of these joints may have apertures as wide as 5 mm. Further, he suggested that all of these macroscopic and structural defects greatly influence the engineering behaviour and the vertical permeability of the clay masses, though the extent of this influence is extremely difficult to assess quantitatively.

2.3.3.1 Gilgais

The term *gilgai* refers to dome-type undulations of the upper surface of the Keswick Clay and Hindmarsh Clay Formation as shown in Figure 2.6. An abundance of gilgai in the Adelaide city area gives rise to marked lateral variation in soil type for the first few metres below the ground surface.

Stapledon (1970) proposed a scenario for the development of gilgai structures, a summary of which is given below, and a graphical representation is shown in Figure 2.7.

1. Firstly, the Keswick and Hindmarsh Clays were deposited in a flocculated state in a river flood plain.

2. Subsequently, the surface of the clay dried, cracked and became desiccated, largely as a result of uplift. This resulted in the formation of numerous vertical shrinkage cracks and the pseudo-consolidation of the clays, referred to earlier.

3. Wind-blown quartz sand and calcareous silt accumulated on the surface of the clay and penetrated and filled the cracks and open joints to form dykes.

4. Subsequent wetting, which led to the deposition of the red-brown Callabonna Clay, resulted in the swelling of the Keswick and Hindmarsh Clays.

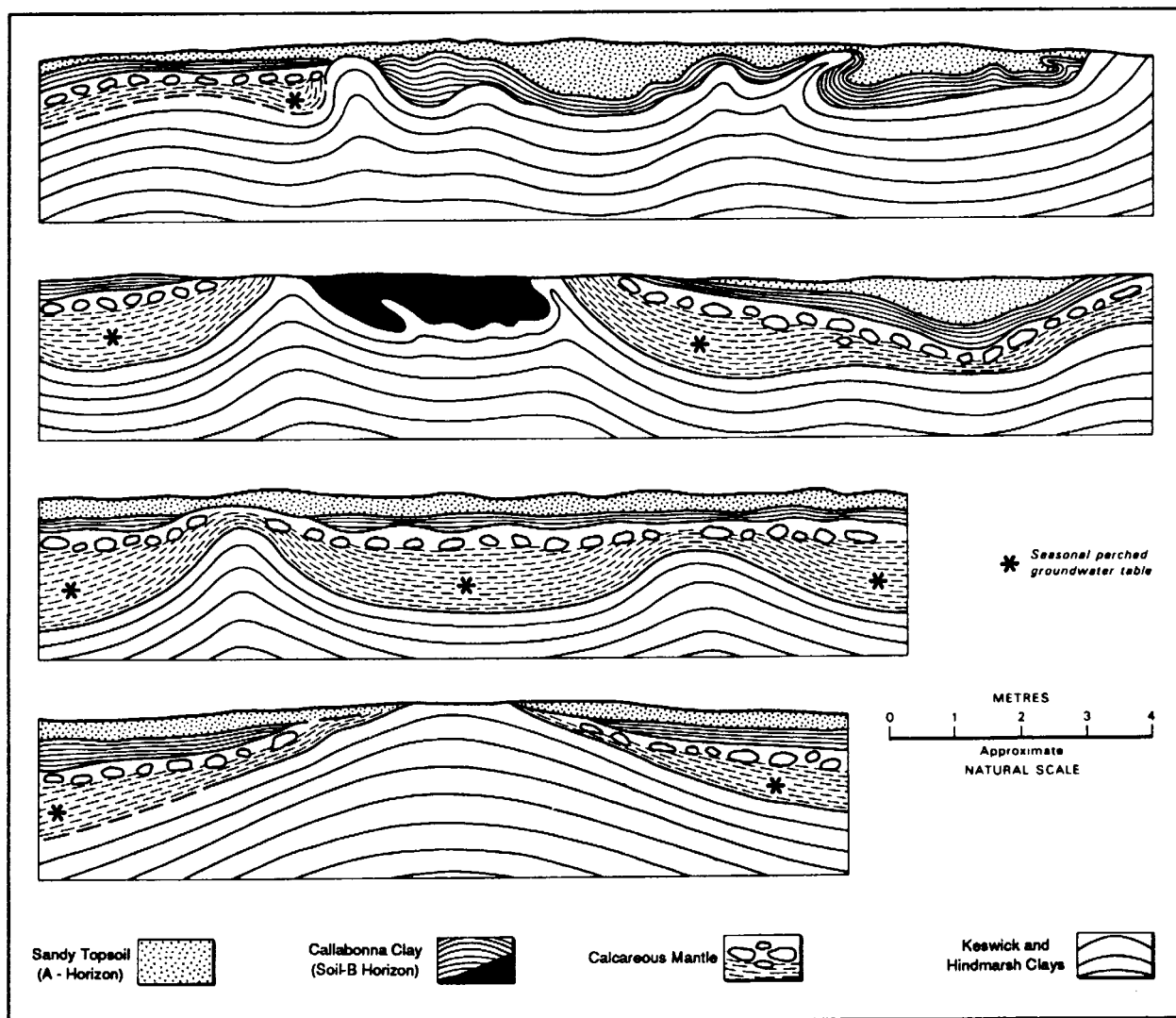


Figure 2.6 Typical gilgai structures within the Adelaide city area.

(After Selby and Lindsay, 1982).

5. The pressures induced by the increased moisture resulted in upward swelling and doming of the clays, as it was largely unconfined in the vertical direction. Horizontally, the clay was confined by the surrounding soil mass and lateral swelling resulted in the formation of the gently dipping joints as a consequence of shear failure.

The gilgai structures appear to be relatively recent in origin as they have displaced soil-profile horizons (Selby and Lindsay, 1982). It appears that most of the gilaigais are inactive, though it is thought that they could be reactivated by a local increase in groundwater flow.

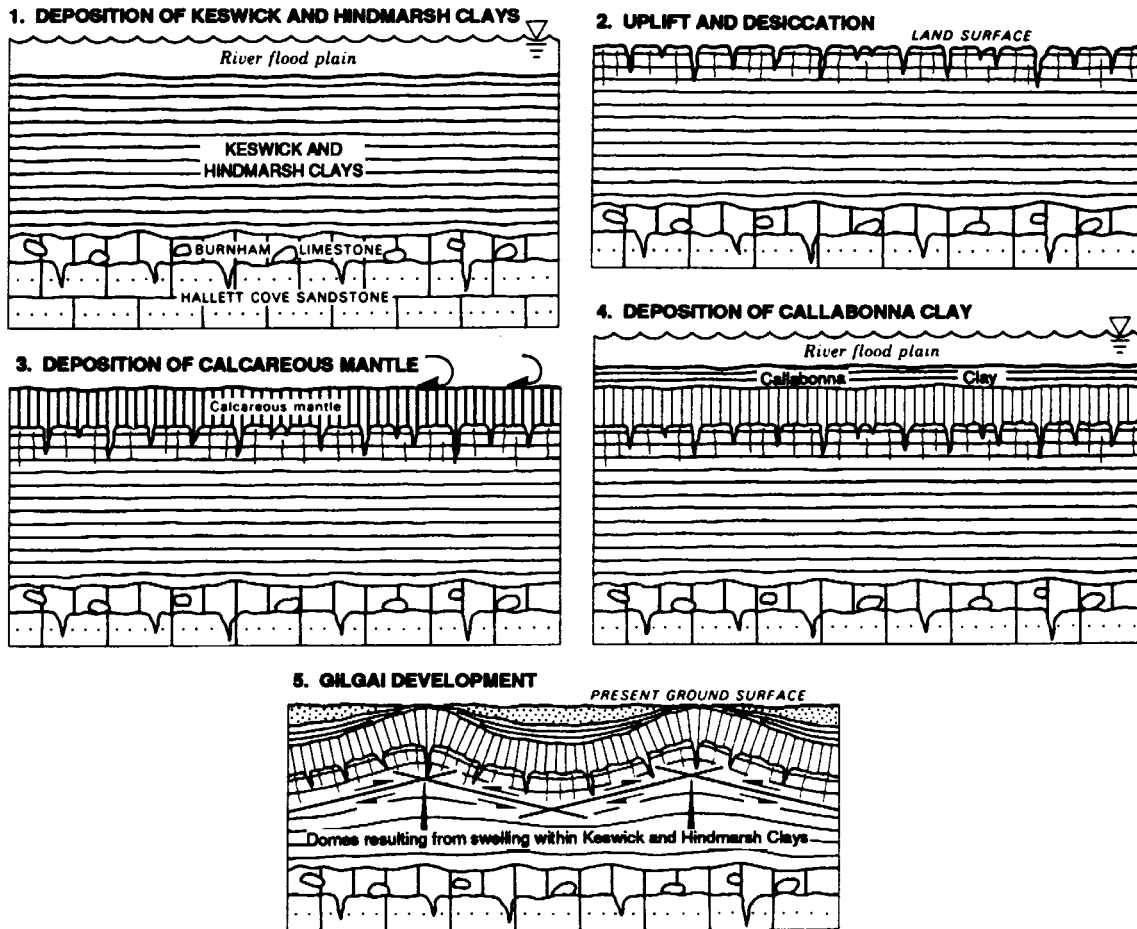


Figure 2.7 Suggested origin of gilgai structures.
(After Stapledon, 1970 and Selby and Lindsay, 1982).

2.3.4 Groundwater

The *general* groundwater table is usually encountered in the Hallett Cove Sandstone and, in addition, perched groundwater tables often occur within the upper three metres of the Keswick Clay (Cox, 1970 referred to this as the *upper perched water table*) and within the sand member of Hindmarsh Clay Formation (the *lower perched water table*). The extent of the upper perched water table varies irregularly over any one site, due mainly to level variations of the boundary between the calcareous mantle and the Keswick Clay, as a result of gilgai. Movement of this groundwater is facilitated by the joints within the clay mass.

Cox (1970) suggested that groundwater within the Adelaide city area originates from the foothills to the east, and Selby and Lindsay (1982) indicated that the Hallett Cove Sandstone has been extensively used as a drainage horizon to take seepage water which collects beneath buildings in the city area.

2.3.5 Summary

This section has examined the geotechnical and structural characteristics of the Keswick and Hindmarsh Clays, as well as the general groundwater regime within the Adelaide city area. It has been shown that these clays are: relatively homogeneous; significantly fissured - both in the macro and micro scales; highly plastic; extremely expansive; and exhibit geotechnical properties similar to those of the well-documented London Clay.

The Keswick and Hindmarsh Clays will form the basis of an experimental investigation to quantify the spatial variability of these soils. This investigation will measure strength parameters of these clays by means of the cone penetration test, which is detailed below.

2.4 THE CONE PENETRATION TEST

This section discusses aspects of the cone penetration test which relate directly to the study of spatial variability. These include: equipment; test procedure; applications and data interpretation; determination of the undrained shear strength; extent of the failure zone; and accuracy of the test itself. As discussed in Chapter 1, the cone penetration test was used in this study to evaluate the small-scale spatial variability of the Keswick and Hindmarsh Clays.

2.4.1 Introduction

The electrical cone penetration test (as distinct from the mechanical cone penetration test, and commonly referred to by the shorter name of *cone penetration test*, CPT) essentially involves pushing a steel cone and rods, of standard dimensions, into the subsurface profile and monitoring the resistance to penetration mobilised in the soil.

Since it was first developed in Holland in 1965, the CPT has continued to gain wide acceptance in many countries throughout the world. De Ruiter (1981) attributed its increased worldwide use to three main factors:

1. The electric cone penetrometer provides more precise measurements, and improvements in the equipment allow deeper penetrations, particularly in dense materials.

2. The need for penetration testing as an in situ technique in offshore foundation investigations, in view of the difficulties in achieving adequate sample quality in marine environments.
3. The addition of other simultaneous measurements to the standard friction penetrometer, such as porewater pressure and soil temperature.

De Ruiter (1981) stated that the CPT is the only available routine technique that provides an accurate continuous profile of soil stratification.

2.4.2 Equipment

The electric cone penetrometer consists, essentially, of two strain gauge load cells; one being attached to the cone tip and measuring cone tip resistance, q_c ; and the other, connected to the side, or sleeve, of the cone penetrometer and measuring sleeve friction, f_s . The cone tip resistance, q_c , is defined as the total force acting on the cone tip, F_c , divided by the area of the base of the cone, A_b , and is usually expressed in units of MPa. The sleeve friction, f_s , is defined as the total force on the friction sleeve, F_s , divided by the surface area of the sleeve, A_s , and is usually expressed in units of kPa. A schematic representation of the electric cone penetrometer is shown in Figure 2.8.

The load cells contain a number of electrical resistance strain gauges which are arranged in such a manner that automatic compensation is made for bending stresses and only axial stress is measured (de Ruiter, 1971). The push rods, used to advance the electric cone penetrometer into the subsurface profile, are usually of a standard length of one metre with a tapered thread, male at the lower end and female at the upper. In addition, the rods have a hollow core so that the cone penetrometer cable can pass through each rod enabling the electronics of the cone to be connected to the recording instruments located at the ground surface.

As will be discussed in greater detail in §3.2, the recording devices generally consist of two types: analogue and digital. These instruments measure q_c and f_s , and in some cases, depth of the cone penetrometer.

The equipment and procedure of the CPT vary throughout the world. Over the years, many committees have been formed in an attempt to establish a consistent, worldwide standard for the CPT; the most recent of these being at the First International Symposium on Penetration Testing (ISOPT-1) (De Beer et al., 1988). In addition, some countries have established individual standards for the CPT, the most relevant of these, for this research,

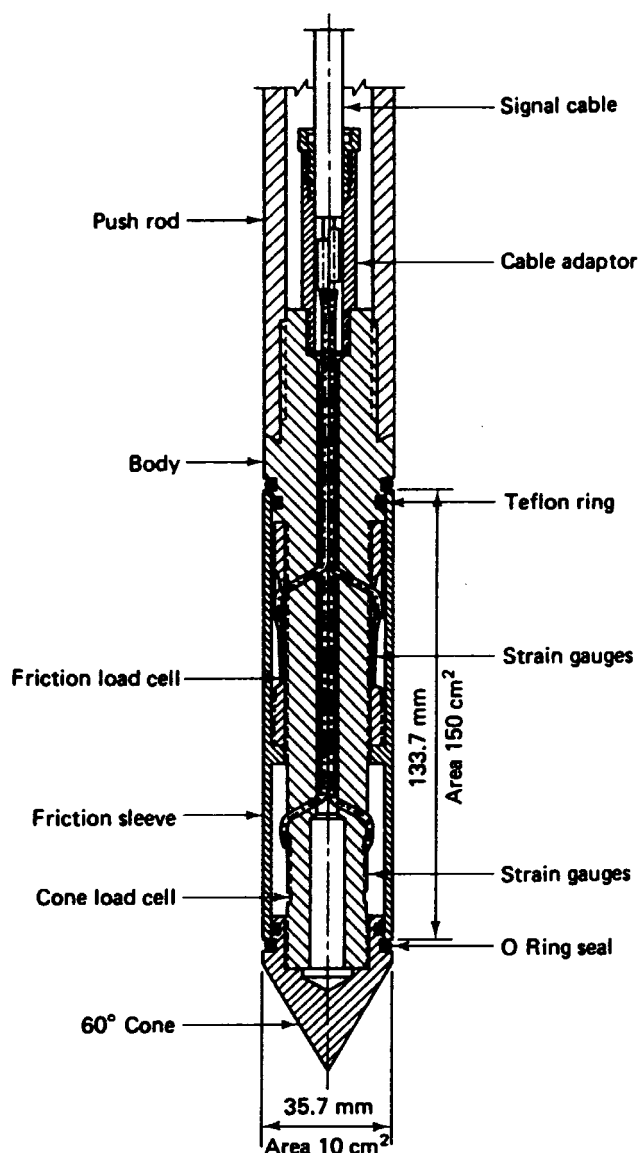


Figure 2.8 Schematic diagram of the electric cone penetrometer.
(After Holtz and Kovacs, 1981).

being the American Standard, *ASTM D3441* (American Society for Testing and Materials, 1986), and the Australian Standard, *AS 1289.F5.1* (Standards Association of Australia, 1977). In general, these three standards agree on the fundamental aspects of the CPT equipment and procedure. Relevant details of the CPT equipment, as specified in these standards, are summarised briefly below and the standard procedure is detailed in §2.4.3.

- The standard cone has a base diameter of 35.7 mm and an apex angle of 60° resulting in a projected area of 1000 mm² (10 cm²). The gap between the cone and other elements of the penetrometer shall not be greater than 5 mm.

- The diameter of the standard friction sleeve is 35.7 mm and has a surface area of 15,000 mm² (150 cm²). The friction sleeve is located immediately above the cone.
- Both the cone and sleeve shall be made from steel of a type and hardness suitable to resist wear due to abrasion by soil. The cone shall have, and maintain with use, a roughness of $\leq 1 \mu\text{m}$, and the friction sleeve shall have a roughness of $0.5 \mu\text{m} \pm 50\%$.
- No standard details for the electrical measuring equipment are given.
- The thrust machine shall have a stroke of at least one metre and shall push the rods into the soil at a constant rate of penetration. The thrust machine shall be anchored and/or ballasted such that it does not move relative to the soil surface during the pushing action.
- Where a *friction reducer*² is used, it shall be located at least one metre above the base of the cone.

2.4.3 Procedure

The standard CPT procedure detailed in ISOPT-1 (De Beer et al., 1988), *ASTM D3441* (American Society for Testing and Materials, 1986), and *AS 1289.F5.1* (Standards Association of Australia, 1977) is summarised as follows:

1. The thrust machine, generally some form of drilling rig, is set up over the test location and is oriented as near to vertical as practicable. The deviation from vertical shall not exceed 2%.
2. The penetrometer and the first length of rod assembly are connected to the thrust machine, the penetrometer being passed through the rod guide at the base of the machine. Prior to connection, the push rods have been pre-threaded with the electrical cable.
3. The cone penetrometer is thrust a short distance into the soil and allowed to remain there until the temperature of the tip has equilibrated with the temperature of the ground, usually between 5 and 10 minutes.
4. The penetrometer is withdrawn from the soil and the cone tip and sleeve friction transducers are zeroed, whilst protecting the cone from direct sunlight.

² narrow local protuberances outside the push rod surface, placed above the penetrometer tip, and provided to reduce the total friction on the push rods.

5. The cone penetrometer is advanced into the subsurface profile at a constant rate of 20 mm/s (± 5 mm/s). Whilst this is occurring, depth, q_c and f_s are recorded. Under no circumstances shall the interval between the readings be greater than 0.2 metres. The depths shall be measured to an accuracy of at least 0.1 metres.
6. Once the thrust mechanism has reached the end of its travel, the rod assembly is disconnected from it, the thrust machine is raised and additional push rods are attached as required.
7. Steps 5 and 6 are continued until the required test depth is reached.
8. On completion of the test, the rod assembly and cone penetrometer are removed from the soil. A final set of readings is taken and compared with the initial readings. If these are not satisfactory, the results are discarded and the penetrometer is either repaired or replaced and the test is repeated.

2.4.4 Applications and Data Interpretation

The CPT is ideally suited for use in fine-grained soils and in sands, both on land and offshore. Due to the probability of cone damage and thrust limitations, the CPT is rarely used in gravels, and weak and weathered rock profiles.

Orchant et al. (1988) suggested that the information obtained from the CPT can be used to interpret the following geotechnical characteristics: soil classification; relative density, RD , of sands; friction angle, ϕ , of sands; undrained shear strength, s_u , of cohesive soils; overconsolidation ratio, OCR ; Young's modulus of elasticity, E ; compressibility of clay; pile bearing capacity; shallow foundation bearing capacity; and liquefaction potential of sands. The *friction ratio*, F_R , is often used in conjunction with q_c to assist in soil classification. The friction ratio is defined as the ratio between f_s and q_c , and is usually expressed as a percentage, as shown in Equation (2.4).

$$F_R = \frac{f_s}{q_c} \times 100\% \quad (2.4)$$

Schmertmann (1978) and *AS 1289.F5.1* (Standards Association of Australia, 1977) emphasised that incorrect calculations of F_R will be made unless a depth correction, or *shift*, is applied to the f_s measurements. This correction is required since the cone tip resistance and sleeve friction load cells are physically separated by a given distance, and hence measurements of q_c do not refer to the same soil as that at which measurements of f_s are taken. Schmertmann (1978) recommended that this *shift distance* be the distance

between the base of the cone and the mid-height of the sleeve which, in standard electric cone penetrometers, is approximately 75 mm. Campanella et al. (1983) suggested that the shift distance, also termed the *friction-bearing offset*, is 100 mm and is dependent on the type of soil being penetrated. The shift distance is examined in detail in §5.3.5.

As mentioned above, CPT data are often used to determine the axial bearing capacity of piled foundations. In fact, the CPT was essentially developed to facilitate the design of driven piles (Orchant et al., 1988). As a consequence, a large number of pile design methods have been developed which are based directly on CPT data. Robertson et al. (1988) compared the results of 6 full-scale pile load tests with the predictions given by 13 separate static axial pile capacity prediction methods, each of which are based on CPT data. Robertson et al. (1988) concluded that, in order of highest to lowest accuracy, the *LCPC Method* (Bustamante and Gianceselli, 1982), the *de Ruiter and Beringen Method* (de Ruiter and Beringen, 1979), and the *Schmertmann and Nottingham Method* (Schmertmann, 1978) yielded the best predictions. Briaud (1988) also compared the predictions of 6 CPT axial pile capacity methods using the results of 98 pile load tests. The 6 CPT pile methods that Briaud examined included: the LCPC Method; the de Ruiter and Beringen Method; and the Schmertmann and Nottingham Method. Briaud (1988) found that, overall, the LCPC Method yielded the best predictions. As a consequence of its performance, the LCPC Method, of Bustamante and Gianceselli (1982), will be used in Chapter 8 to assess the significance of spatial variability on the design of pile foundations. The technique, itself, will be described in detail in §8.3.1.

2.4.5 Determination of the Undrained Shear Strength of a Clay from the CPT

The CPT, and the majority of in situ tests, induce relatively rapid local failures in the soil mass that allow little drainage in the clays. As a result, the cone tip resistance, q_c , is generally related to the undrained shear strength, s_u , by Equation (2.5), which is based on the bearing capacity of a deep, circular foundation (Ladd et al., 1977; Schmertmann, 1978; de Ruiter, 1982; Jamiolkowski et al., 1982; Sutcliffe and Waterton, 1983).

$$s_u = \frac{q_c - \sigma_{v0}}{N_k} \quad (2.5)$$

where:

- q_c is the cone tip resistance;
- σ_{v0} is the total in situ vertical overburden stress;
- N_k is the *cone factor*.

The cone factor, N_k , is an empirically derived parameter usually obtained by cone penetration testing in parallel with reference determinations of s_u . The undrained shear strength, s_u , is normally obtained from triaxial tests performed on high quality specimens, or from in situ vane shear tests - triaxial testing providing better estimates of N_k in most situations (Sutcliffe and Waterton, 1983; Kay and Mayne, 1990). Sutcliffe and Waterton (1983) suggested that the sleeve friction, f_s , of the clay be used as a lower bound for s_u .

Schmertmann (1975) reported that various empirical correlation studies suggest that N_k varies between approximately 5 and 70. Schmertmann suggested that, though many practitioners use Equation (2.5) almost exclusively to evaluate the undrained shear strength of clays, N_k cannot be regarded as a simple constant. He identified a number of factors which cause variation in N_k . These are summarised in Table 2.4.

Table 2.4 Some of the variables which influence N_k . (After Schmertmann, 1975).

Variable	Effect on N_k
Changing the test method for obtaining reference s_u	Better sampling, thinner vanes, use of s_u from pressuremeter test, all decrease N_k
Rigidity index, $I_r = G / s_u$	N_k increases with increasing stiffness
Ratio of increasing/decreasing modulus (E^+ / E^-) at peak s_u	N_k decreases with decreasing ratio
Effective friction, $\tan \phi'$	N_k increases with increasing ϕ'
K_0 or OCR	N_k increases with increasing K_0 or OCR
Shape of penetrometer tip	Reduced diameter above cone can decrease N_k in very sensitive clays
Rate of penetration	Increasing rate increases N_k
Method of penetration	Continuous (electrical tips) penetration decreases N_k compared to incremental (mechanical tips) because of higher pore-water pressures.

An alternative approach to that expressed in Equation (2.5) refers to *cavity expansion theory* as proposed by Bishop et al. (1945). Cavity expansion theory, as adopted by Vesic (1972), assumes that the pressure around the cylindrical surface beneath the cone tip is equal to the limiting stress required during the expansion of a spherical cavity.

Recent studies by Baligh (1975), Keaveny and Mitchell (1986), and Houlsby and Teh (1988), have indicated that N_k may be related to a number of other factors, including: the rigidity index, I_r ; the initial shear stress ratio, f ; and the cone roughness factors, α_f and α_s .

Baligh (1975), and Houlsby and Teh (1988), suggested that Equation (2.5) should strictly be written in terms of the in situ horizontal stress, σ_{h0} , instead of the vertical stress, σ_{v0} . As a result, Equation (2.5) can be rearranged in the following manner:

$$\begin{aligned}
 N_k &= \frac{q_c - \sigma_{v0}}{s_u} = \frac{q_c - \sigma_{v0}}{s_u} - \left(\frac{\sigma_{h0}}{s_u} - \frac{\sigma_{h0}}{s_u} \right) \\
 &= \frac{q_c - \sigma_{h0}}{s_u} - 2 \left(\frac{\sigma_{v0} - \sigma_{h0}}{2s_u} \right) \\
 N_k &= \frac{q_c - \sigma_{h0}}{s_u} - 2f \tag{2.6}
 \end{aligned}$$

where: $f = \frac{\sigma_{v0} - \sigma_{h0}}{2s_u} = \frac{1 - K_0}{2s_u / \sigma_{v0}}$

The parameter, f , is defined as the initial shear stress ratio and was originally proposed by Davis and Poulos (1968) and more recently by Ladd et al. (1977). Theoretically, f can vary between -1 (which represents passive failure in swelling soils under total stress conditions) and $+1$ (which represents conditions at the maximum depth of a shrinkage crack in terms of total stresses) (Kay and Mayne, 1990).

As suggested by Kay and Mayne (1990), it is convenient to use f to compare the various proposals for the determination of N_k . Baligh (1975) proposed that N_k be calculated based on a strain path approach, as follows:

$$N_k = 12 + \ln(I_r) - 2f \tag{2.7}$$

Keaveny and Mitchell (1986) used spherical cavity expansion theory and suggested that N_k be determined using the mean stress, p , instead of σ_{v0} . Kay and Mayne (1990) rewrote Keaveny and Mitchell's equation as:

$$N_k = 3.42 + 1.33(\ln(I_r) - f) \tag{2.8}$$

Baligh (1986) pointed out that an inconsistency in the application of the cavity expansion theory to cone penetration problems is that it does not correctly model the strain paths followed by soil elements. Teh and Houlsby (1991) presented the results of a strain path approach to the steady penetration of a cone in homogeneous soil. This involved changing the frame of reference and treating the penetration process as a steady flow of soil past a stationary penetrometer. As an initial estimate of the flow field, the soil was treated as a viscous fluid. The authors found that the cone factor, N_k , was significantly influenced by the rigidity index, I_r , of the soil and the in situ stress conditions, f , and, to a lesser extent,

by the roughness of the cone and shaft, α_f and α_s ³. In addition, Teh and Houlsby (1991) concluded that the in situ horizontal stresses have a greater influence on N_k than the vertical stress. Using a strain path approach, and assuming initial isotropic soil stresses and a simple, linear, elastic, perfectly-plastic model with a von Mises yield surface, Teh and Houlsby (1991) concluded that N_k can be determined using:

$$N_k = 1.25 + 1.84 \ln(I_r) + 2\alpha_f - 2f \quad (2.9)$$

However, since the stresses derived using the strain path method do not fully satisfy the equilibrium condition, because of errors in the assumed initial displacement field, Teh and Houlsby (1991) carried out a strain path finite element analysis. The authors found that N_k can be determined using Equation (2.10).

$$N_k = \frac{4}{3} [1 + \ln(I_r)] \left[1.25 + \frac{I_r}{2000} \right] + 2.4\alpha_f - 0.2\alpha_s - 1.8f \quad (2.10)$$

where: $50 \leq I_r \leq 500$

The authors stated that, although Equation (2.10) results in higher cone factors than have previously been derived theoretically, the cone factors are closer to those observed in practice and therefore provide a more reasonable solution to the cone penetration problem.

Kay and Mayne (1990) applied Equations (2.5) and (2.10) to CPT and screw plate load test data obtained from a number of site investigations performed in Adelaide (Mitchell and Kay, 1985). Using $f = -0.4$ and $\alpha_f = \alpha_s = 0.8$, values judged to be appropriate for the highly overconsolidated fissured plastic clays and the very stiff silty and sandy clays that constituted the soils tested, Kay and Mayne (1990) found that values of N_k obtained from Equation (2.10) yielded good predictions of undrained shear strength, s_u , when compared to measured values.

The relative importance of the expressions given in Equations (2.5) and (2.7) to (2.10) will be discussed in detail in Chapter 4.

³ both α_f and α_s lie within the range 0 and 1, where $\alpha_f = \frac{\sqrt{3} \tau_f}{2 s_u}$; $\alpha_s = \frac{\sqrt{3} \tau_s}{2 s_u}$; and τ_f and τ_s are the shear stresses on the cone and sleeve respectively.

2.4.6 Extent of the Failure Zone Due to Cone Penetration

As it is advanced into the subsurface profile, the cone penetrometer causes a zone of soil to fail and deform plastically. Teh and Houlsby (1991), using a strain path approach as discussed in the previous section, quantified the extent of this failure zone by the use of two parameters: r_p - the radial distance of the plastic boundary from the axis of penetration measured at a large enough distance above the cone tip; and z_p - the distance between the cone tip and the plastic boundary measured along the axis of the penetrometer. The parameters r_p and z_p , as well as the two possible states of the elasto-plastic boundary as defined by Teh and Houlsby (1991), are shown diagrammatically in Figure 2.9.

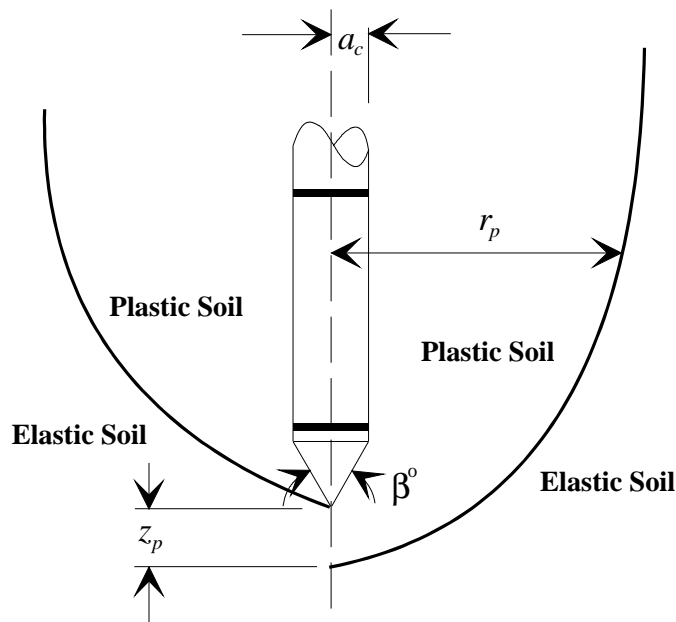


Figure 2.9 Schematic representation of r_p and z_p .
(Adapted from Teh and Houlsby, 1991).

Figure 2.10 illustrates the variation of the parameters r_p and z_p with the rigidity index, I_r . Teh and Houlsby (1991) found close agreement with cylindrical and spherical cavity expansion solutions, as shown in Figure 2.10. For a standard cone with $\beta = 60^\circ$, $a_c = 35.7/2 = 17.9$ mm, and a rigidity index typical for the Keswick and Hindmarsh Clays, that is, $I_r = 100$, Figure 2.10 suggests that $r_p \approx 150$ mm and $z_p \approx 90$ mm. These values compare well to those obtained by Baligh (1986), who, using a spherical cavity expansion model and a Prandtl-Reuss bilinear clay, found that $r_p \approx 180$ mm and $z_p \approx 110$ mm.

These dimensions imply that the measurements of q_c and f_s , obtained by the CPT, are not

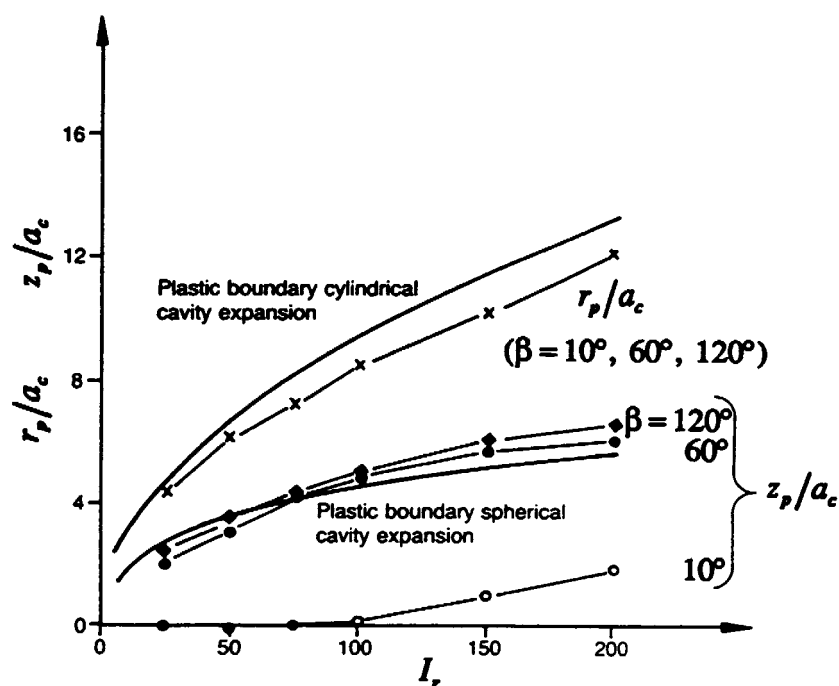


Figure 2.10 Location of the elasto-plastic boundary in cone penetration.
(After Teh and Houlsby, 1991).

point values, but rather *block* values; that is, measurements based on the failure of a volume of soil surrounding both the cone and sleeve. The implications of this will be treated in Chapter 5.

2.4.7 Accuracy of the CPT

Errors associated with measurement can be separated into two categories: *systematic errors* and *random errors* (Lee, White and Ingles, 1983; Baecher, 1986; Orchant et al., 1988; Kay, 1990).

Systematic errors, or bias, are the consistent underestimation or overestimation of a measured parameter. Orchant et al. (1988) separated systematic errors into: *equipment errors* - inaccuracies associated with such effects as drift, non-linearities, zero error of the elements of the measuring instrument; and *operator/procedural errors* - variabilities associated with limitations in existing test standards and between different operators.

Random errors, or scatter, are the variation of test results which cannot be directly attributed to the inherent variability of the material (spatial variability), equipment errors or operator/procedural errors. Random errors are quantified by performing many tests under

identical conditions, and are assumed to have a mean of zero, thus affecting test results equally, and without bias.

Orchant et al. (1988) suggested that the total measurement error can be evaluated by the following model:

$$\sigma_{measure}^2 = \sigma_{equip}^2 + \sigma_{op/proc}^2 + \sigma_{random}^2 \quad (2.11)$$

where: $\sigma_{measure}^2$ = total variance of measurement;
 σ_{equip}^2 = variance of equipment effects;
 $\sigma_{op/proc}^2$ = variance of operator / procedural effects;
 σ_{random}^2 = variance of random testing effects.

Equation (2.11) has two important assumptions: (i) all of the sources of uncertainty can be considered as additive; and (ii) each source of measurement error is considered to be independent, or uncorrelated. In order to simplify the model, Orchant et al. (1988) adopted the second assumption. Otherwise if the sources of error are correlated, covariance terms, expressing the inter-relationship between the parameters, would need to be included and evaluated, thereby complicating the model considerably.

Each of these sources of measurement error are discussed in the following sections.

2.4.7.1 Equipment Errors of the CPT

Orchant et al. (1988) attributed CPT equipment errors to a number of variables. These are summarised in Table 2.5.

Table 2.5 Variables contributing to CPT equipment error.
(After Orchant et al., 1988).

Variable	Relative Effect on CPT Results
Cone Size	Minor
Cone Angle	Moderate to Significant
Manufacturing Defects	Minor to Moderate
Leaky Seals	Minor
Excessive Cone Wear	Minor to Moderate

Durgunoglu and Mitchell (1975) found that the angle of the cone tip has an important effect on CPT results, and that an angle of 60° favours maximum penetration for a given force on the penetrometer. Baligh et al. (1979) also supported this conclusion, having tested cones with angles of 18° , 30° and 60° . The authors found that by using an 18° cone, measurements of q_c and f_s were increased by as much as 30% of those obtained by using the standard 60° cone.

De Ruiter (1981) detailed the use of enlarged cones for special soil conditions. Results obtained from a cone with a 2000 mm^2 base area, used in soft soils, and a 1500 mm^2 cone, used in gravelly and hard deposits, indicated that cone size does not greatly affect measurements of q_c and f_s when compared to the standard cone of 1000 mm^2 base area.

De Ruiter (1982) suggested that minor equipment errors can occur as the result of manufacturing defects which can allow soil to become wedged between the cone and the friction sleeve, yielding inaccurate measurements of f_s . In addition, the author indicated that faulty or leaking seals can lead to corrosion of the electrical components resulting in erroneous measurements; and excessive wear, as a consequence of the penetration of hard and gravelly deposits, can affect test results.

The equipment errors discussed above, can be minimised by regularly maintaining and inspecting the penetrometer, whereas consistent measurements of q_c and f_s can be obtained by the use of a cone penetrometer of standard dimensions, that is, 60° angle and 1000 mm^2 base area.

From an extensive examination of published data, Orchant et al. (1988) concluded that the coefficient of variation, CV , (defined as the ratio of the standard deviation, σ , to the mean, m , usually expressed as a percentage) of CPT results that are attributed to equipment effects is approximately 3%.

2.4.7.2 Operator/Procedural Errors of the CPT

Orchant et al. (1988) identified three variables which can lead to operator/procedural errors of the CPT as shown in Table 2.6.

Schaap and Zuidberg (1982) indicated that the CPT is practically operator-independent provided that prescribed calibration procedures are adequately followed before, during and after the test. Tests performed by Schaap and Zuidberg showed that typical calibration errors are less than 0.4% of the full scale output of the load cell.

Table 2.6 Variables contributing to operator/procedural errors.
(After Orchant et al., 1988).

Variable	Relative Effect on CPT Results
Calibration Error	Minor to Moderate
Rate of Penetration	Minor
Inclined Penetration	Minor to Moderate

Since the CPT provides for the continuous and automatic acquisition of data, the primary procedural variable is the rate of penetration. *ASTM D3441* (American Society for Testing and Materials, 1986), *AS 1289.F5.1* (Standards Association of Australia, 1977) and *ISOPT-1* (De Beer et al., 1988) specified that the rate of penetration shall be constant and between $10 - 20 \text{ mm/s} \pm 25\%$. De Ruiter (1981) showed that q_c tends to increase with higher rates of penetration, however, he concluded that this influence is insignificant for speeds between 10 and 20 mm/s.

Another effect associated with the CPT procedure is drift of the cone tip, or in other words, the deviation from the vertical alignment of the cone tip with depth. This can lead to substantial errors in the evaluation of test results by misinterpreting the depth of the CPT measurements. However, *AS 1289.F5.1* (Standards Association of Australia, 1977) suggests that cone tip drift can occur when testing is carried out at depths greater than 10 to 15 metres. De Ruiter (1981) recommended the use of a slope sensor where penetration exceeds 25 metres and if the site contains gravel or cobbles.

Orchant et al. (1988) concluded that the *CV* associated with operator/procedural effects is less than, or equal to, 5%.

2.4.7.3 Random Errors of the CPT

As discussed above, random errors can be quantified by carrying out a number of tests under identical conditions. Orchant et al. (1988), after examining a number of laboratory calibration studies, found that the variability associated with random errors is approximately 5% for q_c measurements and 10% for f_s measurements.

2.4.7.4 Total Measurement Errors of the CPT

Using the model expressed in Equation (2.11), Orchant et al. (1988) estimated total measurement errors of the CPT of 7% and 12% for q_c and f_s results, respectively. The authors stated that these results were confirmed by several statistical analyses of CPT data in homogeneous clays. In conclusion, Orchant et al. (1988) suggested that, because of the limited data available and the judgement involved in estimating coefficients of variation, the total measurement errors of the CPT are in the range of 5% to 15%. However, Orchant et al. (1988) emphasised that in order to maintain these low values of measurement error it is vital that experienced personnel perform the tests and that the equipment be kept in good working order and regularly calibrated.

2.4.8 Summary

In this section it has been shown that the CPT is a reliable and accurate test procedure with the lowest coefficient of variation of in situ test methods in current use. Furthermore, the CPT has the facility for enabling closely-spaced, geotechnical data to be acquired by computer, reliably and efficiently. Chapter 3 will detail the design and calibration of a micro-computer based data acquisition system developed to record and store these data. The CPT will be used in an extensive field study to investigate and quantify the small-scale spatial variability of the Keswick Clay. This field study is detailed in Chapter 4, and the techniques used to quantify the spatial variability of soils are treated in the next section.

2.5 SPATIAL VARIABILITY OF SOILS

Geotechnical materials and their properties are inherently variable from one location to another. This is due mainly to the complex and varied processes and effects which influence their formation, and include: sedimentation; parent material; weathering and erosion; climate; topography; organisms; structural defects, such as faults, folds, joints, fractures, slickensides and fissures; layering; stress history; suction; and time.

Prior to examining the historical progress of the study of spatial variability in the field of geotechnical engineering, it is necessary, by way of background, to treat the various mathematical techniques used in this area of research.

2.5.1 Mathematical Techniques Used to Model Spatial Variability

Ideally, it would be desirable to assign a tractable deterministic function, say $Y(x)$, to describe the spatial variability of the geotechnical properties of soils and rock. However, this is rarely possible because the variability is often extremely erratic, and hence complex, with many discontinuities and anisotropies. As a result, spatial variability research has focused on a limited number of statistical techniques to quantify, model and estimate the spatial variation of geotechnical materials. These include: *regression*, *random field theory* and *geostatistics*. Regression analyses are based on *classical statistics* which makes use of random variables, with the underlying assumption that all sample values within a soil deposit have equal likelihood of being represented and are independent of one another. Random field theory and geostatistics, on the other hand, make use of *spatial statistics*; that is, the location of the sample is also given consideration. A brief examination of the three statistical techniques of regression, random field theory and geostatistics follows.

2.5.1.1 Regression Analysis

Classical statistics and regression analyses can be applied to many situations in geotechnical engineering and the earth sciences which involve the analysis of bivariate and multivariate data. It is common, when comparing two distributions, to display these in the form of a *scatterplot*. This is an x - y graph on which the x -coordinate corresponds to the value of one variable, and the y -coordinate corresponds to the value of the other variable. The scatterplot represents the correlation, that is the degree of dependence, between the two variables. The correlation is quantified using the *covariance* and the *correlation coefficient*.

The covariance, C_{XY} , between two sets of data $X = X_1, X_2, X_3, \dots, X_n$ and $Y = Y_1, Y_2, Y_3, \dots, Y_n$ is defined as:

$$C_{XY} = \frac{1}{n-1} \sum_{i=1}^n (X_i - \bar{X})(Y_i - \bar{Y}) = \frac{1}{n-1} \left(\sum_{i=1}^n X_i Y_i - \frac{\sum_{i=1}^n X_i \sum_{i=1}^n Y_i}{n} \right) \quad (2.12)$$

where: \bar{X} is the mean of the data $X = X_1, X_2, X_3, \dots, X_n = \frac{\sum_{i=1}^n X_i}{n}$;
 \bar{Y} is the mean of the data $Y = Y_1, Y_2, Y_3, \dots, Y_n$;
 n is the number of data.

The correlation coefficient, r , is defined as:

$$r = \frac{C_{XY}}{\sigma_X \sigma_Y} \quad (2.13)$$

where: σ_X is the standard deviation of the data $X = X_1, X_2, X_3, \dots, X_n = \sqrt{\frac{\sum_{i=1}^n (X_i - \bar{X})^2}{n-1}}$;
 σ_Y is the standard deviation of the data $Y = Y_1, Y_2, Y_3, \dots, Y_n$.

When:

- $r = +1$ the data fit a straight line of positive slope, perfectly;
- $r = 0$ the data exhibit no correlation;
- $r = -1$ the data fit a straight line of negative slope, perfectly.

As a consequence, as $|r|$ approaches 1, the data fit more closely to a straight line. Smith (1986) suggested that for values of $|r|$ between 0 and 1 the following rough guide may be used:

- $|r| \geq 0.8$ strong correlation exists between X and Y , which can be assumed to be completely dependent;
- $0.2 < |r| < 0.8$ correlation exists between X and Y ;
- $|r| \leq 0.2$ weak correlation exists between X and Y , which can be assumed to be independent of each other.

As mentioned previously, the correlation coefficient is a measure of how well the data fits a straight line. This straight line has the form:

$$Y = a + bX \quad (2.14)$$

The y -intercept, a , and the slope, b , can be determined by using relationships found in any standard statistical text. The parameter r^2 is often defined as the *coefficient of determination*, and is commonly determined by means of the expression shown in Equation (2.15). The correlation coefficient, given by Equation (2.13), is simply the square root of r^2 , its sign being the same as b , the slope of the line.

$$r^2 = \frac{a \sum Y + b \sum XY - n\bar{Y}^2}{\sum Y^2 - n\bar{Y}^2} \quad (2.15)$$

This *line of best fit, ordinary least squares straight line, or linear regression line*, by which

names it is known, is achieved by minimising the sum of the squared deviations. That is:

$$\sum_{i=1}^n [Y_i - (a + bX_i)]^2 = \text{minimum} \quad (2.16)$$

In addition, the least squares straight line has the property that the sum of the deviations is equal to zero, that is:

$$\sum_{i=1}^n [Y_i - (a + bX_i)] = 0 \quad (2.17)$$

Other techniques are available for evaluating regression lines other than the *method of ordinary least squares* (OLS) described above. These include: *averages*; *least normal squares* (LNS); and *reduced major axis* (RMA)⁴. The regression lines obtained by each method are shown in Figure 2.11, together with the line given by the method of OLS. In addition, another ordinary least squares line is shown (OLS - D on Q) where the X variable has been made the regressed variable, instead of the usual case of Y. While these other techniques are available, the method of OLS is the most commonly used throughout geotechnical engineering and the earth sciences, since it is the best method to use when one is seeking to predict Y from X (Troutman and Williams, 1987). As a consequence, for the remainder of this thesis, *regression analysis* will refer to the method of ordinary least squares where the Y variable is the regressed variable.

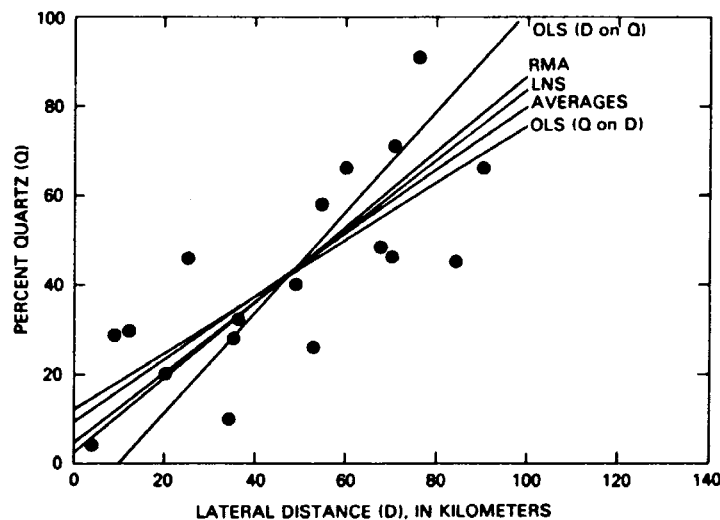


Figure 2.11 Hypothetical sedimentary rock data showing straight lines fitted by different methods.

(After Troutman and Williams, 1987).

⁴ an extensive treatment of each of these alternative techniques is given in Troutman and Williams (1987).

In addition, regression analysis enables non-linear functions, such as quadratic, cubic and logarithmic functions, to be fitted to the data. It should be noted that the largest power in the system of equations used to determine the regression line is always twice the degree of the curve being fitted. Davis (1986) suggested that this can be a major source of error in computer programs which fit high-order polynomials to the data. This can result in rounding-off errors leading to unstable or unreliable solutions to the set of simultaneous equations. As a consequence, regression analyses performed in the following chapters will be limited to fitting polynomials of order no greater than 6. Furthermore, Lumb (1974) stated that, in routine site investigations, there are rarely sufficient data to estimate any form more complicated than a linear trend.

Mann (1987) stated that, theoretically, the linear regression model is valid only when the following assumptions are true:

1. X and Y are measured without error;
2. X and Y are normally distributed, independent variables;
3. A linear relationship exists between X and Y ;
4. X values are linearly independent;
5. Errors of prediction are normally distributed with a mean of zero and a constant variance (*homoscedastic*);
6. Errors of prediction are serially independent (not *autocorrelated* - Discussed briefly below, and in detail in §2.5.1.2(iii)).

In geotechnical engineering and the earth sciences, whilst many of these assumptions may be valid, the first and, more importantly, the sixth assumptions are not. Matheron (1963) demonstrated that concepts of classical statistics, such as regression analyses, are insufficient because geotechnical materials are not serially independent. In fact, they are autocorrelated; that is, neighbouring samples indicate stronger correlation than distant samples which exhibit weak correlation (Matheron, 1963; Journel and Huijbregts, 1978; Tabba and Yong, 1981; Li and White, 1987a; Jaksa et al., 1993). This is partly explained by the randomness of the process governing the formation of the microscopic structural units within the soil mass (Yong, 1984). Rendu (1981) stated that since properties of geotechnical materials are rarely distributed randomly throughout a soil or rock mass, the use of classical statistics techniques such as regression should be limited to preliminary stages of exploration, or when the number of samples available is relatively small and the distances between samples are large.

2.5.1.2 Random Field Theory

Random field theory, as it is known in geotechnical engineering (Vanmarcke, 1977b, 1983), is an n -dimensional extension of classical *time series analysis*. A time series is a chronological sequence of observations of a particular variable usually, but not necessarily, at constant time intervals, and which may be thought of as a one-dimensional random field. A geotechnical example of a time series is the measurement of q_c with depth as obtained from the CPT. Unlike classical statistics, time series analysis incorporates the observed behaviour that values at adjacent time steps are more related, that is *autocorrelated*, than those at large time steps. When applied to the spatial variability of geotechnical materials, the time domain is replaced by the distance domain and the data set is referred to as a *random field*. Hence, for the remainder of this thesis, time series analysis and random field theory will be used interchangeably to refer to the same theoretical framework.

(i) Stationarity

The application of random field theory is greatly simplified if the data are *stationary*; that is, the probabilistic laws which govern the series must be independent of the location of the samples. Data are said to be stationary, in a *strict sense*, if (Brockwell and Davis, 1987):

- the mean, m , is constant with distance, that is, no trend or *drift* exists in the data;
- the variance, σ^2 , is constant with distance, that is, homoscedastic;
- there are no seasonal variations;
- there are no irregular fluctuations.

In practice it is usual to define stationarity in terms of *second-order*, or *weak*, stationarity. A data set is said to satisfy second-order stationarity if its mean is constant, and its autocovariance function depends only on the *lag*, that is, the distance between two random variables in a random field (Chatfield, 1975; Brockwell and Davis, 1987). These aspects are defined, and treated in some detail in §2.5.1.2(iii).

An example of a non-stationary data set, that is, measurements of q_c from a CPT, is shown in Figure 2.12. As can be seen from this figure, the level, indicated by a quadratic trend, and the variance, are both a function of depth.

An important implication of the assumption of stationarity is that the statistical properties

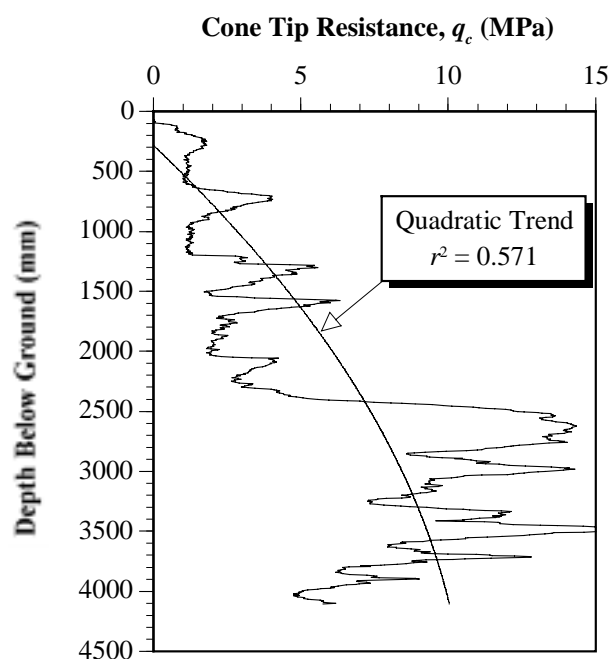


Figure 2.12 An example of a non-stationary data set.

of the time series are unaffected by a shift of the spatial origin. For example, the statistical relationships between n samples at origin i , say $X_i, X_{i+1}, \dots, X_{i+n-1}$, are the same as the statistical relationships between n samples at origin $i+j$, say $X_{i+j}, X_{i+j+1}, \dots, X_{i+j+n-1}$ (Brockwell and Davis, 1987). A stationary process is therefore invariant under spatial translation (Bennett, 1979).

Bennett (1979) suggested that non-stationarity falls into three separate forms, namely: trend; variance; and relationship; each of which are shown in Figure 2.13. Non-stationarity of trend describes the phenomenon that a random field is subject to a trend which may be either deterministic or stochastic; whereas non-stationarity of variance describes the pattern by which the variance is subject to change as a function of distance. On the other hand, non-stationarity of relationship occurs when the process which controls the random field itself, is a function of distance.

Vanmarcke (1983) stated that stationarity is the one-dimensional equivalent of two- and three-dimensional homogeneity and, in particular, he referred to *statistical homogeneity*. However, as the application of both random field theory and geostatistics are facilitated by stationary data, treatment must first be given to *data transformation*, that is, the process by which a non-stationary data set is transformed to a stationary one.

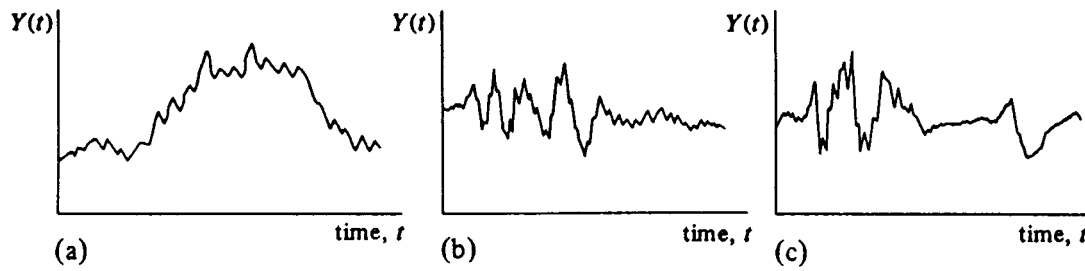


Figure 2.13 Forms of non-stationarity: (a) trend non-stationarity, (b) variance non-stationarity, (c) relationship non-stationarity. (After Bennett, 1979).

(ii) Data Transformation

In the analysis of any random field, or time series, the first step is to plot the data and to identify any apparent discontinuities that may exist in the series. If there are any, it is advisable to first separate the series into a number of statistically homogeneous segments, and then to carry out the analyses on these segments (Brockwell and Davis, 1987). Secondly, it is desirable to transform the data so that they are stationary. Two techniques are commonly used to transform non-stationary data which exhibit a trend: *classical decomposition* and *differencing*. In addition, *variance transformation* is used for data which exhibit a non-stationary variance. These are treated, in turn, below.

(a) Classical Decomposition

Classical decomposition assumes that a random field, X_t , is made up of a number of additive components (Brockwell and Davis, 1987):

$$X_t = t_t + \varepsilon_t \quad (2.18)$$

where: t_t is a slowly changing function termed the *trend component*;
 ε_t is a *random, or white noise component*.

In general, time series analysis also considers an additional component, s_t , which is due to *seasonal effects*. However, since the majority of geotechnical engineering data do not contain a seasonal component (Lumb, 1974), including the data examined in the present study, no further discussion of seasonality will be given. Such treatment, however, can be

found in a large number of time series analysis texts, such as Box and Jenkins (1970), Anderson (1976), Cryer (1986), and Brockwell and Davis (1987).

The aim of classical decomposition is to estimate and remove the deterministic component, t_t , in the hope that the residual random component, ε_t , will be stationary. This trend component can be removed in a number of ways. In the geotechnical engineering literature the technique of OLS regression tends to be the most widely used method for trend estimation (Lumb, 1974; Alonso and Krizek, 1975; Lumb, 1975; Baecher, 1979; Kulatilake and Southworth, 1987; Spry et al., 1988; Ravi, 1992), with polynomial trends of up to order 4 being reported. Other techniques, such as smoothing by means of: *a moving average*, *spline fitting* and *exponential smoothing*, have been suggested in various time series analysis texts (Brockwell and Davis, 1987); however, these have not found use in the geotechnical engineering community, probably because of the suitability of the OLS method.

(b) *Differencing*

An alternative technique which is used extensively in time series analysis, though has found limited use in geotechnical engineering, is that of *differencing* (Chatfield, 1975; Bowerman and O'Connell, 1979; Brockwell and Davis, 1987). If the time series, or random field, does not contain seasonal variation, stationarity can frequently be attained by taking the *first-difference*, ∇X_t , of the original data, X_t , where:

$$\nabla X_t = X_t - X_{t-1} = (1 - B)X_t \quad (2.19)$$

where, B , is the *backshift operator* given by:

$$BX_t = X_{t-1} \quad (2.20)$$

In fact, any polynomial trend of degree, k , can be removed by applying the ∇^k difference operator. That is, by starting with a model, $X_t = t_t + \varepsilon_t$, where $t_t = \sum_{j=0}^k a_j t^j$, and ε_t is stationary with zero mean, then:

$$\nabla^k X_t = k! a_k + \nabla^k X_t \quad (2.21)$$

is a stationary process with a mean of a_k . While differencing to any order, k , can be performed, first-, or second-order differencing is usually sufficient (Brockwell and Davis, 1987). In fact, Cryer (1986) recommended that care be taken to avoid *over-differencing*, which tends to introduce unnecessary correlations and complicate relatively simple models.

(c) Variance Transformation

As detailed in §2.5.1.2(i), the condition of stationarity is violated if the variance of the data is *heteroscedastic*, that is, it varies with distance. A random field, X_t , with a non-constant variance can often be transformed into a stationary data set, W_t , by means of either:

1. *Logarithmic transformation* by using:

$$W_t = \ln(X_t) \quad (2.22)$$

2. The *Box-Cox transformation* by using:

$$f(x) = \begin{cases} \frac{x^\lambda - 1}{\lambda}, & \lambda \neq 0, \\ \log(X_t), & \lambda = 0. \end{cases} \quad (2.23)$$

Often the variance can be stabilised by choosing $\lambda = 0$ (Brockwell and Davis, 1991).

A number of tools are available, firstly, to ascertain whether the data are stationary, and secondly, to enable the data to be modelled. These tools, namely the *autocovariance*, *autocorrelation function*, *partial autocorrelation function*, and *cross-correlation function* are treated below.

(iii) Autocovariance and the Autocorrelation Function

Two essential statistical properties used in time series analysis are the *autocovariance*, c_k , and the *autocorrelation coefficient*, ρ_k , at lag, k , which are defined as:

$$c_k = \text{Cov}(X_i, X_{i+k}) = E[(X_i - \bar{X})(X_{i+k} - \bar{X})] = E[X_i X_{i+k}] - \bar{X}^2 \quad (2.24)$$

and

$$\rho_k = \frac{c_k}{c_0} \quad (2.25)$$

where:

c_0	is the autocovariance at lag 0;
c_k	$= c_{-k}$;
ρ_k	$= \rho_{-k}$.

The autocorrelation coefficient, ρ_k , measures the correlation between any two random field observations separated by a lag of k units (Bowerman and O'Connell, 1979).

It is not possible to know c_k nor ρ_k with any certainty, but only to estimate them from samples obtained from a population, say X_1, X_2, \dots, X_n . As a result, the *sample autocovariance*, c_k^* , and the *sample autocorrelation coefficient*, at lag k , r_k , are defined, respectively, as:

$$c_k^* = \frac{1}{n} \sum_{i=1}^{n-k} (X_i - \bar{X})(X_{i+k} - \bar{X}) \quad (2.26)$$

and

$$r_k = \frac{c_k^*}{c_0^*} = \frac{\sum_{i=1}^{n-k} (X_i - \bar{X})(X_{i+k} - \bar{X})}{\sum_{i=1}^n (X_i - \bar{X})^2} \quad (2.27)$$

where: \bar{X} is the average of the observations X_1, X_2, \dots, X_n ;
 $0 \leq k < n$.

The *sample autocovariance function* (ACVF), or *autocovariogram*, is the plot, or graph, of c_k^* , for lags $k = 0, 1, 2, \dots$. The *sample autocorrelation function* (ACF), or *correlogram*, is the graph of r_k for lags $k = 0, 1, 2, \dots, K$; where K is the maximum number of lags that r_k should not be calculated beyond. While the sample autocorrelation function can be evaluated for all lags up to $n - 1$, it is not advisable since, as k tends toward n , the number of pairs reduces and, as a consequence, the reliability of the estimate r_k of the true autocorrelation function, ρ_k , also decreases. Various authors have suggested the following values for K :

- $K = \frac{n}{4}$ (Box and Jenkins, 1970; Chatfield, 1975; Anderson, 1976; Pankratz, 1983; Davis, 1986);
- $K = 12$ for non-seasonal time series (Bowerman and O'Connell, 1979);
- $K = \sqrt{n} + 10$ (Cryer, 1986);
- $20 \leq K \leq 40$ (Brockwell and Davis, 1987; Hyndman, 1990; Brockwell and Davis, 1991).

As one might expect, the accuracy of the sample autocorrelation and autocovariance functions are directly related to the number of observations, n , in the random field. Little guidance is given regarding the minimum number of observations, though Box and Jenkins (1970), Anderson (1976), and Davis (1986) recommended that n be greater than 50. With particular reference to the spatial variability of soils, Lumb (1975) suggested that, for a full three-dimensional analysis, the minimum number of test results needed to give reasonably precise estimates is of the order of 10^4 , which is prohibitively large, even for a special

research project. On the other hand, Lumb (1975) recommended that the best that can be achieved in practice is to study the one-dimensional variability, either vertically or laterally, using n of the order of 20 to 100.

The autocorrelation function (ACF) is used widely throughout the time series analysis literature, whereas the use of the autocovariance function is far more limited. The ACF enables the characteristics of the random field to be determined. For example, an ACF exhibiting slowly decaying values of r_k with increasing k suggests long term dependence, whereas rapidly decaying values of r_k suggest short term dependence (Chatfield, 1975; Hyndman, 1990). However, no guidance is given with regard to distinguishing between the two, other than subjectively. A purely random time series, or *white noise*, is characterised by an ACF with the following properties:

$$\rho_k = \begin{cases} 1 & \text{for } k = 0 \\ 0 & \text{for } k \neq 0 \end{cases} \quad (2.28)$$

In addition, the ACF provides information which is used when estimating values of the time series, as will be discussed later in this chapter. Moreover, many authors (Box and Jenkins, 1970; Chatfield, 1975; Bennett, 1979; Bowerman and O'Connell, 1979; Davis, 1986) have suggested that the stationarity of a random field can be determined from an inspection of the ACF. These authors stated that non-stationarity is punctuated by an ACF which slowly dies-down over large lags. Conversely, ACFs which die-down rapidly are thought to represent stationary random fields. While these rules are somewhat subjective, it is difficult to define quantitative limits (for example, the maximum number of lags beyond which the autocorrelations should essentially be equal to zero), as these are very much dependent on the scale of the problem. A number of other techniques for the evaluation of stationarity are available, and these will be examined later in this section.

The theoretical ACF of a stationary random field tends to either cut-off after a particular lag $k = q$, or die-down with increasing lag, k (Bowerman and O'Connell, 1979). Since r_k is an estimation of ρ_k , it is difficult to know, with certainty, when $\rho_k = 0$. Many authors, however, have provided some guidance to the calculation of q , that is, the lag number at which the theoretical ACF is thought to be equal to zero. That is, $\rho_k = 0$ for $k > q$, if:

- $|r_k| = \frac{2}{\sqrt{n}} \left(1 + 2 \sum_{i=1}^{k-1} r_i^2 \right)^{1/2} \approx \pm \frac{1.96}{\sqrt{n}}$, often referred to as *Bartlett's approximation*, which corresponds to two standard errors of the estimates (Box and Jenkins, 1970; Chatfield, 1975; Anderson, 1976; Brockwell and Davis, 1987; Hyndman, 1990; Brockwell and Davis, 1991);

- $|r_k| = \frac{2}{\sqrt{n+1}} \left(1 + 2 \sum_{j=1}^q r_j^2 \right)^{1/2}$ for $k > q$; a rough rule of thumb suggested by Bowerman and O'Connell (1979).

Of these methods, the former appears to be the most widely used throughout the time series literature.

(iv) Partial Autocorrelation Function

Another useful function applied to the analysis of time series is the *partial autocorrelation coefficient*, ϕ_{kk} , at lag, k , which is defined by the solution of the *Yule-Walker* equations (Box and Jenkins, 1970):

$$\begin{bmatrix} 1 & \rho_1 & \rho_2 & \cdots & \rho_{k-1} \\ \rho_1 & 1 & \rho_1 & \cdots & \rho_{k-2} \\ \vdots & \vdots & \vdots & \ddots & \vdots \\ \rho_{k-1} & \rho_{k-2} & \rho_{k-3} & \cdots & 1 \end{bmatrix} \begin{bmatrix} \phi_{k1} \\ \phi_{k2} \\ \vdots \\ \phi_{kk} \end{bmatrix} = \begin{bmatrix} \rho_1 \\ \rho_2 \\ \vdots \\ \rho_k \end{bmatrix} \quad (2.29)$$

The partial autocorrelation coefficient, ϕ_{kk} , can be thought of as the autocorrelation between any two observations, X_i and X_{i+k} , separated by a lag of k units, with the effects of the intervening observations, $X_{i+1}, X_{i+2}, \dots, X_{i+k-1}$, removed (Bowerman and O'Connell, 1979).

Like c_k and ρ_k , it is not possible to know ϕ_{kk} with any certainty, but only to estimate it from samples obtained from a population. As a result, r_{kk} is defined as the *sample partial autocorrelation coefficient at lag k* , and is given by the following equation:

$$r_{kk} = \begin{cases} r_1 & \text{if } k = 1 \\ \frac{r_k - \sum_{j=1}^{k-1} r_{k-1,j} r_{k-j}}{1 - \sum_{j=1}^{k-1} r_{k-1,j} r_j} & \text{if } k > 1 \end{cases} \quad (2.30)$$

$$\text{where: } r_{kj} = r_{k-1,j} - r_{kk} r_{k-1,k-j} \quad \text{for } j = 1, 2, \dots, k-1$$

The graph of r_{kk} , calculated for lags $k = 0, 1, 2, \dots, K$, is known as the *sample partial autocorrelation function* (PACF). The parameter K is the maximum number of lags that r_{kk}

should not be calculated beyond, and is identical to the parameter K used for the ACF, discussed previously.

The PACF is a useful tool in identifying an appropriate estimation model for the random field, as well as assisting to identify the stationarity of the data. Like the ACF, the theoretical PACF of a stationary random field tends to either cut-off after a particular lag, $k = q$, or die-down with increasing lag, k (Bowerman and O'Connell, 1979). Again, since r_{kk} is an estimation of ϕ_{kk} , it is difficult to know, with certainty, when $\phi_{kk} = 0$. Many authors, however, provide some guidance for the calculation of q , that is, the lag number at which the theoretical PACF is thought to be equal to zero. These limits are identical to those detailed in the previous section, with Bartlett's formula being the most widely adopted.

(v) Estimation - Random Field Models

Once the autocorrelation, and partial autocorrelation, functions have been determined for a stationary data set, time series analysis provides a framework whereby values at other spatial locations may be estimated. The process, known as the *Box-Jenkins Procedure*, involves a number of steps which are summarised in Figure 2.14. The stages of *model identification*, *parameter estimation*, *diagnostic checking* and *forecasting*, are treated below.

(a) Model Identification and Parameter Estimation

Once the data are made stationary, the ACF and PACF are together used to determine which probability model will best fit the random field under consideration. Models which are in common use include:

- Moving average (MA) models;
- Autoregressive (AR) models;
- Mixed autoregressive-moving average (ARMA) models;
- Integrated mixed autoregressive-moving average (ARIMA) models.

In deciding which of these models best fits the data, the first step is to calculate the autocorrelation and partial autocorrelation functions. The choice of model will depend on the manner in which the ACF and PACF die-down. Each of these models will be briefly described below, with treatment confined to *non-seasonal* models.

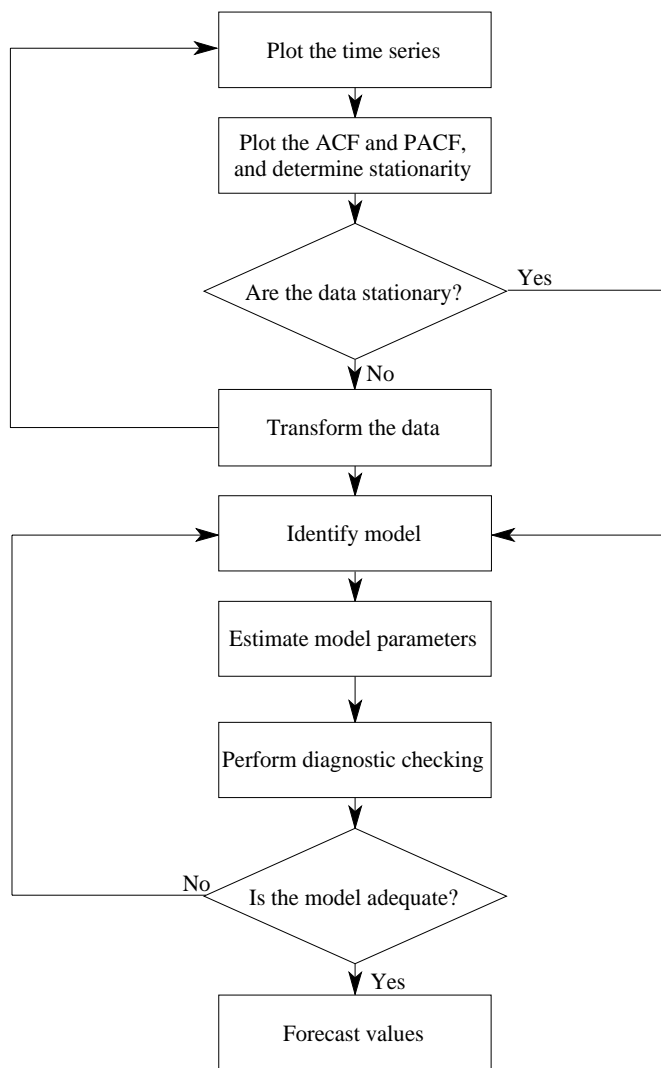


Figure 2.14 Summary of the Box-Jenkins procedure.
(After Maier and Dandy, 1994).

1. Moving Average Models of Order, q

If a_t is a purely random process with a mean of zero and a variance of σ_a^2 then the process, Z_t , is said to be a *moving average process* of order, q , if:

$$Z_t = \theta_0 a_t + \theta_1 a_{t-1} + \cdots + \theta_q a_{t-q} \quad (2.31)$$

where: θ_i are constants, with the a_i 's scaled such that $\theta_0 = 1$.

A moving average process is characterised by:

- an ACF that cuts-off after lag q ;

- a PACF that dies-down.

The manner in which the PACF dies-down identifies the order of the MA process. For example:

- First order MA process The PACF dies-down in a damped exponential decay fashion;
- Second order MA process The PACF dies-down according to a combination of damped exponential and sine wave decays.

The parameters $\theta_0, \theta_1, \dots, \theta_q$, are estimated using a numerical optimisation algorithm such as a *grid search*, the *Gauss-Newton approach* (Cryer, 1986), or the *innovations algorithm* (Brockwell and Davis, 1987).

As an example, for the MA(1) case (a first-order moving average process) the parameter, θ_1 , and the variance of the white noise, σ_a^2 , are determined by the following relationships:

$$\theta_1 = \frac{-1 + (1 - 4r_1^2)^{\frac{1}{2}}}{2r_1} \quad (2.32)$$

$$\sigma_a^2 = \frac{c_0}{1 + \theta_1^2}$$

2. Autoregressive Models of Order, p

If a_t is a purely random process with a mean of zero and a variance of σ_a^2 then the process, Z_t , is said to be an *autoregressive process* of order, p , if:

$$Z_t = \phi_1 Z_{t-1} + \phi_2 Z_{t-2} + \dots + \phi_p Z_{t-p} + a_t \quad (2.33)$$

where: ϕ_i are constants.

An autoregressive process is characterised by:

- an ACF that dies-down;
- a PACF that cuts-off after lag p .

The manner in which the ACF dies-down identifies the order of the AR process. For example:

- First order AR process The ACF dies-down in a damped exponential decay fashion;
- Second order AR process The ACF dies-down according to a combination of damped exponential and sine wave decays.

Consider an AR process of order m and mean, μ , (Chatfield, 1975):

$$Z_t - \mu = \phi_1(Z_{t-1} - \mu) + \phi_2(Z_{t-2} - \mu) + \dots + \phi_m(Z_{t-m} - \mu) + a_t \quad (2.34)$$

Given N observations, Z_1, Z_2, \dots, Z_n , the parameters, $\mu, \phi_1, \phi_2, \dots, \phi_m$, can be estimated by least squares by minimising S , usually called the *conditional sum-of-squares function* (Cryer, 1986), where:

$$S = \sum_{t=m+1}^n [(Z_t - \mu) - \phi_1(Z_{t-1} - \mu) - \dots - \phi_m(Z_{t-m} - \mu)]^2 \quad (2.35)$$

As an example, for the AR(1) case (a first-order autoregressive process) the parameter, ϕ_1 , and the variance of the white noise, σ_a^2 , are determined by the following relationships:

$$\begin{aligned} \phi_1 &= r_1 \\ \sigma_a^2 &= c_0(1 - \phi_1 r_1) \end{aligned} \quad (2.36)$$

3. Mixed Autoregressive-Moving Average Models of Order, p, q

The *mixed autoregressive-moving average process* (ARMA) is a useful class of time series model since a stationary random field can often be described using fewer parameters than a purely MA or AR process (Chatfield, 1975). An ARMA process of order (p, q) is defined as:

$$Z_t = \phi_1 Z_{t-1} + \phi_2 Z_{t-2} + \dots + \phi_p Z_{t-p} + a_t + \theta_1 a_{t-1} + \theta_2 a_{t-2} + \dots + \theta_q a_{t-q} \quad (2.37)$$

An ARMA process is characterised by:

- an ACF that dies-down;
- a PACF that dies-down.

The manner in which the ACF and PACF die-down identifies the order of the ARMA

process. For example:

- ARMA process of order (1, 1) Both the ACF and PACF die-down in a damped exponential decay fashion.

4. Integrated Mixed Autoregressive-Moving Average Models

Finally, the *integrated mixed autoregressive-moving average process* (ARIMA) is a class of time series model that incorporates non-stationary data. The ARIMA process is one that, after performing several differences, as outlined in §2.5.1.2(ii), reduces to an ARMA process (Brockwell and Davis, 1987). If Z_t , a non-stationary random field, is differenced to order d , that is:

$$W_t = \nabla^d Z_t \quad (2.38)$$

such that W_t is a stationary random field, then the ARIMA process is of the form:

$$W_t = \phi_1 W_{t-1} + \phi_2 W_{t-2} + \cdots + \phi_p W_{t-p} + a_t + \theta_1 a_{t-1} + \theta_2 a_{t-2} + \cdots + \theta_q a_{t-q} \quad (2.39)$$

If W_t is an ARMA(p, q) process, then X_t is an ARIMA(p, d, q) process. Cryer (1986) stated that for practical purposes, d is usually taken to 1 (first-difference), or at most 2 (second-difference).

Estimation of the parameters in both the ARMA and ARIMA models use the same techniques adopted for the MA and AR models, detailed previously.

(b) Diagnostic Checking

Once a preliminary model has been identified and its associated parameters estimated, a number of diagnostic checks are available to determine how well the model fits the observed random field. Each technique analyses the *residuals*, that is, the differences between the observations and the fitted values, as well as the autocorrelation coefficient of the residuals, \hat{r}_k . A brief discussion of the more commonly used techniques follows.

1. Box-Pierce Method

Box and Pierce (1970) showed that $1/\sqrt{n}$ supplies an upper bound for the standard error of the \hat{r}_k 's calculated from the residuals. Chatfield (1975) suggested that a correlogram of the residuals be calculated and any values of \hat{r}_k that lie outside the range $\pm 2/\sqrt{n}$ are considered to be significantly different from zero, indicating an inappropriate model. However, for low lags, values of \hat{r}_k that lie inside the range $\pm 2/\sqrt{n}$ may still be significantly different from zero and require further investigation.

2. Portmanteau Test

Box and Pierce (1970) suggested that, instead of considering the \hat{r}_k 's individually, K coefficients of \hat{r}_k be taken as a whole, by calculating, Q , the *Box-Pierce chi-square statistic*:

$$Q = n \sum_{k=1}^K \hat{r}_k^2 \quad (2.40)$$

where: n is the number of terms in the differenced series;
 K = 20 (Box and Jenkins, 1970);
 = 12, 24, or 36 (Bowerman and O'Connell, 1979);
 = \sqrt{n} (Hyndman, 1990).

If the model accounts for relationships between the observations, as it should, the residuals should be unrelated and, hence, Q should be small. Thus, a large value of Q indicates that the model is inadequate. Bowerman and O'Connell (1979) stated that it is common practice to accept the adequacy of the model if:

$$Q < \chi_5^2(K - n_p) \quad (2.41)$$

where: $\chi_5^2(z)$ is the point on the scale of the chi-square distribution having z degrees of freedom, such that, there is an area of 5% under the curve of this distribution above this point;
 n_p is the number of parameters that must be estimated in the model under consideration, = $p - q$, where p , q are the number of AR and MA terms, respectively.

Brockwell and Davis (1987, 1991) suggested that the portmanteau test is useful for disqualifying unsatisfactory models, but often fails to reject poorly fitting models. As a consequence, Brockwell and Davis (1991) recommended that the portmanteau test should not be used on its own.

In addition, Brockwell and Davis (1987, 1991) suggested a number of diagnostic tests which examine the randomness of the residuals. These include: *a test based on turning points*; *the difference-sign test*; and *the rank test*. However, in the interests of brevity, these are not treated in this thesis. Further details regarding these tests are given by Brockwell and Davis (1987, 1991).

(c) *Forecasting*

Having identified an appropriate model, estimated its parameters and performed diagnostic checks to confirm its validity, the user is then in a position to employ the model to forecast future values of the random field, or in terms of the spatial domain, estimate values at locations other than those measured. In essence, forecasting is one of the primary objectives of time series analysis. Focusing solely on univariate stochastic processes, several forecasting techniques have been traditionally applied to time series. These include: *extrapolation of trend curves* (regression); *exponential smoothing*; *Holt-Winters forecasting technique*; and the *Box-Jenkins approach* (Chatfield, 1975). Whilst each of these methods are frequently applied with good results, the Box-Jenkins methodology, detailed above and summarised in Figure 2.14, is the most versatile, and provides a more systematic framework for building, analysing and forecasting with time series models (Chatfield, 1975; Bowerman and O'Connell, 1979). In addition, the Box-Jenkins methodology tends to give more accurate forecasts than other methods. On the other hand, the Box-Jenkins approach suffers from a number of limitations:

- At least 50 to 100 observations are necessary to build a reliable Box-Jenkins model, and even greater if a seasonal component, or a relationship non-stationarity are present (Bowerman and O'Connell, 1979). In addition, these authors recommended that, because of the large amount of data required, the Box-Jenkins methodology is best suited to time series with small sampling intervals.
- Several ARIMA models may be found to fit the data equally well. While these models are usually almost equivalent, occasionally each model will generate different forecasts (Chatfield, 1975).
- There are currently no procedures available for automatically updating the model parameters as new data are measured. As additional observations are added to the

random field, the complete model-building procedure must be repeated (Bowerman and O'Connell, 1979).

- The Box-Jenkins procedure is complex, time-consuming and expensive (Chatfield, 1975; Bowerman and O'Connell, 1979).
- Considerable experience is required to identify an appropriate ARIMA model (Chatfield, 1975).

(vi) Cross-Covariance and the Cross-Correlation Function

Just as the autocovariance and the autocorrelation functions are used to measure dependencies by comparing a time series with itself at successive lags, it is also possible to compare two separate time series with each other to calculate positions of strong correlation. The tools used to do this are the *cross-covariance* and the *cross-correlation function* (CCF). The cross-covariance coefficients, between two time series, $X = X_1, X_2, X_3, \dots, X_n$ and $Y = Y_1, Y_2, Y_3, \dots, Y_n$, at lag k , $c_{k_{XY}}$, are given by (Box and Jenkins, 1970):

$$c_{k_{XY}} = E[(X_i - \bar{X})(Y_{i+k} - \bar{Y})] \quad k = 0, 1, 2, \dots \quad (2.42)$$

and the cross-covariance between Y and X at lag k , $c_{k_{YX}}$, is:

$$c_{k_{YX}} = E[(Y_i - \bar{Y})(X_{i+k} - \bar{X})] \quad k = 0, 1, 2, \dots \quad (2.43)$$

where, in general, $c_{k_{XY}} \neq c_{k_{YX}}$. However, since:

$$c_{k_{XY}} = E[(X_{i-k} - \bar{X})(Y_i - \bar{Y})] = E[(Y_i - \bar{Y})(X_{i-k} - \bar{X})] = c_{-k_{YX}} \quad (2.44)$$

$c_{k_{XY}}$ need only be calculated for $k = 0, \pm 1, \pm 2, \pm \dots$

Since the time series, X and Y , may be expressed in different units, it is useful to define the cross-correlation coefficient at lag k , $\rho_{k_{XY}}$, as:

$$\rho_{k_{XY}} = \frac{c_{k_{XY}}}{\sigma_X \sigma_Y} \quad k = 0, \pm 1, \pm 2, \pm \dots \quad (2.45)$$

Again, only estimates can be made of $c_{k_{XY}}$ and $\rho_{k_{XY}}$, and hence the *sample cross-covariance coefficient at lag k* , $c_{k_{XY}}^*$, and the *sample cross-correlation coefficient at lag k* , $r_{k_{XY}}$, are defined as:

$$c_{k_{XY}}^* = \begin{cases} \frac{1}{n} \sum_{i=1}^{n-k} (X_i - \bar{X})(X_{i+k} - \bar{X}) & k = 0, 1, 2, \dots \\ \frac{1}{n} \sum_{i=1}^{n+k} (X_i - \bar{X})(X_{i-k} - \bar{X}) & k = 0, -1, -2, \dots \end{cases} \quad (2.46)$$

$$r_{k_{XY}} = \frac{c_{k_{XY}}^*}{s_X s_Y} \quad k = 0, \pm 1, \pm 2, \pm \dots \quad (2.47)$$

where: s_X is the sample standard deviation of $X = \sqrt{c_{0_{XX}}^*}$;
 s_Y is the sample standard deviation of $Y = \sqrt{c_{0_{YY}}^*}$.

Again, the accuracy of the sample cross-correlation function (CCF), that is the graph of $r_{k_{XY}}$ against lag, k , is directly related to the number of observations in the time series, n . As for the sample autocorrelation function, Box and Jenkins (1970) recommended that n be greater than 50.

Again, Box and Jenkins (1970) recommended that Bartlett's approximation be used as a crude check to ascertain whether certain values of the CCF can be regarded as being effectively equal to zero. The CCF will be used in §5.3.5 to compare series of q_c measurements to f_s measurements, to determine the optimal value of the shift distance mentioned previously in §2.4.4.

2.5.1.3 Geostatistics

The mathematical technique, which is now universally known as *geostatistics*, was developed to assist in the estimation of changes in ore grade within a mine, and is largely a result of the work of Krige (1951) and Matheron (1965). Since its development in the early 1960's, geostatistics has been applied to many disciplines including: groundwater hydrology and hydrogeology; surface hydrology; earthquake engineering and seismology; pollution control; geochemical exploration; and geotechnical engineering. In fact, geostatistics can be applied to any natural phenomena that are spatially or temporally associated (Journel and Huijbregts, 1978; Hohn, 1988).

As mentioned previously, geostatistics is based on the *regionalised variable*, that is, one that can be represented by random functions, rather than the classical approach which treats samples as independent random variables. The regionalised variable has properties that are partly random and partly spatial and has continuity from point to point, however, the changes are so complex that they cannot be described by a tractable deterministic function (Davis, 1986).

One of the basic statistical measures of geostatistics is the *semivariogram*, which is used to express the rate of change of a regionalised variable along a specific orientation. The semivariogram is treated below.

(i) Semivariogram

The semivariogram is a measure of the degree of spatial dependence between samples along a specific orientation, and represents the degree of continuity of the property in question. The semivariogram, γ_h , is defined by the following equation:

$$\gamma_h = \frac{1}{2} E[(X_{i+h} - X_i)^2] \quad (2.48)$$

where: X_i is the value of the property, X , at location, i ;
 X_{i+h} is the value of the property, X , at location, $i+h$;
 h is the displacement between the data pairs;
 $E[\dots]$ is the expected value.

Thus, the semivariogram is defined as half the expected value, or mean, of the squared difference between pairs of points, X_i and X_{i+h} , separated by a displacement, h . If the regionalised variable is stationary and normalised to have a mean of zero and a variance of 1.0, the semivariogram is the mirror image of the autocorrelation function, as shown in Figure 2.15.

Even though a regionalised variable is spatially continuous, like the ACF and PACF, it is not possible to know its value at all locations. Instead its values can only be determined from samples taken from a population. Thus, in practice, the semivariogram must be estimated from the available data, and is generally determined by the following relationship:

$$\gamma_h^* = \frac{1}{2N} \sum_{i=1}^N (X_{i+h} - X_i)^2 \quad (2.49)$$

where: γ_h^* is the experimental semivariogram, that is, one based on the

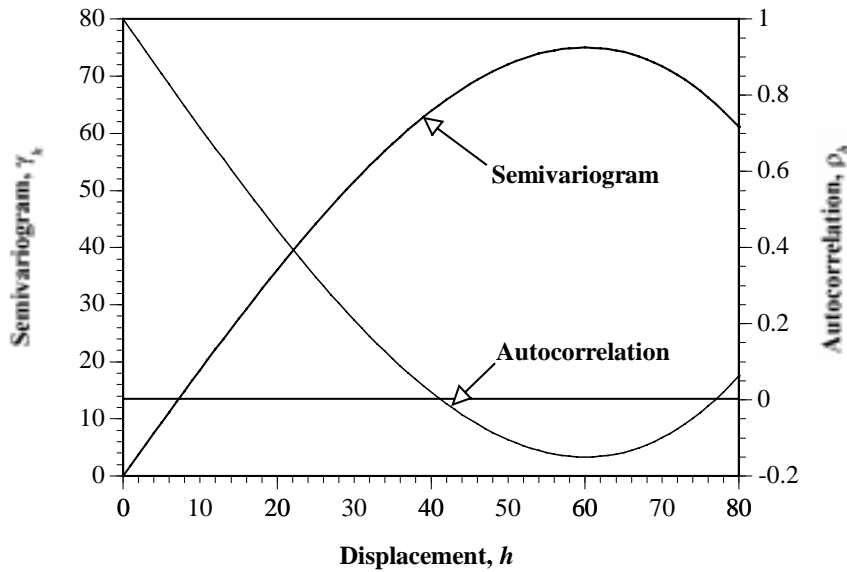


Figure 2.15 Relationship between the semivariogram, γ_h , and the autocorrelation, ρ_h , for a stationary regionalised variable.
(After Davis, 1986).

sampled data set;

N is the number of data pairs separated by the displacement, h .

Clark (1980) stated that the experimental semivariogram is theoretically restricted to distances of one-quarter of the total extent of the sampled information, however, in practice, one-half is generally used (Journel and Huijbregts, 1978; Clark, 1979; Clark, 1980; Brooker, 1989). (For example, if a CPT sounding is performed to a depth of 5,000 mm, its corresponding semivariogram would normally be calculated for values of h from 0 to 2,500 mm). In addition, the accuracy of γ_h^* is directly related to the number of data pairs, N (Brooker, 1991), with the minimum number of pairs needed for a reliable estimate of γ_h^* being between 30 and 50 (Journel and Huijbregts, 1978; Brooker, 1989); with some authors suggesting as many as 400 to 500 (Clark, 1980).

The strength of geostatistics is that it provides, through the semivariogram, a framework for the estimation of variables. In fact, it can be shown that geostatistics provides the *best, linear, unbiased estimator* (BLUE) (Journel and Huijbregts, 1978; Clark, 1979; Rendu, 1981). Whilst the experimental semivariogram is known only at discrete points, the estimation procedure, known as *kriging*, and discussed in the next section, requires the semivariogram values be known for all h . Thus, it is necessary to model the experimental semivariogram, γ_h^* , as a continuous function, γ_h . Table 2.7 and Figure 2.16 present a

Table 2.7 Commonly used model semivariograms.

Model	Mathematical Function	Remarks
Pure Nugget	$\gamma_h = C_0$	$C_0 = \text{Nugget}$
Spherical	$\gamma_h = C \left(\frac{3h}{2a} - \frac{h^3}{2a^3} \right) + C_0$ when $h \leq a$ $\gamma_h = C + C_0$ when $h \geq a$	$C + C_0 = \text{Sill};$ Range = a
Exponential	$\gamma_h = C(1 - e^{-h/a}) + C_0$	Effective Range = $3a^\dagger$
Gaussian	$\gamma_h = C(1 - e^{-h^2/a^2}) + C_0$	Effective Range = $\sqrt{3}a^\dagger$
Linear	$\gamma_h = ph + C_0$	$p = \text{slope}$
Power	$\gamma_h = ph^\alpha + C_0$	$0 < \alpha < 2$
de Wijsian	$\gamma_h = 3\alpha \ln(h) + C_0$	$\alpha = \text{absolute dispersion}$

Note: In addition, each of the models, above, obey $\gamma_0 = 0$.

[†] From Olea (1991).

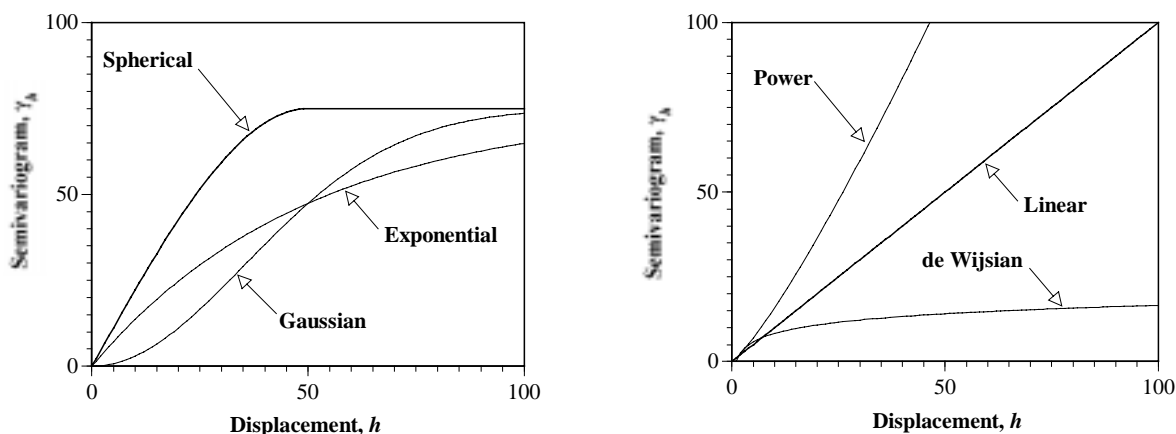


Figure 2.16 Commonly used model semivariograms with C_0 set to zero.

number of semivariogram models that are commonly used in the literature, the most widely applied of these being the *spherical* model.

With particular reference to the spherical model, three parameters are used:

C_0 is defined as the *nugget effect* and arises from the regionalised variable being so erratic over a short distance that the semivariogram goes from zero to the level of the nugget in a distance less than the sampling interval. The nugget effect is the result of three separate phenomena (Rendu, 1981):

1. *microstructures within the geological material* - which have been observed from the study of the spatial variability of mineral concentrations of core samples. Two adjacent cores will exhibit a nugget effect when one of them contains a nugget and the other does not (Journel and Huijbregts, 1978). Several researchers have stated that soils also exhibit this behaviour (Calle et al., 1987; Li and White, 1987a; Soulié et al., 1990; Jaksa et al., 1993);
2. *sampling, or statistical, errors* - as will be detailed in §2.5.2.1, C_0 depends greatly on the spacing between individual samples (Brooker, 1977; Journel and Huijbregts, 1978; Clark, 1979; Clark, 1980; de Marsily, 1982);
3. *measurement errors* - if it were possible to obtain a repeat measurement at precisely the same location, the observations would differ by an amount directly dependent on the measurement technique. Measurement errors are also manifested by a non-zero value of the semivariogram at zero lag.

It has been standard practice in the treatment of the spatial variability of soils to attribute the nugget effect solely to measurement errors associated with the testing method (Baecher, 1986; Wu and El-Jandali, 1985; Filippas et al., 1988). However, Li and White (1987a) suggested that while some of the nugget effect can be attributed to measurement errors, the possibility of small-scale random effects, that is, microstructures, cannot be ignored in geotechnical properties. The relationship between measurement errors and the nugget effect will be examined in some detail in §5.5.

$C + C_0$ is known as the *sill* which measures half the maximum, on average, squared difference between data pairs.

a is defined as the *range of influence*, or *range*, and is the distance at which samples become independent of one another. Data pairs separated by distances up to a are correlated, but not beyond.

Clark (1979) described the process of fitting a model to an experimental semivariogram as essentially a trial-and-error approach, usually achieved by eye. Brooker (1991) suggested the following technique as a first approximation in determining the appropriate parameters for a spherical model:

- The experimental semivariogram and variance of the data are plotted;
- The value of the sill, $C + C_0$, is approximately equal to the variance of the data;

- A line is then drawn with the slope of the semivariogram near the origin, which intersects the sill at two thirds the range, a ;
- This line intersects the ordinate at the value of the nugget effect, C_0 .

In addition, Brooker (1991) stated that the accuracy of the modelling process depends on both, the number of pairs in the calculation of the experimental semivariogram, and the lag distance at which it is evaluated.

Journel and Huijbregts (1978) suggested that automatic fitting of models to experimental semivariograms, such as least squares methods, should be avoided. This is because each estimator point, γ_h^* , of an experimental semivariogram is subject to an estimation error and fluctuation which is related to the number of data pairs associated with that point. Since the number of pairs varies for each point so, too, does the estimation error. The authors recommended that the weighting applied to each estimated point, γ_h^* , should come from a critical appraisal of the data, and from practical experience.

Similar to the autocorrelation function of random variables, the semivariogram is greatly facilitated by stationarity, that is, the semivariogram depends only on the separation distance and not on the locality of the data pairs. The regionalised variable can be regarded as consisting of two components: the *residual* and the *drift*. If a drift, or trend, exists in the data, which leads to non-stationarity, it must first be removed (Journel and Huijbregts, 1978; Henley, 1981). It has been shown by Davis (1986), that if the drift is subtracted from the regionalised variable, the residuals will themselves be a regionalised variable and will have local mean values of zero. In other words, the residuals will be stationary and the semivariogram can be evaluated.

(ii) Estimation - Kriging

Once the form of the semivariogram is known, it is possible to estimate the values of the measured parameter at any unsampled location. The estimation procedure is known as *kriging*, named after D. G. Krige, a South African mining engineer who pioneered the application of statistical techniques to the estimation of ore bodies. Kriging essentially involves the determination of a series of weights, $w_1, w_2, w_3, \dots, w_n$, that are applied to the sample data set, $Y_1, Y_2, Y_3, \dots, Y_n$, to yield a linear estimate, Y_p^* , at an unsampled location, p , such that:

$$Y_p^* = w_1 Y_1 + w_2 Y_2 + w_3 Y_3 + \dots + w_n Y_n \quad (2.50)$$

and:

$$w_1 + w_2 + w_3 + \dots + w_n = 1 \quad (2.51)$$

It is expected that the estimate, Y_p^* , will differ from the actual (but unknown) value, Y_p , by an amount known as the estimation error, ε_p , (the same as the *residual* used in random field theory), such that:

$$\varepsilon_p = Y_p^* - Y_p \quad (2.52)$$

Provided that no local trend exists within the sample data set, and the weights sum to one, as indicated by Equation (2.51), the estimate, Y_p^* , will be unbiased. That is, the average of the estimation errors will be zero, and linear, since the estimate is a linear combination of the sample values. The variability of the errors, or the *estimation variance*, σ_ε^2 , for the general *linear unbiased* estimator can be shown to be equal to (Clark, 1979; Brooker, 1991):

$$\sigma_\varepsilon^2 = 2 \sum_{i=1}^n w_i \bar{\gamma}(S_i, U) - \sum_{i=1}^n \sum_{j=1}^n [w_i w_j \bar{\gamma}(S_i, S_j)] - \bar{\gamma}(U, U) \quad (2.53)$$

where:

- $\bar{\gamma}(S_i, U)$ is the average value of the semivariogram, γ_h , as one end of the vector h is in S_i , and the other independently sweeps the unknown element U ;
- U is a point, line, area, or block;
- $\bar{\gamma}(S_i, S_j)$ is the average value of the semivariogram between points S_i and S_j ;
- $\bar{\gamma}(U, U)$ is the average of the semivariogram between all pairs of points within the element U .

For the continuous case, Equation (2.53) can be expressed as:

$$\sigma_\varepsilon^2 = \frac{2}{U} \int_U \sum_{i=1}^N w_i \gamma(x - x_i) dx - \sum_{i=1}^N \sum_{j=1}^N w_i w_j \gamma(x_i - x_j) - \frac{1}{U^2} \iint_U \gamma(x - y) dx dy \quad (2.54)$$

By calculating the estimation variance, σ_ε^2 , it is possible to rank any estimation regime⁵. Kriging enables an optimal set of weights, $w_1, w_2, w_3, \dots, w_n$, to be determined so that σ_ε^2 can be minimised. This is achieved by differentiating σ_ε^2 with respect to the weights, and setting this differential equal to zero, as:

⁵ A methodology used to estimate the value of a domain, based on applying a series of weights, $w_1, w_2, w_3, \dots, w_n$, to a set of sample data. Such estimation regimes include: *polygonal*, *inverse distance*, and *inverse distance squared*. Each of these estimation procedures are examined in §7.4.2.

$$\frac{\partial \sigma_{\varepsilon}^2}{\partial w_i} = 0 \quad \text{where: } i = 1, 2, 3, \dots, n \quad (2.55)$$

Solving this equation will yield n -equations and n -unknowns. However, an additional equation needs to be satisfied so that the estimator will be unbiased; that is, the weights must sum to equal one:

$$\sum_{i=1}^n w_i = 1 \quad (2.56)$$

After differentiation, the following system of equations is obtained:

$$\left[\begin{array}{ccc|c} \bar{\gamma}(S_i, S_j) & & & 1 \\ & & & \vdots \\ & & & w_i \\ \hline & \dots & 1 & 0 \\ \hline & & & \mu \end{array} \right] \begin{bmatrix} \vdots \\ \vdots \\ \vdots \\ \mu \end{bmatrix} = \begin{bmatrix} \vdots \\ \bar{\gamma}(S_i, U) \\ \vdots \\ 1 \end{bmatrix} \quad (2.57)$$

where: μ is the Lagrange multiplier.

This results in $n+1$ equations and $n+1$ unknowns. In this way, kriging provides the minimum estimation variance and the best, linear, unbiased estimation (BLUE) regime, as mentioned previously. The estimation variance associated with kriging, or the kriging variance, σ_k^2 , can be evaluated using Equation (2.53), or alternatively:

$$\sigma_k^2 = \left[\dots \quad w_i \quad \dots \quad \mu \right] \begin{bmatrix} \vdots \\ \bar{\gamma}(S_i, U) \\ \vdots \\ 1 \end{bmatrix} - \bar{\gamma}(U, U) \quad (2.58)$$

Brooker (1980) detailed the following key steps involved in the kriging method of geostatistical estimation:

1. A structural study to determine the semivariogram.
2. Selection of the samples to be used in evaluating the element, U .
3. Calculation of the $\bar{\gamma}$ of the kriging system of equations.
4. Solution of the system of equations to obtain the optimal weights.
5. Use of these results to calculate the estimate of U and its associated estimation variance.

Since the geostatistical process of kriging was first formalised in the 1960's, several modifications to this process have been proposed by various researchers. These are generally sub-divided into two forms: *linear kriging*, and *non-linear kriging*. These two forms include:

Linear Kriging:

- *ordinary kriging* (Isaaks and Srivastava, 1989; Olea, 1991) - the technique defined previously in §2.5.1.3(ii) simply as ‘kriging’;
- *simple kriging* (Journel and Huijbregts, 1978; Olea, 1991) - the same as ordinary kriging, except that the mean is known and, hence, the final row is deleted from all matrices, as is the final column of the square matrix. Simple kriging is the best of all minimum mean square error estimators only when a multinormal distribution is used as a model for the random function (Olea, 1991);
- *universal kriging* (Journel and Huijbregts, 1978; Rendu, 1981; Olea, 1991) - simple kriging of the residuals of a regionalised variable after automatically removing optimal estimates of the drift. It is used for non-stationary data, that is, when a deterministic trend exists in the measured data.

Non-Linear Kriging:

- *disjunctive kriging* (Journel and Huijbregts, 1978; Clark, 1979; Olea, 1991) - a distribution-dependent estimator which is used when a bias exists in the measured data, and is the most demanding of the kriging procedures in terms of stationarity conditions, computer resources, and mathematical understanding on the part of the user;
- *lognormal kriging* (Olea, 1991) - simple kriging or ordinary kriging of a logarithmically transformed set of observations, having a multivariate lognormal distribution;
- *indicator kriging* (Journel, 1983; Olea, 1991) - simple kriging or ordinary kriging applied to indicator data (samples which have been transformed into binary numbers) sharing the same threshold;
- *probability kriging* (Olea, 1991) - an enhancement of indicator kriging which also includes rank order transformations of the original data;
- *Bayesian kriging* (Kulkarni, 1984; Omre, 1987; Omre and Halvorsen, 1989) - an enhancement of indicator kriging which is used when a small number of observations is available, and when significant experience and knowledge about the phenomenon should be accounted for in the estimation process.

Indicator, probability and Bayesian kriging are methods of non-parametric geostatistics; that is, a branch of geostatistics which comprises techniques that do not rely on a prior multivariate distribution hypothesis (Olea, 1991). The geostatistical process of kriging will be examined in detail in Chapters 5 and 7.

2.5.1.4 Tests for Non-Stationarity

As discussed in the previous sections, the application of both random field theory and geostatistics is facilitated by stationary data. Various authors have proposed techniques for ascertaining the stationarity of the data.

Bennett (1979) proposed five methods for the detection of non-stationary data:

1. *Eyeballing* - Mere inspection of the scatterplots of the data is often sufficient to detect non-stationarity, as was shown by Figure 2.12. Eyeballing, however, is not sufficient to detect the form of the trend, nor most cases of non-stationary variance.
2. *Histogram plots* - A simple, though crude technique, is to split the random field into a number of subsections and to plot each of their histograms. Comparison of these histograms enables shifts in the means and variances to be detected.
3. *Inspection of the ACF* - As discussed previously, several authors (Box and Jenkins, 1970; Chatfield, 1975; Bowerman and O'Connell, 1979; Davis, 1986) have suggested that a process that is non-stationary in trend, or mean, is indicated by an ACF which dies-down slowly. Box and Jenkins (1970) suggested that a stationary time series is observed by a rapidly damping ACF, whilst Bennett (1979) stated that it is difficult to determine if a slowly dying-down ACF is the result of non-stationarity, or of autoregressive parameters very close to unity.
4. *The number of significant autocorrelations* - This method determines the appropriate degree of differencing necessary to achieve stationarity, and is implicit in the previous technique described above. As a result, this method should be combined with the inspection technique (3), above (Bennett, 1979).
5. *Significance tests on trends* - This technique is applied in four stages:
 - (i) The trend component, t_t , is estimated by least-squares regression;
 - (ii) The residuals, E_t , from this model are calculated and the parameters of an autoregressive model are estimated, that is:

$$e_t = \phi_1 e_{t-1} + \phi_2 e_{t-2} + \dots + \phi_p e_{t-p} \quad (2.59)$$

- (iii) The original data, X_t , are transformed using the estimates of the residual auto-

correlation parameters:

$$x_t = X_t - \phi_1 X_{t-1} - \phi_2 X_{t-2} - \dots - \phi_p X_{t-p} \quad (2.60)$$

- (iv) The new filtered sequence, x_t , is then used to re-estimate the trend and then cycling from step (ii), a new set of autoregressive parameters is calculated, repeating the process until convergence has occurred.

Possibly one of the first techniques proposed in the geotechnical engineering literature to detect the presence of non-stationary data, was the nonparametric, statistical *runs test* suggested by Alonso and Krizek (1975), and used later by Campanella et al. (1987). In fact, these authors used the runs test to check the homogeneity of the data. A *run* is defined as a sequence of like events, items, or symbols that is preceded and followed by an event, item, or symbol of a different type, or by none at all (Daniel, 1990). In specific application terms, a run is a sequence of observations that are either all above, or all below, the mean of the observations. According to Alonso and Krizek (1975) and Campanella et al. (1987), the test is carried out in the following manner:

1. The data set is separated into a series of n sub-sets, each of some arbitrary length, Δ .
2. The local means and variances for each of the n sub-sets are then compared to the global mean and variance of the entire data set. Two outcomes are possible: either the local mean is above the global mean; or the local mean is below, or equal to, the global mean.
3. The hypothesis of stationarity, or homogeneity, of the data is then either accepted or rejected by comparing the resulting distribution with standard percentage tables of the run distribution.

If the runs test is used to assess the stationarity of a data set, the data need not be divided into smaller sub-sets (Daniel, 1990). Daniel (1990) defined the parameters, n_1 , as the number of observations greater than the mean and, n_2 , as the number of observations less than the mean. However, the parameters n_1 and n_2 make no allowance for ties, that is, when the observations equal the mean. If we let the parameter, n_3 , be the number of tied observations, then n_1 and n_2 can account for ties if modified as follows:

$$\begin{aligned} n_1 &= (\text{no. of observations} > \text{mean}) + \frac{n_3}{2} ; \\ n_2 &= (\text{no. of observations} < \text{mean}) + \frac{n_3}{2} ; \\ n_1 + n_2 &= n \end{aligned} \quad (2.61)$$

where: n is the total number of observations.

This technique of allowance for ties is similar to that suggested by Noether (1991) for use with Kendall's τ test, which is discussed in detail below. The runs test, when used to assess stationarity of a data set, however, is given by the following steps (Daniel, 1990):

1. The parameters, n_1 , n_2 , and n_3 are evaluated.
2. The number of runs, R , are calculated.
3. If the data are determined by a random process, that is, a stationary one, then the calculated number of runs, R , must lie within upper and lower critical bounds, as given by standard runs test tables, for example Daniel (1990). However, these tables are generally limited to situations where $n \leq 20$. For large values of n , Daniel (1990) recommended the use of Equation (2.62), where z_R is distributed normally, with a mean of zero and variance of unity. As a consequence, the value of z_R can be compared with values given in standard, normal distribution tables. Hence, if $z_R \leq \pm 1.96$, then the data can be assumed to be stationary with 95% confidence.

$$z_R = \frac{R - \frac{2n_1n_2}{n_1 + n_2} + 1}{\sqrt{\frac{2n_1n_2(2n_1n_2 - n_1 - n_2)}{(n_1 + n_2)^2(n_1 + n_2 - 1)}}} \quad (2.62)$$

The runs test, although used by Alonso and Krizek (1975) and Campanella et al. (1987) as a test for homogeneity, has found little use elsewhere in the geotechnical engineering literature.

Journel and Huijbregts (1978) suggested that an experimental semivariogram which increases as rapidly as $|h|^2$ for large distances, h , most often indicates the presence of a trend, and hence non-stationary data. This technique was also proposed by Kulatilake and Southworth (1987) and Kulatilake and Ghosh (1988) for the detection of non-stationarities in geotechnical engineering data. This technique is the geostatistical equivalent of the time series method of a slowly decaying ACF (the third method suggested by Bennett (1990), as detailed previously).

Ravi (1992) stated that the most powerful test for non-stationarity is *Kendall's τ test*. The test essentially involves the calculation of the test statistic, τ , which measures the probability of *concordance* minus the probability of *discordance* (Daniel, 1990). The observation pairs, (X_i, Y_i) and (X_j, Y_j) , are said to be concordant if the difference between X_i and X_j is in the same direction as the difference between Y_i and Y_j . That is, if either $X_i > X_j$ and $Y_i > Y_j$, or $X_i < X_j$ and $Y_i < Y_j$, then the pairs are concordant. Discordance, on the other hand, is when the directions of the differences are not the same. If $X_i = X_j$ and/or $Y_i = Y_j$,

then the pairs are neither concordant nor discordant. The test statistic, τ , is given by (Daniel, 1990; Noether, 1991):

$$\tau = \frac{S}{\frac{1}{2}n(n-1)} \quad (2.63)$$

where: n is the number of pairs of (X, Y) observations.

To obtain S the following process is used:

1. The observations (X_i, Y_i) are ranked in a column according to the magnitude of the X 's, with the smallest X first, through to the largest X last. The X 's are thus arranged in their *natural order*.
2. Each Y value is then successively compared with each Y value appearing below it. In making these comparisons, a pair of Y values, that is, the value of Y in question and the value of Y below it, is said to be in *natural order* if the Y below is larger than the Y above. On the other hand, a pair of Y values is in *reverse natural order* if the Y below is smaller than the Y above.
3. The parameter, P , is the number of pairs in natural order, and the parameter, Q , is the number of pairs in reverse natural order.
4. S is then simply the difference between P and Q , that is, $S = P - Q$.

The value of Kendall's τ lies between $+1$ and -1 with: $\tau = +1$ indicating perfect positive correlation; $\tau = -1$ indicating perfect negative correlation; and $\tau = 0$ indicating no correlation. Hence, when applied to the assessment of stationarity, a value of τ close to zero indicates that the data are stationary, whereas a value of τ near $+1$ or -1 indicates non-stationary data. Usually, for some confidence level specified by the user, the value of τ is compared with critical values of τ tabulated in many statistics texts; for example Daniel (1990) and Noether (1991). As with the runs test, tables of critical τ values are rarely given for data sets where n exceeds about 40. For large values of n , Daniel (1990) recommended the use of the following equation:

$$z_\tau = \frac{3\tau\sqrt{n(n-1)}}{\sqrt{2(2n+5)}} \quad (2.64)$$

Again, z_τ is normally distributed with a mean of zero and variance of unity and, as a consequence, the value of z_τ can be compared with values given in standard, normal distribution tables. Hence, if $z_\tau \leq \pm 1.96$ then the data can be assumed to be stationary with

95% confidence. Additionally, Noether (1991) suggested the use of the parameter, c , given by:

$$c = \frac{1 + \tau}{1 - \tau} \quad (2.65)$$

The parameter, c , suggests that the probability of concordance, P , is c times more likely than the probability of discordance, Q .

In summary, of the various techniques for assessing data stationarity, as detailed above, it is generally accepted that none have been found to be entirely suitable on their own. Perhaps the most suitable and most widely used in the field of geotechnical engineering are: inspection of a scatterplot of the data; examination of the ACF; inspection of the experimental semivariogram; the runs test; and Kendall's τ test. It will be these five techniques which will be used to assess the stationarity of the data, detailed in Chapter 4, and examined in Chapter 5.

In the next section treatment will be given to the historical progress of the understanding of the spatial variability of geotechnical materials. This discussion will focus essentially on soils, as much work has already been done in the field of rocks, particularly in the evaluation of ore bodies. Where possible, this treatment follows a chronological sequence.

2.5.2 Historical Studies Concerned with the Spatial Variability of Geotechnical Materials

The development of the understanding of the spatial variability of soils has evolved along two, essentially separate streams - one involving random field theory, and the other focusing on geostatistics. In general, the evolution of each stream has occurred independent of the other, with a few exceptions. As a result, this treatment of the historical development of the spatial variability of geotechnical materials will be separated into these two streams.

Since the very early days of soil mechanics, it was recognised that geotechnical materials varied from one location to another. Karl Terzaghi, universally regarded as the *father of geotechnical engineering*, in his Presidential Address to the First International Conference on Soil Mechanics and Foundation Engineering in 1936, stated: "...*the earth in its natural state is never uniform*" (Terzaghi, 1936). However, it was not until 1966 that this aspect, that is, the spatial variability of soils, began to be examined rigorously.

2.5.2.1 Random Field Theory

Probably the first detailed investigation of the spatial variability of soils was that by Lumb (1966), where he examined the statistical properties of London Clay and four Hong Kong soils, namely: *Marine Clay*; *Alluvial Sandy Clay*; *Residual Silty Sand*; and *Residual Clayey Silt*. Lumb (1966) stated that any soil property such as the void ratio, undrained shear strength, and so on, is generally not constant, but depends on the location of the point within the soil mass. He stated that the properties can be taken as independent of lateral position and, at most, linearly dependent on the depth, z_k , below the ground surface. Thus, for a particular soil property, v_k , at a point k within a soil mass, Lumb (1966) proposed the following *random variable model*:

$$v_k = a + bz_k + \varepsilon_k \quad (2.66)$$

where: a, b are constants;
 z_k is the depth of point k below the ground surface;
 ε_k is a random variable at point k with a mean of zero.

In this model, $a + bz_k$ accounts for a linear trend of the property, v_k , with depth, and ε_k represents the random fluctuation of this property about the trend. In addition, Lumb (1966) suggested that it is occasionally more convenient to express the random variable, ε_k , in the form: $\varepsilon_k = \sigma u_k$, since σ may itself be a function of depth. Lumb (1966) defined the variable, u_k , as a *standardised random variable* having a mean of zero and a standard deviation equal to unity. In addition, Lumb (1966) proposed three different cases of the form of the standard deviation, as shown in Figure 2.17.

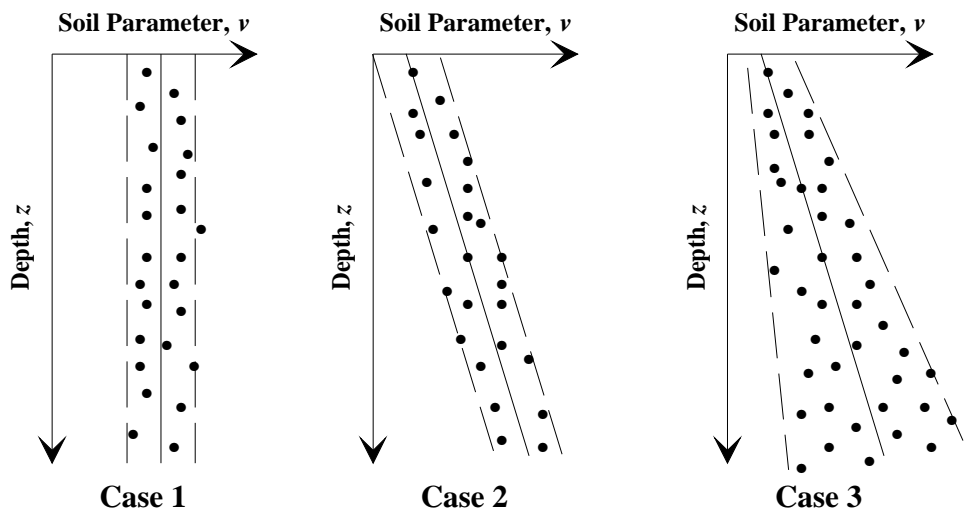


Figure 2.17 Different forms of a soil parameter, v , with depth, z . (After Lumb, 1966).

Case 1 refers to the soil property, v , being normally distributed about the mean value, m , whereas Case 2 refers to v being normally distributed about a linear trend, $a + bz$, and, in both cases, the variance is independent of depth. Case 3 represents the situation where v is normally distributed about a linear trend, $a + bz$, and the variance increases with depth. By plotting the standardised random variable, u , against the *standardised normal variate*, ζ (Pearson and Hartley, 1956), and applying the χ^2 test to a combination of vane shear and carefully sampled, unconfined compression test results, Lumb (1966) was able to show that the undrained shear strength, s_u , and drained internal angle of friction, ϕ_d , of the three soils follow normal distributions, and possess statistical properties which are summarised in Table 2.8. In addition, Lumb (1966) suggested that a rational choice of design parameter can be made from the mean, or linear trend provided that the form of the variance is known. As can be seen from Table 2.8, the spatial variability models, represented by the mean linear trends, provide relatively basic models of the variability structure of these geotechnical properties.

Table 2.8 Summary of statistical properties. (After Lumb, 1966).

Soil	Property	Mean, m	Std. Deviation, σ	Coeff. of Variation, CV
Marine Clay	s_u (kPa)	$1.04z + 1.89$	$0.19z + 0.35$	18.4% (3)*
London Clay	s_u (kPa)	$22.1z$	$3.58z$	16.2% (3)
Silty Sand	$\tan\phi_d$	0.692	0.0958	13.8% (1)

Note: z is the depth below the ground surface in metres;
* (1) and (3) refer to the cases shown in Figure 2.17.

Hooper and Butler (1966) presented the results of a large number of undrained triaxial tests performed on undisturbed samples of London Clay, and also found that the undrained shear strength follows a normal distribution.

Lumb and Holt (1968) examined undrained shear strength results obtained from vane shear tests; and unconfined compression tests, carried out on remoulded and high quality undisturbed specimens of the soft Marine Clay of Hong Kong. The results, combined from approximately 100 boreholes, indicated Case 3 behaviour with a high degree of scatter about the linear trend. From 270 test results, the authors suggested a CV of at least 20%, and the best linear relationship for the mean value to be:

$$s_u = (1.012 \pm 0.012)z + 1.85 \quad (2.67)$$

where: s_u is the undrained shear strength, in kPa;
 z is the depth below the ground surface, in metres.

Again, the use of a linear trend to depict the variability of s_u represents a relatively elementary model. Agterberg (1970), for probably the first time, summarised the use of the autocorrelation function (ACF) with respect to geotechnical engineering materials; in his case, rocks. Based on a general model:

$$v_k = t_k + s_k + \varepsilon_k \quad (2.68)$$

where:

v_k	is the value of a parameter v in a random field at location k ;
t_k	is the trend component at k , which expresses the global systematic change and any test method bias;
s_k	is the signal component at k , which expresses the local correlated portion of the spatial variation;
ε_k	is the random uncorrelated portion.

Agterberg (1970) proposed the following procedure for estimating the ACF:

1. Eliminate spatial heteroscedasticity from the data, if present, by data transformation.
2. Estimate the trend by fitting deterministic functions by the method of least squares.
3. Remove the trend component from the data; the remaining data being the *residuals*.
4. Estimate the ACF of the residuals.
5. Fit a model to the ACF of the residuals.

Agterberg suggested that the ACF for a continuous random variable is exponential. By analysing elevations of the surface of a geological stratum from 200 boreholes, Agterberg (1970) concluded that the best results can be obtained by first fitting a low degree trend function (e.g. a quadratic) and using an estimation procedure based on the residuals.

While Lumb (1966) stated that soil properties can be regarded as laterally independent, Lumb (1974) later acknowledged lateral dependence, in addition to depth dependence. Lumb (1974) re-examined the results of Lumb and Holt (1968) and, for probably the first time in the geotechnical engineering literature, used the ACF to investigate the spatial dependence of *soil* properties by making use of the work of Agterberg (1970). Lumb (1974) suggested that soil properties which are depth dependent generally follow a first order autoregressive model, also known as a *unilateral Markov process*, as shown in Equation (2.69) in the backward direction, and Equation (2.70) in the forward direction. On the other hand, Lumb (1974) stated that laterally dependent soil properties usually follow a *bilateral Markov process*; that is, one with dependence extending in both directions, as shown in Equation (2.71).

$$v_k = \phi_1 v_{k-1} + \varepsilon_k \quad (2.69)$$

$$v_k = \phi_1 v_{k+1} + \varepsilon_k \quad (2.70)$$

$$v_k = \phi_1 v_{k-1} + \phi_2 v_{k+1} + \varepsilon_k \quad (2.71)$$

where: ϕ_1, ϕ_2 are constants generally less than 1.

Lumb (1974) stated that the ACF for the unilateral and bilateral Markov processes are, respectively, of the following form:

$$\rho_k = e^{-\alpha k} \quad (2.72)$$

$$\rho_k = (\beta k) K_1(\beta k) \quad (2.73)$$

where: α, β are constants;
 k is the distance, in metres;
 $K_1(x)$ is the modified Bessel function of the second kind and first order.

Lumb (1974) went on to fit these models to sample ACFs produced from data obtained from various sources, and concluded that:

- The lateral variation of the liquid limit of the *Bear Paw Shale* (a clay shale from Saskatchewan, Canada) followed satisfactorily a combination of a white noise process and a bilateral Markov process:

$$\rho_k = 0.42(1.44k) K_1(1.44k) \quad (2.74)$$

- The lateral variation of the modulus of subgrade reaction of a fine dry sand fill could be satisfactorily represented, again, by a combination of a white noise process and a bilateral Markov process, via:

$$\rho_k = 0.59(6.35k) K_1(6.35k) \quad (2.75)$$

- The variation with depth of the liquid limit, natural moisture content and the submerged unit weight of the Hong Kong Marine Clay (Lumb and Holt, 1968) followed a unilateral Markov process:

$$\rho_k = e^{-1.23k} \quad (2.76)$$

- The variation of the undrained shear strength with depth of the Hong Kong Marine Clay could be modelled using either a white noise process, or a unilateral Markov process:

$$\rho_k = e^{-0.33k} \quad (2.77)$$

From the results of these analyses, Lumb (1974) stated that the spatial autocorrelations for the Bear Paw Shale and the Marine Clay were not particularly large, the converse of what would have been expected for these very uniform deposits. On this basis, and from the limited data available, Lumb (1974) concluded that no great error would be made in assuming the properties to be uncorrelated for spacings of the order of 1 to 2 metres.

Wu (1974) also used the ACF to study the spatial correlation of the undrained shear strength of the soils, in his case, the *Chicago Clay*. Positive correlation was found to occur within a vertical distance of 0.9 metres, which is equal to the approximate thickness of the different geological units within the Chicago area. In addition, Wu (1974) approximated the ACF by the following relationship:

$$\rho_k = e^{-0.234k} \quad (2.78)$$

Lumb (1975) re-examined the results presented by Lumb (1974) using first- and second-differences, the ACF, and the partial autocorrelation function (PACF). Lumb (1975) found that, in all cases, no more than a first-difference was necessary to minimise the variance of the population; implying that a linear trend component was always sufficient. Since the soils that he examined showed weak autocorrelations, Lumb (1975) concluded that the autocovariances and autocorrelations could be neglected and, as a result, their omission should produce no serious error in the design predictions. This conclusion, in particular, will be examined in greater detail later in this thesis, with reference to the measured CPT values of Keswick Clay⁶.

Diaz Padilla and Vanmarcke (1974) proposed a property, the *correlation distance*, v_o , which expresses the extent of spatial variation of some parameter, v . The authors defined v_o as the distance required for the ACF to decay from 1 to e^{-1} (0.3679). Diaz Padilla and Vanmarcke (1974) suggested that v_o be determined by fitting the following exponential decay models to the sample ACF:

$$\rho_{\Delta z} = e^{-(|\Delta z|/v_o)} \quad (2.79)$$

⁶ Lumb (1975) also made reference to the *spectral density function* (SDF); that is, the Fourier transform of the ACF; as an additional spatial variability descriptor. Lumb suggested that there are some theoretical advantages in using a *frequency* domain, instead of the more natural distance domain. However, since the vast majority of research reported in the geotechnical engineering literature has focused on the distance domain, the theory associated with the SDF will not be applied in the present study. A detailed treatment of the analysis of properties in the frequency domain; that is, *spectral analysis*; is given by Vanmarcke (1983).

$$\rho_{\Delta z} = e^{-(\Delta z/v_0)^2} \quad (2.80)$$

where: Δz is the spacing between samples.

Using these relationships, Diaz Padilla and Vanmarcke (1974) were able to calculate vertical correlation distances for the moisture content, void ratio and preconsolidation pressure of a soft organic, silty clay from California, as 1.5, 1.5, and 0.3 metres, respectively. In addition, the authors found that the horizontal correlation distance of the preconsolidation pressure of this clay was of the order of 90 metres. However, Diaz Padilla and Vanmarcke (1974) commented that, since the smallest lateral spacing between boreholes was 90 metres, they could not detect smaller scale correlation effects. The usefulness of the parameter, v_0 , was not emphasised until Vanmarcke (1977a) presented his treatment of random field theory, which is discussed below.

Matsuo and Asaoka (1977) compared the undrained shear strengths of many undisturbed samples of a normally consolidated Japanese marine clay, obtained from unconsolidated undrained triaxial tests. While extending the number of cases proposed by Lumb (1966) from three to ten, the authors found that the results fell into Lumb's Case 3, and a small number into Case 2. Matsuo and Asaoka (1977) concluded that it was difficult to determine the exact spatial autocorrelation of s_u because of sample disturbance. In addition, the authors found that significant autocorrelation of s_u in the vertical direction usually occurs within a distance of 1.5 metres.

Vanmarcke (1977a, 1977b, 1978, 1983, 1984) provided a major contribution to the study of spatial variability of geotechnical materials by the use of random field theory. Vanmarcke (1977a) stated that, in order to describe a soil property, v , stochastically, three parameters are needed: (i) the mean, m ; (ii) the standard deviation, σ (or the variance, σ^2 , or the coefficient of variation, CV); and (iii) the *scale of fluctuation*, δ_v . He introduced the new parameter, δ_v , which accounts for the distance within which the soil property, v , shows relatively strong correlation, or persistence, from point-to-point. Furthermore, when the property is plotted as a function of distance, the scale of fluctuation is closely related to the average distance between intersections, or crossings, of v and m . Small values of δ_v imply rapid fluctuations about the mean, whereas large values suggest a slowly varying property, with respect to the average. While δ_v is closely related to the correlation distance, v_0 (Diaz Padilla and Vanmarcke, 1974), Vanmarcke (1977a) recommended the use of δ_v . Vanmarcke (1983) suggested that δ_v has an important property, namely:

$$\delta_v = \int_{-\infty}^{+\infty} \rho_{\Delta z} d(\Delta z) = 2 \int_0^{+\infty} \rho_{\Delta z} d(\Delta z) \quad (2.81)$$

That is, the scale of fluctuation, δ_v , is the area beneath the entire ACF, or twice the area beneath the positive part of the ACF. To be more specific than Vanmarcke (1977a), with regard to the three parameters needed to stochastically model a soil profile, in order to describe a random field in terms of first- and second-order moments, one must quantify the mean or trend function, the variance, and the correlation structure. As suggested by Vanmarcke (1977a), the variance of the soil profile may be expressed by σ , CV , or the variance, σ^2 , itself. Whilst Vanmarcke (1977a) argued that δ_v is a simple characterisation of the correlation structure, as in fact it is, the autocovariance function, ACVF, spectral density function, SDF, and the *variance function*, may also be used as descriptors of the correlation structure. The variance function, $\Gamma_v^2(\Delta z)$, proposed by Vanmarcke (1977a), measures the point variance under local averaging, and its value is bounded by 0 and 1. The variance function is a particularly useful relationship, since it implies that the variability of *spatial averages* is lower than the point values. This results from the fact that fluctuations of v are smoothed in the averaging process. Vanmarcke (1977a, 1983) defined the *standard reduction factor*, $\Gamma_v(\Delta z)$, as the square root of $\Gamma_v^2(\Delta z)$, and by the following relationship:

$$\Gamma_v(\Delta z) = \frac{\sigma_{\Delta z}}{\sigma} \quad (2.82)$$

where: $\sigma_{\Delta z}$ is the standard deviation of v spatially averaged over a depth interval, Δz ;
 σ is the standard deviation of the point values of v .

Or, in terms of volume averages:

$$\Gamma_v(V) = \frac{\sigma_V}{\sigma} \quad (2.83)$$

where: σ_V is the standard deviation of v spatially averaged over a volume, V .

In addition, Vanmarcke (1977a) defined the scale of fluctuation, δ_v , in terms of $\Gamma_v^2(\Delta z)$, as:

$$\delta_v = \Gamma_v^2(\Delta z)\Delta z \quad (2.84)$$

which is valid when Δz becomes large.

Vanmarcke (1977a) proposed that the variance function may be represented by:

$$\text{Model 1:} \quad \Gamma_v^2(\Delta z) = \begin{cases} 1 & \text{for } \Delta z \leq \delta_v \\ \frac{\delta_v}{\Delta z} & \text{for } \Delta z \geq \delta_v \end{cases} \quad (2.85)$$

Vanmarcke (1983) later refined Equation (2.85) to Equation (2.86), because the resulting ACF is inconsistent with the requirement that δ_v be equal to the area under $\rho_{\Delta z}$ (Equation (2.81)).

$$\text{Model 2: } \Gamma_v^2(\Delta z) = \begin{cases} 1 & \text{for } \Delta z \leq \frac{\delta_v}{2} \\ \frac{\delta_v}{\Delta z} \left(1 - \frac{\delta_v}{4\Delta z} \right) & \text{for } \Delta z \geq \frac{\delta_v}{2} \end{cases} \quad (2.86)$$

Examples of variance function Models 1 and 2 are shown in Figure 2.18.

Vanmarcke (1978) suggested that there are several advantages in expressing second-order information in terms of δ_v . Firstly, the scale of fluctuation is simple to use and to interpret. Secondly, δ_v directly expresses the effect of correlation on the variance of spatial averages. Finally, δ_v can be used to determine the minimum number of uncorrelated observations within Δz needed to correctly predict the standard deviation, $\sigma_{\Delta z}$. Furthermore, Vanmarcke (1978) argued that $\Gamma_v^2(\Delta z)$ is a useful parameter, since the performance of geotechnical engineering systems are generally influenced by spatially averaged soil properties. For example, the average undrained shear strength along a potential failure surface of an earth embankment must be sufficiently low for a slide to occur. In addition, a braced excavation may fail when the average lateral earth pressure exceeds some critical value.

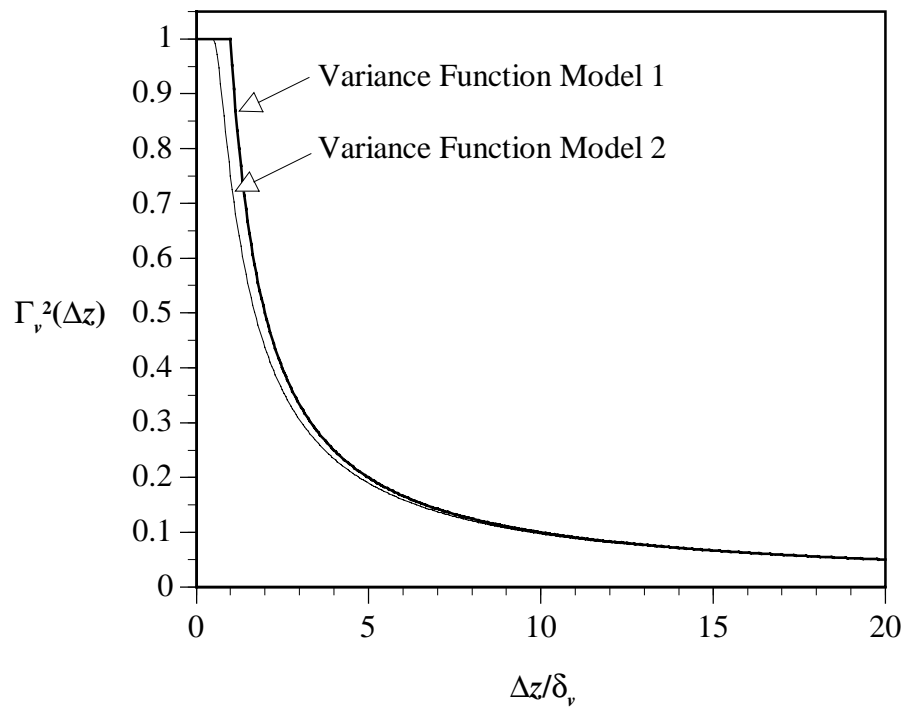


Figure 2.18 Examples of variance functions.
(After Vanmarcke, 1977a).

Vanmarcke (1977a, 1978 and 1983) proposed a number of methods for estimating the scale of fluctuation, δ_v , with particular reference to CPT data. In each of these methods, Vanmarcke used *statistically homogeneous* data, that is, the n -dimensional equivalent of 1D stationarity. Vanmarcke (1977a) suggested that statistical homogeneity could be obtained by *standardising* the data by means of the following relationship:

$$v_s(z) = \frac{v(z) - \bar{v}}{\sigma_v} \quad (2.87)$$

where: $v_s(z)$ is the standardised data;
 \bar{v} is the mean of $v(z)$;
 σ_v is the standard deviation of $v(z)$.

Vanmarcke (1983) later recognised that, in some instances, a further transformation, such as the logarithmic variance transformation (discussed previously in §2.5.1.2(ii)), may be needed to obtain homogeneity. The more relevant techniques for estimating δ_v are presented below.

1. Variance function method for estimating δ_v

Vanmarcke (1977a) suggested that, firstly, the mean, \bar{v} , and standard deviation, σ_v , of the measured *point* values are determined. Adjacent observations are then averaged pairwise, and standard deviation of the resulting *spatial averages* are calculated. This yields an estimate of $\sigma_v \Gamma(2)$. This result is plotted on a standard reduction factor graph, $\Gamma(n)$ versus n , which is similar in nature to that shown in Figure 2.18. (The parameter, n , denotes the number of adjacent observations of v which are averaged). Subsequently, for each value of n , the standard deviation of the spatial averages is computed, and $\Gamma(n)$ evaluated by dividing the result by σ . Vanmarcke (1977a) suggested that the predicted values of $\Gamma(n)$ will approach the theoretical values given by:

$$\Gamma(n) = \sqrt{\frac{\delta_v}{n\Delta z_0}} \quad (2.88)$$

where: Δz_0 is the sampling interval.

Finally, δ_v is estimated by fixing n , observing $\Gamma(n)$, and substituting into:

$$\delta_v = n\Gamma^2(n)\Delta z_0 \quad (2.89)$$

2. Autocorrelation function method for estimating δ_v

Vanmarcke (1978, 1983) and Li and White (1987a) proposed that δ_v could be evaluated from the ACF by the relationships shown in Table 2.9. As a result, δ_v may be estimated by fitting one of the ACF models to the sample ACF by using standard curve fitting techniques, such as ordinary least squares.

Table 2.9 Theoretical autocorrelation functions used to determine the scale of fluctuation, δ_v . (After Vanmarcke, 1977a, 1983; Li and White, 1987a).

Model No.	Autocorrelation Function	Model (Process)	Scale of Fluctuation, δ_v
1	$\rho_{\Delta z} = \begin{cases} 1 - \frac{ \Delta z }{a} & \text{for } \Delta z \leq a, \\ 0 & \text{for } \Delta z \geq a \end{cases}$	Triangular model	a
2	$\rho_{\Delta z} = e^{- \Delta z /b}$	Simple Exponential, AR(1)	$2b$
3	$\rho_{\Delta z} = e^{-(\Delta z /c)^2}$	Squared Exponential, or Gaussian, model	$\sqrt{\pi} c$
4	$\rho_{\Delta z} = e^{- \Delta z /d} \left(1 + \frac{ \Delta z }{d} \right)$	AR(2)	$4d$
5	$\rho_{\Delta z} = e^{- \Delta z /\alpha} \cos(\Delta z/\alpha)$	Cosine Exponential	α

Note: AR(1) is a first-order, autoregressive process;
AR(2) is a second-order, autoregressive process.

3. Mean-crossings approximation of δ_v

An alternative technique, proposed by Vanmarcke (1977a), is to use the approximate relationship:

$$\bar{d}_v \approx \sqrt{\frac{\pi}{2}} \delta_v \approx 1.25 \delta_v \quad (2.90)$$

where: \bar{d}_v is the average distance between the intersections of the fluctuating property, $v(z)$, and its mean, \bar{v} .

Since the introduction of these techniques, the ACF method appears to be the most widely adopted in the geotechnical engineering community, with the variance function method being somewhat less popular. This is possibly due to the fact that the variance function

method involves a degree of subjectivity with regard to the choice of the number of observations, n , whereas the ACF method is somewhat less subjective. The latter, however, implicitly assigns equal weighting to each autocorrelation coefficient. This is slightly erroneous, since more data pairs contribute to the coefficients at lower lags than those at higher lags. However, this effect becomes somewhat negligible when the number of data pairs is large.

Vanmarcke (1977b) applied the theory of random fields to earth slopes in an attempt to make reliable forecasts of slope failure events. He used data obtained from the site investigation of the failure of a 6.5 metre high, and 100 metre long, embankment in a deep deposit of varved clay in Ontario, Canada (Lacasse and Ladd, 1973). Based on measurements of s_u obtained from vane shear tests performed in a number of vertical boreholes, Vanmarcke (1977b) calculated the vertical scale of fluctuation, δ_v , to be 5 metres, and the horizontal scale of fluctuation, δ_H , to be 46 metres. Vanmarcke (1977b), however, gave no information regarding the number and spacing of the data used in the calculation of δ_v and δ_H . Furthermore, no details were provided with respect to transformations, if any, that were performed on the data. Vanmarcke (1977b) subsequently used these values to estimate the probability of failure of the slope. Most importantly, however, Vanmarcke (1977b) provided a theoretical framework for the three-dimensional probabilistic analysis of the classical, limit-equilibrium, slope stability problem.

Since its introduction, several researchers have applied random field theory to the stability analysis of slopes (Anderson et al., 1984; Li and White, 1987b; Li and Lumb, 1987; Bergado and How, 1991; Mostyn and Soo, 1992), as well as other geotechnical problems (Baker, 1984; Tang and Sidi, 1984; Baker and Zeitoun, 1987; Vanmarcke, 1987; Vanmarcke, 1989; Cherubini and Garrasi, 1991; Ditlevsen and Gluwer, 1991; Fenton and Vanmarcke, 1991; Bergado et al., 1992). Random field theory, as applied to slope stability analyses, will be examined in Chapter 8.

Based on the work of Vanmarcke (1977a, 1977b, 1978 and 1983), several researchers have since estimated the ACF and the scale of fluctuation, δ_v , of several geotechnical properties of many different soil types. Their results are summarised in Table 2.10.

The relationships between the scale of fluctuation, δ_v , and the correlation distance, v_o , for each model given in Table 2.9, are summarised in Table 2.11.

Baecher et al. (1980) and DeGroot and Baecher (1993) defined the correlation distance as the distance at which the autocovariance function decays to e^{-1} , not the ACF, as defined by Diaz Padilla and Vanmarcke (1974). However, this is not a generally accepted definition

Table 2.10 Autocorrelation functions, correlation distances and scales of fluctuations given by various researchers.
(Adapted from Li and White, 1987a).

Soil Type	Geotechnical Property	Direction (H: Horizontal, V: Vertical)	Test Type*	Autocorrelation Function ρ_z	Correlation Distance v_o (m)	Scale of Fluctuation δ_v (m)	Sampling Interval Δz_0 (m)	Researcher(s)
Bear Paw Shale	Liquid Limit, w_L	H	-	$0.605zK_1(1.44)z$	≈ 0	≈ 0	0.15	Lumb (1974)
Hong Kong Marine Clay	Index Properties	V	-	$e^{-1.23z}$	0.8	1.6	0.3	
	s_u	V	TUC	$e^{-0.33z}$	3.0	6.0	0.3	
Soft Organic Silty Clay, California	Moisture Content, w	V	-	$e^{-0.66z}$	1.5	3.0	1.5	Diaz Padilla and Vanmarcke (1974)
	Void ratio, e	V	-	$e^{-0.66z}$	1.5	3.0	1.5	
	Preconsolidation Pressure, σ'_p	V	-	$e^{-3.3z}$	0.3	0.6	1.5	
		H	-	$e^{-0.011z}$	90	180	90	
Chicago Clay	s_u	V		$e^{-0.234z}$	4.3	8.6	?	Wu (1974)
Bear Paw Shale	Liquid Limit, w_L	H	-	$0.445zK_1(1.31)z$	≈ 0	≈ 0	0.15	Lumb (1975)
Fine Dry Sand Fill	Subgrade Modulus	H	PLT	$e^{-6.1z}$	0.16	0.33	0.1	
Soft Clay, Louisiana	γ	V	-	?	1.2	?	?	Vanmarcke and Fuleihan (1975)
Clean Sand, Florida Clay	q_c	V	CPT	$e^{-0.9z}$	1.1	2.22	0.2	Alonso and Krizek (1975)
	f_s	V	CPT	$e^{-1.6z}$	0.6	1.25	0.2	
	q_c	V	CPT	$e^{-1.91z}\cos(2.62z)$	0.5	?	0.05	
Soft Silty Loam, Coast of the Ariake Sea, Japan	Moisture Content, w	?	-	$e^{-0.16z}\cos(0.3z)$	6.3	?	0.5	
	Liquid Limit, w_L	?	-	$e^{-0.23z}\cos(0.31z)$	4.3	?	0.5	
	Void ratio, e	?	-	$e^{-0.191z}\cos(0.31z)$	5.2	?	0.5	
	Bulk unit weight, γ	?	-	$e^{-0.253z}\cos(0.41z)$	4.0	?	0.5	

Note: * : Abbreviations for test types are given in the *Glossary*.

continued on the following pages...

Table 2.10 Autocorrelation functions, correlation distances and scales of fluctuations given by various researchers. (...continued).
(Adapted from Li and White, 1987a).

Soil Type	Geotechnical Property	Direction (H: Horizontal, V: Vertical)	Test Type*	Autocorrelation Function ρ_z	Correlation Distance ν_o (m)	Scale of Fluctuation δ_v (m)	Sampling Interval Δz_0 (m)	Researcher(s)
Marine Clay, Japan	s_u	V	TUU	$e^{-\alpha z}$ $\alpha = 0.75 - 1.6$	0.6 - 1.3	1.3 - 2.7	1.0 - 7.7	Matsuo (1976)
New Liskeard Varved Clay, Canada	s_u	V	VST	?	?	5	≈ 1.5	Vanmarcke (1977b) and Lacasse and Ladd (1973)
	s_u	H	VST	?	?	46	≈ 25	
Sand Deposit	D_{10} to D_{90}	V	-	$e^{-0.33z}$	3.0	6.1	1.5	Fardis (1979)
		H	-	$e^{-0.041z}$	24	49	61	
	ln(RD)	V	SPT	$e^{-0.547z}$	1.8	3.7	1.5	
		H	SPT	$e^{-0.030z}$	34	67	61	
Seabed Deposits, Nth. Sea	q_c	H	CPT	$e^{-(z/30)^2}$	30	53	> 20	Tang (1979)
Coastal Sand	q_c	?	CPT	?	5	?	?	Baecher et al. (1980)
Compacted Clay	γ_d	V	-	?	5	?	?	
	γ_d	H	-	?	5	?	?	
Dune Sand	SPT-N	?	SPT	?	20	?	?	
Pleistocene Quadra Sand, Vancouver, Canada	Hydraulic Conductivity	H	-	?	?	≈ 3.5	1.52 - 3.0	Smith (1981)
		V	-	?	?	≈ 1.7	1.52 - 3.0	
	Porosity	H	-	?	?	≈ 3.3	1.52 - 3.0	
		V	-	?	?	≈ 6.5	1.52 - 3.0	
	D_{50}	V	-	?	?	≈ 0.9	1.52 - 3.0	

Note: * : Abbreviations for test types are given in the *Glossary*.

continued on the following page...

Table 2.10 Autocorrelation functions, correlation distances and scales of fluctuations given by various researchers. (...continued).
(Adapted from Li and White, 1987a).

Soil Type	Geotechnical Property	Direction (H: Horizontal, V: Vertical)	Test Type*	Autocorrelation Function ρ_z	Correlation Distance ν_o (m)	Scale of Fluctuation δ_v (m)	Sampling Interval Δz_0 (m)	Researcher(s)
Sand Deposit	$\ln(RD)$	V	SPT	$e^{-0.547z}$	1.8	3.7	1.5	Fardis and Veneziano (1981)
		H	SPT	$e^{-0.030z}$	34	67	61	
Soft Clay, New York	s_u	V	VST	$e^{-0.826z}$	1.2	2.4	1.0 - 3.3	Asaoka and A-Grivas (1982)
	s_u	V	VST	$e^{-0.322z}$	3.1	6.2	3.0 - 4.8	
Alluvial Deposits, Spain	$1/q_c$	V	CPT	$e^{-\alpha z}$ $\alpha = 0.78 - 23.1$	0.04 - 1.3	0.09 - 2.6	0.05	Ximenez de Embun & Romana (1983)
Soft Glacial Clay, North Sea	s_u	V	TUC	?	1.0	?	0.4	Wu and El-Jandali (1985)
	s_u	V	VST	?	1.0	?	0.4	
Fine Silty Sand, Nth. Sea	q_c	V	CPT	?	1.4	?	0.2	
Deltaic Soils, Canada	q_c	V	CPT	$e^{-1.18z} \cos(2.63z)$	0.85	0.13 - 0.71	0.025	Campanella et al. (1987)
Silty Clay, California	q_c	V	CPT	$e^{-2.94z}$	0.34	0.68	0.1	Spry et al. (1988)
Various, California	Permeability	H/V	-	?	-	$\delta_H / \delta_V \approx 40$	-	Fenton and Vanmarcke (1991)
Silty Clays, Bangkok	Embankment Settlement	V	-	$e^{-\alpha z}$ $\alpha = 0.5 - 2.0$	0.5 - 2.0	1.0 - 4.0	> 1	Bergado and How (1991)
Silty Clay	q_c	V	CPT	e^{-10z}	0.1	0.2	0.020	Li and Lee (1991)
Deltaic Soils, Canada	q_c	V	CPT	?	?	0.24 - 0.32	0.025	Wickremesinghe and Campanella (1993)
	f_s	V	CPT	?	?	0.35 - 0.40	0.025	
	Pore Pressure, u_{bt}	V	CPT	?	?	0.14 - 0.42	0.025	

Note: * : Abbreviations for test types are given in the *Glossary*.

Table 2.11 Relationship between the scale of fluctuation, δ_v , and the correlation distance, ν_o , for various ACF models.

Model No.	Autocorrelation Function	Scale of Fluctuation, δ_v	$\frac{\nu_o}{\delta_v}$
1	$\rho_{\Delta z} = \begin{cases} 1 - \frac{ \Delta z }{a} & \text{for } \Delta z \leq a, \\ 0 & \text{for } \Delta z \geq a \end{cases}$	a^\dagger	1
2	$\rho_{\Delta z} = e^{- \Delta z /b}$	$2b^\dagger$	$\frac{1}{2}$
3	$\rho_{\Delta z} = e^{-(\Delta z /c)^2}$	$\sqrt{\pi} c^\dagger$	$\frac{1}{\sqrt{\pi}}$
4	$\rho_{\Delta z} = e^{- \Delta z /d} \left(1 + \frac{ \Delta z }{d} \right)$	$4d^\dagger$	$\frac{1}{4}$
5	$\rho_{\Delta z} = e^{- \Delta z /\alpha} \cos(\Delta z/\alpha)$	α^\ddagger	1

Note: † from Vanmarcke (1983);
 ‡ from Vanmarcke (1978).

of ν_o and, as a result, the interpretation suggested by Diaz Padilla and Vanmarcke (1974) and Vanmarcke and Fuleihan (1975) will be used. While some authors use the correlation distance (Baecher et al., 1980; Li and White, 1987a; DeGroot and Baecher, 1993) to express the autocorrelation of geotechnical properties, the majority of researchers use the scale of fluctuation, δ_v .

Asaoka and A-Grivas (1982) presented the results of 56 field vane shear tests performed on a saturated, soft, organic, silty clay from New York, obtained from four separate vertical boreholes, A1, A2, B1 and B2. The tests were nominally spaced at 1.0 metre intervals, but varied between 0.85 and 1.25 metres. Asaoka and A-Grivas (1982) normalised the measurements of s_u , with respect to depth, z , by introducing the parameter, u_i , which they defined as:

$$u_i = \frac{s_{u_i}}{z_i} \quad (2.91)$$

where: s_{u_i} is the undrained shear strength of sample i ;
 z_i is the depth below ground of the i th sample.

Asaoka and A-Grivas (1982) modelled the variability of the undrained shear strength by

means of the straight line function:

$$\bar{s}_u = \frac{\beta_0}{1 - \beta_1} z \quad (2.92)$$

where: \bar{s}_u is the mean estimate of the undrained shear strength;
 β_0, β_1 are parameters obtained from ordinary least squares, OLS, such that: $u_i = \beta_0 + \beta_1 u_{i-1} + \varepsilon_i$;
 ε_i is an error term, with zero mean and constant variance.

The authors found that for the four boreholes \bar{s}_u varied between $1.50z$ and $2.49z$, with a CV of between 17.8% and 30.2%. However, because the spatial variability was modelled by means of a straight line, the function given in Equation (2.92) provides a relatively poor fit of the actual measured variability, as shown in Figure 2.19. In addition, the model proposed by Asaoka and A-Grivas (1982) makes no allowance for irregularly spaced data and, as has been pointed out above, the data from each of the boreholes were not sampled at regular intervals.

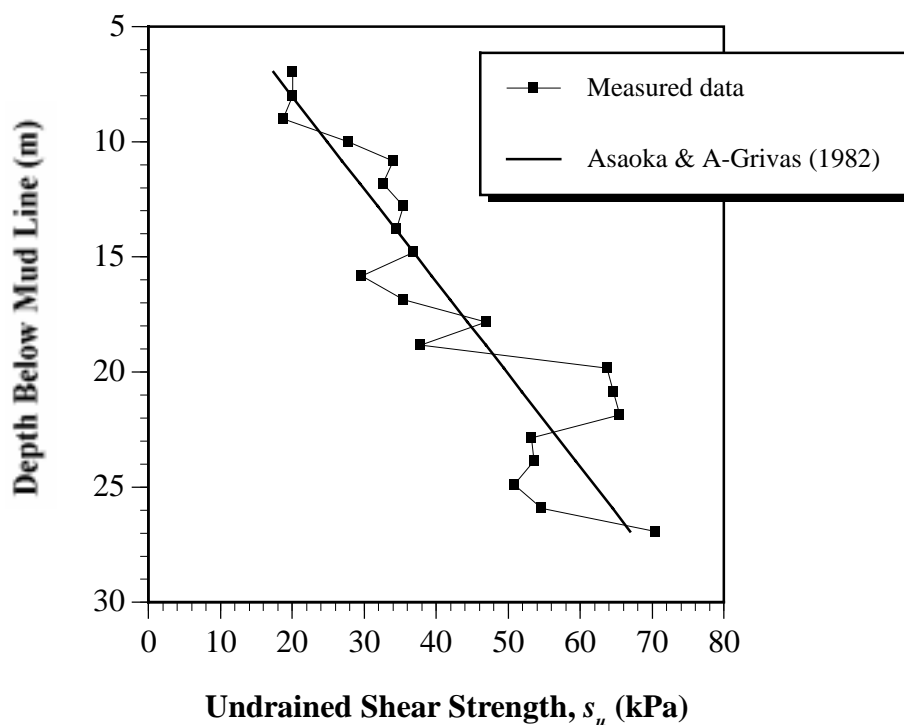


Figure 2.19 Spatial variability model of \bar{s}_u at borehole A1.
(After Asaoka and A-Grivas, 1982).

Using random field theory, Baecher (1982) proposed a useful method for separating the scatter observed in geotechnical data into its two component sources: the spatial variability of the material; and the random measurement error associated with the test itself. Baecher (1982) suggested, as did Agterberg (1970) and Lumb (1974) before him, that the spatial variation of some parameter, v_x , at a location x within a soil mass, may be treated as a combination of a deterministic component, as well as a stochastic, or random, component, as shown in the following equation:

$$v_x = t_x + \xi_x \quad (2.93)$$

where: t_x is the trend component at location x , usually determined by OLS regression;
 ξ_x is the random perturbation from the trend at x .

In addition, Baecher (1982) suggested that the random measurement error is presumed to be independent from one test to another, to have zero mean, and to have constant variance. As a consequence, the measurement, m_{v_x} , of the parameter, v_x , may be expressed as:

$$m_{v_x} = t_x + \xi_x + \zeta_x \quad (2.94)$$

where: ζ_x is the random measurement error at x .

After some algebraic manipulation, Baecher (1982, 1986) stated that the autocovariance, $c_{k(m_v)}$, of the measurement, m_v , at lag, k , may be shown to equal:

$$c_{k(m_v)} = c_{k(v)} + c_{k(\zeta)} \quad (2.95)$$

where: $c_{k(v)}$ is the autocovariance function (ACVF) of v at lag, k ;
 $c_{k(\zeta)}$ is the autocovariance function of the random measurement error, ζ , at lag, k .

A similar relationship can be derived that incorporates the ACF, rather than the ACVF. Baecher (1982, 1986) proposed that, since $c_{k(\zeta)}$ is equal to the variance of ζ at $k = 0$, and $c_{k(\zeta)}$ is equal to zero at $k \neq 0$, the random measurement error may be determined by extrapolating the observed ACVF, or ACF, back to the origin, as shown in Figures 2.20 and 2.21.

Baecher (1986) stated that, by using this method, typical in situ measurements of soils have been found to contribute random measurement errors anywhere between 0% and 70% of the data scatter. It will be shown in §5.5 that Baecher's approach suffers from a number of

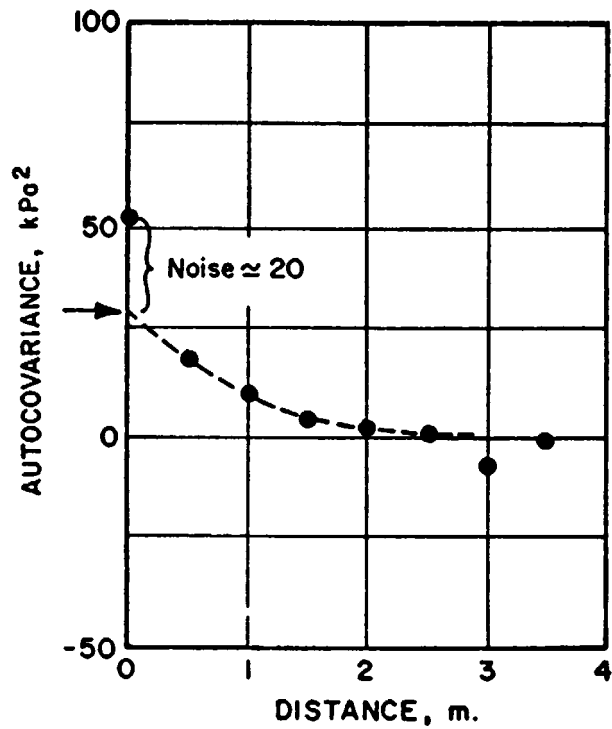


Figure 2.20 Procedure for estimating the random measurement component from the ACVF. (After Baecher, 1982).

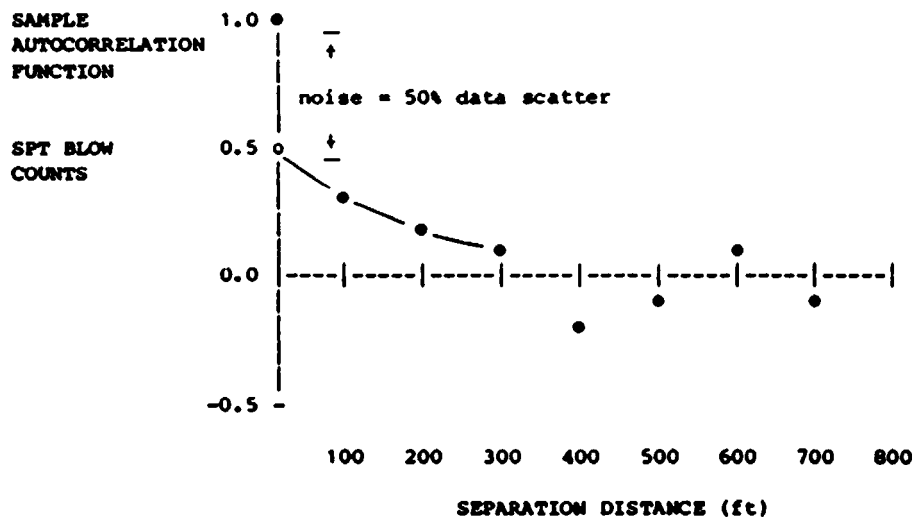


Figure 2.21 Procedure for estimating the random measurement component from the ACF. (After Baecher, 1986).

limitations. As a consequence, the technique should be used with care, and with attention given to the factors discussed in §5.5.

Wu and El-Jandali (1985) suggested a slightly different technique to Baecher's for estimating the random measurement error associated with geotechnical testing. Wu and El-Jandali proposed a method which incorporates time series analysis and, in particular, the Box-Jenkins methodology, and accounts for the random testing error by including an error term, ε_t , in the ARMA model, as shown in the following equation:

$$Z_t = \phi_1 Z_{t-1} + \phi_2 Z_{t-2} + \dots + \phi_p Z_{t-p} + a_t - \theta_1 a_{t-1} - \theta_2 a_{t-2} - \dots - \theta_q a_{t-q} + \varepsilon_t \quad (2.96)$$

Wu and El-Jandali (1985) proposed the parameter, *PRE*, the percentage random testing error, and expressed it as:

$$PRE = \frac{\sigma_e^2}{\sigma_z^2} \times 100\% \quad (2.97)$$

where: σ_e^2 is the variance of the random testing error;
 σ_z^2 is the variance of the observed, or transformed, data.

The technique proposed by Wu and El-Jandali (1985) essentially involves fitting an ARMA model to the observed or transformed data (or an ARIMA model to the differenced data) and calculating σ_e^2 by substituting into Equation (2.98). Since σ_z^2 is equal to the autocovariance at lag 0, that is c_0 , *PRE* can be directly obtained by substituting into Equation (2.97).

$$c_0 = \phi_1 c_1 + \dots + \phi_p c_p + \sigma_a^2 - \theta_1 c_{za}(-1) - \dots - \theta_q c_{za}(-q) + \sigma_e^2 \quad (2.98)$$

where: $c_{za}(-k) = (\phi_k - \theta_k) \sigma_a^2$;
 ϕ_i are coefficients of the AR process;
 θ_i are coefficients of the MA process.

Using this technique, Wu and El-Jandali (1985) found that:

- unconfined compression tests performed on Oslo clay were best represented by an ARMA(1,3) model, and that the percentage random testing error, *PRE*, was found to equal 54.9%, as compared with 24% using Baecher's technique;
- undrained shear strengths obtained from field vane tests in Oslo clay were best represented by an MA(2) model, and *PRE* was found to equal 5.7%, as compared with 5% using the method proposed by Baecher (1982);

- measurements of q_c obtained from a typical cone penetration test in sand were best modelled using an ARIMA(0,1,1), and PRE was found to equal 6.2%, as compared with 0% using Baecher's technique.

Kulatilake and Varatharajah (1986) proposed a weighted regression approach to model and estimate the trend component of geotechnical properties in one dimension. The technique, used to transform heteroscedastic data to satisfy stationarity, applies a series of weights to the covariance matrix of the residuals in an iterative fashion. Using mechanical cone penetrometer data performed in Florida sands, from Schmertmann (1969), Kulatilake and Varatharajah (1986) found that a fourth-order polynomial best fitted the data and that weighted regression was not needed, since the data exhibited constant variance with depth.

Kulatilake and Southworth (1987) extended this work and proposed a technique for the estimation of the spatial variability of geotechnical properties in one dimension, based on random field theory. Their method is summarised in Figure 2.22. Again using the data reported by Schmertmann (1969), Kulatilake and Southworth (1987) found that an ARMA(6,1) process best represented the residual data. In addition, the authors recommended that the semivariogram be used as a check of the stationarity of the data. Kulatilake and Southworth suggested that stationary data are indicated by an experimental semivariogram which is modelled using a *transitive* semivariogram function; that is, one with a finite sill⁷.

Kulatilake and Ghosh (1988) later formalised this indirect test for data stationarity, and Kulatilake and Miller (1987) extended the theoretical framework to incorporate three dimensions. The technique involves: the estimation of the trend component by fitting a polynomial surface by OLS regression; transformation of the data by removing the trend surface; evaluation of the ACF of the residuals; and, finally, estimation by means of the geostatistical process of kriging. It is evident from this that the technique proposed by Kulatilake and Miller (1987) makes use of various aspects proposed by others, such as Agterberg (1970), Asaoka and A-Grivas (1982), and Wu and El-Jandali (1985). However, the procedure uses the geostatistical estimation technique of kriging and, as such, is a hybrid method incorporating aspects of both random field theory and geostatistics. Kulatilake (1989) applied this three-dimensional estimation technique to potentiometric data from the Wolfcamp aquifer in Texas. He was able to demonstrate the usefulness of his estimation framework and showed that the estimates, generated by including a stationary stochastic component, were superior to those obtained using the more common deterministic approach.

⁷ In a formal sense, however, stationary data may also be represented by a non-transitive model semivariogram, for example, a linear semivariogram.

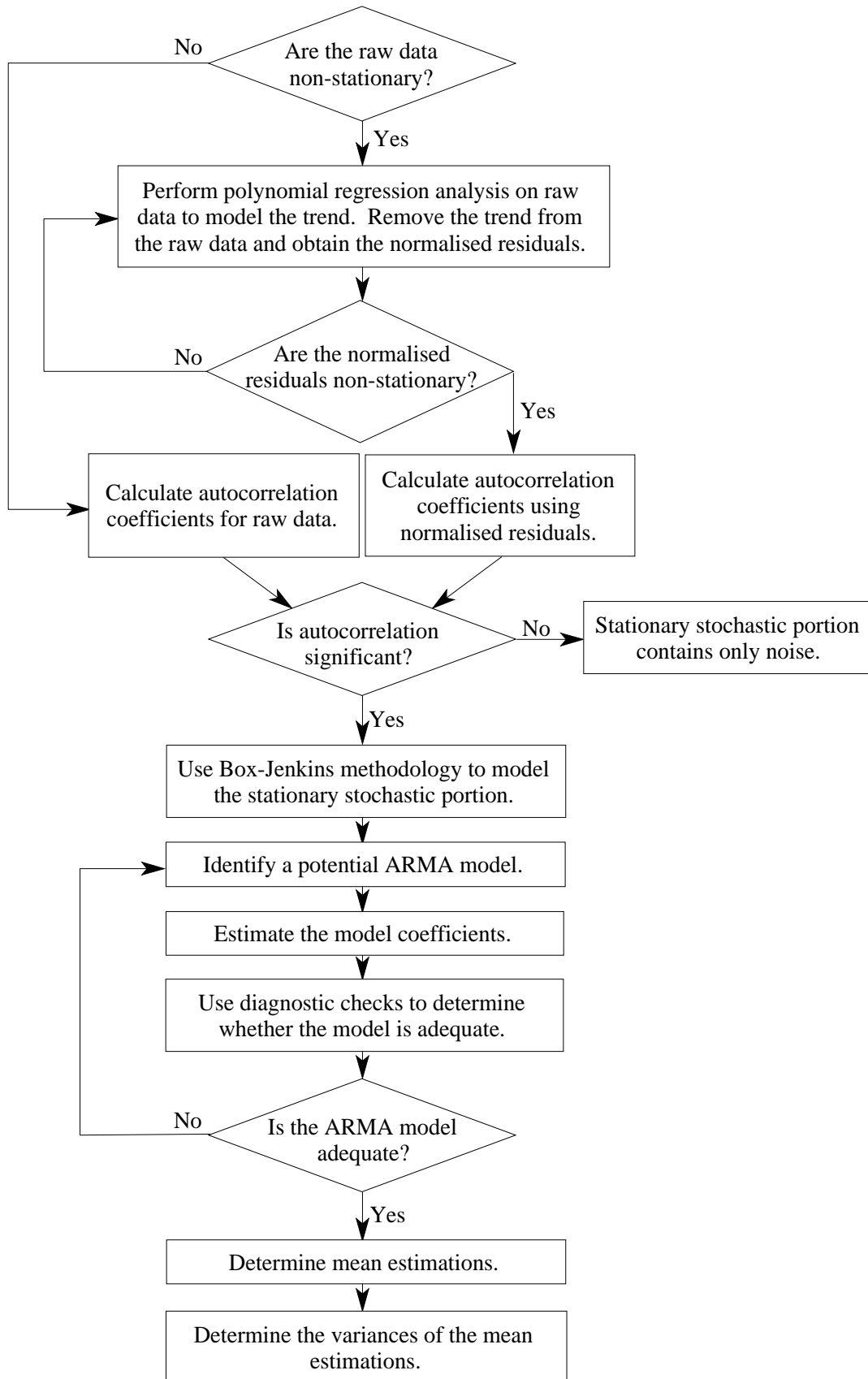


Figure 2.22 Estimation technique proposed by Kulatilake and Southworth (1987).

Sulikowska et al. (1991) examined the results of relative density, RD , data obtained from 45 replicate CPTs performed in sand. The authors indicated that the measurement error associated with the testing was relatively small, with a variance of RD of 0.002298. However, Sulikowska et al. (1991) gave no indication of the conditions under which the tests were performed, no global mean, nor any details regarding the sampling interval. As a consequence, without this additional information, it is difficult to compare the variance with other similar results. In addition, the authors used random field theory to model the spatial variability of the data and, subsequently, concluded that the data were best modelled by an AR(2), or an ARMA(2,2) process.

Ravi (1992) re-examined the data presented by Asaoka and A-Grivas (1982) using the Box-Jenkins methodology. Instead of normalising the measurements of s_u with respect to depth, as suggested by Asaoka and A-Grivas (1982), Ravi (1992) used the standard Box-Jenkins approach of classical decomposition of the data by removing both a linear, and a quadratic, trend by means of OLS, as suggested by others before him (Agterberg, 1970; Asaoka and A-Grivas, 1982; Wu and El-Jandali, 1985; Kulatilake and Ghosh, 1988). In this manner, Ravi (1992) found that an AR(1) model best fitted the residual data and that, in all but one of the boreholes, removing the OLS quadratic trend provided a better representation of the measured data than that obtained by removing the OLS linear trend. Using the sum of the squares of the difference between the measurements and the estimated values, Ravi (1992) was able to demonstrate that the standard Box-Jenkins approach provided a better model of the spatial variability of the undrained shear strength than the technique proposed by Asaoka and A-Grivas (1982). In addition, Ravi used Kendall's τ test to assess the stationarity of the residuals and concluded that, in all cases, the removal of a linear or quadratic trend provided stationary data. On the other hand, the technique of normalising with respect to depth, as proposed by Asaoka and A-Grivas (1982), did not always provide stationary data. Some of Ravi's results will be re-examined in Chapter 5, in order to provide a check of the numerical procedures contained within computer software, specifically written to perform random field theory and geostatistical analyses presented therein.

The foregoing treatment of random field theory, as applied to the field of geotechnical engineering, has demonstrated its usefulness as a tool for characterising the spatial variability of soils and rocks, as well as providing a framework for the estimation of properties at unsampled locations. While much research effort has been directed towards the application of random field theory in the field of geotechnical engineering, it has been almost exclusively applied to one-dimensional situations. Two- and three-dimensional random field theory frameworks have been suggested (Lumb, 1974; Li and White, 1987a; Kulatilake and Ghosh, 1988), but no such field studies have yet been published. In

addition, it is evident from the literature that the vast majority of spatial variability studies have been based on limited data, and on data obtained at relatively large sample spacings.

The following sub-section examines the historical development and application of geostatistics to the field of geotechnical engineering.

2.5.2.2 Geostatistical Analyses

The study of the spatial variability of soil properties by means of geostatistics has found far less use in the geotechnical community than that using random field theory. Over the last 5 to 10 years, there has been a growing number of researchers who are directing their efforts towards the field of geostatistics. While a number of researchers have suggested that geostatistics is a useful tool in the field of geotechnical engineering, many have relied on scant or fictitious data (Bogárdi et al., 1983; Nguyen and Baafi, 1986; Ims and Toolan, 1988). This section, however, examines the more significant contributions made with respect to the application of geostatistics to the study of the spatial variability of soil properties, and again follows a chronological sequence where possible.

Perhaps the first application of geostatistics to the study of the spatial variability of geotechnical properties was made by Soulié et al. (1983). In their paper, Soulié et al. (1983) examined the results of 371 in situ compaction tests which were performed during the construction of an earth dam, and the locations of which were randomly selected in three dimensions. Because the data were spatially sparse, 1 test every 3,500 m³, the authors used a *temporal* scale rather than a spatial one; that is, the data were sorted according to their date of testing, rather than their location. The authors then generated an experimental semivariogram and used this as a basis for ordinary kriging. The kriged estimates were then used to assess the efficiency of the control testing, the probability of whether further compaction was necessary or not, and the probability of whether any incorrect decisions were made. The authors concluded that the application of geostatistics to this kind of geotechnical problem was very useful. However, the results are questionable because of the sparsity of the data, and the fact that a temporal scale was used instead of a spatial one.

Soulié (1984) presented the results of 12 CPTs performed in alluvial deposits of sand and gravel in the Mississippi River flood plain, in the state of Missouri. Measurements of q_c were recorded at vertical intervals of 12.5 mm. The vertical experimental semivariograms of these data indicated: no nugget, and hence no random measurement error; a periodicity of 1.5 metres, which the authors attributed to sample disturbance due to a reaming process which was performed at 1.5 metre intervals in order to reduce lateral stresses on the drilling rods; and a sill value, C , of 13 MPa² and a range, a , of 1.2 metres.

In addition, Soulié (1984) and Soulié et al. (1990) presented the results of about 300 field vane shear tests (VSTs), performed in an intact clay within the James Bay area of Québec, Canada. Though not expressly stated, the tests appear to have been spaced at vertical intervals of 0.5 metres, and at irregular horizontal spacings of greater than one metre. Examination of the vertical VSTs indicated no definite trend with depth and, as a result, the authors performed no transformation of the data. The vertical semivariograms indicated a sill of 50 kPa² and a range, a , of 3 metres; whereas one horizontal semivariogram exhibited pure nugget behaviour, and another indicated a sill of 25 kPa² and a range, a , of 7 metres. In order to account for a measurement bias which was found to exist within the data, the authors performed a shift of 8 kPa to the s_u profiles; and the resulting horizontal semivariogram indicated a sill of 50 kPa² and a range of 30 metres, with each point on the semivariogram being represented by generally less than 30 data pairs. While the authors could not isolate the cause of this bias, it is likely that, since the tests were obtained from four separate investigations which were carried out over a 3 year period, equipment, operator, or environmental effects may have influenced the measurements.

By examination of the experimental semivariograms, Soulié et al. (1990) found the measurement errors to be extremely small and, as a result, they excluded a measurement error term, and hence a nugget effect, from their spatial variability model. The authors then used the experimental semivariograms and the spatial variability model to perform ordinary kriging and presented a cross-sectional elevation, contour plot of estimates of s_u . Soulié (1984) and Soulié et al. (1990) were able to demonstrate the value of geostatistics as a tool for site characterisation and quantifying the spatial variability of the undrained shear strength of clay soils.

Baecher (1984), on the other hand, presented a number of reasons why geostatistics should be treated with caution when applied to geotechnical engineering situations. Baecher (1984) identified three aspects where traditional geotechnical reliability, statistical data analysis and geostatistics differ.

1. For geotechnical applications, population sizes are often small and, as a consequence, statistical estimation error plays an important role in geotechnical reliability.
2. The characterisation of soil or rock properties for geotechnical reliability serves as input to complicated, and often non-linear, numerical transformations, rather than being an end in itself.
3. While average soil or rock properties, throughout a deposit, are often of interest to geotechnical problems, just as often it is the geological detail, or extremes, which control the performance of geotechnical facilities.

While agreeing that the work presented by Soulié (1984) was a valid and useful application of geostatistics to the field of geotechnical engineering, Baecher (1984) recommended that its use should be tempered with caution, particularly in relation to the three aspects listed above. However, the three factors which Baecher (1984) identified apply not only to geostatistics, but also to random field theory. While Baecher expressed some reservations in regard to geostatistics, he offered no alternative technique for estimating the spatial variability of geotechnical materials.

A number of other researchers have applied geostatistics to the study of various geotechnical engineering parameters, and these are summarised in Table 2.12. In addition, several researchers have used kriging to estimate and characterise various properties of soils and rock. These are summarised below.

- Oullet et al. (1987) performed 3D ordinary kriging in order to estimate the modulus of rigidity of a Colorado rock mass. The authors found that the geostatistical analysis yielded different results to those reported in a former study, which were obtained using conventional contouring techniques. As a consequence, Oullet et al. (1987) questioned the results of the former study.
- Nowatzki et al. (1989) used 2D indicator kriging to predict the occurrence of collapsing soils in the Tucson area of Arizona. Data were obtained from job files, from a number of consulting firms, from 411 separate locations yielding 992 data measurements. The authors found that the theory of geostatistics could be applied successfully to geotechnical engineering problems where large amounts of reliable data are available.
- Soulié et al. (1990) estimated the undrained shear strength of an intact marine clay, using 2D ordinary kriging. The authors concluded that the power of geostatistics was made very apparent by the estimation of values where no measurements were taken, with the semivariogram enabling local estimations to be made.
- Nobre and Sykes (1992) used 2D universal kriging and Bayesian kriging to estimate the elevation of bedrock near Lake Erie in Ontario. Universal and Bayesian kriging were used, in contrast to ordinary kriging, because of the presence of a significant trend in the bedrock elevations. The authors found that the estimates from both the universal kriging and Bayesian kriging methods were superior to those obtained by ordinary kriging. In addition, Nobre and Sykes (1992) suggested that Bayesian kriging is particularly useful when only a small number of observations are available, and when significant experience and knowledge can be added to the estimation process.
- Brooker et al. (1995) performed 2D ordinary kriging in order to estimate values of

Table 2.12 Model semivariograms and their parameters as given by various researchers.

Soil Type	Geotechnical Property	Direction (H: Horizontal, V: Vertical)	Test Type*	Model Semivariogram γ_h	Model Parameters	Nugget Effect C_0	Sampling Interval Δz_0 (m)	Researcher(s)
Sand & Gravel, Missouri	q_c	V	CPT	Spherical	$a = 1.2$ m, $C = 13$ MPa ²	0	0.0125	Soulié (1984)
Sandy Clay, France	q_c	V	CPT	Spherical	$a = 0.6$ m, $C = 1.0$ MPa ²	0	0.1	Azzouz et al. (1987) and Azzouz & Bacconnet (1991)
	q_c	H	CPT	Spherical	$a = 25$ m, $C = 0.44$ MPa ²	0.42	1 and 5	
Rock, Colorado	Modulus of Rigidity	V & H	CSMD	Spherical	$a = 3$ m, $C = 92$ GPa ²	20	0.3	Oullet et al. (1987)
Intact Marine Clay, James Bay, Québec	s_u	V	VST	Spherical	$a = 3$ m, $C = 50$ kPa ²	0	≈ 0.5	Soulié et al. (1990)
	s_u	H	VST	Spherical	$a = 30$ m, $C = 50$ kPa ²	0	> 1	
Alluvial Clay, North of Tokyo	s_u	V	TUC	Spherical	$a = 6.5$ m, $C = 125$ kPa ²	0	≈ 0.5	Honjo and Kuroda (1991)
	s_u	H	TUC	Spherical	$a = 200$ m, $C = 125$ kPa ²	0	40	
Sands and Clays, Riverland, South Australia	Readily Available Water (RAW)†	H	-	Spherical	$a = 200$ to 650 m, $C = 130$ mm ²	100	75 × 75 grid	Brooker et al. (1995)
	Topsoil Depth	H	-	Spherical	$a = 220$ to $1,000$ m, $C = 2950$ cm ²	600		
Lightly Over- consolidated, Highly Sensitive Clay, Montréal, Canada	q_c	V	Piezo- cone	Spherical	$a = 2$ m, $C = 5,400$ kPa ²	0	< 2 cm	Chiasson et al. (1995)
	f_s				$a = 2$ m, $C = 4.6$ kPa ²	0		
	Porewater Pressure				$a = 2$ m, $C = 1,180$ kPa ²	0		
	s_u	V	VST	Spherical	$a = 2$ m, $C = 24 - 27$ kPa ²	0	0.5 m	

Note: * : Abbreviations for test types are given in the *Glossary*.

† : An irrigation/soil science parameter which measures the water reservoir of the soil between full point, -8 kPa, and refill point, -60 kPa, and is expressed in mm.

readily available water, *RAW*, and topsoil depth. The authors concluded that geostatistical analyses were valuable adjuncts to the more traditional information available to irrigation system designers.

- Chiasson et al. (1995) used geostatistics to characterise the spatial variability of a lightly overconsolidated and highly sensitive clay. The study was based on measurements obtained from piezocone and vane shear tests (VSTs) which were observed to increase linearly with depth. The authors found that the results of the piezocone and VSTs yielded the same spatial covariance and statistical distribution, indicating that the assessed variability is independent of the mode of operation of the testing device. In addition, Chiasson et al. (1995) found that the piezocone and the VST exhibited no measurement error.

As can be seen from the treatment of geostatistical analyses in the field of geotechnical engineering, given above, geostatistics is particularly useful as a technique for characterising the spatial variability of soils and rocks, and also provides a framework for the estimation of parameters at locations where no measurements are available. Furthermore, there has been relatively little research directed towards the application of geostatistics to the assessment of the spatial variability of soils, when compared to that relating to random field theory.

2.6 SUMMARY

It is evident from the foregoing treatment of the available literature, that both random field theory and geostatistics provide adequate frameworks for quantifying and estimating the spatial variability of geotechnical engineering properties. In addition, it has been demonstrated that the vast majority of analyses using these two techniques have been based on limited data, and on data obtained at relatively large sample spacings. This is particularly so in studies dealing with the lateral variability of geotechnical properties. As mentioned previously, one of the aims of this research is to obtain a large quantity of accurate and closely-spaced data on which subsequent spatial variability analyses will be based.

Furthermore, it has been demonstrated that the CPT provides the facility to measure and record accurate and reliable data, and possesses the lowest level of measurement error of any commonly-used in situ test procedure; provided that the equipment is well-maintained and well-calibrated. The following chapter details a micro-computer based data acquisition system which was developed in order to provide an accurate, reliable and efficient means by which to measure and store these CPT data.

Chapter Three

Development of a Micro-Computer Based Data Acquisition System for the Cone Penetration Test

3.1 INTRODUCTION

This section describes the design, development, calibration and use of a micro-computer based data acquisition system for the CPT. The system was developed by the author in order to obtain accurate and reliable, closely-spaced data for subsequent spatial variability analyses.

3.2 EXISTING DATA ACQUISITION SYSTEMS

As discussed in §2.4.1, the electric cone penetrometer was first developed in Holland in 1965. At that time, measurements of cone tip resistance, q_c , and sleeve friction, f_s , were recorded using analogue instruments. De Ruiter (1971) detailed one of the first data acquisition systems as consisting of a Wheatstone bridge instrument which recorded load variations directly onto a continuous chart. Depth of the cone penetrometer was measured by a magnetic reduction coupling installed between the loading frame, which was connected to the push rods, and the transport mechanism of the chart recorder. In this way, the chart paper advanced 10 mm for every metre of cone penetration.

Analogue systems, such as the one described by de Ruiter (1971), have several limitations. These include:

- *Scaling is Required to Determine Numerical Values* - Since data are stored solely on the chart plots, should data manipulation and calculation be required, (as is the case with the

evaluation of the friction ratio and the undrained shear strength of the soil), this is only possible once the data have been scaled from the plots and re-input into a computer or calculator. This results in: *inefficiencies*, both from a time and economic perspective; and *inaccuracies* from the scaling process itself.

- *Stiction and Overshoot* - Pen-based chart recorders are affected by: *stiction* - the friction developed between the pen and the paper, resulting in delayed response of the chart recorder; and *overshoot* - the amount of over-, or under- measurement as a result of the pen assembly having a finite inertia. These effects combine to reduce the accuracy of the q_c and f_s plots.
- *Limitations of Thermal Paper* - While thermal paper chart recorders can overcome the effects of stiction and overshoot, the quality of their output deteriorates with exposure to ultra-violet light. As a result, care needs to be taken when operating these chart recorders in bright field situations. In addition, the quality of thermal paper deteriorates with time resulting in a loss of resolution in the q_c and f_s plots.

In order to overcome these limitations modern CPT data acquisition systems are based on digital computers. Jamiolkowski et al. (1985) suggested that the potential of the CPT has been greatly improved by recent advances in data acquisition systems.

De Ruiter (1981, 1982) described a system, used by Fugro Consultants International Pty. Ltd. in Holland, designed to produce precise data with a high degree of resolution, which is shown in Figure 3.1. De Ruiter (1981, 1982) stated that the most important part of the data acquisition system is the signal conditioner, to which all major elements are connected. The conditioning unit supplies the excitation voltages for the penetrometer, and amplifies the returned signal to useable and calibrated levels. In addition, it receives pulses from a rotary encoder which measures depth of the cone penetrometer. These pulses, 1,000 per metre, are used to control chart displacement, and to trigger a digital data-logger. The system uses an analogue chart recorder, in addition to the digital acquisition system, to verify equipment operation and to allow on-site evaluation of the CPT.

Currently, there are a limited number of data acquisition systems that are commercially available for the CPT. However, those that can be purchased are generally:

- *Spacing of measured data may not suit spatial variability research* - As discussed previously, studies focusing on spatial variability require large amounts of relatively closely-spaced data. Many of the data acquisition systems commercially available record data at spacings not ideal for this research.
- *Expensive* - Their cost is generally prohibitive to research projects with limited budgets.

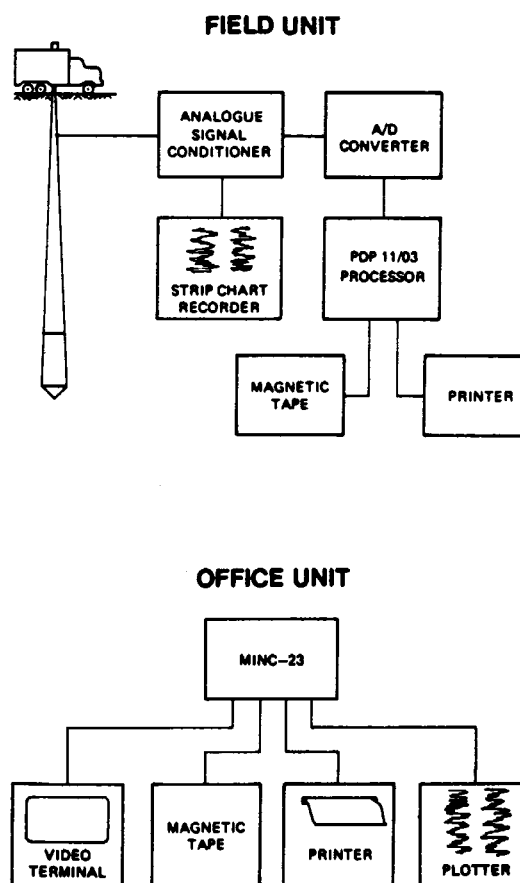


Figure 3.1 Fugro Consultants International Pty. Ltd. data acquisition system.
(After de Ruiter, 1982).

- *Difficult to modify* - Often the design and details of the elements of the data acquisition system are not supplied. Consequently the individual components are difficult to modify to suit requirements that may arise in research. In addition, maintenance of the system is made more difficult because of the unavailability of these design specifications.
- *Errors and limitations of the system and individual components are uncertain* - Since the design details are generally not supplied with the system, any errors, limitations, or uncertainties associated with the elements of the system are difficult to identify and quantify.

Due to the limitations of commercially available data acquisition systems for the CPT, it was decided to design and develop a system at the University of Adelaide, primarily suited to the investigation of spatial variability of soils. In addition, the Department of Civil and Environmental Engineering at the University of Adelaide uses the CPT for consulting projects and, as a result, the data acquisition system should also meet the criteria necessary for this type of work.

3.3 DESIGN CRITERIA FOR DATA ACQUISITION SYSTEM

As mentioned in §2.4.2, three standards have been established for the CPT that are relevant to this research, namely: ISOPT-1 (De Beer et al., 1988); *ASTM D3441* (American Society for Testing and Materials, 1986); and *AS 1289.F5.1* (Standards Association of Australia, 1977). Minimum requirements for the accuracy of CPT measurements have been specified by these standards, as well as other aspects of the CPT. They have, however, not given exclusive specifications regarding all aspects of the CPT and, where relevant, other literature has been examined. Summarised below are criteria that the data acquisition system and associated CPT equipment should meet.

- *Depth measurements* - De Ruiter (1981) stated that depth measurements obtained by the Fugro Consultants Pty. Ltd. depth encoder has an accuracy of 50 mm in 20 metres, that is, 0.25%.
- *Measurements of q_c and f_s* - ISOPT-1 (De Beer et al., 1988) specified that the precision of measurements of q_c and f_s shall be the greater of 5% of the measured value and 1% of the maximum value of the measured resistance in the layer under consideration.
- *Closely-spaced data* - Measurements of q_c , f_s , and depth should be recorded at spacings close enough to enable accurate assessments of spatial variability to be carried out (Jamiolkowski et al. (1985) suggested at least 20 mm).
- *Data storage* - The CPT measurements shall be stored on computer disk to enable reliable and efficient processing of data.
- *Direct accessibility of data during testing* - ISOPT-1 (De Beer et al., 1988) recommended that data should not be stored directly on a tape without the facility to view the data throughout the test.
- *Sampling rate of data* - Jamiolkowski et al. (1985) recommended that the data should be sampled at a rate of between 0.1 and 1 second, whilst Lunne et al. (1986) suggested a 1 second sample interval is normally adequate.
- *Robust equipment* - The data acquisition system and associated equipment shall be robust enough to withstand the rigours of field testing in a variety of weather conditions.

In designing the University of Adelaide data acquisition system each of the criteria listed above were specified and, in order to obtain ample data for spatial variability analyses, a

measurement spacing of 5 mm was targeted. The following section details the design and construction of this data acquisition system.

3.4 DESIGN AND CONSTRUCTION OF UNIVERSITY OF ADELAIDE DATA ACQUISITION SYSTEM

3.4.1 Equipment

The cone penetration test requires that three parameters be measured: cone tip resistance, q_c ; sleeve friction, f_s ; and the depth of the cone penetrometer, z . As detailed in Chapter 2, the electric cone penetrometer is the basis of the CPT which measures both q_c and f_s . However, there is no technique that is specifically referred to by ISOPT-1 (De Beer et al., 1988), *ASTM D3441* (American Society for Testing and Materials, 1986), or *AS 1289.F5.1* (Standards Association of Australia, 1977) for the measurement of depth. The electric cone penetrometer and the *depth box* - the instrument developed by the author to measure depth, are discussed below.

3.4.1.1 Electric Cone Penetrometer

The University of Adelaide electric cone penetrometer was manufactured by Macsil Pty. Ltd. and meets the guidelines specified by ISOPT-1 (De Beer et al., 1988), *ASTM D3441* (American Society for Testing and Materials, 1986), or *AS 1289.F5.1* (Standards Association of Australia, 1977). These guidelines were briefly summarised in §2.4.2.

3.4.1.2 Depth Box

In order to measure accurately the depth of the electric cone penetrometer a device, termed the *depth box*, was developed. This instrument was designed to meet the criteria detailed in §3.3. The depth box, which is seated on the ground, consists of a thin metallic cable, one end of which is attached to the hydraulic ram which drives the cone penetrometer into the ground, and the other end is wound around a metal drum, as shown in Figure 3.2.

A shaft encoder is connected to the shaft of the drum and, as a result, a pulse is transmitted every one-five-hundredth of a revolution of the drum. Since the metal drum has an external diameter of 100 mm, each pulse corresponds to 0.62832 mm of travel of the cable and, hence, depth of the cone penetrometer. A light torsional spring is also attached to the

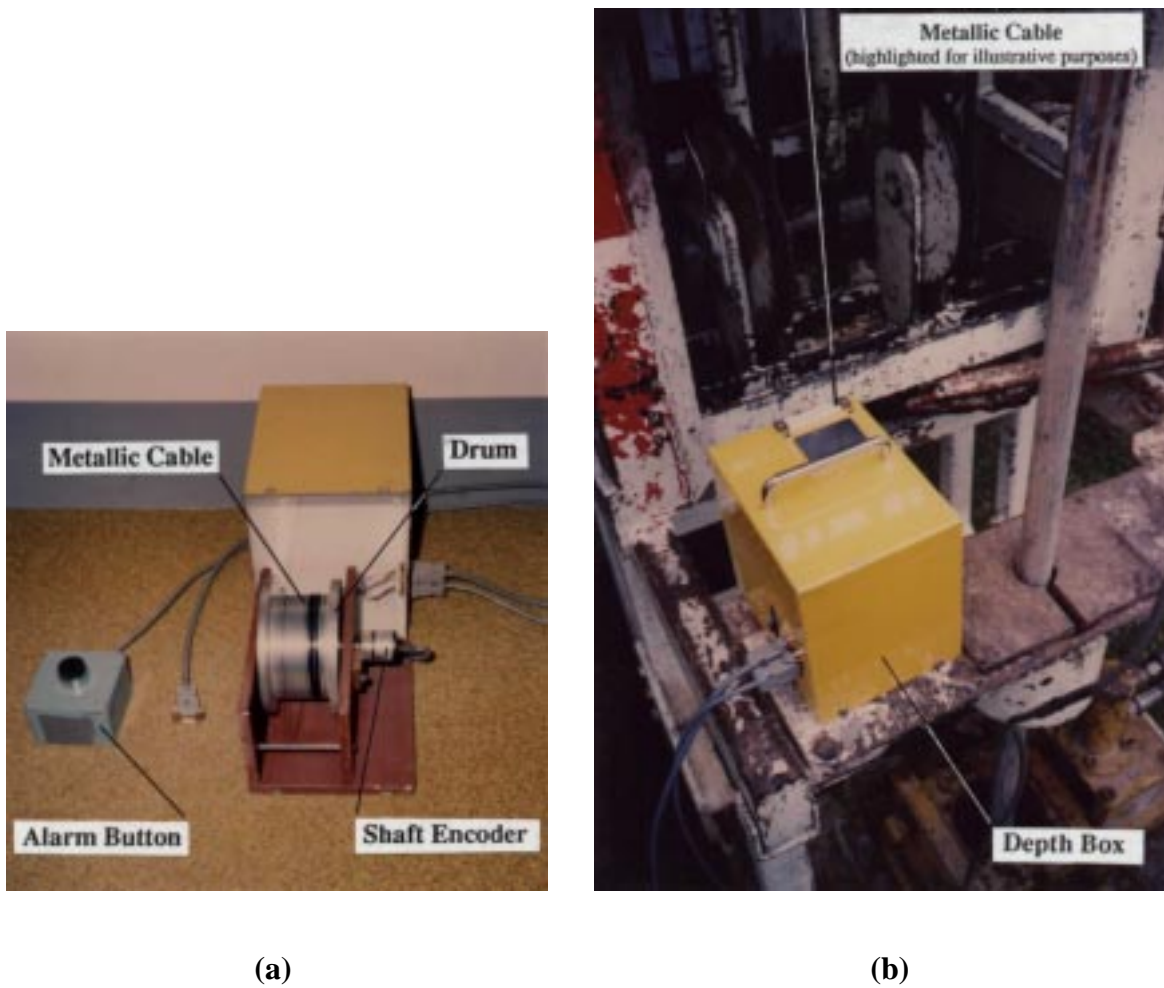


Figure 3.2 Depth box: (a) internal details, (b) attached to drilling rig.

metal drum so that as the cable is retracted into the depth box, which corresponds to the cone penetrometer being driven into the ground, it is automatically rewound onto the drum. By counting the number of pulses, and the phase of each pulse, it is possible to accurately determine the depth of the cone penetrometer and whether it is being driven into the soil, or whether it is being removed from it.

Connected to the depth box is an *alarm button* which consists of a warning alarm and an electronic button. The purpose of the alarm button is to signify that the CPT has commenced, or continued, after the addition of further drilling rods. The alarm button will be described in greater detail in §3.4.2.1(iii).

3.4.2 Measurement and Recording

In order to convert the electrical signals being transmitted by the electric cone penetrometer and the depth box to measurements of q_c , f_s and depth, a system of electric components are required. These include amplifiers, signal conditioners and analogue-to-digital (A/D) converters. In addition, software is required to interpret and convert the electrical information to meaningful units, such as MPa, kPa and mm, and to store these data for subsequent post-processing. Details of the hardware and software developed to measure q_c , f_s and depth are described below.

3.4.2.1 Hardware

The measurements of q_c , f_s and depth are acquired, interpreted and stored by two elements of hardware; the *microprocessor interface* and the *micro-computer*. In addition, the *alarm button* is used to signify the commencement, or continuation, of the CPT. Each of these elements are treated in turn, below.

(i) Microprocessor Interface

The microprocessor interface, shown schematically in Figure 3.3, consists of the following components:

- Microprocessor unit (MPU);
- 8 kb (kilobytes) \times 8 bit EPROM chip (erasable programmable read only memory);
- 8 kb \times 8 bit RAM (random access memory);
- Operational amplifiers;
- RS232 interface;
- Liquid crystal displays (LCD).

The microprocessor interface performs a variety of tasks. These include the following:

- *Multiplexing* - The MPU reads two input channels: cone tip resistance and sleeve friction. Software stored on the EPROM controls when the MPU reads each of these two channels. This software is discussed in §3.4.2.2((i)). Depth measurements, that is, pulses from the depth box's shaft encoder, are *interrupt driven*. In other words, the MPU immediately processes these measurements as soon as an interrupt signal is received.

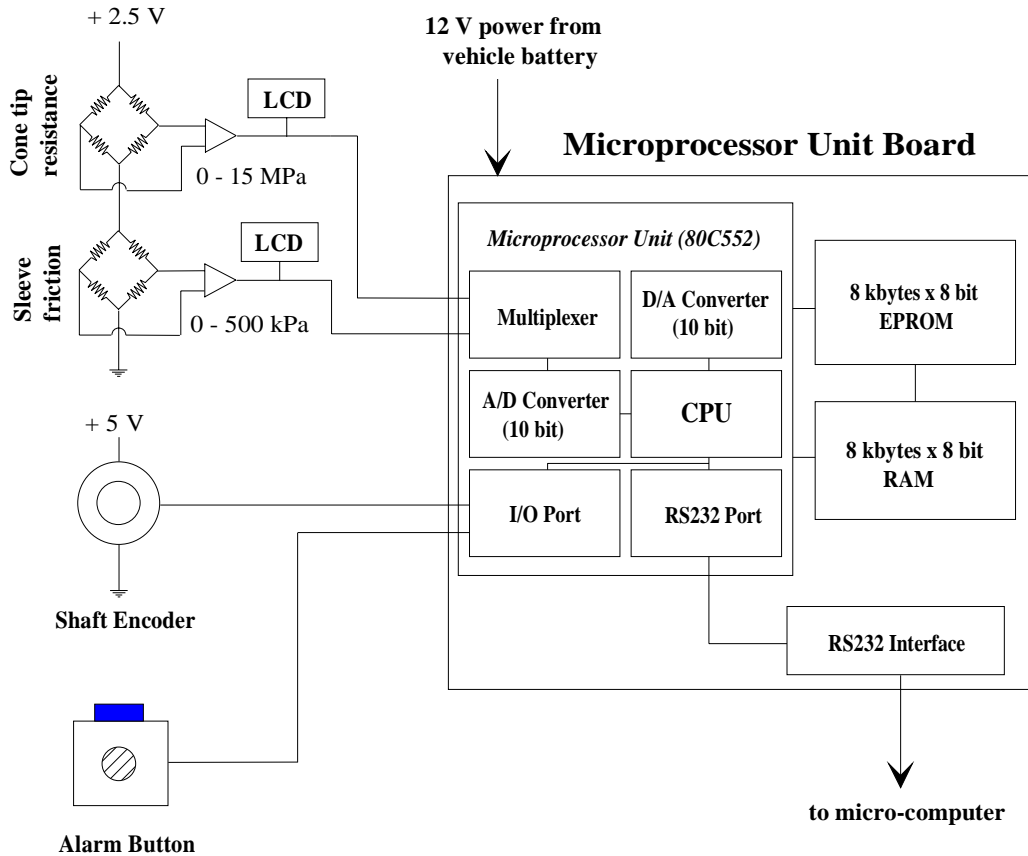


Figure 3.3 Schematic diagram of the microprocessor interface.

- *I/O Port Data Transmission* - The depth box and alarm button are read via the I/O (input/output) port.
- *Signal Conditioning and Amplification* - The q_c and f_s analogue signals arrive from the electrical cone penetrometer at microvolt level, and are scaled by the operational amplifiers to 0 to 1V, so that q_c is in the range 0 to 15 MPa, and f_s is in the range of 0 to 500 kPa. This scaling is attained by setting an appropriate gain on each of the two operational amplifiers. In addition, the microprocessor interface is fitted with a *cone amplification switch* which, when activated, multiplies the cone measurements by a factor of five. This facility is useful when taking measurements in soft soils, as it increases the resolution of the q_c measurements by 5 times. Because of the range of q_c measurements, the cone amplification switch can be used only for values of q_c less than, or equal to, 3 MPa.
- *Analogue to Digital (A/D) Conversion* - So that the analogue information can be transferred to the micro-computer, data are converted to digital format. This is performed by a 10 bit A/D converter located on the MPU chip. As a result, q_c and f_s have a resolution of 2^{10} , or 1,024 bits.

- *Data Storage and Transfer* - Data are temporarily stored in RAM and transferred to the micro-computer via the RS232 serial data bus every 5 mm travel of the cone penetrometer. Data are transferred to the micro-computer in the following format:

$D\oplus\oplus\oplus\oplus\oplus^8$	depth measurements (number of pulses from the shaft encoder);
$c\otimes\otimes\otimes\otimes^9$	q_c measurements;
$C\otimes\otimes\otimes\otimes$	q_c measurements when the cone amplification switch has been activated, that is, 5 times the actual value;
$S\otimes\otimes\otimes\otimes$	f_s measurements;
$M\otimes\otimes\otimes\otimes$	maximum depth reached before the cone penetrometer was raised;
X	when the cone has been raised more than 200 mm.

(ii) Micro-Computer

Measurements of q_c , f_s and depth which are amplified, conditioned, stored and transmitted by the microprocessor interface are scaled, displayed and saved onto floppy disk on an IBM compatible micro-computer. An AMSTRAD PPC640 portable personal computer was chosen for this task, and is shown in Figure 3.4. It is a relatively inexpensive unit, with a cost below \$1,000, and supports the following features:

- IBM PC-XT compatible with an 8 MHz clock;
- 640 kb of Random Access Memory (RAM);
- $2 \times 3.5''$, 720 kb floppy disk drives;
- Liquid Crystal Display Monitor with in built facility for external CGA monitor;
- Compact and fully portable with facility for mains, 12V and battery power supplies;
- Modem.

A number of these features make this computer attractive for field data acquisition of CPT measurements, particularly: its portability and relative robustness; IBM compatibility; low initial operation and maintenance costs; its facility to be powered by either 12V supply or dry cell batteries; and its ability to store the measured data onto floppy disks.

(iii) Alarm Button

The alarm button, mentioned earlier, is located adjacent to the drilling rig operator and its primary function is to transmit a signal to the microprocessor interface to commence

⁸ $\oplus\oplus\oplus\oplus\oplus$ refers to a 16 bit number; that is, in the range 0 and 65,535 (examples are given in §3.1.1.2).

⁹ $\otimes\otimes\otimes\otimes$ refers to a four digit, 10 bit number in the range 0 and 1,023.



Figure 3.4 Micro-computer and microprocessor interface.

sampling. That is, once the cone penetration test is ready to commence, or continue, the operator presses the button, thereby communicating to the microprocessor interface to begin reading its inputs.

A warning alarm sounds when the drilling head has been raised by more than 200 mm, indicating that sampling has ceased. This situation occurs when additional drilling rods are connected to the cone penetrometer in order to continue the CPT sounding, or the sounding has been completed and the cone penetrometer is being withdrawn from the ground. The alarm continues to sound, informing the operator that data acquisition will not continue until the button is depressed.

3.1.1.2 Software

The microprocessor interface and micro-computer are each controlled by software stored in their respective memories. The microprocessor interface software, *CPTRead*, and the micro-computer software, *CPTest*, are each discussed in the following sections.

(i) *CPTRead*

CPTRead, is permanently stored on the EPROM chip of the microprocessor interface. This software, written in assembly language, essentially reads the cone tip resistance and sleeve friction load cells, as well as the depth box and alarm button. In addition, *CPTRead* temporarily stores these data in the microprocessor interface's RAM, and at various stages, transfers the data to the micro-computer. A simplified flowchart of the *CPTRead* software is shown in Figure 3.5.

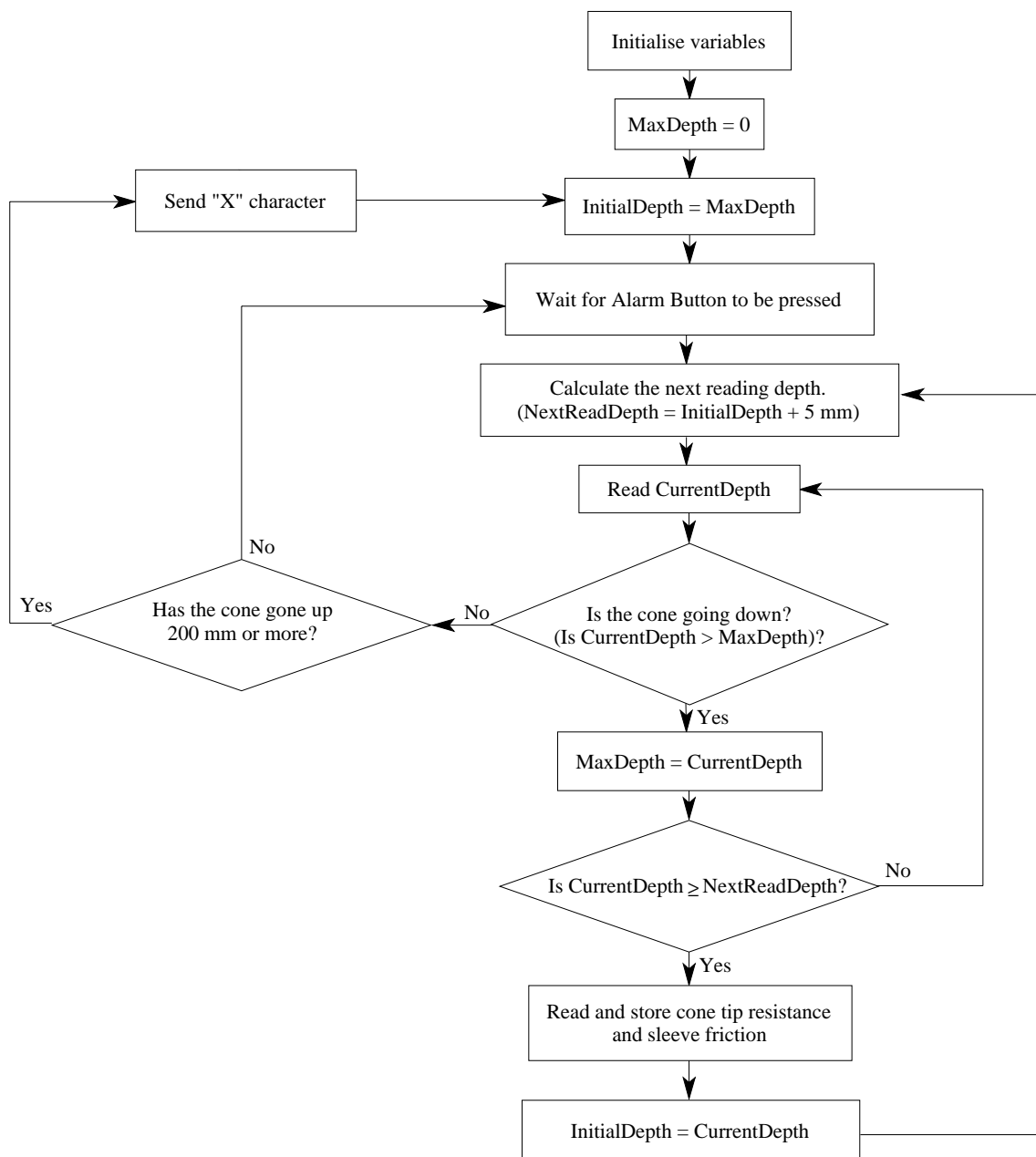


Figure 3.5 Flowchart of the microprocessor interface software, *CPTRead*.

In addition, *CPTRead* has an in built filtering algorithm for reducing the effects of electrical noise. This aspect of *CPTRead* is detailed in §3.2.3.

(ii) *CPTTest*

The program *CPTTest*, written in Turbo Pascal^{®10} Version 6.0, is the interface between the operator of the CPT and the data acquisition system. Every 5 mm of travel of the cone penetrometer, the microprocessor interface reads the cone and sleeve load cells and sends depth, cone tip resistance and sleeve friction data to the RS232 port of the micro-computer. An example of these data is shown below.

D2438
c0167
S0271

CPTTest continually scans the RS232 port of the micro-computer for data being transferred from the microprocessor interface. Data are read, one character at a time, and then reassembled to form a series of three, string variables. Referring to the example above, the first string would be “D2438”; the second “c0167”; and the third “S0271”. The first letter of each string identifies the type of measurement. For example, a “D” character refers to a depth measurement; a “c” character refers to a cone tip resistance measurement; and so on, as described previously in §3.4.2.1.

In order to obtain the scaled values of depth, q_c and f_s , the digital values are multiplied by conversion factors, as shown in Table 3.1, which were calculated using the relationships shown in Table 3.2. Both of these tables are discussed in greater detail in §3.2.1.

Table 3.1 Data conversion factors.

First Character	Measurement	Conversion Factor	Unit	Range
D or M	Depth	0.62832	mm	0 to 41,176 mm
c	q_c	0.014648	MPa	0 to 15 MPa
C	$q_c \times 5$	0.0029296	MPa	0 to 3 MPa
S	f_s	0.48828	kPa	0 to 500 kPa

¹⁰ Turbo Pascal is a registered trademark of Borland International, P.O. Box 660001, Scotts Valley, CA, USA, 95066-0001.

Table 3.2 Relationships used to calculate data conversion factors.

Measurement	Relationship
Depth	$1 \text{ pulse}^{11} = \frac{\pi D}{500} = \frac{\pi \cdot 100}{500} = \frac{\pi}{5} \text{ mm}$
q_c	$1 \text{ mpb}^{12} = \frac{15}{1024} \text{ MPa}$
f_s	$1 \text{ mpb} = \frac{500}{1024} \text{ kPa}$

Once the data have been read and converted to string variables, the data are then scaled and stored in an array. Again referring to the example shown above, the first string being a depth measurement, and hence the number of pulses read from the depth box's shaft encoder, is multiplied by the depth conversion factor of 0.62832, as shown in Table 3.1. This yields the depth of cone travel since the alarm button was last pressed. In this example the depth read is 2,438 pulses, or 1,532 mm¹³. This depth reading of 1,532 is then added to the variable *MaxDepth*, the depth of the cone penetrometer below the ground surface prior to the addition of further drilling rods, in order to obtain the depth of the cone penetrometer. For the purpose of illustration, let us assume that *MaxDepth* = 3,538 mm. The depth of the cone penetrometer is then 3,538 + 1,532 = 5,070 mm. This value of *total depth* is then stored in the micro-computer's RAM in an array variable, *Depth[i]*; *i* being the integer number of measurements read since the alarm button was last pressed. Again, for illustrative purposes, let us assume that this reading is the 302nd since the CPT continued. As a result, *Depth[302]* would be given the value 5,070.

Succeeding data are controlled in the same fashion. The second string, "c0167", a cone tip resistance reading, is multiplied by the cone conversion factor of 0.014648 to obtain a q_c measurement of 2.45 MPa. This value is then stored in the array variable *qc[i]*. In this example, *qc[302]* would be given the value 2.45. Similarly, the third reading of "S0271", a sleeve friction measurement, is multiplied by the sleeve conversion factor of 0.48828 to obtain an f_s measurement of 132.3 kPa. This value is then stored in the array variable *fs[i]*. Again, in this example, *fs[302]* would be given the value 132.3.

As data are being read, they are simultaneously shown graphically on the micro-computer's display, an example of which is shown in Figure 3.6. In this way, data can be visually

¹¹ 1 pulse refers to a signal output by the depth box's shaft encoder.

¹² 1 mpb refers to 1 microprocessor bit. e.g. c0001 = 15 / 1024 MPa (cf. §3.5.1).

¹³ 2438 × 0.62832 = 1,532 mm.

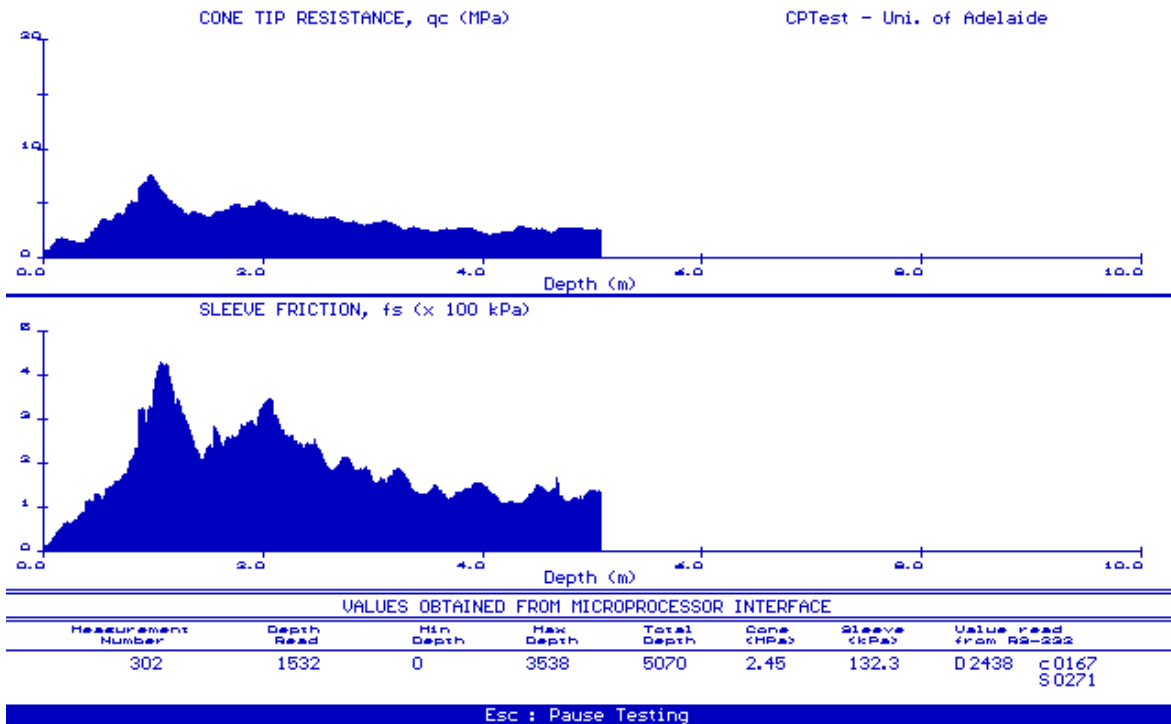


Figure 3.6 An example of the *CPTest* screen.

monitored and interrogated in order to assess whether the test is being performed correctly and whether it is giving sensible results. This is in accordance with ISOPT-1 (De Beer et al., 1988) as described in §3.3.

Once the cone penetrometer has been raised more than 200 mm, the microprocessor interface sends an “X” character to the micro-computer. Upon receiving this signal, which implies that sampling has temporarily ceased due to the addition of further drilling rods, *CPTest* again reads the depth box to determine the depth of the cone penetrometer and assigns this depth to the variable *MaxDepth*. It is necessary for *CPTest* to read the depth box at this *maximum depth*, since the depth of the cone penetrometer tip may not be at a multiple of 5 mm. As a consequence, the depth of the penetrometer tip can be monitored more accurately.

In addition, *CPTest* saves all data previously stored in the array variables, $Depth[i]$, $qc[i]$ and $fs[i]$, in the micro-computer’s RAM, to a file on a 3.5” floppy disk for later post-processing. Data in the file are arranged in three columns: Depth of the cone tip below the ground surface (mm); q_c (MPa); and f_s (kPa); and are saved in ASCII format - each column being separated by a *tab* (ASCII #9) character.

3.1.2 Post-Processing

A number of computer programs have been developed to enable post-processing of the CPT data recorded by *CPTest*. All programs were written in Turbo Pascal Version 6.0, because of its excellent speed and graphical capabilities at the time of development. A brief description of each of the programs is given below.

3.1.2.1 *CPTView*

The program *CPTView* was developed to allow the user to inspect, visually, the cone penetration test data on the screen, both in the field and at a later date. Cone tip resistance, sleeve friction and friction ratio are simultaneously plotted on the screen, an example of which is shown in Figure 3.7. In addition, *CPTView* provides the following facilities:

- The entire CPT sounding can be plotted on a single screen;
- A range of depths can be plotted on a single screen, for example 2.5 metres to 5.0 metres;
- The entire recorded depth can be plotted and stepped in windows of user-specified depth;
- The numerical values of q_c , f_s and F_R , can be displayed for inspection.

3.1.2.2 *CPTPlot*

The program *CPTPlot* was developed to enable the user to prepare report quality plots and tables of the CPT data stored on disk. Figure 3.8 shows an example of a graphical plot and Figure 3.9 an example of the recorded CPT data printed in tabular format, each of which has been produced by the *CPTPlot* program.

CPTPlot creates a PostScript¹⁴ file (*filename.ps*) which enables the plot, or table, to be output to a laser printer which supports the PostScript language, such as the Apple Laser-Writer.

In addition, *CPTPlot* shifts the sleeve friction data back by 75 mm. As detailed in §2.4.4, this is necessary because the cone tip and the friction sleeve are physically separated by a distance of 75 mm. As discussed previously, the microprocessor interface simultaneously

¹⁴ PostScript is a graphical language for laser printers developed by Adobe Systems, Inc.

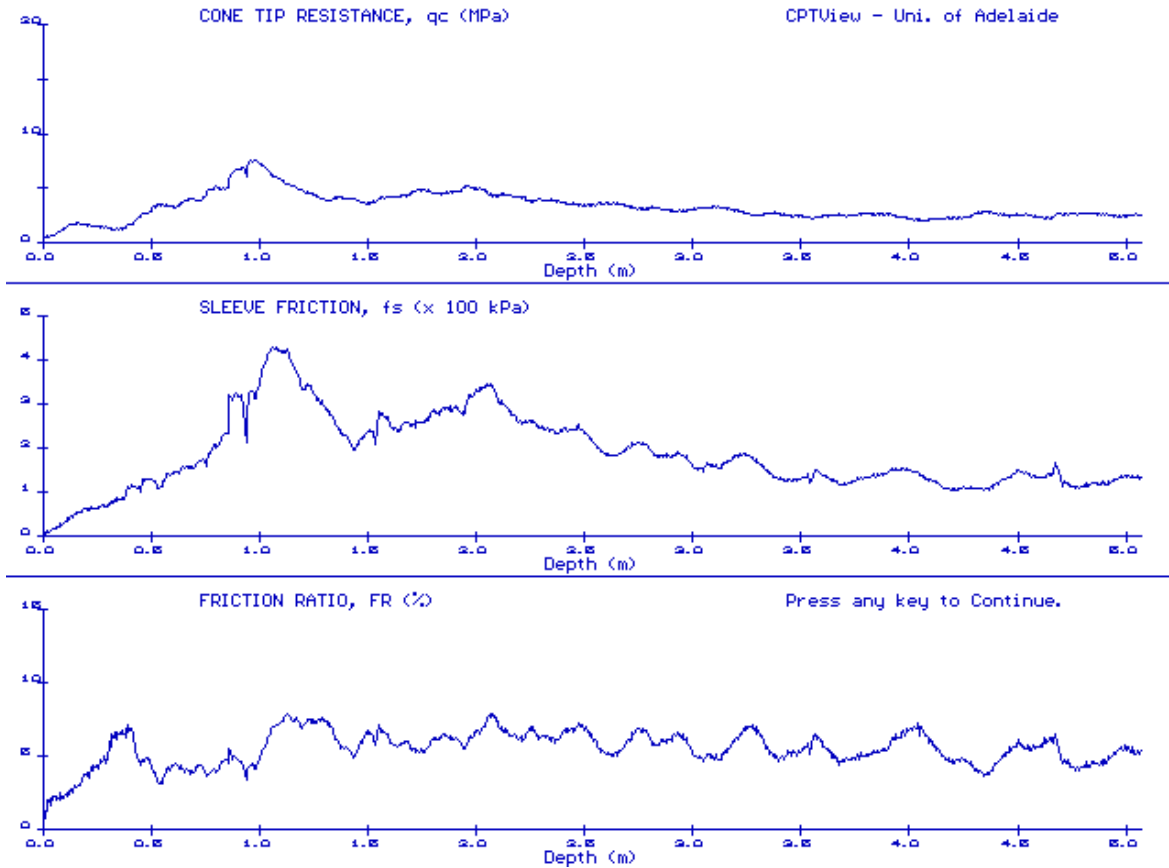


Figure 3.7 An example of a screen plot produced by *CPTView*.

reads values of q_c and f_s at the depth of the cone penetrometer tip. As a result, the actual depth corresponding to the f_s measurements is 75 mm less than that indicated by the depth box. Hence, friction ratio, F_R , calculations, based on data that has not been corrected for this shift, will yield misleading results (Schmertmann, 1978).

As discussed previously in §3.1.1.2(ii), measurements of q_c and f_s are read at depth intervals of 5 mm. However, while the recorded depths are separated by 5 mm, they need not be divisible by 5. This is due to the fact that *MaxDepth*, the maximum depth of the cone penetrometer tip prior to the addition of further drilling rods, may not be at a depth divisible by 5. For example, *MaxDepth* may be 797 mm and, when the CPT is continued, the next depth at which readings are taken will be $797 + 5$ mm, or 802 mm; a depth not divisible by 5. When the f_s measurements are shifted by 75 mm, there may not be a value of q_c corresponding to this depth, ie 652 mm. As a result, two columns of depths would need to be provided: one for values of q_c , and the other for the shifted values of f_s .

So that only one column of depth measurements need be maintained, *CPTPlot* first

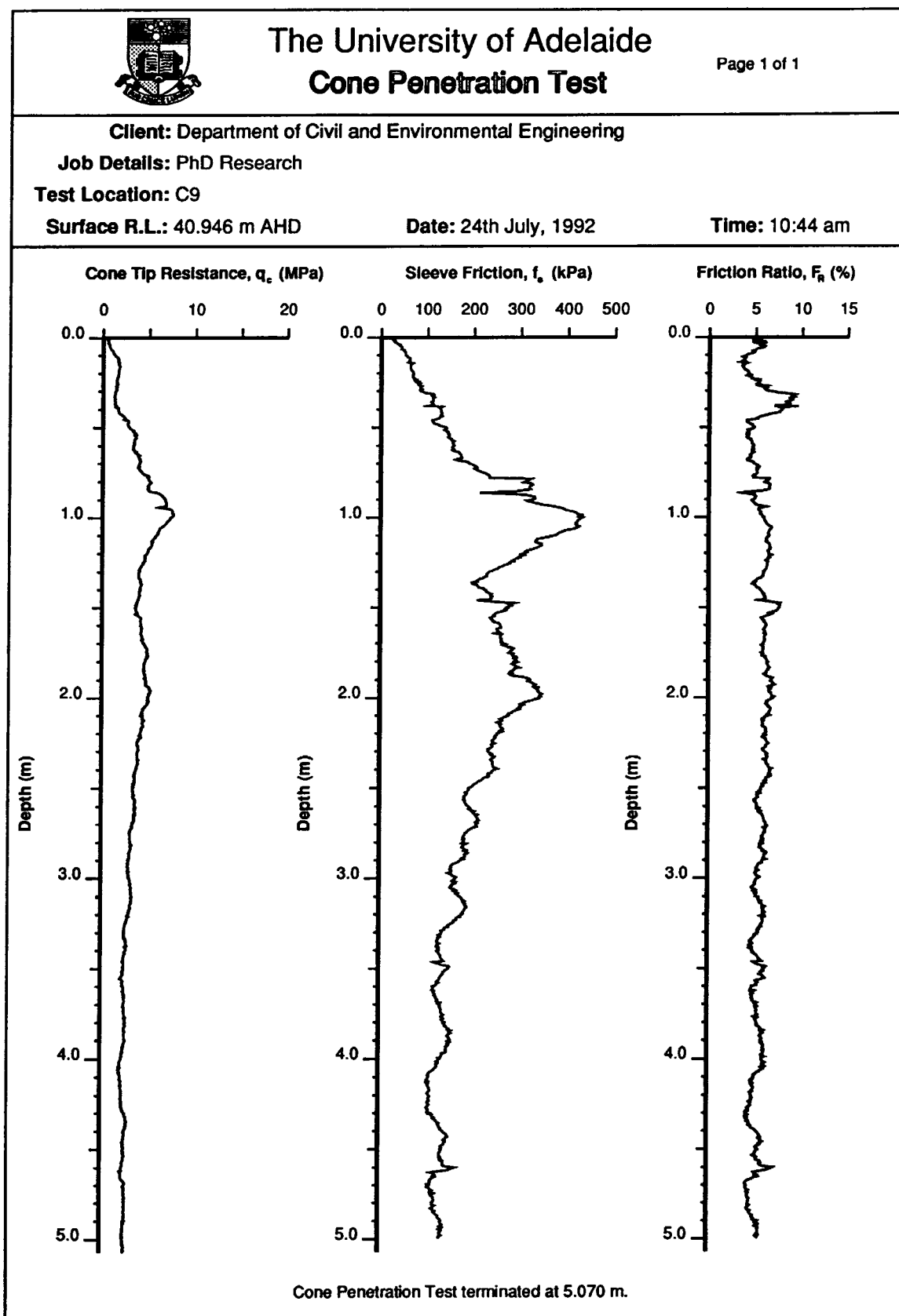


Figure 3.8 An example of a graphical plot produced by *CPTPlot*.

		The University of Adelaide Cone Penetration Test		Page 1 of 12			
Client: Department of Civil and Environmental Engineering Job Details: PhD Research Test Location: C9 Surface R.L.: 40.946 m AHD Date: 24th July, 1992 Time: 10:44 am							
Depth (m)	Cone Tip Resistance q_c (MPa)	Sleeve Friction f_s (kPa)	Friction Ratio F_R (%)	Depth (m)	Cone Tip Resistance q_c (MPa)	Sleeve Friction f_s (kPa)	Friction Ratio F_R (%)
0.005	0.48	21.00	4.38	0.215	1.66	67.00	4.04
0.010	0.56	27.40	4.89	0.220	1.55	67.40	4.35
0.015	0.51	24.90	4.88	0.225	1.52	69.40	4.57
0.020	0.53	28.80	5.43	0.230	1.57	70.40	4.48
0.025	0.62	28.30	4.56	0.235	1.45	76.20	5.26
0.030	0.54	33.20	6.15	0.240	1.47	73.30	4.99
0.035	0.66	34.20	5.18	0.245	1.48	79.70	5.39
0.040	0.70	39.60	5.66	0.250	1.44	76.20	5.29
0.045	0.72	39.10	5.43	0.255	1.55	83.10	5.36
0.050	0.72	43.00	5.97	0.260	1.55	78.70	5.08
0.055	0.75	44.00	5.87	0.265	1.47	79.70	5.42
0.060	0.81	44.00	5.43	0.270	1.42	85.50	6.02
0.065	0.87	43.50	5.00	0.275	1.51	82.60	5.47
0.070	1.01	49.40	4.89	0.280	1.42	83.10	5.85
0.075	1.06	49.40	4.66	0.285	1.38	85.00	6.16
0.080	1.04	50.30	4.84	0.290	1.48	87.50	5.91
0.085	1.09	52.30	4.80	0.295	1.38	82.60	5.99
0.090	1.17	52.30	4.47	0.300	1.35	84.10	6.23
0.095	1.26	52.30	4.15	0.305	1.30	91.40	7.03
0.100	1.30	52.30	4.02	0.310	1.28	93.80	7.33
0.105	1.42	55.20	3.89	0.315	1.29	110.50	8.57
0.110	1.54	55.20	3.58	0.320	1.23	113.40	9.22
0.115	1.57	61.10	3.89	0.325	1.23	109.00	8.86
0.120	1.63	61.60	3.78	0.330	1.26	111.90	8.88
0.125	1.61	61.10	3.80	0.335	1.26	115.30	9.15
0.130	1.66	60.10	3.62	0.340	1.29	110.90	8.60
0.135	1.61	61.10	3.80	0.345	1.29	111.40	8.64
0.140	1.73	58.20	3.36	0.350	1.26	111.90	8.88
0.145	1.66	66.50	4.01	0.355	1.28	110.90	8.66
0.150	1.72	63.00	3.66	0.360	1.30	108.00	8.31
0.155	1.72	63.50	3.69	0.365	1.29	110.90	8.60
0.160	1.80	62.60	3.48	0.370	1.26	109.50	8.69
0.165	1.77	63.00	3.56	0.375	1.29	111.90	8.67
0.170	1.74	63.50	3.65	0.380	1.45	101.70	7.01
0.175	1.72	63.50	3.69	0.385	1.36	130.00	9.56
0.180	1.69	64.50	3.82	0.390	1.66	125.10	7.54
0.185	1.63	65.00	3.99	0.395	1.60	127.10	7.94
0.190	1.63	67.90	4.17	0.400	1.61	N/A	N/A
0.195	1.63	67.90	4.17	0.405	1.66	128.50	7.74
0.200	1.63	68.90	4.23	0.410	1.69	128.50	7.60
0.205	1.64	67.90	4.14	0.415	1.70	129.50	7.62
0.210	1.58	69.40	4.39	0.420	1.82	131.00	7.20

Figure 3.9 An example of a data table produced by *CPTPlot*.

rationalises the depths to values divisible by 5. For example, a depth of 797 mm would be rationalised to 795 mm. The rationalisation algorithm obeys the following rules:

1. If the last digit is a 0, 1, or 2, then the last digit becomes a 0.
e.g. 200, 201 and 202 become 200 mm.
2. If the last digit is a 3, 4, 5, 6, or 7, then the last digit becomes a 5.
e.g. 203, 204, 205, 206, and 207 become 205 mm.
3. If the last digit is an 8, or 9, then the depth is increased by 2, or 1, respectively.
e.g. 208, and 209 become 210 mm.

The rationalisation process assumes that each measurement of q_c and f_s is constant within its soil element of 5 mm in height. Such an assumption is appropriate for elements of soil with such small dimensions. Once rationalisation of depths has been performed, the sleeve friction values can then be easily shifted back by 75 mm.

Occasionally, the distance between two successive depth measurements is 6 mm instead of 5 mm. The reason for this is explained in §3.2. As a result, rationalisation causes some depths to have no associated q_c or f_s measurements. For example, two successive depths may be 207 mm and 213 mm, that is, separated by 6 mm. Upon rationalisation, the 207 mm depth becomes 205 mm; and the 213 mm depth becomes 215 mm. Hence, the 210 mm depth has no associated q_c or f_s measurements. When this occurs, *CPTPlot*, assigns this *missing depth* of 210 mm with values of q_c and f_s equal to -99.99, implying that there are missing data associated with this depth. When plotting takes place, *CPTPlot* (and *CPTView*) ignores these missing data and draws a straight line from the next depth above and below this missing depth.

Rationalised plots of data spaced at 5 mm intervals are indistinguishable from unrationalised plots. Figure 3.8 shows an example of a plot performed on rationalised data, and Figure 3.10 shows the same data but plotted without depth rationalisation. As can be seen clearly from these figures, these missing data have negligible effect on the plots obtained by *CPTPlot*. Note the effect of rationalisation and sleeve friction shift on the plot of friction ratio versus depth. Omission of the shift can greatly affect the calculation of F_R yielding misleading results, as mentioned previously.

In addition, it will be seen later, in Chapter 5, that the rationalisation process simplifies the calculation of the semivariogram, autocorrelation and partial autocorrelation functions, as well as reducing their calculation times.

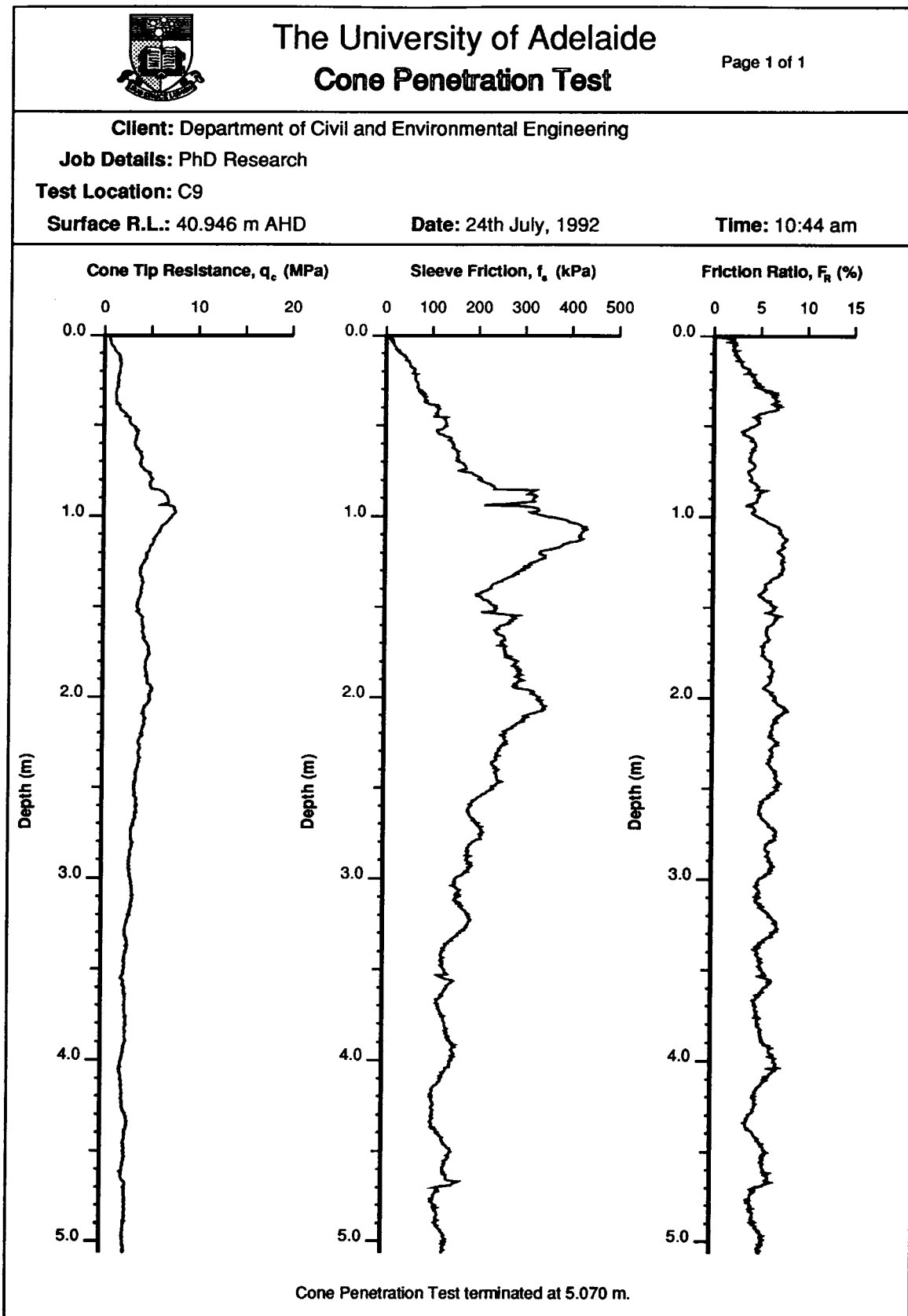


Figure 3.10 An example of an unrationalised graphical plot produced by *CPTPlot*.

In addition to those discussed previously, *CPTPlot* provides the following features:

- One, two or five metres of data, or the entire data set, can be plotted on a single page;
- Either of the following formats can be plotted:
 - cone tip resistance, sleeve friction and friction ratio, or
 - cone tip resistance, friction ratio and undrained shear strength.

3.1.2.3 *CPTPrint*

CPTPrint is a utility program which enables files created by *CPTPlot* to be printed by the Apple LaserWriter, or other PostScript printing device. So that the University of Adelaide crest can be printed at the top left hand corner of each plot, *CPTPrint* either copies or concatenates (depending on whether the user has a stand-alone PC¹⁵ connected to the printer, or a networked PC) the plot file with the university crest file (*crest.ps*). In this way, plot files can be stored more efficiently without duplicating the crest in each plot file. A typical 5 metre plot file is approximately 80 kb in size, whereas *crest.ps* is about 17 kb in size.

3.1.3 Description of Overall Data Acquisition System

The University of Adelaide data acquisition system was developed to enable closely-spaced CPT data to be measured and stored reliably, efficiently and accurately. As discussed previously, the data acquisition system can be divided into hardware and software. The hardware of the system consists of: the electric cone penetrometer; depth box; alarm button; microprocessor interface; and the micro-computer. The software of the data acquisition system consists of: *CPTRead*; *CPTTest*; *CPTView*; *CPTPlot*; and *CPTPrint*. A summary of the University of Adelaide data acquisition system for the cone penetration test is shown in flowchart form in Figure 3.11.

Each of the elements of the data acquisition system is powered by a 12V DC¹⁶ source, which is normally supplied by the lead-acid battery on board the drilling rig. The battery provides a stable power source which readily accommodates the requirements of the individual components of the system.

¹⁵ Personal Computer

¹⁶ Direct Current.

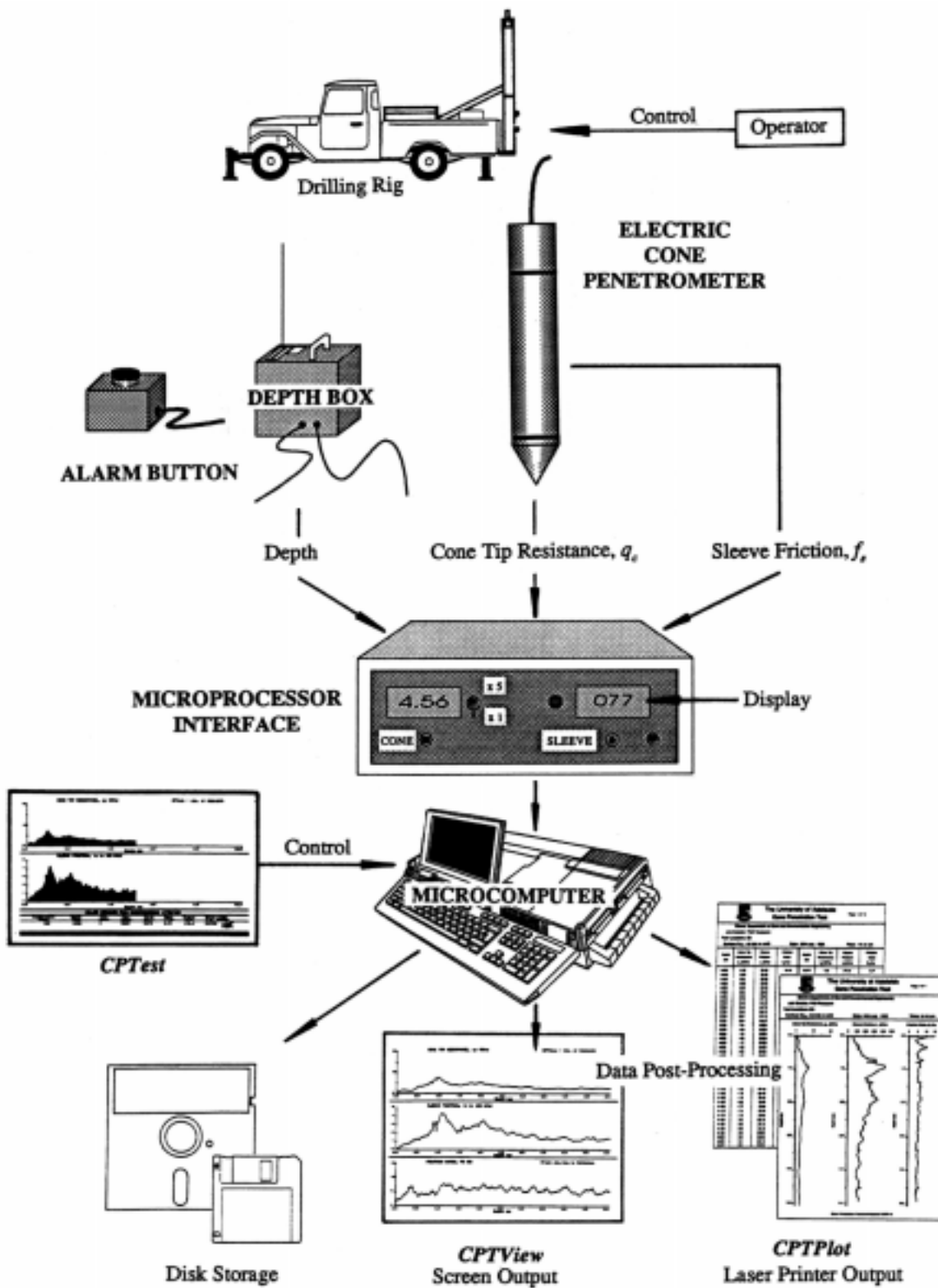


Figure 3.11 Flowchart of the University of Adelaide CPT data acquisition system.

3.2 CALIBRATION AND ACCURACY OF EQUIPMENT

Micro-computer based data acquisition systems, by themselves, do not increase the accuracy of the recorded data. The accuracy is derived from the design and quality of the individual elements and electrical components, as well as the quality and resolution of the microprocessor interface and associated software. This section details the procedures and the results of calibration tests undertaken to quantify the resolution, accuracy and errors associated with the University of Adelaide data acquisition system for the CPT, and compares these to the criteria specified in §3.3.

3.2.1 Resolution of Measured Data

The accuracy of the CPT data is governed by the resolution of the microprocessor interface and the depth box. Since the acquisition system stores and transfers data digitally, the recorded values of depth, cone tip resistance and sleeve friction, have a finite resolution. The resolution of depth measurements is dictated by the specifications of the shaft encoder, that is, 500 pulses per revolution of the encoder. Since the depth box drum has a diameter of 100 mm, the resolution of depth measurements is $\pi/5$, or 0.628 mm, as indicated previously in Tables 3.1 and 3.2.

The resolution of q_c and f_s measurements is governed by the number of bits that the A/D converter of the MPU can accommodate. The University of Adelaide microprocessor interface contains an MPU with a 10 bit A/D converter, as shown in Figure 3.5. Hence, since the MPU can accommodate 2^{10} , or 1,024 values, and the range of q_c and f_s measurements is 15 MPa and 500 kPa respectively, the resolution of cone tip resistance measurements is $15/1024$, or 14.65 kPa, and the resolution of sleeve friction measurements is $500/1024$, or 0.488 kPa, as shown in Tables 3.1 and 3.2.

3.2.2 Calibration Tests to Quantify Measurement Errors

This section discusses the results of calibration tests undertaken to quantify errors in the measurement of q_c , f_s and depth, and examines how well each of these compares with the criteria specified in §3.3.

3.2.2.1 Depth Box and Depth Measurements

The depth box, and the resulting measurement of depth, was calibrated by comparing the results output by the microprocessor interface to those given by a 500 mm long vernier and an 8 metre long steel tape. The results of the calibration are shown in Figure 3.12.

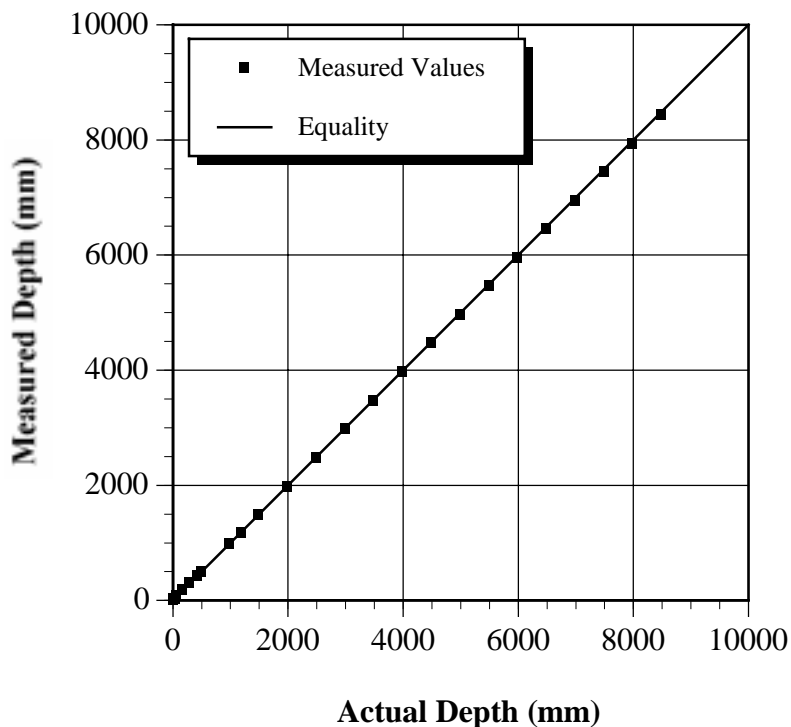


Figure 3.12 Depth box calibration curve.

The results of the calibration indicate that the accuracy of the depth box is 0.8%, that is, an error of 160 mm in 20 metres. While this error is approximately 3 times greater than that specified by de Ruiter (1981), it still represents a relatively high degree of accuracy.

This error can, in part, be attributed to the diameter of the metal drum of the depth box. As discussed in §3.1.1.2(ii), the microprocessor interface reads both the cone tip load cell and the sleeve friction load cell at depth intervals of 5 mm. However, every 38th measurement the distance between two successive depth readings is 6 mm instead of 5 mm. This is because of rounding of the depth conversion factor, indicated in Table 3.1. The microprocessor interface reads the q_c and f_s load cells every 8 pulses of the shaft encoder. However, a penetration depth of 5 mm actually corresponds to 7.9577 pulses, not eight. Every 38 readings, or 190 mm, this error accumulates to add 1 mm to the depth, that is, an inaccuracy of 0.53%.

3.2.2.2 Measurements of q_c and f_s

The electrical cone penetrometer that was used exclusively throughout the field testing phase of this research (discussed in Chapter 4) was calibrated using a 1,000 kN Avery loading frame, measured within a 0 to 50 kN loading range. This loading frame was considered to be suitably accurate, as it is regularly calibrated to NATA¹⁷ specifications. The calibration curves for the cone tip and sleeve friction load cells of the cone penetrometer are shown in Figures 3.13 and 3.14 respectively.

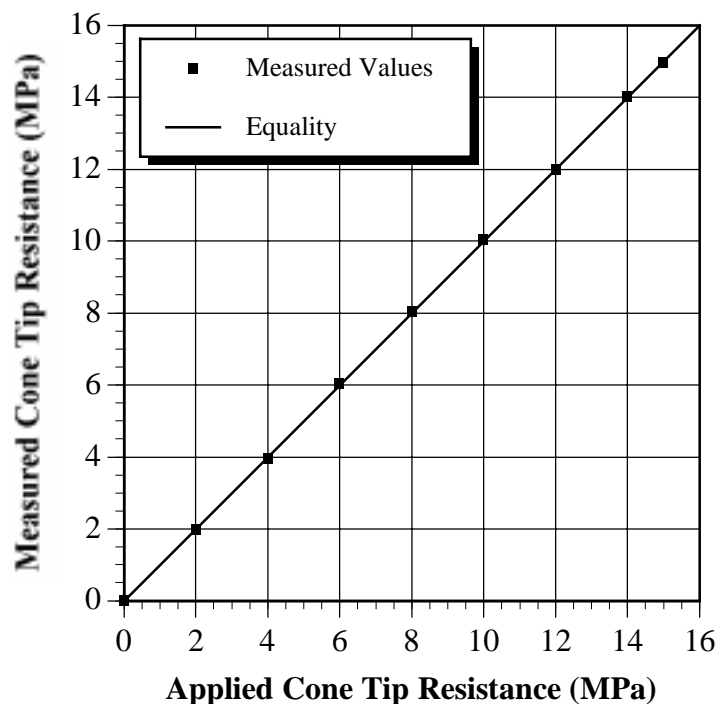


Figure 3.13 Cone penetrometer calibration curve - cone tip resistance.

The calibration of the cone tip resistance and sleeve friction load cells indicated a maximum measurement error of $\pm 1.0\%$ and $\pm 2.6\%$, respectively. These errors are well below the maximum allowable errors specified by ISOPT-1 (De Beer et al., 1988); that is, the greater of 5% of the measured value and 1% of the maximum value of the measured resistance in the layer under consideration, as discussed in §3.3.

¹⁷ National Association of Testing Authorities, Australia - an organisation which accredits testing and calibration laboratories.

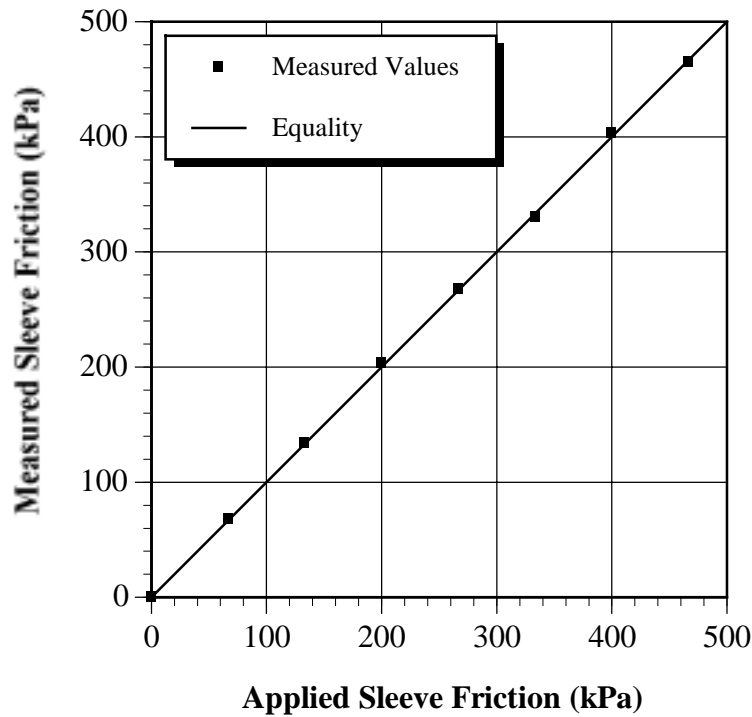


Figure 3.14 Cone penetrometer calibration curve - sleeve friction.

3.2.2.3 Microprocessor Interface Sampling Rate

The microprocessor interface has a sample interval of approximately 0.1 second. As mentioned in §3.3, Jamiolkowski et al. (1985) recommended that CPT data be sampled within the range of 0.1 to 1 second; whereas Lunne et al. (1986) suggested a 1 second sample interval is generally adequate. Depth measurements, or pulses from the depth box's shaft encoder, are *interrupt driven*. That is, the MPU immediately processes these measurements as soon as an interrupt signal is received. As a result, depth measurements can be recorded at a maximum sampling rate of 75 μ s, the sample and conversion rate of the microprocessor. At the standard penetration rate of 20 mm/s, the shaft encoder transmits approximately 32 pulses per second, which is equivalent to one pulse every 31 ms. As a result, a sample rate of 75 μ s, which is approximately 2,500 times greater than the rate of pulse transmission, is more than adequate to measure depth, q_c and f_s .

3.2.3 Random Measurement Errors

Random measurement errors, such as electrical noise, although generally small, are always present in this type of system in one form or another. In order to minimise random measurement errors, a filtering algorithm was built into the program *CPTRead*. This algorithm effectively uses a four level stack. Measured data are placed at the bottom of the

stack and each previous measurement is *rolled up* to the next level on the stack, the uppermost value being *rolled off* the stack. An average of the four values on the stack is calculated each time new data are measured. In this way a *rolling average* of the data is recorded. Davison and Hills (1983) suggested a similar method for reducing the fluctuation in readings due to electrical noise, described as *12% trimmed means*. This method stores 24 readings which are ranked, the top and bottom four are discarded, and the result stored in memory being the average of the remaining 16. Calibration tests, detailed in the preceding section, indicated that the rolling average method is an effective and adequate means of minimising the effect of electrical and random noise, and there was no need to adopt Davison and Hills' 12% trimmed means technique.

3.3 FIELD PERFORMANCE

Tests to assess the field performance of the University of Adelaide data acquisition system showed that it is relatively robust and performs well in a variety of weather conditions. The tests, however, highlighted two problems with the equipment and associated software: *falling off*; and *noise spikes*. These are shown in Figure 3.15 and are treated in-turn, below.

3.3.1 Falling Off

Assessment of the data measured during preliminary cone penetration tests indicated that at every addition of a drill rod the measured values of q_c and f_s dropped to zero, or a value well below that recorded immediately above it. This phenomenon, known as *falling off*, as shown in Figure 3.15, is indicated only at the addition of further drill rods and at no other point in the CPT sounding. The cause of falling off is likely to be due to a number of factors, which include:

- *Soil rebound* - Since much of the soil surrounding the electric cone penetrometer remains in an elastic condition, as shown in Figure 2.9, when load is removed from the drill rod stem to enable further rods to be added, the surrounding soil rebounds thereby lifting the penetrometer slightly and reducing the measurements of q_c and f_s to values approaching zero.
- *Response of electrical components* - The time taken for the cone tip resistance and sleeve friction load cells to respond to large changes may be such that the response recorded is principally that of the equipment and not the soil.

The effect of falling off has been removed by modifications to the control program *CPTest*.

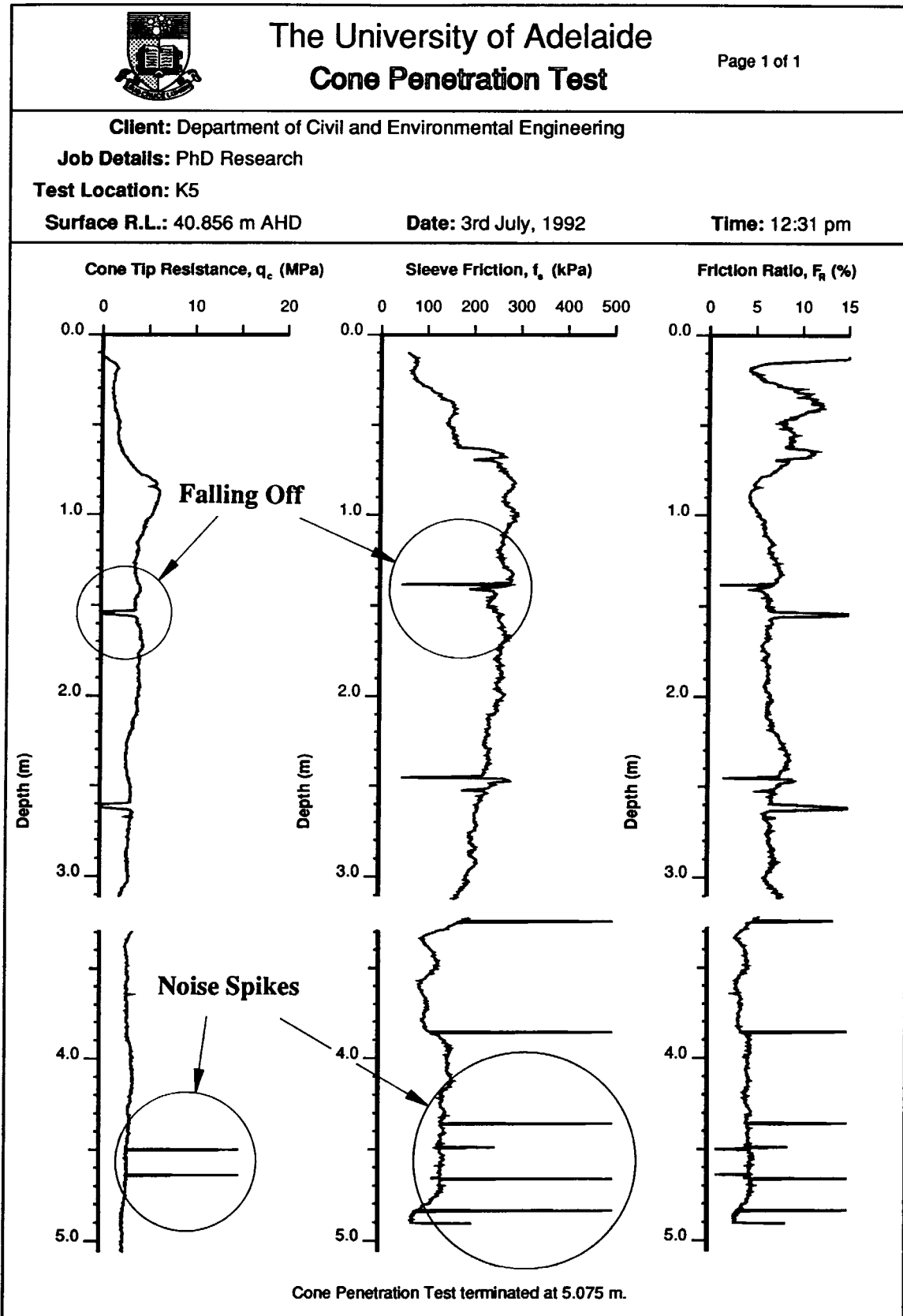


Figure 3.15 An example of q_c and f_s falling-off at rod changes and noise spikes.

Measurements of q_c and f_s are recorded at intervals of 5 mm from the initiation and continuation of the CPT. However, as discussed previously, when the data are saved to the data file on the floppy disk, *CPTest* does not save the first 2 readings. This removes the falling off effect in q_c and f_s measurements, but adds to the number of missing depths in the data file, as discussed in §3.1.1.2(ii).

3.3.2 Noise Spikes

An uncertainty associated with the measurement of q_c and f_s , discovered during the development of the data acquisition system, was the random presence of *noise spikes*. These were identified as sudden increases in q_c and f_s values that were not associated with any geotechnical phenomena. Figure 3.15 shows examples of noise spikes obtained during cone penetration testing. These spikes were found to be related to earthing within the CPT cable, and rectified by connecting the shielding that surrounds the cable and individual wires, to ground.

3.3.3 Limitations of Data Acquisition System

A computer based data acquisition system has two drawbacks. Firstly, minor undetected defects, such as gradual breakdown of the electrical instruments, amplifiers and electrical components, give rise to data inaccuracy and an increased measurement error (defined as the difference between the actual parameter and that measured) with time. This error can be minimised, however, by regular calibration. ISOPT-1 (De Beer et al., 1988) recommends that calibration be carried out at least every three months.

Secondly, total failure of the system can occur due to failures of the micro-computer, or microprocessor interface, which usually occur due to external power supply failure. The University of Adelaide system is less likely to suffer from power supply failure since the external power source is derived from the vehicle's 12V battery - the power required to drive the various electrical elements of the data acquisition system being insignificant in comparison to that stored in the battery itself.

3.4 SUMMARY

This chapter has examined the development of a micro-computer based data acquisition system for the CPT. It has been shown that the system satisfies each of the criteria

specified in §3.3. As a result, the data acquisition system is a robust and reliable means of accurately measuring, recording and storing closely-spaced CPT data.

The data acquisition system will be used in a field study to measure the small-scale spatial variability of the Keswick and Hindmarsh Clays. This field study is detailed in the next chapter.

Chapter Four

Experimental Programme

4.1 INTRODUCTION

As mentioned previously, in order to quantify small-scale variation (that is, within the range of millimetres to metres) it is necessary to obtain data at closely spaced intervals - both vertically and horizontally. This chapter details the results of a field study undertaken to quantify the small-scale variation of the undrained shear strength, s_u , of the Keswick and Hindmarsh Clays. Chapter 6, on the other hand, will discuss the compilation of a data base which will be used to quantify the large-scale variability of these clays.

4.2 LOCATION OF SITE FOR FIELD STUDY

In selecting the site for the field investigation, it was decided that it should meet a number of criteria. That is, the site should:

- *be located within the Adelaide city area* - so that the field study data can be incorporated with the large-scale database (discussed in Chapter 6);
- *have minimum dimensions of 50 × 50 metres* - in order to enable the number of required tests to be carried out;
- *be relatively free of trees and vegetation* - Trees and vegetation draw water from the upper region of the subsurface profile resulting in moisture changes with depth. These moisture variations influence the shear strength of the soil which, in turn, can distort spatial variability analyses. In addition, the locations of the trees will influence the positions of the individual tests and unnecessarily complicate the testing programme;

- *have the Keswick and Hindmarsh Clays relatively close to the ground surface* -in order to optimise the testing programme by obviating the need for unnecessary drilling and penetration;
- *be relatively flat and free of fill, previous construction and services* - thereby reducing the number of aspects likely to hinder the testing programme and uncertainties associated with the measurements;
- *have clear access to the site* - enabling the drilling rig and associated equipment to enter the site and successfully carry out the testing programme.

A suitable site, which satisfied the criteria listed above, was located in the South Parklands of the City of Adelaide. The location of the field study site is shown in Figure 4.1.

4.3 FIELD TESTING - SOUTH PARKLANDS SITE

As discussed in Chapters 1 and 2, the cone penetration test (CPT) was used as the basic field testing procedure to quantify the small-scale variability of the Keswick and Hindmarsh Clays because:

- *In situ testing has a number of advantages over laboratory testing;*
- *Large amounts of data can be acquired efficiently and economically;*
- *The CPT has the lowest measurement error of any in situ test method in current use;*
- *CPT equipment and technicians proficient in its operation were available.*

4.3.1 Layout of Field Testing

In order to determine the small-scale variability of the Keswick and Hindmarsh Clays in the vertical direction, as well as in a number of horizontal directions, a grid layout of cone penetration tests was chosen, as shown in Figure 4.2.

The layout consisted of 100 CPTs at a grid spacing of 5 metres in both directions, and 101 CPTs set out in a *cross* arrangement at lateral spacings of 1 metre. For ease of referencing, an alpha-numeric grid-numbering system was adopted, as shown in Figure 4.2. The referencing system used for the CPTs in the cross arrangement is shown in Figure 4.3. It was proposed that each cone penetration sounding would be performed to a depth of 5 metres below ground. Thus, for each sounding, a total of 1,000 measurements of cone tip

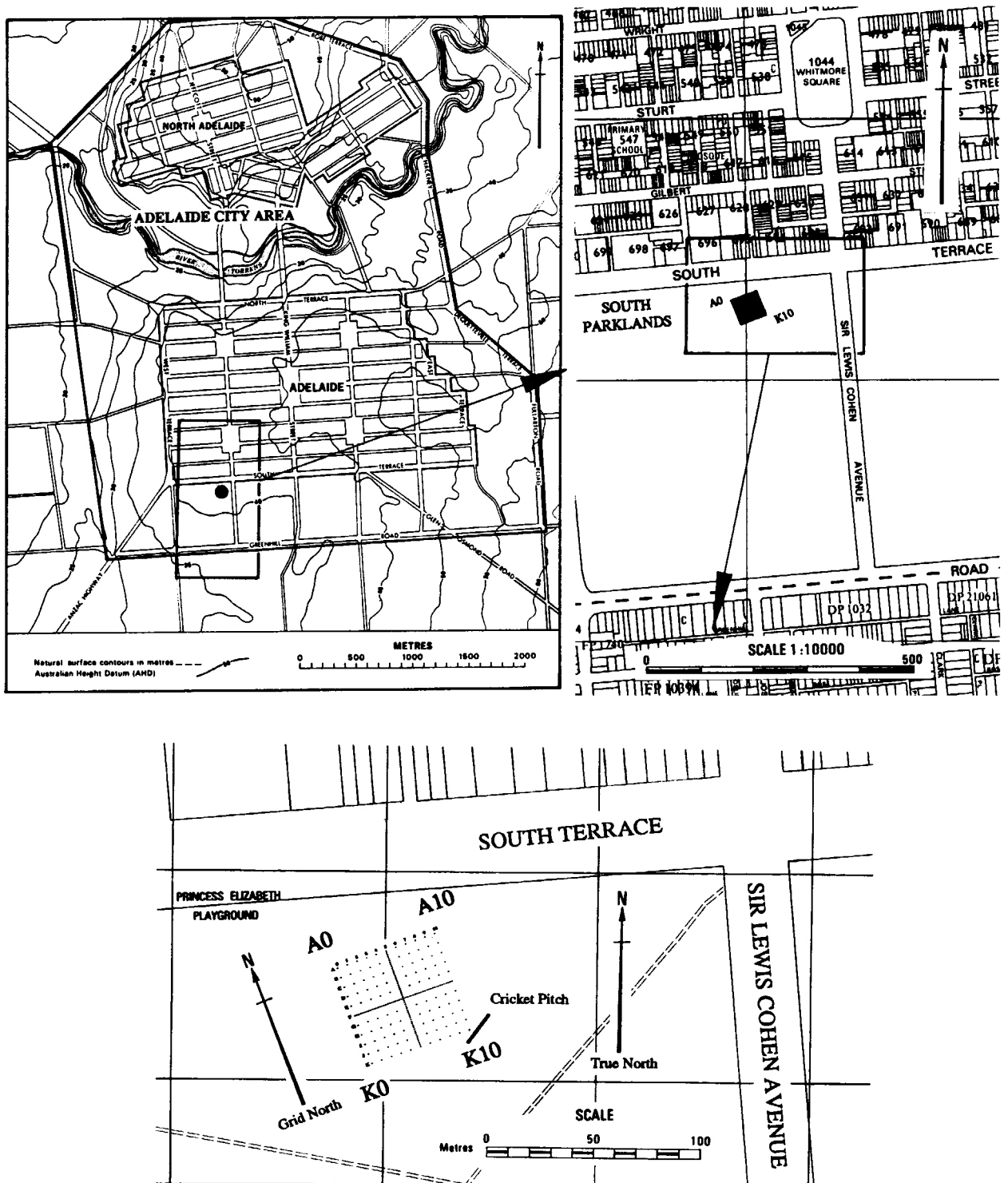


Figure 4.1 Location of field study site.

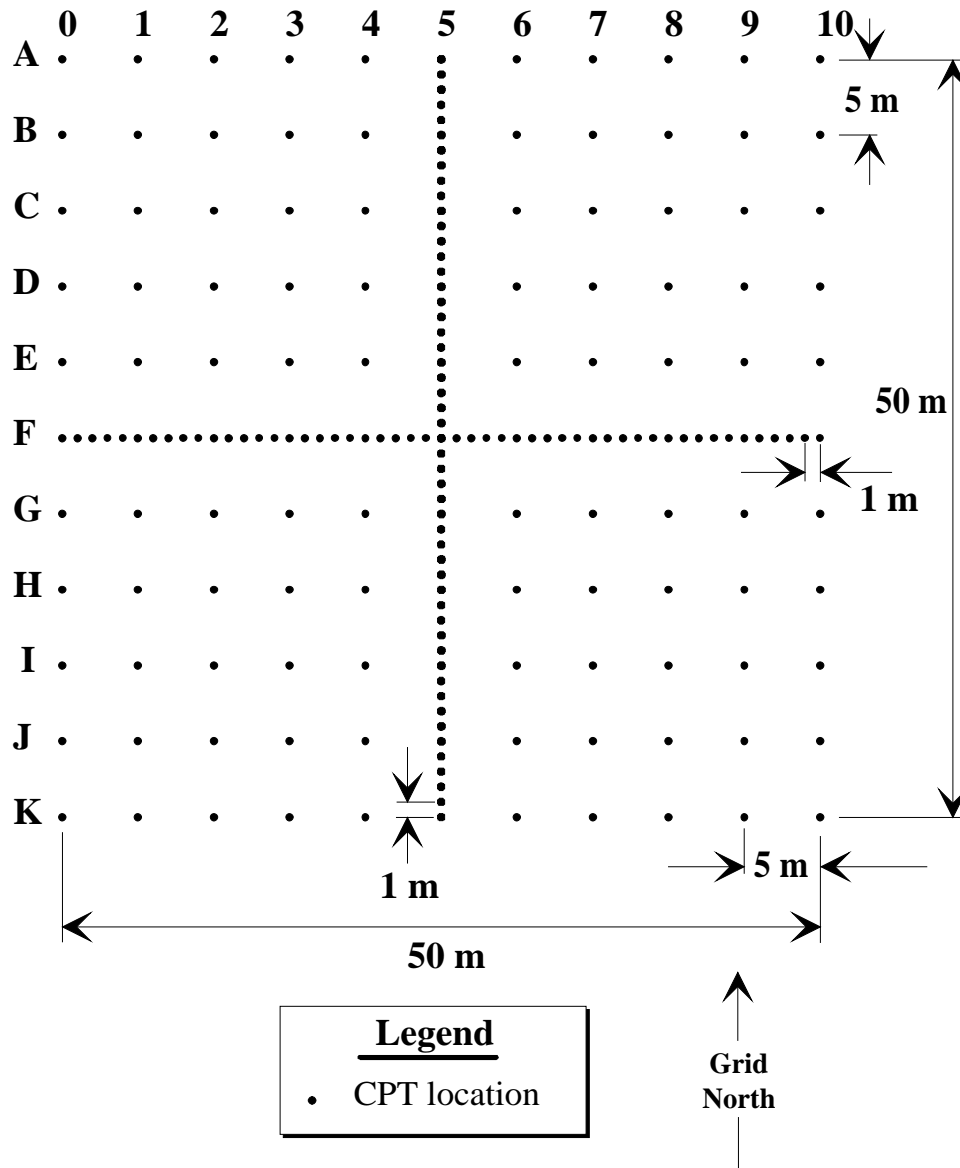


Figure 4.2 Initial layout of field testing.

resistance, q_c , and sleeve friction, f_s , would be recorded, due to the spacing of measurements being 5 mm, as detailed in Chapter 3. The orientation of the CPTs, as shown in Figure 4.1, was chosen to avoid large trees, overhead electrical cables and a concrete cricket pitch.

It is common practice, when investigating the spatial variability of soils and rock, to use a sampling pattern which is regular and either in the form of a square grid, or along a straight line. In particular, in the field of geostatistics, it is common place to use regular square grid sampling (Brooker, 1975; Journel and Huijbregts, 1978; Clark, 1979; Rendu, 1981; Azzouz and Bacconnet, 1991; Brooker, 1991). Journel and Huijbregts (1978) recommended that, initially, sampling should be carried out on a large, and more or less, regular grid which is

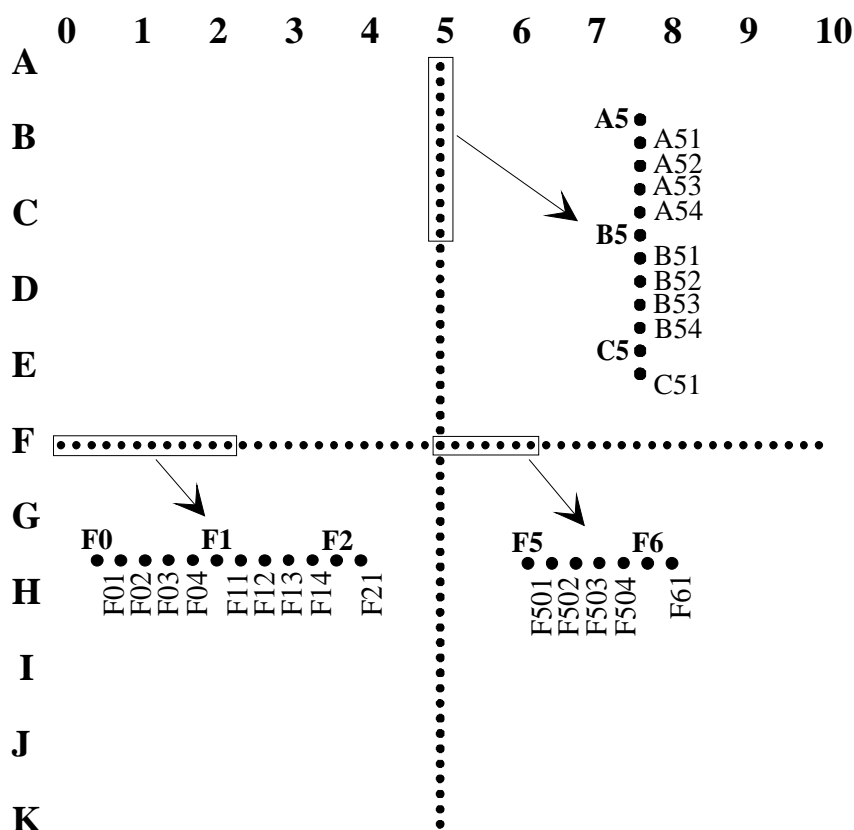


Figure 4.3 Referencing system used for the one metre, laterally spaced CPTs.

then followed by *in-fill drilling*, that is, sampling on a progressively smaller grid. Furthermore, it is possible to show, using geostatistics, that samples located on a regular, or near regular grid, provide more information than randomly located samples (Matheron, 1963; Rendu, 1981).

In the application of random field theory to the spatial variability of geotechnical materials, it is common practice to use either: samples taken along straight lines at regular, or irregular, intervals (Lumb, 1974, 1975; Anderson et al., 1984; Bergado et al., 1992); or samples obtained from regular, or near regular, square grids (Tang, 1979; Smith, 1981; Fardis and Veneziano, 1981). As shown in Figure 4.2, the proposed testing layout conforms with sampling regimes generally accepted in both the fields of geostatistics and random field theory.

4.3.2 Equipment and Methods

So that the results of the field testing would enable an accurate assessment of the spatial variability of undrained shear strength to be made, it was essential that testing be carried

out over as short a period of time as possible. This was to ensure that moisture variations within the subsurface profile, caused by seasonal effects, would be kept to a minimum. In order to achieve this, the use of a large-capacity drilling rig was necessary. The Department of Road Transport of South Australia owns and operates two such rigs: an *Edson*; and a *Proline*. These are shown in Figures 4.4 and 4.5, respectively. Subsequent to a request by the author, the Department generously agreed to provide a rig and an operator for the duration of this study. With the use of these rigs, it was anticipated that the testing programme would be completed within a period of one month.



Figure 4.4 Edson drilling rig.

In addition, the Department of Civil and Environmental Engineering at the University of Adelaide owns and operates a light-weight, *Toyota*, four-wheel-drive, drilling rig, as shown in Figure 4.6. It weighs approximately 2 tonnes and has a driving capacity of around 4 tonnes when fitted with two ground anchors.

The hydraulic feed rate, or the rate of cone penetration, of both the Edson and Proline drilling rigs is controlled manually by the operator. In order to minimise the uncertainties associated with the cone penetration tests, one driller, Mr. Ian Forrester, exclusively operated the Edson and Proline drilling rigs throughout the testing programme. On the other hand, the Toyota drilling rig is fitted with an hydraulic pressure regulator which



Figure 4.5 Proline drilling rig.



Figure 4.6 Toyota 4WD drilling rig.

ensures that the rate of penetration is maintained at 20 mm/s regardless of the resistance offered by the soil. As a consequence, the cone penetration rate is effectively operator-independent. However, throughout the testing programme, the Toyota drilling rig was exclusively operated by Mr. Tad Sawosko.

The hydraulic feed rate of the Edson and Proline rigs was monitored throughout the field study and the CPTs were maintained at a penetration rate of between 10 and 20 mm/s, as specified by *AS 1289.F5.1* (Standards Association of Australia, 1977). Field testing occurred over three periods: from July to August 1992; in September 1992; and from February to March 1993. Table 4.1 details the schedule of the cone penetration tests.

The CPTs were carried out in accordance with *AS 1289.F5.1* (Standards Association of Australia, 1977) and ISOPT-1 (De Beer et al., 1988) using a standard, 35.7 mm diameter, electrical friction-cone penetrometer, as detailed in §2.4.2, §2.4.3 and §3.4.1.1. Typical results obtained from the cone penetration tests are included in Appendix A.

The field testing programme extended for a total of approximately 7 months, far greater than that initially expected. This was due mainly to the fact that the drilling rigs were often needed for other commitments and, as a consequence, the rigs were often unavailable for the study. In addition, a period of heavy winter rain was experienced in late August and September 1992, causing disruption to the testing programme. Tests performed on the 29th September 1992 indicated that the recent rainfall had significantly affected the subsurface moisture regime and, hence, subsequent testing could not be used in the same data set. Thus, it was decided to abort the original testing programme and layout. From the beginning of testing to the 29th September 1992, 177 CPTs were successfully carried out. Five (those that were performed on the 29th September) were deemed to be unacceptable because of the recent winter rains and, hence, were discarded from the data set, leaving 172 CPTs that could be used for the assessment of the small-scale variability of the Keswick and Hindmarsh Clays. It will be shown in §4.3.4 that during the period of the 3rd July 1992 to the 14th August 1992, when these 172 CPTs were measured, the climatic conditions were relatively constant and, hence, the subsurface moisture regime was also relatively stable.

Preliminary analyses of the spatial variability of the test results obtained to that date showed that, in order to quantify the lateral variability of the Keswick Clay, samples should be taken at intervals of less than one metre (Jaksa et al., 1993). As a consequence, it was decided to amend the testing layout to include 50 CPTs at lateral spacings of 0.5 metres. These tests, CD1 to CD50, were performed between the 16th - 18th February 1993. The layout of all field tests that were carried out at the South Parklands site are summarised in Figure 4.7.

Table 4.1 Cone penetration testing programme.
(CPT reference system is shown in Figures 4.3 and 4.7).

Date	Drilling Rig	No. of CPTs	CPTs
3rd July 1992	Proline	14	K5, J54, J53, J52, J51, J5, I54, I53, I52, I51, I5, H54, H53, H52
7th July 1992	Edson	15	F5, F51, F52, F53, F54, G5, G51, G52, G53, G54, H5, H51, A5, A51, A52
9th July 1992	Edson	20	A53, A54, B5, B51, B52, B53, B54, C5, C51, C52, C53, C54, D5, D51, D52, D53, D54, E5, E51, E52
10th July 1992	Proline	5	E53, E54, F44, F43, F42
14th July 1992	Proline	19	F10, F94, F93, F92, F91, F9, F84, F83, F82, F81, F8, F74, F73, F72, F71, F7, F64, F63, F62
15th July 1992	Proline	10	F61, F6, F504, F503, F502, F501, F33, F32, F31, F24
16th July 1992	Proline	16	F22, F21, F2, F14, F13, F12, F11, F1, A10, B10, C10, D10, G10, H10, I10, J10
17th July 1992	Proline	13	E10, K10, K9, K8, K7, K6, K4, K3, K2, A0, A1, A4, A6
24th July 1992	Proline	15	A8, B9, C9, D9, E9, G9, H9, I9, J9, B8, C8, D8, E8, G8, H8
29th July 1992	Proline	14	J8, B7, C7, D7, E7, G7, H7, I7, J7, B6, C6, D6, E6, G6
31st July 1992	Proline	10	H6, I6, J6, B4, C4, D4, E4, G4, I4, J4
14th August 1992	Edson	21	B0, C0, D0, E0, F0, G0, H0, I0, J0, B1, C1, D1, E1, G1, H1, I1, J1, K1, K0, A2, B2
29th September 1992	Edson	5	A3, B3, C3, D3, E3
16th February 1993	Edson	18	CD50, CD49, CD48, CD47, CD46, CD45, CD44, CD43, CD42, CD41, CD40, CD39, CD38, CD37, CD36, CD35, CD34, CD33
17th February 1993	Edson	14	CD32, CD30, CD29, CD28, CD27, CD26, CD25, CD24, CD23, CD22, CD21, CD20, CD19, CD17
18th February 1993	Edson	18	CD31, CD18, CD16, CD15, CD14, CD13, CD12, CD11, CD10, CD9, CD8, CD7, CD6, CD5, CD4, CD3, CD2, CD1
26th February 1993	Edson	3	A10A, A10B, A10C
4th March 1993	Toyota	3	F5A, F5B, F5C

4.3.3 Sampling and Logging

In order to correlate cone tip resistances, measured in the field study, with undrained shear strengths, obtained from the data base, *KESWICK*, to be discussed in Chapter 6, it was necessary to obtain samples for unconsolidated undrained triaxial testing. Such tests would enable the determination of the cone factor, N_k , as detailed in §2.4.5. Two boreholes, A10 and F5, were drilled for this purpose, the locations of which are shown in Figure 4.7.

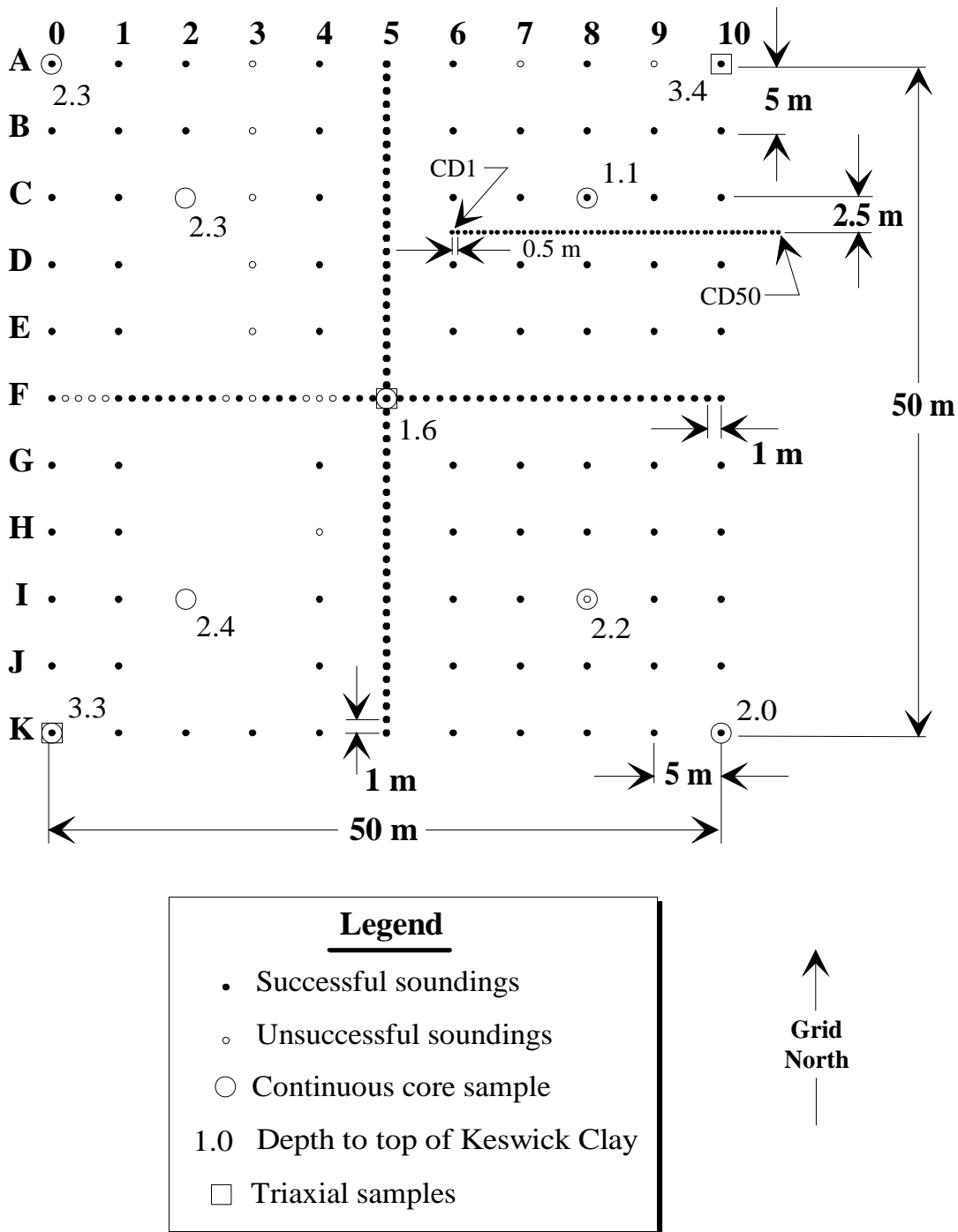


Figure 4.7 Amended testing layout.

The first of these boreholes, A10, was drilled on 26th February 1993 using the Department of Road Transport’s Edson rig. The second borehole, F5, was drilled on 4th March 1993 using the University’s Toyota 4WD drilling rig. Each sample consisted of a 70 mm diameter thin-walled tube which was sealed against moisture loss using screw-fit plastic seals. A total of 12 undisturbed samples of Keswick Clay were subsequently tested in the laboratory, the results and discussion of which are detailed in §4.5.

Eight boreholes were drilled on 15th August 1992, to a depth of 5 metres below ground, to provide continuous cores for the purpose of visual inspection and logging of the subsurface profile. These were achieved using the dynamic-push technique; that is, where a series of 40 mm diameter tubes, 1.0 metres in length, are dynamically driven into the soil, thereby providing a continuous, although disturbed, core of the subsurface material. The locations of these boreholes are also shown in Figure 4.7. A summary of the borehole logs is shown in Table 4.2 and Figure 4.8, and the complete borehole logs are included in Appendix B.

Table 4.2 Summary of borehole logs.

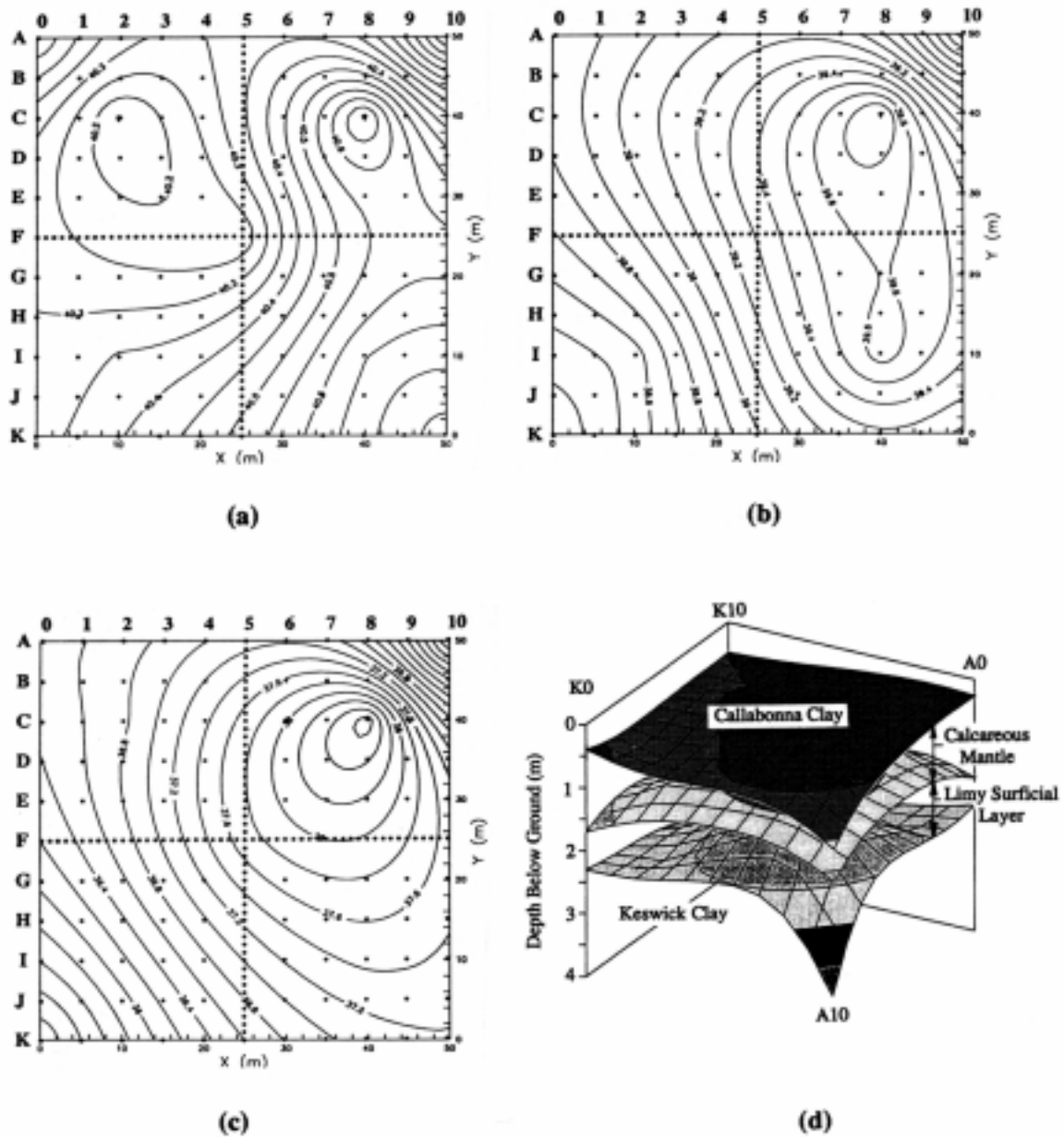
Borehole	Depth to top of calcareous layer (m)	Depth to top of Keswick Clay (m)
A0	0.4	2.3
A10	1.1	3.4
C2	0.7	2.3
C8	0.2	1.1
F5	0.3	1.6
I2	0.5	2.4
I8	1.0	2.2
K0	0.5	3.3
K10	0.3	2.0

4.3.4 Reduction of Errors During Field Testing

In order to measure the spatial variability of any geotechnical materials it is essential to eliminate variabilities associated with other effects, such as equipment, operator and procedural variabilities, as well as temporal climatic changes. As discussed previously, so that equipment and operator errors would be minimised, a single cone penetrometer, data acquisition system and operator were used throughout the field testing programme. In addition, the procedure adopted for each of the CPTs conformed with the standards specified by *AS 1289.F5.1* (Standards Association of Australia, 1977) and *ISOPT-1* (De Beer et al., 1988).

So that the temperature of the cone penetrometer was relatively constant throughout testing, the following procedure was adopted:

1. Prior to each group of CPTs (at the commencement of each day, or after a refreshment break), the cone penetrometer was inserted about 300 mm into the ground for approximately 5 to 10 minutes. This was performed in accordance with *AS 1289.F5.1*, so that the cone was able to equilibrate with the subsurface temperature.



Lateral drift of the cone penetrometer, that is, its deviation from the vertical, was not monitored during testing. *AS 1289.F5.1* states that drift can occur when penetration depths exceed 10 to 15 metres, whereas de Ruiter (1981) recommended that slope sensors are advisable where final penetration is greater than 25 metres, and if the site contains gravels or cobbles. Since the final depth of penetration was approximately 5 metres, the testing site contains no gravel nor cobbles, and the drilling rig was carefully levelled prior to each CPT, it is concluded that errors resulting from drift are negligible.

Figures 4.9 to 4.12 show the climatic conditions in the Adelaide city area during 1992 and 1993. Figures 4.13 to 4.16, on the other hand, show the climatic conditions in the Adelaide city area during the field testing periods of 3rd July 1992 to 14th August 1992, and 16th February 1993 to 4th March 1993. The data for each of these figures were obtained from the Bureau of Meteorology. As can be seen from these figures, the climatic conditions during the field testing periods of 3rd July 1992 to 14th August 1992, and 16th February 1993 to 4th March 1993, were relatively stable and, as a result, it can be assumed that climatic effects have not contributed significantly to the variability indicated by the CPT results.

Since equipment, procedural, operator and climatic variations during the field testing programme have been shown to be relatively negligible, the variation between CPT results can be assumed to represent the spatial variation of the soil deposit.

4.3.5 Level Survey of South Parklands Site

In order to correlate the cone penetration tests, and to combine the data base with the field study, it was necessary to carry out a level survey of the South Parklands site, as well as the individual CPTs. Using an automatic level, staff and theodolite, each CPT was levelled and, by means of a permanent mark, each CPT was related to the Australian Height Datum¹⁸. A contour plot of the South Parklands site is shown in Figure 4.17, and a three-dimensional projection is shown in Figure 4.18. As is evident from these figures, the site falls from A10 to K0, that is, approximately south west, with a slope of around 1 in 330. The CPT with the highest level is A9, having a reduced level (RL) of 41.078 m AHD, and the lowest CPT is K1, having an RL of 40.816 m AHD.

¹⁸ a standard datum surface, effectively a mean sea level, which is adopted by the National Mapping Council, and to which all vertical control for mapping is referred.

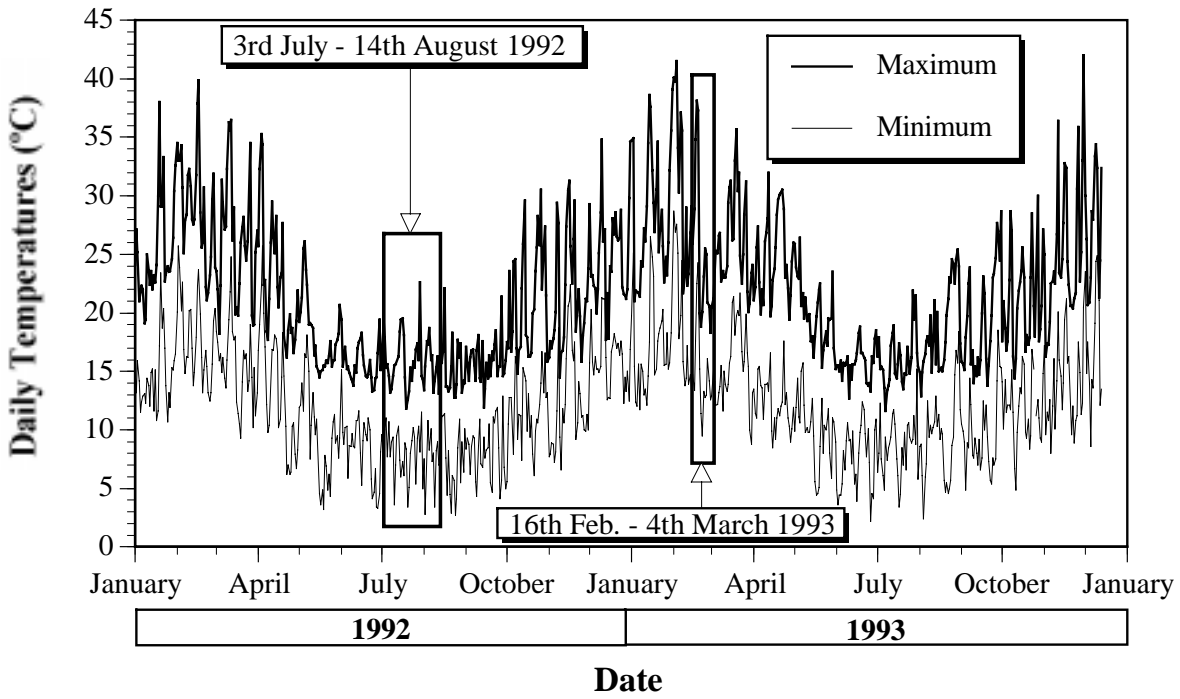


Figure 4.9 Maximum and minimum daily temperatures for the Adelaide city area for 1992 and 1993. (Data provided by Bureau of Meteorology).

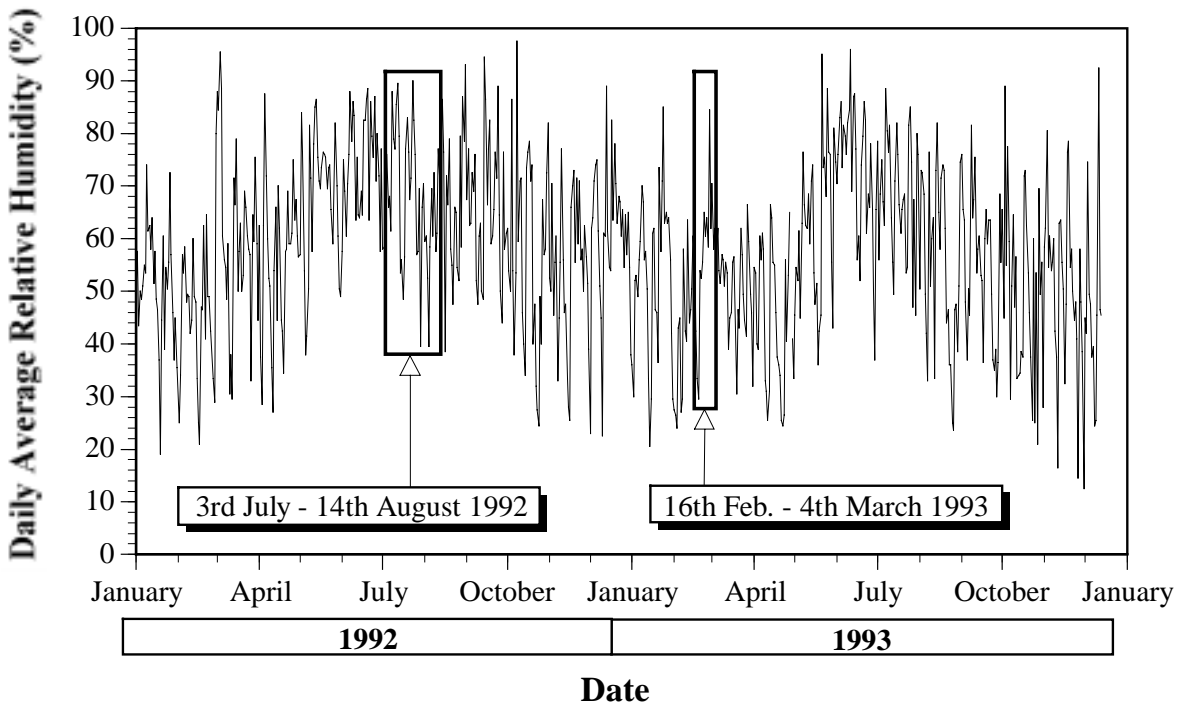


Figure 4.10 Average daily relative humidity for the Adelaide city area for 1992 and 1993. (Data provided by Bureau of Meteorology).

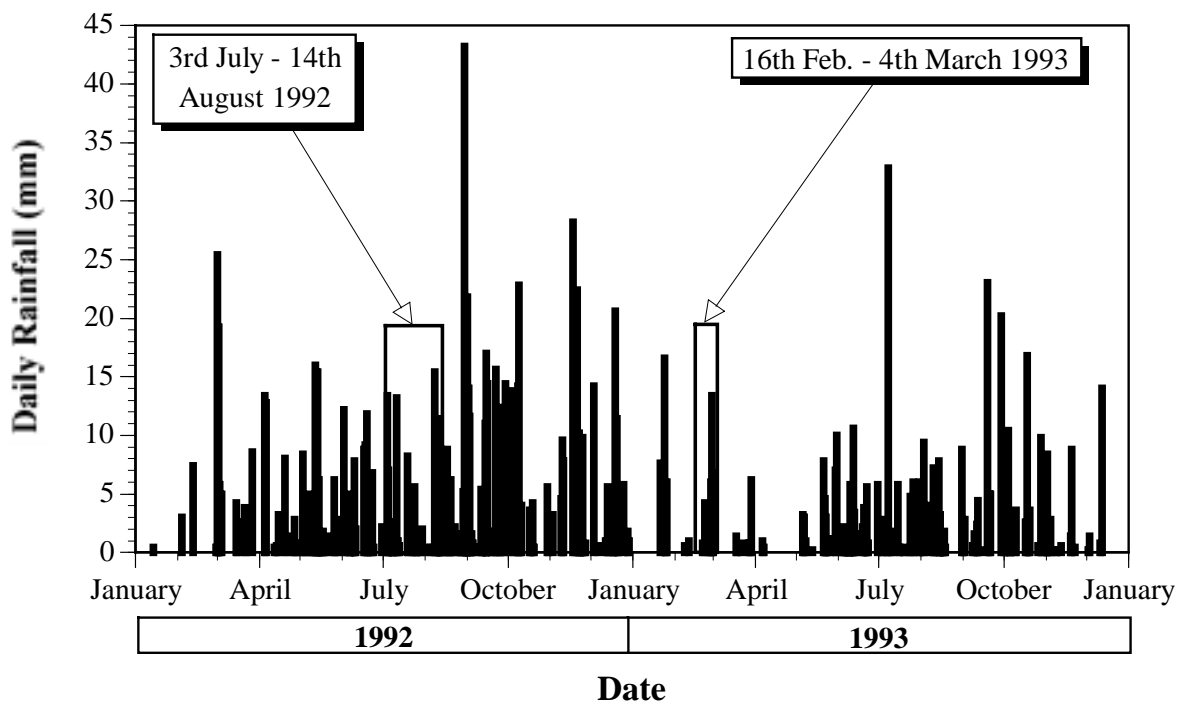


Figure 4.11 Daily rainfall for the Adelaide city area for 1992 and 1993.
 (Data provided by Bureau of Meteorology).

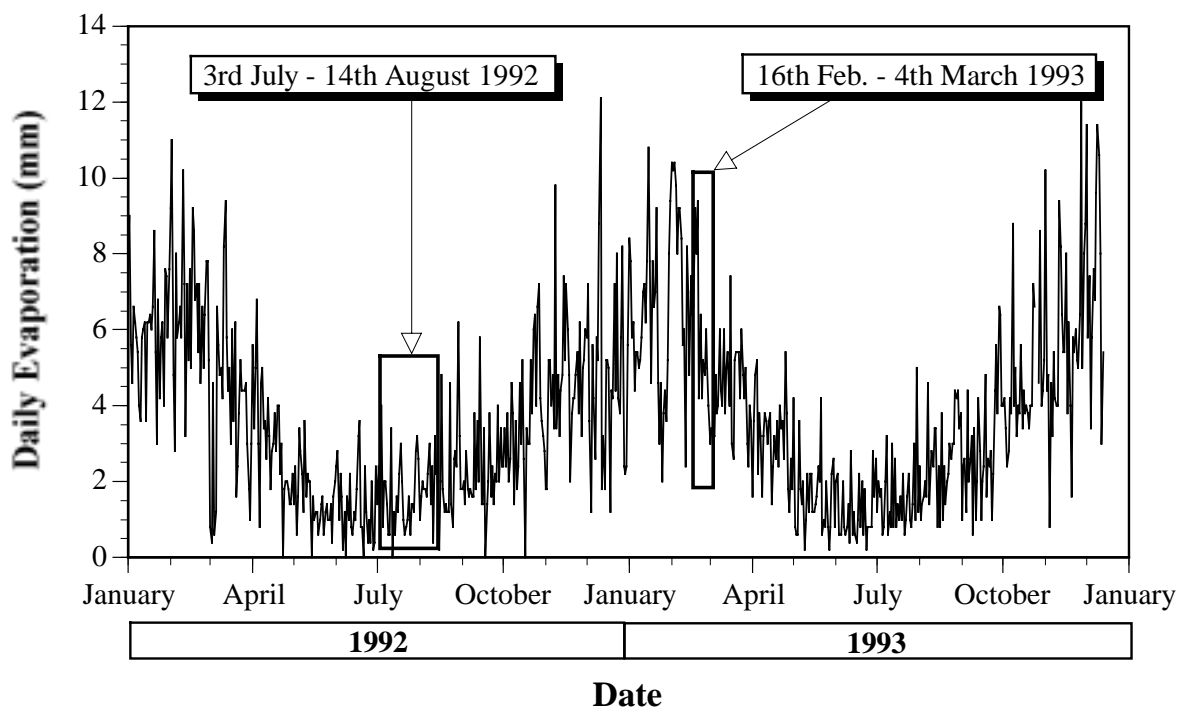


Figure 4.12 Daily evaporation for the Adelaide city area for 1992 and 1993.
 (Data provided by Bureau of Meteorology).

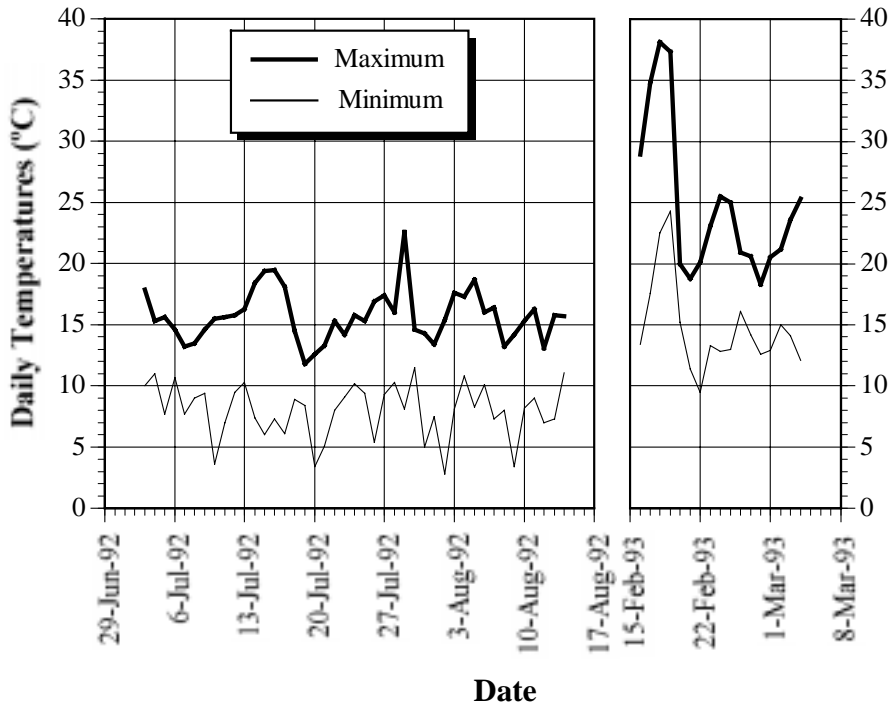


Figure 4.13 Maximum and minimum daily temperatures for the Adelaide city area for 3rd July 1992 - 14th August 1992 and 16th February 1993 - 4th March 1993. *(Data provided by Bureau of Meteorology).*

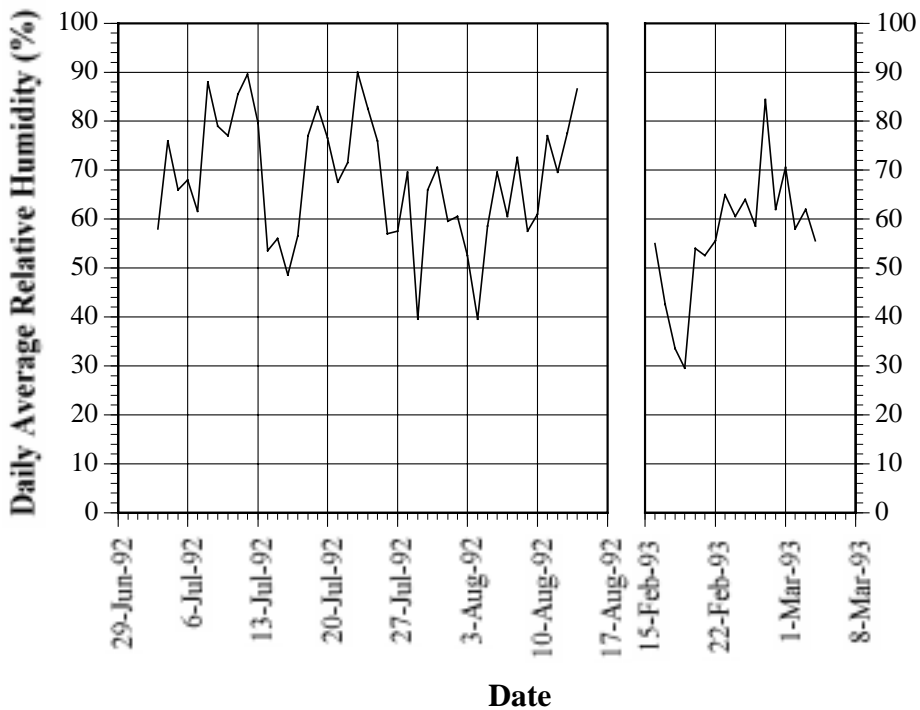


Figure 4.14 Average daily relative humidity for the Adelaide city area for 3rd July 1992 - 14th August 1992 and 16th February 1993 - 4th March 1993. *(Data provided by Bureau of Meteorology).*

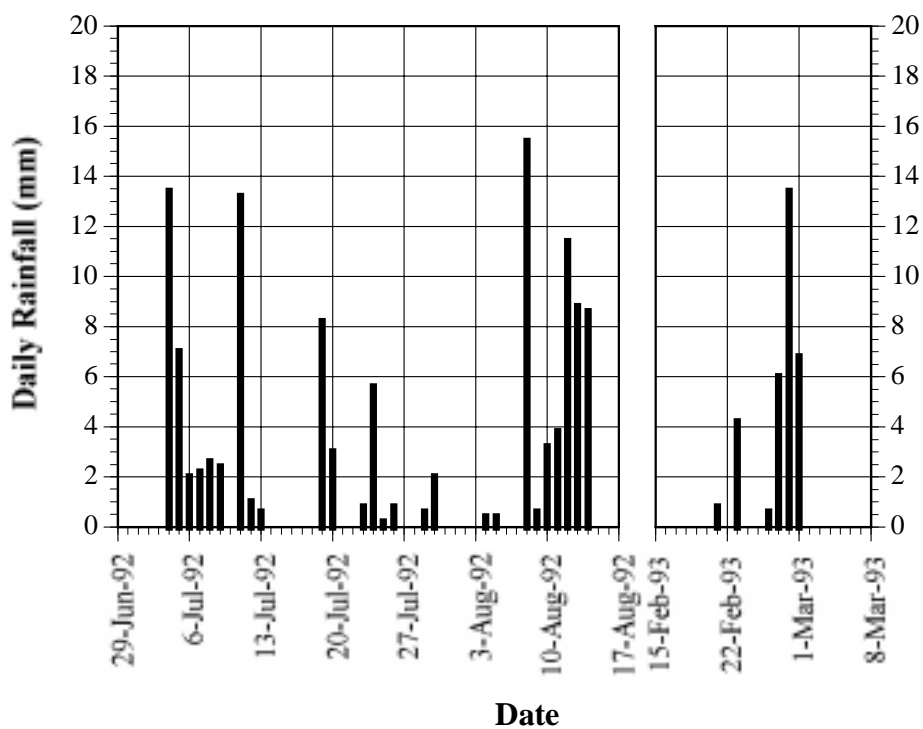


Figure 4.15 Daily rainfall for the Adelaide city area for 3rd July 1992 - 14th August 1992 and 16th February 1993 - 4th March 1993. (Data provided by Bureau of Meteorology).

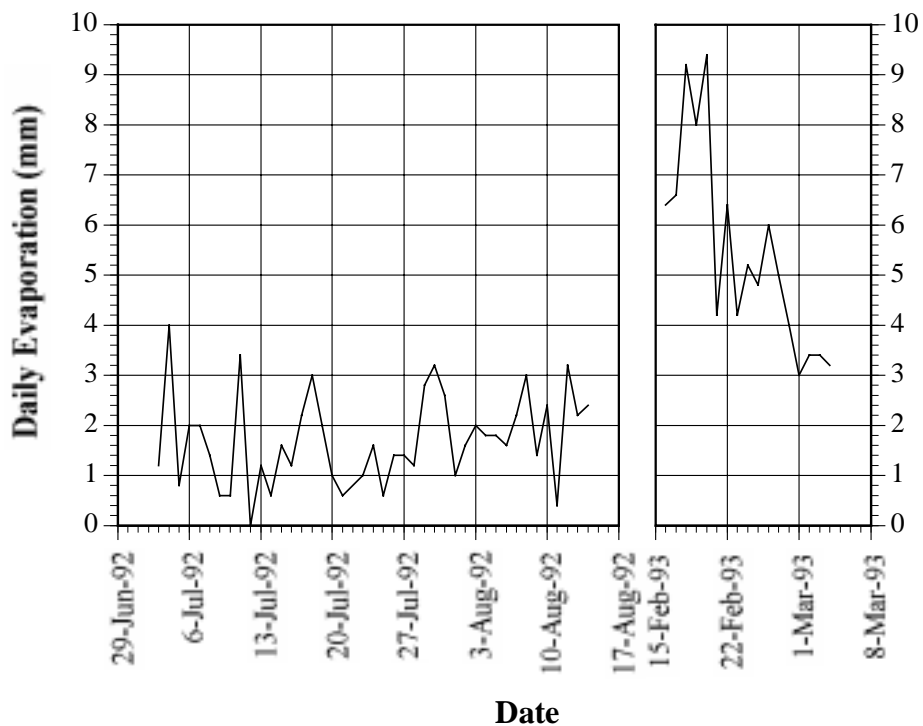


Figure 4.16 Daily evaporation for the Adelaide city area for 3rd July 1992 - 14th August 1992 and 16th February 1993 - 4th March 1993. (Data provided by Bureau of Meteorology).

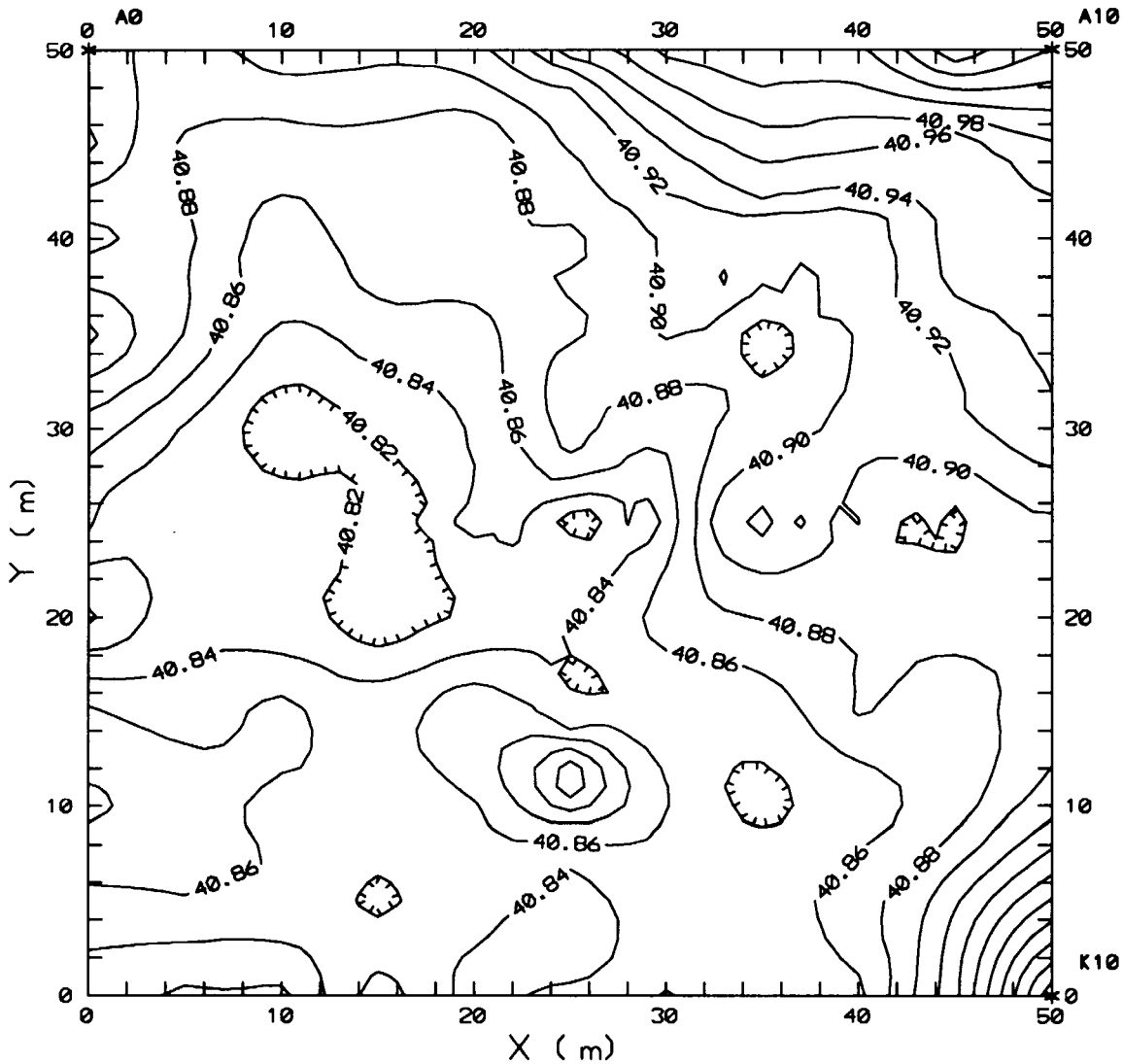


Figure 4.17 Contour plot of South Parklands site.
(Contours in metres AHD at 0.02 m intervals).

4.4 FIELD TESTING - KESWICK SITE

Preliminary analyses of the spatial variability of CPT results obtained to September 1992 showed that, in order to determine the lateral variability of the Keswick Clay, samples should be taken at intervals of less than one metre (Jaksa et al., 1993). As mentioned previously, this prompted the drilling of 50 additional CPTs (CD1 - CD50), which were spaced at 0.5 metre centres, as shown previously in Figure 4.7. However, these additional CPTs still provide only sparse data with which to examine the horizontal spatial variability of the Keswick and Hindmarsh Clays. Ideally, a CPT performed in the horizontal direction would provide a great number of data points with which to make this examination.

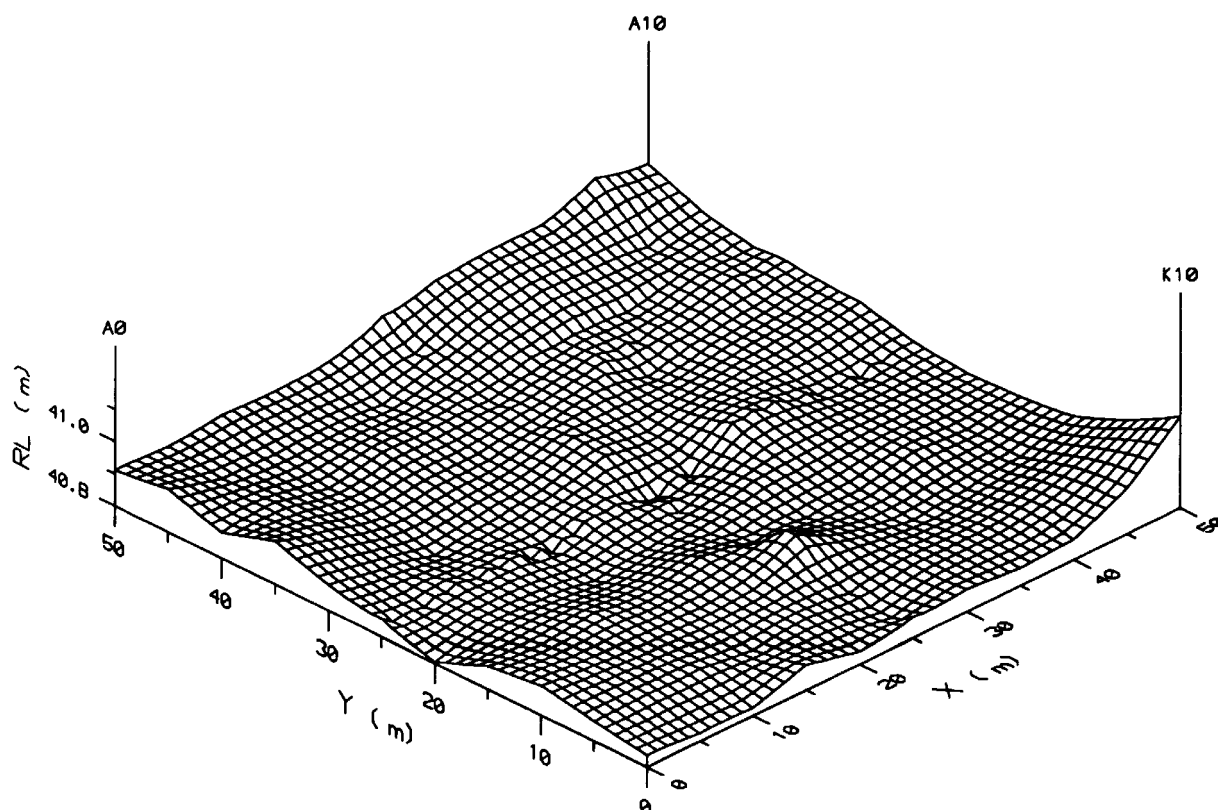


Figure 4.18 3-dimensional surface plot of South Parklands site.
(Reduced level, RL, in metres AHD and exaggerated by 25).

However, a horizontal CPT presents many physical problems, the most significant of which, is locating an exposed face, or excavating an embankment, consisting of Keswick Clay.

Previous experience in consulting engineering, obtained by the author, suggested that such an exposed face was located at the Australian National railway yards at Keswick. As a result, it was decided to investigate the possibility of using this site to perform a horizontal CPT.

4.4.1 Location of Site for Horizontal Spatial Variability Field Study

The site chosen to perform the horizontal spatial variability field study is located adjacent to the railway lines, and the Australian National office building, at Keswick; as shown in

Figure 4.19. As can be seen from this figure, the Keswick site is located within the Adelaide city area.

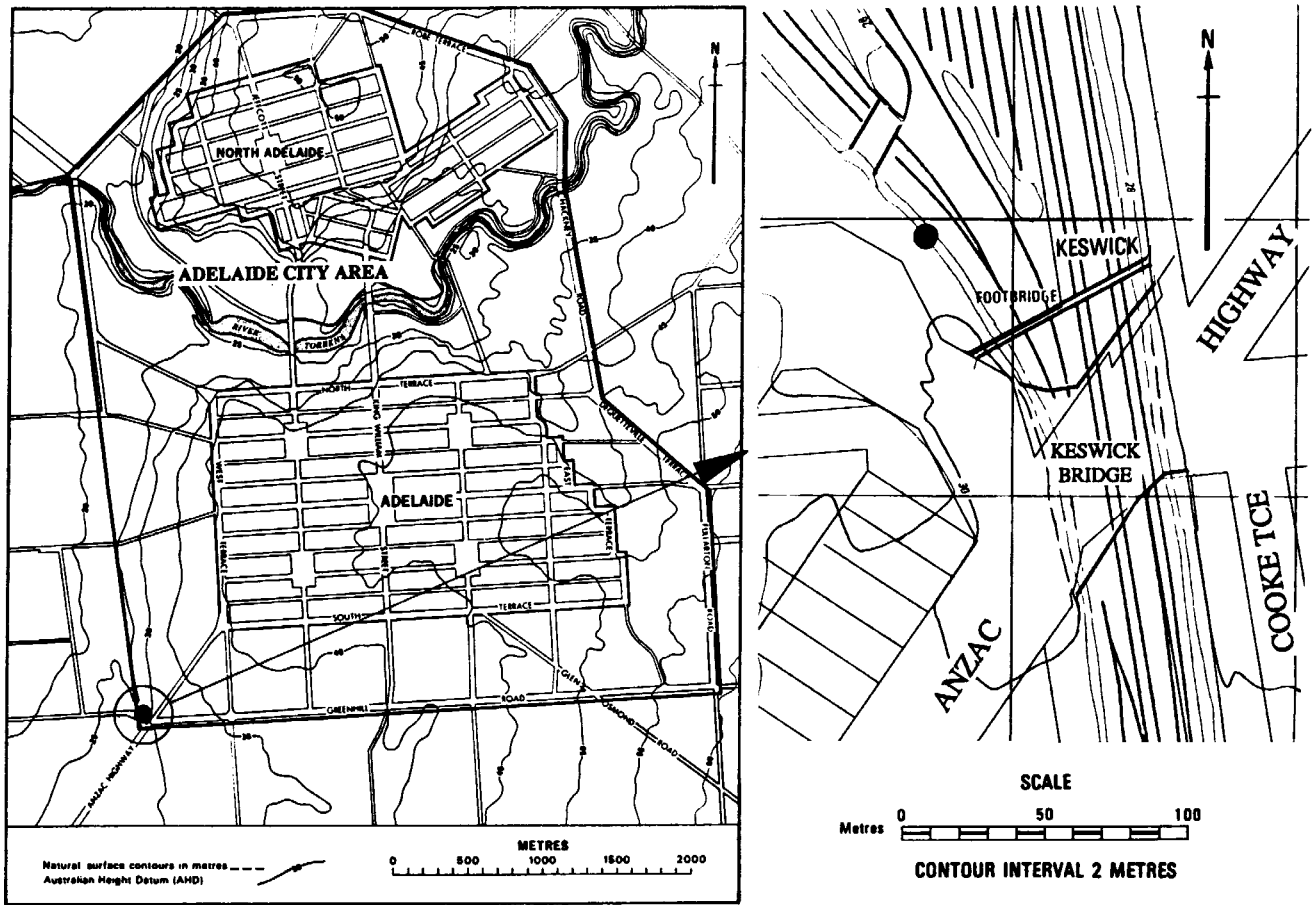


Figure 4.19 Location of site for horizontal spatial variability field study.

4.4.2 Horizontal CPT Equipment and Methods

In order to perform a cone penetration test in the horizontal direction, it is necessary to modify extensively existing CPT equipment. This involved mounting an hydraulic ram on a single axle trailer, as shown in Figure 4.20. The hydraulic ram was attached to the University's Toyota 4WD drilling rig, by means of flexible hoses and couplings. In this way, the horizontally mounted ram was operated by the hydraulic pump, reservoir and controls, associated with the Toyota rig. As a result of this, relatively minimal work was needed to manufacture a thrusting device for carrying out horizontal cone penetration tests. In addition, the trailer mounted CPT provided an extremely manoeuvrable and light-weight thrusting rig that could perform the test in the limited available space and time constraints.



Figure 4.20 Trailer mounted CPT equipment for testing in the horizontal direction.

In order to provide reaction to the horizontal thrust produced by the hydraulic ram, the trailer was stabilised by two steel lateral restraint piers, drilled into the soil adjacent to the trailer. One of these steel piers is shown in Figure 4.20. Two, 200 mm diameter, piers were drilled to a depth of approximately 1.5 metres adjacent to the sides of the trailer, shown in Figure 4.21, by means of the Toyota drilling rig. Each pier, a 2.5 metre steel 100UC¹⁹ section, was then placed in each of the holes, which were subsequently backfilled with compacted quarry rubble to facilitate their removal. The trailer was connected to the steel piers by 5-tonne capacity steel chains which were bolted to the front and rear of the trailer and wound around the steel piers, as shown in Figure 4.20.

As shown in Figure 4.21, an asymmetric arrangement was used for the pier locations. This layout was chosen to enable the trailer to be moved laterally, allowing a borehole to be drilled adjacent to the CPT hole. It was proposed that this borehole would provide undisturbed samples of Keswick Clay for identification purposes, as well as for unconsolidated undrained triaxial testing, so that a lateral value of N_k could be evaluated.

¹⁹ universal column - a mild steel I beam 100 mm overall depth, 100 mm flange width, 7 mm thick flanges and 5 mm thick web.

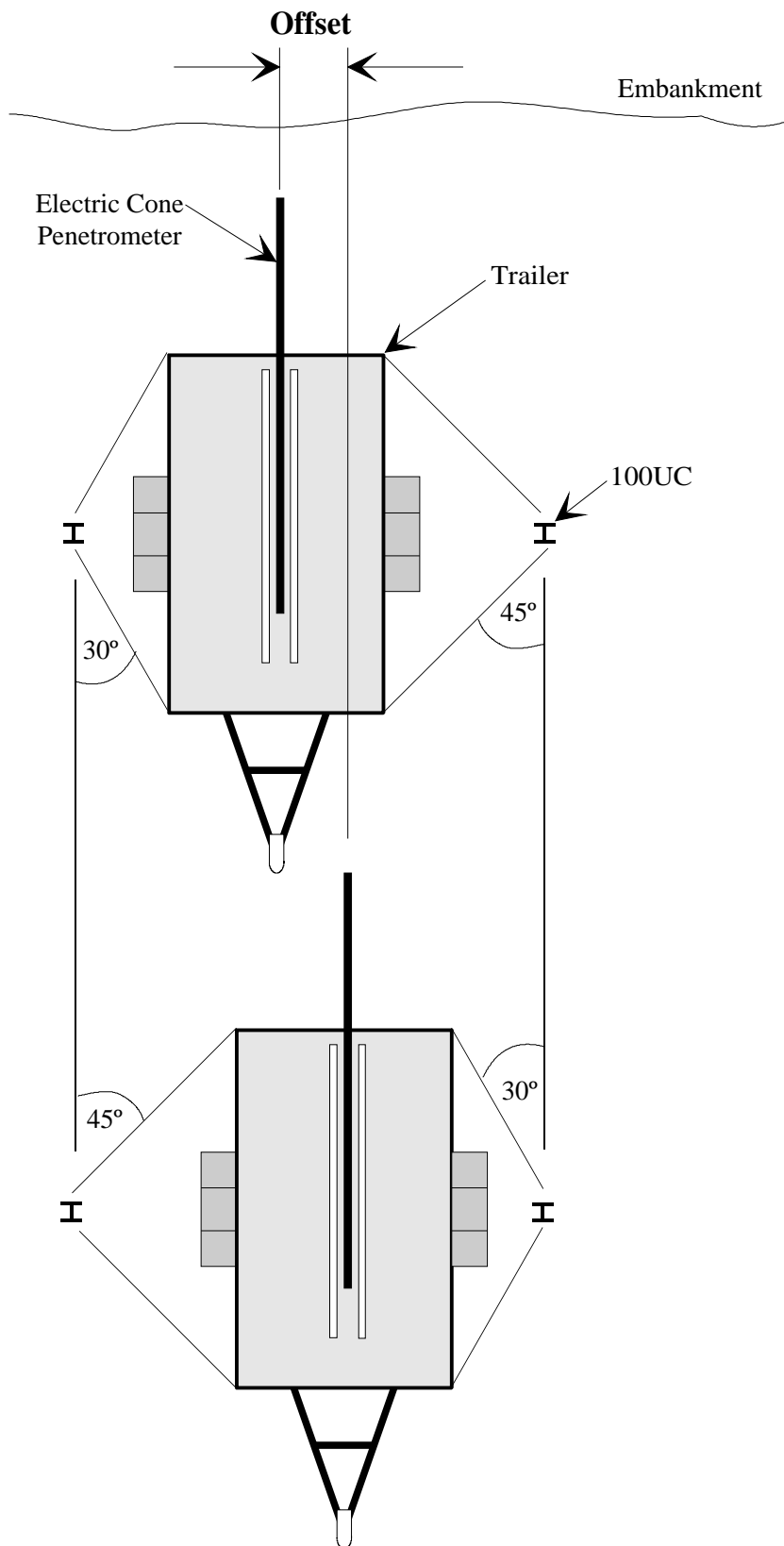


Figure 4.21 Layout of steel lateral restraint piers.

The micro-computer based data acquisition system, detailed in Chapter 3, was used to record the horizontal CPT data. So that penetration depths could be monitored in the

horizontal direction, a pulley and timber post were employed in conjunction with the depth box, as shown in Figure 4.22. The tension of the torsional spring within the depth box, as described in §3.4.1.2, and the low self-weight of the metallic cable, are such that it is expected that depth measurements were minimally influenced by the effect of catenary.



Figure 4.22 Depth box arrangement used to measure horizontal penetration depths.

One CPT was carried out, on Friday 16th July 1993, in accordance with *AS 1289.F5.1* (Standards Association of Australia, 1977) and *ISOPT-1* (De Beer et al., 1988) and with the details specified in §4.3.2 and §4.3.4. Unfortunately, due to limitations imposed by the Australian National railways authority; the owners of the site, only one horizontal CPT was able to be performed. The CPT was carried out to a total horizontal depth of 7.62 metres from the face of the embankment, and the results are shown in Figure 4.23.

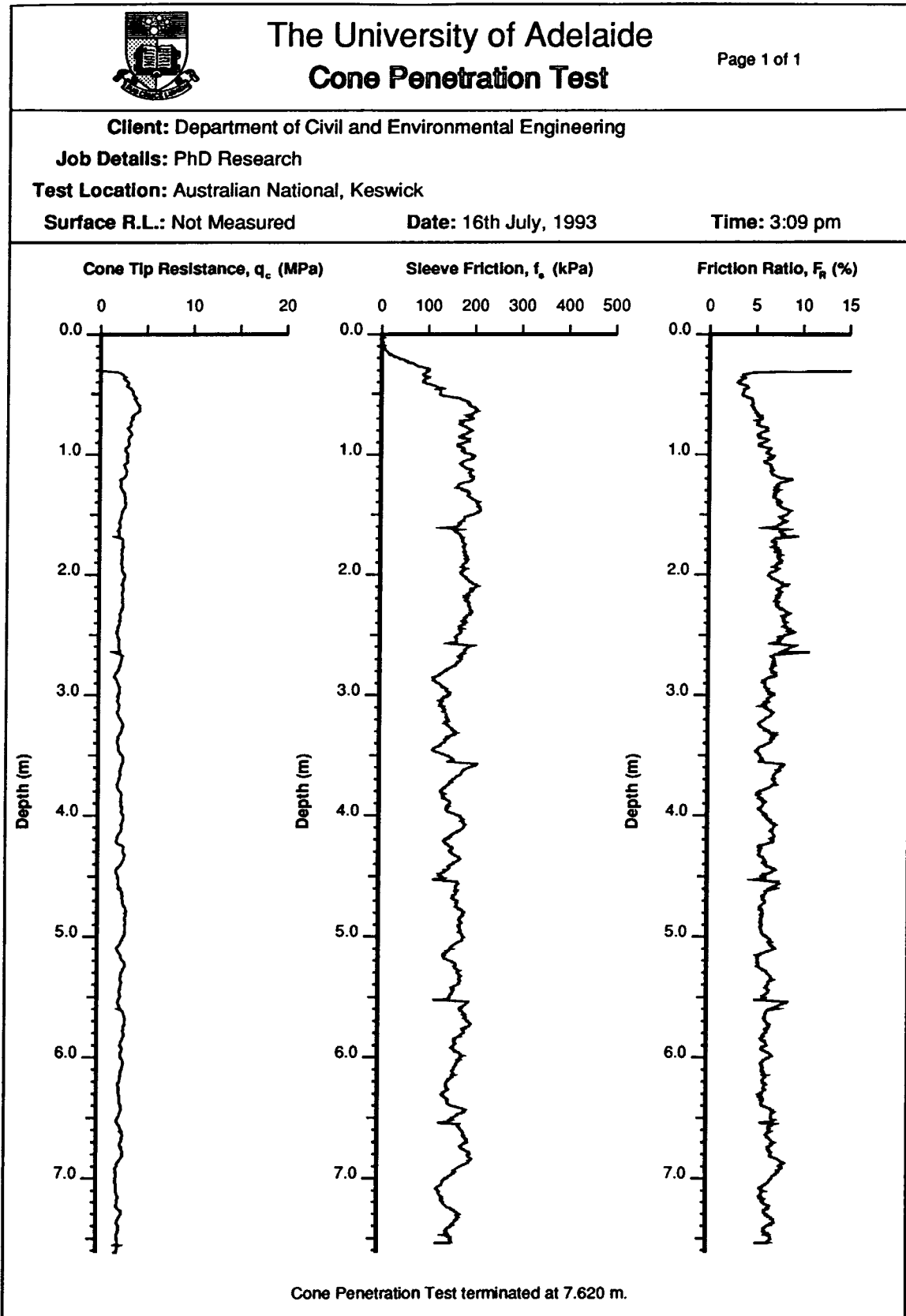


Figure 4.23 Results of the horizontal CPT at Keswick.

Furthermore, due to complications caused by trailer movements, only two undisturbed tube samples of Keswick Clay were obtained. However, these were unsuitable for triaxial testing purposes because of weathering and the presence of plant roots in the region adjacent to the embankment face. Inspection of these samples, on the other hand, indicated that the material tested by the CPT was, indeed, Keswick Clay as originally anticipated.

The measurements obtained from the horizontal CPT will be analysed, with respect to spatial variability, in the following chapter. However, before the spatial variability of the undrained shear strength of the Keswick Clay can be assessed, it is necessary to convert the measurements of q_c to estimates of s_u . This is discussed in the following section.

4.5 DETERMINATION OF CONE FACTOR, N_k

In order to convert the CPT measurements to values of undrained shear strength, s_u , via the relationships given by Equations (2.5), and (2.7) to (2.10), it is necessary to quantify the cone factor, N_k . As described previously in §2.4.5, this is usually achieved by performing a series of unconsolidated undrained (UU) triaxial tests on high-quality samples obtained from a location adjacent to the CPT. As a consequence, and as mentioned in §4.4.3.3, several 70 mm diameter undisturbed samples were taken so that UU tests could be performed in the laboratory.

A total of 12 unconsolidated undrained triaxial tests were performed on undisturbed samples of Keswick Clay, obtained from boreholes A10 and F5. The tests were performed using standard triaxial apparatus, and the results of these tests are summarised in Table 4.3. Each of the 12 samples failed by shearing along a readily identifiable failure plane. As can be seen from Table 4.3, many of the triaxial tests were carried out well after the samples were obtained - some up to a month after. This was not intended, nor desired, and resulted from the triaxial testing apparatus, and technicians, being obligated to other projects during this period.

Furthermore, it was originally intended to obtain the samples for triaxial testing immediately after the completion of the cone penetration testing, so that the CPT results could be compared with the triaxial test results in order to determine N_k . However, due to the disruption in testing and the heavy rains that occurred in late August and September 1992, this was not possible. As a result, four additional CPTs were performed adjacent to the boreholes A10 and F5, where the undisturbed samples were obtained. Three CPTs (A10A, A10B, and A10C) were conducted adjacent to borehole A10, and one CPT (F5A) adjacent to borehole F5, as shown in Figure 4.24. The dates that these CPTs were drilled, and the rigs that were used to perform them, were shown previously in Table 4.1. A

Table 4.3 Summary of unconsolidated undrained triaxial tests.

Test No.	Borehole	Date Sampled	Date Tested	Sample Depth (m)
1	A10	26th February 1993	26th March 1993	3.72 - 3.86
2	A10	26th February 1993	3rd March 1993	3.95 - 4.09
3	A10	26th February 1993	3rd March 1993	4.20 - 4.34
4	A10	26th February 1993	2nd March 1993	4.34 - 4.60
5	A10	26th February 1993	2nd March 1993	4.65 - 4.79
6	A10	26th February 1993	2nd March 1993	4.80 - 5.04
7	F5	4th March 1993	26th March 1993	1.61 - 1.76
8	F5	4th March 1993	26th March 1993	1.77 - 1.92
9	F5	4th March 1993	26th March 1993	2.09 - 2.24
10	F5	4th March 1993	26th March 1993	2.25 - 2.40
11	F5	4th March 1993	26th March 1993	3.13 - 3.28
12	F5	4th March 1993	26th March 1993	3.29 - 3.44

Test No.	σ_3 (kPa)	s_u (kPa)	$E_{u(50)}$ (MPa)	I_r	w (%)	γ (kN/m ³)	γ_d (kN/m ³)	S_r (%)	e
1	60	134.4	16.4	40.6	26.63	19.36	15.29	95.77	0.765
2	70	158.1	14.6	30.7	29.05	19.27	14.93	99.07	0.806
3	100	158.9	35.8	75.1	28.60	19.35	15.05	99.18	0.793
4	100	117.0	32.6	92.8	29.96	19.09	14.69	98.44	0.837
5	100	132.8	26.7	67.0	33.19				
6	100	132.9	26.3	66.0	33.69	18.67	13.97	99.44	0.932
7	40	56.0	10.6	63.0	33.70	17.91	13.39	91.36	1.014
8	40	76.5	15.3	66.6	28.93	18.39	14.26	89.25	0.892
9	40	105.4	26.7	84.4	24.98	18.71	14.97	85.65	0.802
10	40	154.1	42.0	90.7	29.57	18.75	14.47	94.09	0.864
11	60	146.5	6.6	15.0	25.83	19.23	15.28	92.85	0.765
12	60	126.9	44.4	116.5	26.30	19.15	15.16	92.78	0.779

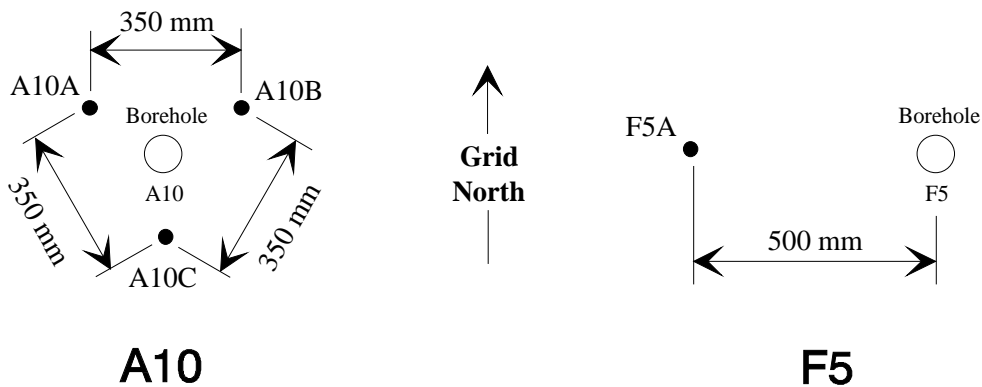


Figure 4.24 Locations of additional CPTs performed in the determination of N_k .

summary of the relevant results of the additional CPTs, together with values of N_k calculated from Equations (2.5) and (2.7) to (2.10), are given in Table 4.4.

Table 4.4 Summary of additional CPT results and calculated values of N_k .

Test No.	s_u (kPa)	I_r	\bar{q}_c (MPa)	Calculated Cone Factor, N_k				
				Eq. (2.5)	Eq. (2.7)	Eq. (2.8)	Eq. (2.9)	Eq. (2.10)
1	134.4	40.6	2.23	16.4	16.8	9.2	9.7	10.9
2	158.1	30.7	2.54	15.1	16.5	8.8	9.2	10.4
3	158.9	75.1	2.47	15.1	17.5	10.2	11.1	12.4
4	117.0	92.8	2.30	19.0	17.9	10.7	11.8	13.3
5	132.8	67.0	2.20	15.9	17.5	10.2	11.1	12.4
6	132.9	66.0	2.14	15.4	17.5	10.2	11.0	12.3
7	56.0	63.0	1.39	24.2	17.4	10.1	10.9	12.2
8	76.5	66.6	1.55	19.8	17.3	9.9	10.7	12.0
9	105.4	84.4	3.26	30.5	17.5	10.1	11.0	12.3
10	154.1	90.7	3.36	21.5	17.5	10.1	11.0	12.3
11	146.5	15.0	3.21	21.5	15.7	7.9	7.9	9.1
12	126.9	116.5	3.93	30.5	17.8	10.6	11.7	13.1

- where: \bar{q}_c the average of the measured values of cone tip resistance over the length of the triaxial specimen (typically the average of 30 values);
 s_u undrained shear strength determined by UU tests;
 f initial shear stress ratio, taken as -0.4 , used in Equations (2.7) to (2.10), (Kay and Mayne, 1990);
 α_f, α_s roughness factors of the cone face and cone shaft, respectively, both taken as equal to 0.8 , used in Equations (2.9) and (2.10), (Kay and Mayne, 1990).

A number of authors (de Ruiter, 1981, 1982; Campanella et al., 1983; Jamiolkowski et al., 1985; Lunne et al., 1986; Kay and Mayne, 1990) have discussed the importance of correcting q_c for the influence of hydrostatic pressures acting downwards on the notched section of the cone, at the location of the o-ring. The corrected cone tip resistance, q_t , is given by:

$$q_t = q_c + u_{bt}(1 - A_{cn}) \quad (4.1)$$

- where: u_{bt} is the porewater pressure associated with the q_c measurements;
 A_{cn} is the net area ratio of the cone = $\frac{d_o^2}{D^2}$;

- d_o is the smallest diameter of the cone, at the o-ring seal;
 D is the diameter of the base of the cone, usually 35.7 mm.

Since none of the CPTs encountered a water table, no correction to q_c was required, since $u_{bt} = 0$.

Figure 4.25 shows the variation of N_k , evaluated from Equation (2.5), that is,

$$N_k = \frac{q_c - \sigma_{v0}}{s_u} \quad (4.2)$$

with the undrained shear strength, s_u , determined from unconsolidated undrained triaxial tests, and cone tip resistance, q_c measured from the CPTs, shown in Figure 4.24. As can be seen clearly from Figure 4.25, and from Table 4.4, there is a relatively wide scatter in the values of N_k , that is, between 15.1 and 30.5. However, if one concentrates on the results of N_k determined from borehole A10, a much narrower scatter exists; namely, between 15.1 and 19.0. The relatively large scatter, associated with values obtained from borehole F5, is likely to have been caused by the time delay between sampling and triaxial testing, up to one month, as described previously. Such a time delay is likely to have caused greater stress relief within the Keswick Clay samples, yielding lower shear strengths than if the soil had been tested immediately after sampling. As a consequence, lower measurements of s_u resulted in higher values of N_k . The scatter in the values of N_k , obtained from borehole F5, is likely to have resulted from variability in the amount of stress relief between individual tube samples.

During 1992 and 1993 two final year undergraduate research projects were conducted, under the supervision and guidance of the author, to investigate the variability of N_k of the Keswick Clay. Do and Potter (1992) carried out a CPT to five metres and obtained ten undisturbed samples of Keswick Clay for unconsolidated undrained triaxial testing. The field work was undertaken on the 28th July 1992 at Victoria Square, which is located within the Adelaide city area. The location of the boreholes is shown in Figure 4.26.

In order to provide more reliable estimates of N_k , van Holst Pellekaan and Cathro (1993) carried out similar testing at the Victoria Square site, on the 13th April 1993 and 5th July 1993. However, instead of performing a single CPT, the authors conducted three CPTs around the sampling borehole in an arrangement similar to that shown in Figure 4.24. Like Do and Potter, van Holst Pellekaan and Cathro carried out their tests to a depth of approximately 5 metres and obtained a total of 20 undisturbed samples for unconsolidated undrained triaxial testing. The location of the boreholes is also shown in Figure 4.26.

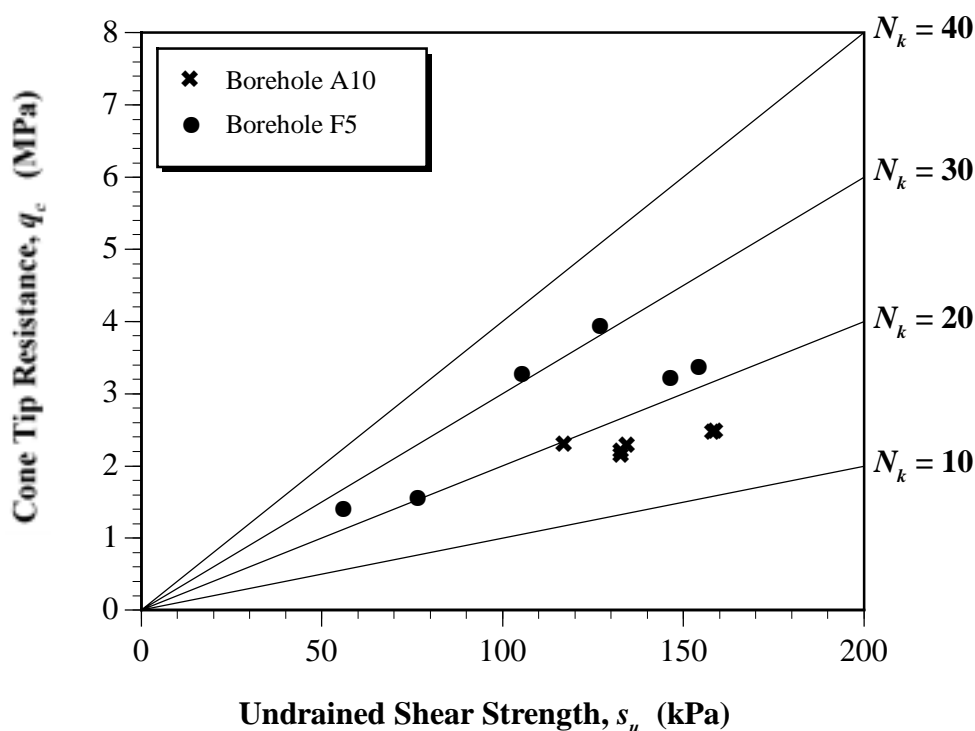
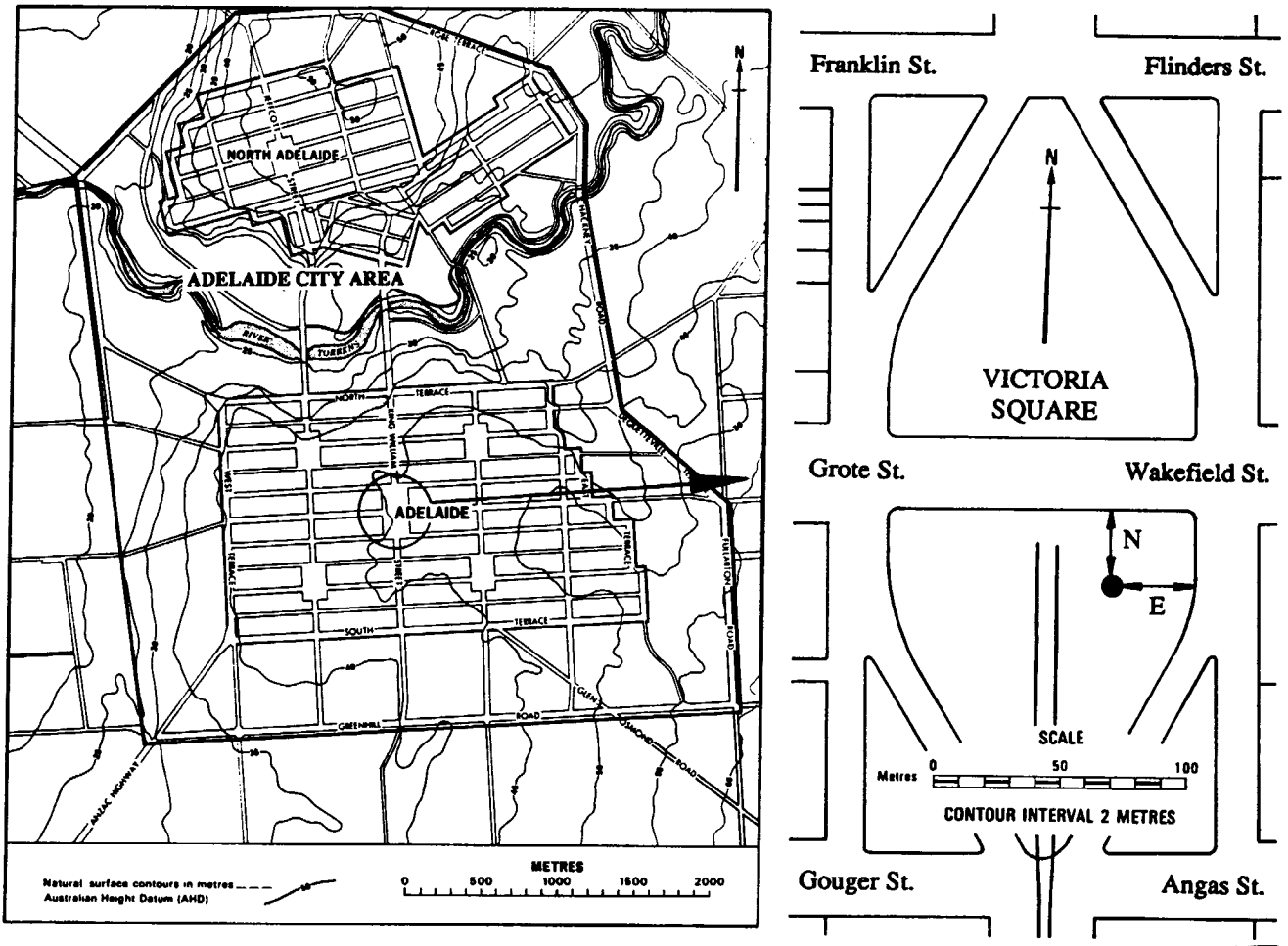


Figure 4.25 Variation of N_k with undrained shear strength, s_u .

In order to confirm the value of $f = -0.4$ suggested by Kay and Mayne (1990), van Holst Pellekaan and Cathro (1993) performed 7 Marchetti flat plate dilatometer tests (DMTs) in the Keswick Clay at the Victoria Square site. The tests were carried out using a standard 95 mm wide by 14 mm thick blade at 0.5 metre depth intervals. The authors found that f varied between -0.30 and -0.44 , with an average of -0.36 , which compares well with that suggested by Kay and Mayne (1990).

The results of the work carried out by Do and Potter (1992) and van Holst Pellekaan and Cathro (1993), together with the results from boreholes A10 and F5 shown in Table 4.4, are summarised in Figure 4.27. The unconsolidated undrained triaxial tests performed by Do and Potter (1992) were carried out 7 days after sampling, whereas the tests performed by van Holst Pellekaan and Cathro were conducted between one and two days after sampling. As can be seen from Figure 4.27, the values of N_k derived from Equation (2.5) exhibit a relatively wide scatter. A number of authors (Ladd and Lambe, 1963; Davis and Poulos, 1967; Germaine and Ladd, 1988; Kulhawy, 1993) have shown that the UU test is a poor indicator of the undrained shear strength of clay. This is primarily due to:

- *sample disturbance* - the inevitable mechanical disturbance and localised residual stress changes and stress relief associated with the sampling, handling and preparation process (Bjerrum, 1973; Ladd, 1964; Davis and Poulos, 1967; Koutsoftas and Fischer, 1976;



LOCATION OF CONE PENETRATION TESTING

Cone Penetration Testing	Northing, N (m)	Easting, E (m)
Do and Potter (1992)	43.6	18.9
van Holst Pellekaan and Cathro (1993) - April	44.0	19.0
van Holst Pellekaan and Cathro (1993) - July	45.3	18.8

Figure 4.26 Locations of tests performed by Do & Potter (1992) and van Holst Pellekaan & Cathro (1993).

Germaine and Ladd, 1988; Long and O’Riordan, 1988; Chandler et al., 1992; Vaughan et al., 1993);

- *initial consolidation* - the differences between the field and the laboratory initial stress states (Ladd, 1964; Davis and Poulos, 1967; Sagaseta, 1993);
- *strength anisotropy* - the variation of undrained shear strength upon the orientation of the sample (Ladd et al., 1977; Mayne, 1985);

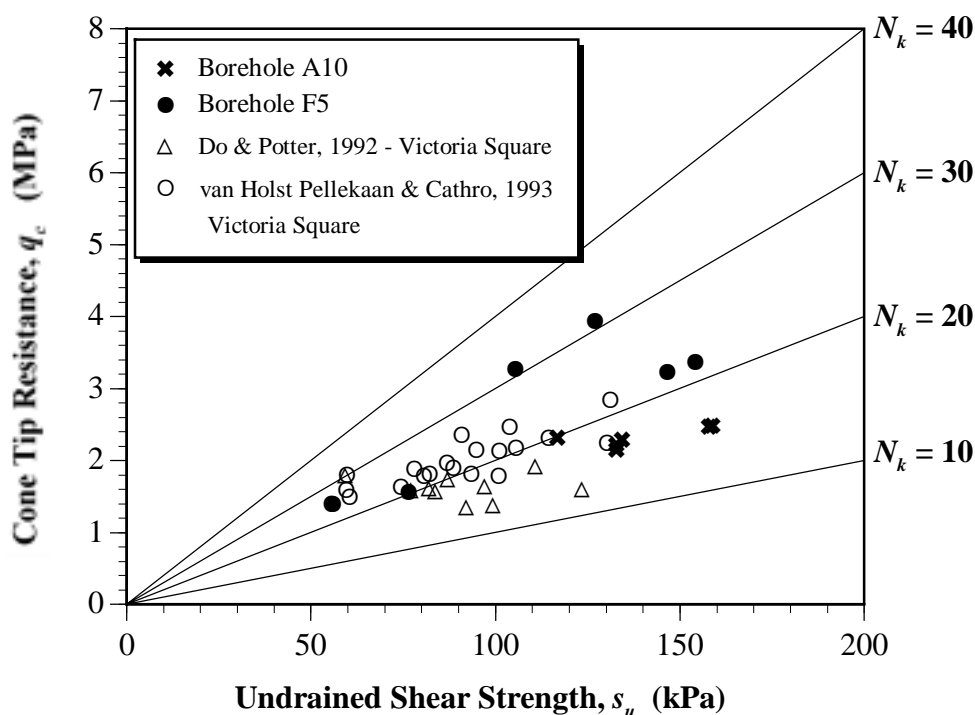


Figure 4.27 Variation of N_k with undrained shear strength, s_u , including results from Do & Potter (1992) and van Holst Pellekaan & Cathro (1993).

- *testing strain rate* - the rate at which strain is applied to the sample (Ladd and Foott, 1974; Germaine and Ladd, 1988).

In order to overcome some of these limitations, many authors (Ladd and Lambe, 1963; Davis and Poulos, 1967; Mitachi and Kitago, 1979; Wroth, 1984; Germaine and Ladd, 1988; Jamiolkowski et al., 1988; Chen and Kulhawy, 1993; Kulhawy, 1993) have suggested that CIU^{20} or CK_0U^{21} tests should be used as an alternative to UU tests. Koutsoftas and Fischer (1976), who compared the results of CPT tests to UU and field vane shear tests, found that greater scatter exists between values of N_k determined from UU tests than from those determined from field vane tests, and consequently advocated the use of the latter.

The variability of N_k may be better understood by examining the results of borehole A10, given previously in Table 4.4 and Figure 4.25. The measured values of \bar{q}_c vary from 2.14 to 2.54 MPa, or 19%, whereas s_u varies from 117.0 to 158.9 kPa, or 36%. That is, the measured values of s_u vary to a larger extent than the measurements of q_c , resulting in greater variations in the derived values of N_k .

²⁰ isotropically consolidated, undrained triaxial compression tests.

²¹ undrained triaxial tests where the sample is reconsolidated to in situ K_0 conditions prior to shear.

As detailed in Table 2.4, the cone factor, N_k , depends on many more factors than is suggested by Equation (2.5). Figures 4.28 and 4.29 show the cone factors determined by Equation (2.5), compared with those suggested by Teh and Houlsby (1991) given in Equation (2.10).

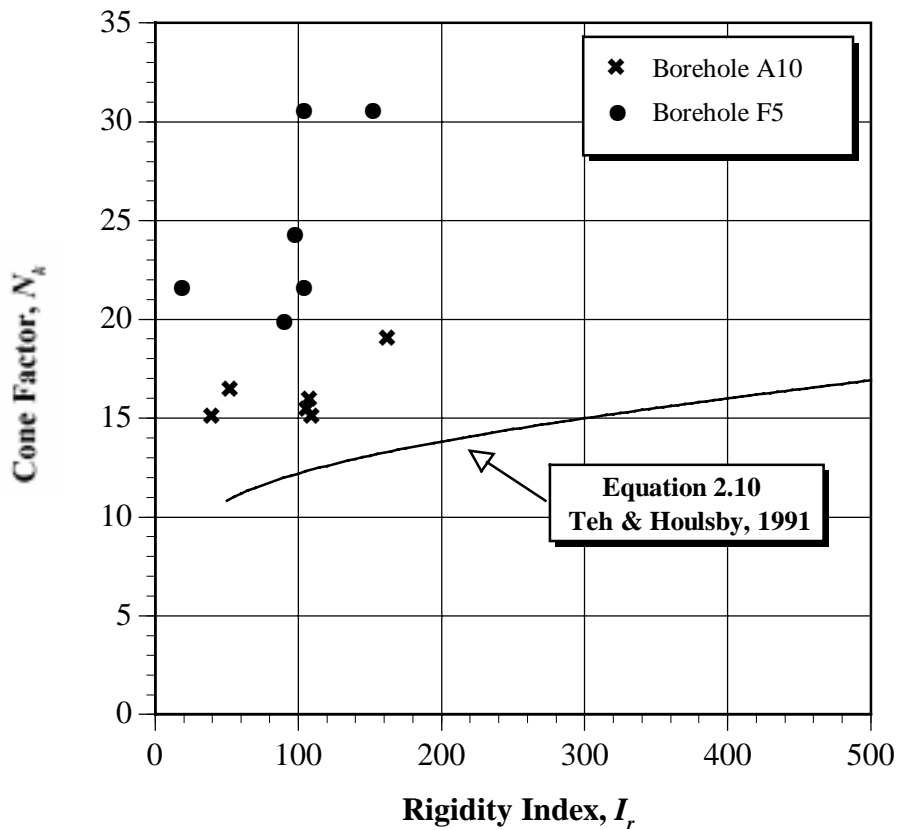


Figure 4.28 Values of N_k determined from Equation (2.5) compared with those obtained by Teh and Houlsby (1991).

As can be seen from Figures 4.28 and 4.29, the experimentally determined results bear little resemblance to the relationship suggested by Teh and Houlsby (1991). This is likely to be due to the fact that UU tests are a poor indicator of s_u , as discussed earlier.

In order to compare the various relationships for evaluating N_k , the measured values of s_u are plotted against the undrained shear strengths, s_u^* , predicted by Equations (2.5) and (2.7) to (2.10). A summary of these is shown in Table 4.5 and Figures 4.30 to 4.33.

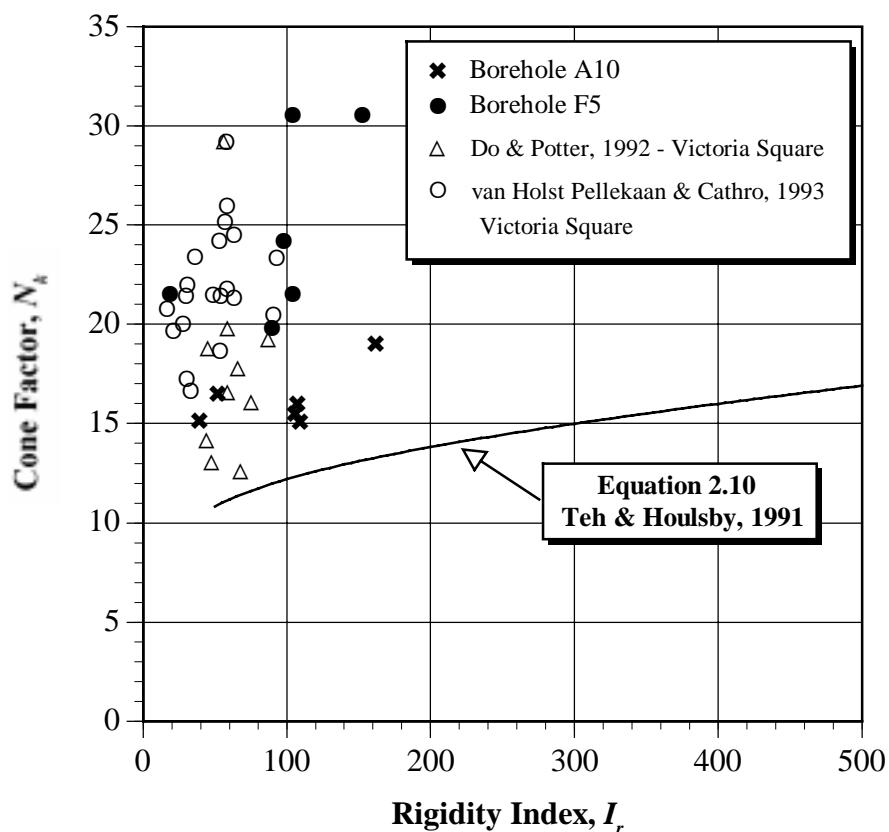


Figure 4.29 Values of N_k determined from Equation (2.5) compared with those obtained by Teh and Houlsby (1991) including results from Do & Potter (1992) and van Holst Pellekaan & Cathro (1993).

Table 4.5 Undrained shear strengths, s_u^* , predicted from values of N_k determined from Equations (2.5) and (2.7) to (2.10).

Test No.	s_u (kPa)	Undrained Shear Strength, s_u^* , (kPa) Predicted by N_k from:			
		Eq. (2.7)	Eq. (2.8)	Eq. (2.9)	Eq. (2.10)
1	134.4	131.8	239.7	227.0	202.4
2	158.1	144.6	269.4	258.6	229.1
3	158.9	136.7	234.5	215.6	193.0
4	117.0	124.0	207.0	187.8	167.0
5	132.8	121.0	207.8	191.2	171.2
6	132.9	117.4	201.9	185.8	166.4
7	56.0	77.9	134.8	124.4	111.5
8	76.5	87.6	152.4	141.1	126.5
9	105.4	184.4	317.6	292.5	262.0
10	154.1	189.9	327.0	301.2	269.7
11	146.5	200.1	400.7	400.8	346.3
12	126.9	217.0	363.7	330.7	294.5

where: s_u undrained shear strength determined by UU tests.

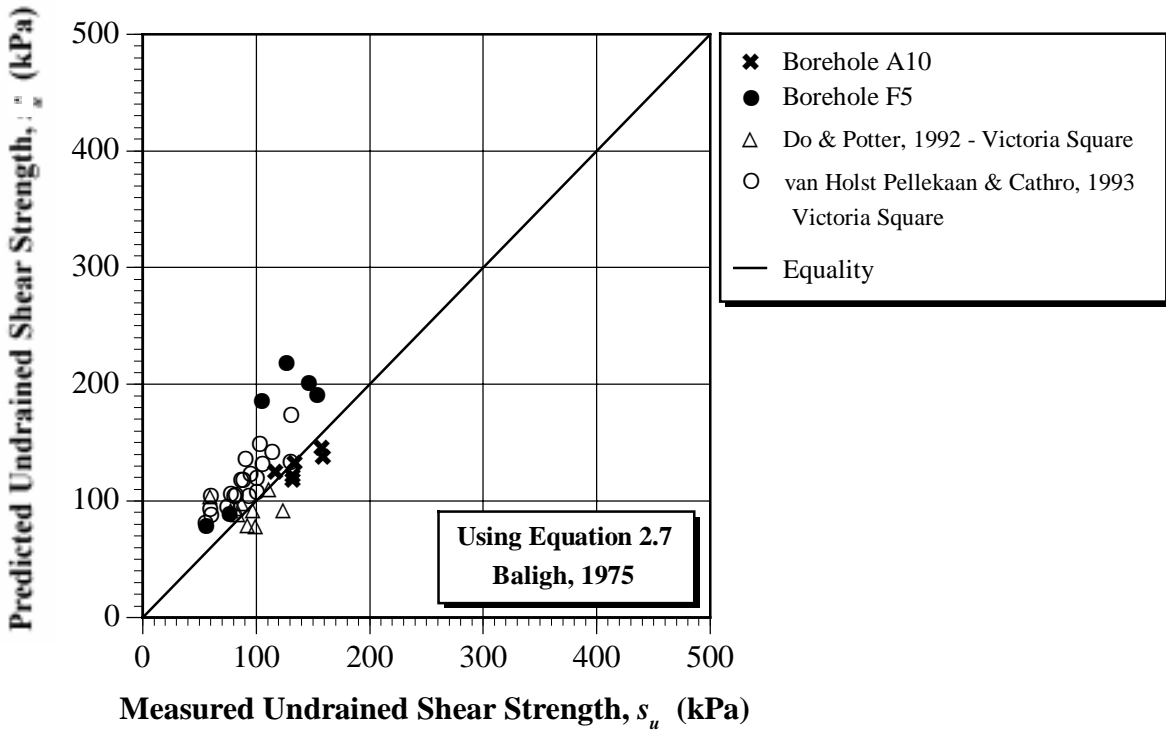


Figure 4.30 Measured values of s_u compared with s_u^* predicted by Equation (2.7) from Baligh (1975).

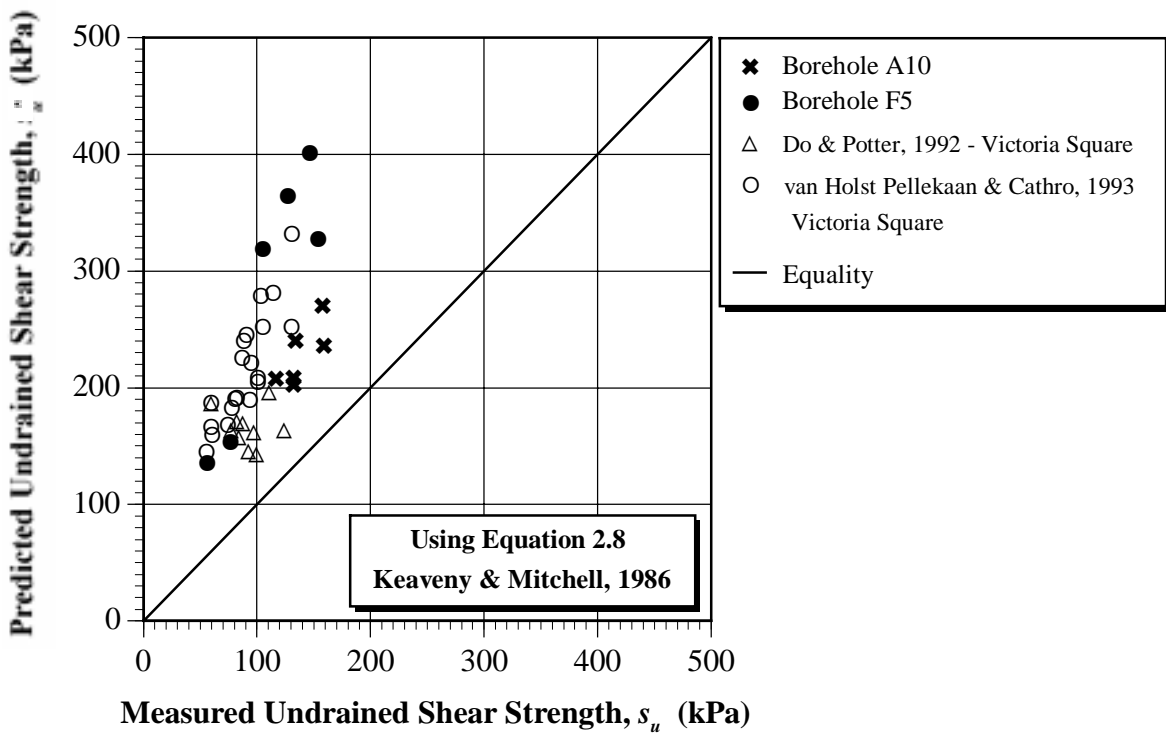


Figure 4.31 Measured values of s_u compared with s_u^* predicted by Equation (2.8) from Keaveny and Mitchell (1986).

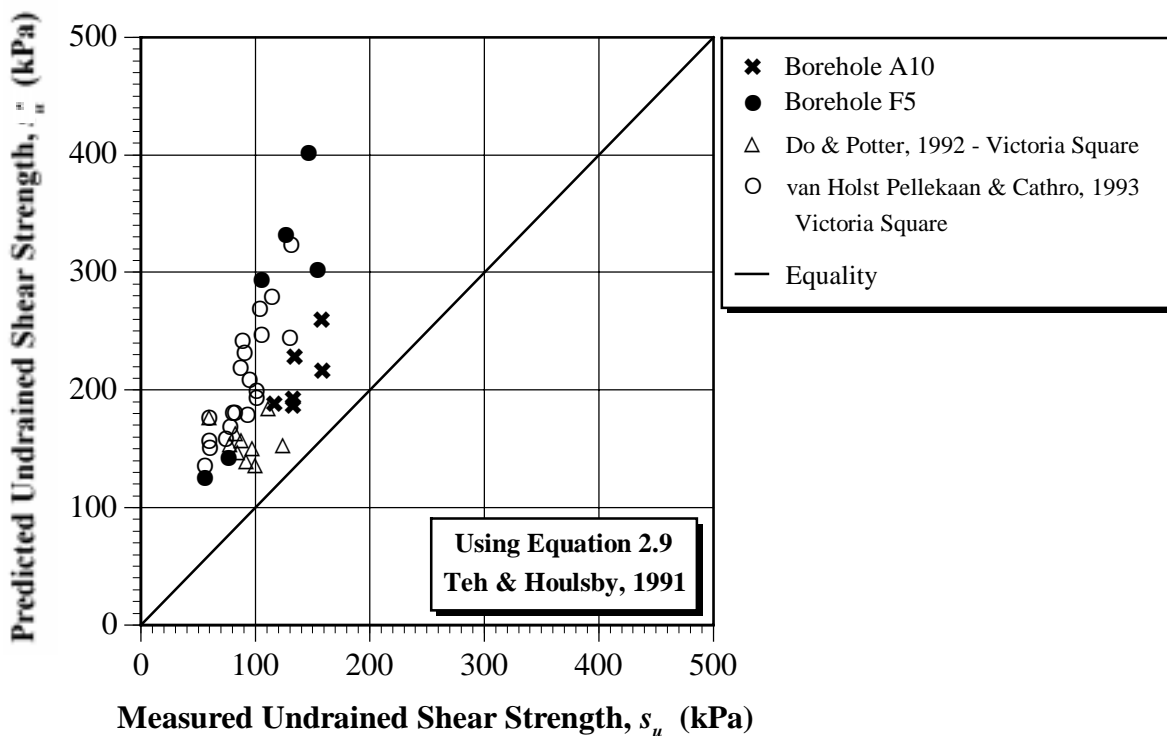


Figure 4.32 Measured values of s_u compared with s_u^* predicted by Equation (2.9) from Teh and Housby (1991).

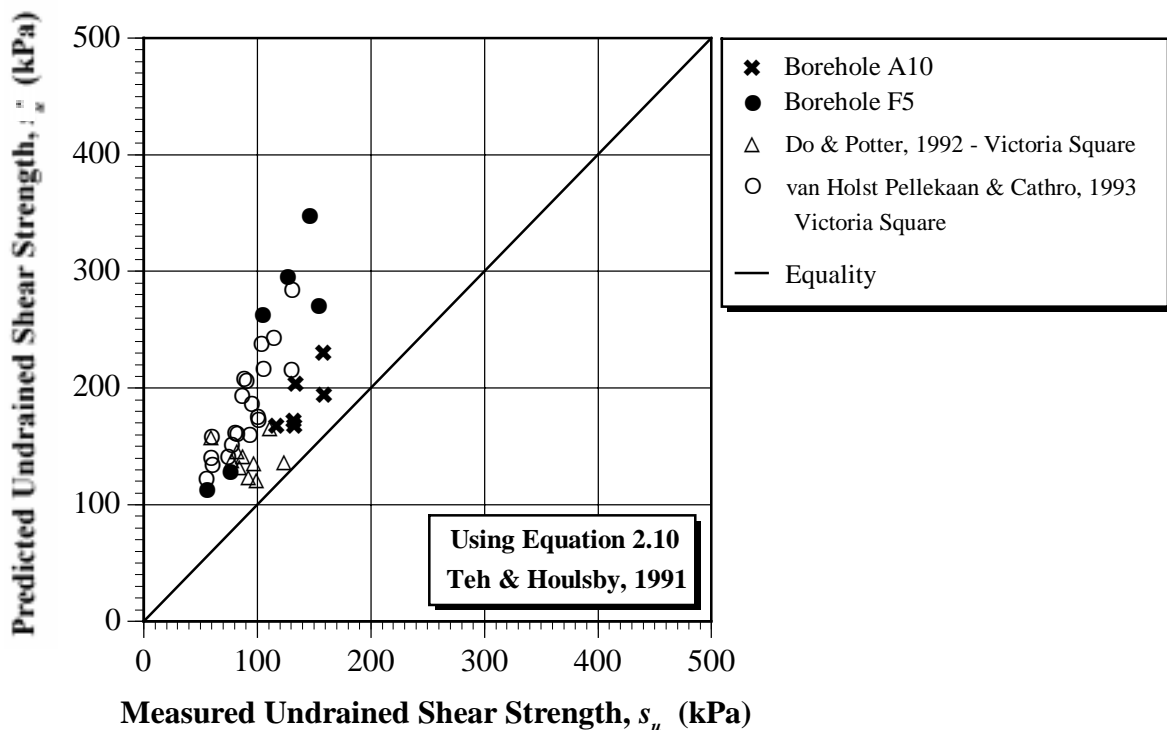


Figure 4.33 Measured values of s_u compared with s_u^* predicted by Equation (2.10) from Teh and Housby (1991).

Examination of Figures 4.30 to 4.33 indicate that Equation (2.7), repeated here:

$$N_k = 12 + \ln(I_r) - 2f \quad (4.3)$$

yields the best comparison of measured, to predicted, undrained shear strengths.

Furthermore, in almost every case, the predicted undrained shear strength is greater than that measured. Chandler et al. (1992) conducted a study which involved comparing the results of driven tube samples of London Clay to block samples. The authors concluded that the process of driving thin-walled tubes to obtain undisturbed samples of soil significantly increases the effective stress, leading to over-optimistic estimates of the undrained shear strength and excessive values of K_0 . This is confirmed by the results shown in Figures 4.30 to 4.33.

It is imperative in the study of spatial variability to eliminate as many sources of error as possible, so that the structure of the spatial variation can be identified and isolated from other causes of variability. Germaine and Ladd (1988) stated that UU tests on specimens having varying degrees of disturbance will give misleading indications of spatial variability, due to bias in the measurements. In addition, Jamiolkowski et al. (1988) stated that the use of q_c to obtain s_u should be limited to non-fissured clays, without highly developed macrofabric. Since a consistent level of disturbance between samples cannot be guaranteed (Chandler et al., 1992) and, as discussed in Chapter 2, the Keswick Clay is heavily fissured, the conversion of q_c measurements to s_u will introduce further variability to the measured data. As a result, subsequent analyses of these data will be based directly on the measured values of q_c and f_s , *not* derived values of s_u .

4.6 SUMMARY

It has been shown that cone factors derived from Equation (2.7), from Baligh (1975), yield the best comparison of measured, to predicted, undrained shear strengths. However, considerable scatter still exists: s_u^*/s_u between 0.86 to 1.06 for borehole A10; and 1.15 to 1.75 for borehole F5. So that additional uncertainties are not introduced into the measured data, thereby clouding the spatial variability of the soil mass, subsequent analyses of these data will not be based on derived values of s_u ; but rather on the measured values of q_c and f_s . These analyses are presented in the following chapter.